An investigation into the role of mutant p53-dependent extracellular vesicles and their impact on the extracellular matrix

David Novo

M.Sci.

Submitted in fulfilment of the requirements for the Degree of Doctor of Philosophy

Institute of Cancer Sciences

College of Medical, Veterinary and Life Sciences

University of Glasgow

September 2019

Abstract

Mutant forms of p53 with impaired DNA binding ability – termed mutp53 – promote cancer aggressiveness. As this occurs, in part, through mutp53's ability to influence membrane trafficking pathways, we have investigated whether mutp53 influences extracellular vesicle (EV) production and/or function, using both cancer cell lines and mouse models of cancer.

To understand whether mutp53 promotes the release of pro-invasive factors, we set up a co-culture approach, using cancer isogenic cell lines differing in their p53 status. We found that poorly invasive H1299 cells lacking p53 (H1299-p53$^{-/-}$ cells) displayed increased invasiveness in 3D microenvironments when cultured in the same media as mutp53-expressing H1299 cells. We then used differential centrifugation to collect EVs from H1299 cells of differing p53 status (p53$^{-/-}$ or mutp53-EVs). We characterised these EV preparations using a range of techniques and found that mutp53 expression in cancer cells does not influence the number or size of EV released by these cells. Nevertheless, when used to pre-treat H1299-p53$^{-/-}$ cells, mutp53-EVs promoted migration of recipient cells indicating that they were qualitatively different from p53$^{-/-}$-EVs. Further investigation determined that mutp53-EVs stimulate RCP- and DGKα-dependent recycling in recipient p53$^{-/-}$ cancer cells, and that inhibition of these pathways in recipient cells prevented their migratory response to mutp53-EVs.

We then used quantitative proteomic approaches to characterise EVs from H1299 cells and found that mutp53 influences levels of EV-associated podocalyxin, a sialomucin with previous described roles in metastasis. Mutp53 suppressed podocalyxin levels in EVs by repressing cellular levels of podocalyxin, and we demonstrated that this likely occurs via inhibition of mutp53's binding partner, p63. Furthermore, we showed that levels of EV-associated podocalyxin must be within a certain range to influence the behaviour of recipient cancer cells, as manipulation of EV-associated podocalyxin impaired the ability of EVs in modulating migration and integrin recycling in recipient cancer cells. Although EV release in many cell types occurs via Rab27-dependent mechanisms, we found that loss of this Rab GTPase did not compromise the ability of mutp53-EVs to influence recipient cell behaviour. Instead, we found that another Rab GTPase, Rab35 is required for the production of phenotype-altering EVs, and it does so, not by influencing EV production, but by regulating EV-associated podocalyxin levels. In particular, we found that Rab35 associates with podocalyxin in mutp53-expressing cells which promotes podocalyxin sorting to the cell

surface, thereby reducing the level of podocalyxin in EVs to a range that allows non-cell autonomous communication to occur.

Fibroblasts are known to be key to the acquisition of pro-invasive tumour microenvironments. We therefore evaluated the effect of EVs on fibroblasts and found that mutp53-EV promote RCP- and DGKα-dependent integrin recycling and, in turn, increased migration of these cells. Integrins are key for the deposition of ECM, and we found that mutp53-EVs encouraged fibroblasts to deposit ECM with altered (more orthogonal) morphology and that this depended on DGKα-dependent integrin recycling. We then found that cancer cells invade more efficiently in this "orthogonal" ECM, and this is likely owing to the reduced adhesiveness of this ECM.

To investigate whether mutp53-expressing tumours influence ECM deposition in a non-cell autonomous fashion *in vivo*, we used quantitative second harmonic generation microscopy and evaluated the organisation of ECM in various organs in autochthonous models of pancreatic cancer. We found that KPC mice, which express mutp53 and develop highly metastatic tumours, display increased ECM orthogonality in the liver and lung prior to metastasis. Furthermore, we used xenograft transplantation models to demonstrate that subcutaneous tumours derived from mutp53-expressing H1299 cells also promote deposition of orthogonal ECM in the lung, and loss of podocalyxin or Rab35 in these tumours impaired their ability to do so. These data suggest that mutp53 expressing tumours promote ECM deposition in pre-metastatic niches and indicate the likelihood of this occurring via EVs and through the regulation of EV-associated podocalyxin levels.

Taken together, these data provide evidence for a novel non-cell autonomous gain-of-function of mutp53 that is mediated by EVs and involves modulation of integrin recycling in recipient cells. We propose that this mechanism might contribute to the aggressiveness of mutp53-expressing cancers, by affecting both tumour cell migration and ECM deposition by fibroblasts. Thus, we have discovered an intercellular/inter-organ communication pathway comprising a number of well-characterised components, which might inform for future therapies and may also act as novel biomarkers to indicate the presence of metastatic tumours.

Table of contents

List of Tables

List of Figures

Acknowledgements

I would like to thank Jim Norman for giving me the opportunity to join the lab and for his supervision and guiding throughout my PhD. I would also like to thank all the members of the R20 lab, not only for their feedback and engaging scientific discussions, but also for being a very nice group of people. I enjoy spending time with you in and out of the lab, and will miss you dearly when I leave. My special thanks to Louise Mitchel, for her input in the project and for her support and friendship over the last 4 years, and to Michalis Gounis, for being a great mate and keeping me sane. And I also thank Nikki Heath, for her contribution in the project and guidance in the first months of my PhD.

This work also progressed through the effort of collaborators. From the Beatson, I thank Jen Morton, Karen Blyth, Leo Carlin, Amanda McFarlane and Dide Reijmer, for their input and advice on the *in vivo* experiments. I would also like to thank Sara Zanivan and David Sumpton for collaborating on the mass spectrometry experiments. My thanks to Peter Bailey and Giuseppina Caligiuri, for collaborating with the experiments using patient-derived cell lines. I am also grateful to the services at the Beatson, as well as BSU/BRU staff, that made this work possible. My thanks to the BAIR, in particular Ewan McGee, for his input and advice on the multiphoton microscope and imaging analysis. Beyond the Beatson, I am grateful to Huabing Yin and Laura Charlton, for collaborating with their AFM expertise; and Arnaud Echard and Kerstin Klinkert, for having provided plasmids.

I am forever grateful to my love, partner and friend Lucy. Who made me feel happy over these 4 years and continues to do so. Also, Lucy contributed with the drawing of the cell types which I used in some of my thesis diagrams... I am lucky. I am grateful to have the support of my 2 good friends Mauro and Afonso, who have been with me since we first met when I started my BSc back in 2009. Finally, I thank my family for their unconditional love and support. And to my nan, Maria. You always believed in me… I did it nan!

Author’s Declaration

I declare that, except where explicit reference is made to the contribution of others, this thesis is the result of my own work and has not been submitted for any other degree at the University of Glasgow or any other institution.

David Novo

Abbreviations

AFM	Atomic force microscopy
AMAP1	A Multiple-domain Arf-GAP Protein 1
Arf6	ADP-ribosylation factor 6
ATM	Ataxia-Telangiectasia mutated
BM	Basement membrane
BMDCs	Bone marrow-derived cells
BSA	Bovine serum albumin
CAFs	Cancer-associated fibroblasts
CCL2	Chemokine (C-C motif) ligand
CD	Cluster differentiation
cDNA	Complementary deoxyribonucleic acid
CM	Conditioned medium
CRISPR	Clustered regularly interspaced short palindrome repeats
CTD	Carboxy-terminal domain
CTL	CD8+ cytotoxic T lymphocytes
DABCO	1,4-Diazabicyclo-octane
DBD	DNA-binding domain
DICER	Endoribonuclease Dicer
DMEM	Dulbecco's Modified Eagle Medium
DMSO	Dimethyl sulfoxide
DNA	Deoxyribonucleic acid
ECM	Extracellular matrix
EGFR	Epidermal Growth Factor receptor
EV	Extracellular vesicle
FMI	Forward migration index
GFP	Green fluorescent protein
GLCM	Gray-level co-occurrence matrix
GLUT1	Glucose transporter 1
GOF	Gain-of-function
HGF	Hepatocyte growth factor
HSP90	Heat-shock protein 90
ILVs	Intraluminal vesicles
IP	Intraperitoneal

KC	LSL-Kras$^{G12D/+}$; Pdx-1-Cre
KPC	LSL-Kras$^{G12D/+}$; LSL-Trp53$^{R172H/+}$; Pdx-1-Cre
KP$_{fl}$C	LSL-Kras$^{G12D/+}$; LSL-Trp53$^{fl/+}$; Pdx-1-Cre
LCMS	Liquid chromatography-mass spectrometry
LFS	Li-Fraumeni syndrome
LOX	Lysyl oxidases
LysC	Lysyl ndopeptidase
Mdm2	Mouse double minute 2 homolog
MDSCs	Myeloid-derived suppressor cells
MIF	Migration inhibitory factor
MMP	Matrix metalloproteinases
mRNA	Messenger ribonucleic acid
mutp53	Mutant p53
MVE	Multivesicular endosomes
MVP	Mevalonate pathway
NETS	Neutrophil extracellular traps
NRF2	Nuclear factor erythroid 2-related factor 2
NT	Non-targeting
NTA	Nanoparticle tracking analysis
OD	Oligomerisation domain
PAGE	Polyacrylamide gel electrophoresis
PBS	Phosphate-buffered saline
PCR	Polymerase chain reaction
PDAC	Pancreatic ductal adenocarcinoma
PDCLs	Patient derived cell lines
PDGF	Platelet-derived growth factor
PDGFR2	Platelet-derived growth factor alpha receptor
PGP	Proline-Glycine-Proline
Pin1	Peptidyl-prolyl cis-trans isomerase NIMA-interacting 1
PMN	Polymorphonuclear neutrophils
PMN	Premetastatic niche
PODXL	Podocalyxin
PRD	Proline-rich domain
PVDF	Polyvinylidene difluoride
RCP	Rab-coupling protein

RDG	Arginine-glycine-aspartic acid motif
RHOA	Ras homolog gene family member A
RTK	Receptor Tyrosine Kinase
SDS	Sodium dodecyl sulphate
SEM	Standard error of the mean
SHARP1	basic helix-loop-helix family member e41
SHG	Second harmonic generation
SILAC	Stable isotope labelling with amino acids in cell culture
SLRPs	Small leucine-rich repeat proteoglycan
SMA	Smooth muscle actin
SNARE	Soluble NSF attachment proteins receptor
TAD	Tandem transactivation domain
TBS	Tris-buffered saline
TEM	Transmission electron microscopy
TF	Transcription factor
TGF-β	Transforming growth factor beta
TME	Trimethylolethane
TME	Tumour Microenvironment
TnfR	Tumour necrosis factor receptor
TOPBP1	DNA topoisomerase 2-binding protein 1
TP53	Tumour protein 53
Treg	Regulatory T cells
Tyr	Tyrosine
UDPase	Uridine 5'-disphosphatase
VDR	Vitamin D Receptor
VEGF	Vascular endothelial growth factor
VPS32	Vacuolar-protein sorting –associated protein 32
WT	Wild-type
YAP	Yes-associated protein

Chapter 1 Introduction

1.1 p53 as a tumour suppressor

Evolution has shaped the appearance of mechanisms that maintain tissue homeostasis. The protein p53, encoded by the TP53 gene that is located in 17p13.1 chromosome, is arguably the most important hub for such mechanisms in humans (Levine and Oren, 2009). p53 is a transcription factor that is stabilised in times of stress. One example of this is when DNA damage arises from spontaneous mutagenesis or sustained oncogenic signalling (Kastan et al., 1991). The stabilisation of p53 allows it to recognise a specific DNA motif in the genome and to activate transcription of target genes (el-Deiry et al., 1992), thereby modulating cellular processes that preserve genomic integrity. Given the fact that cancer is enabled by the accumulation of genomic abnormalities (Hanahan and Weinberg, 2000), it is often characterised by the acquisition of mutations in TP53, leading to loss of tumour-suppressive functions (Olivier et al., 2010).

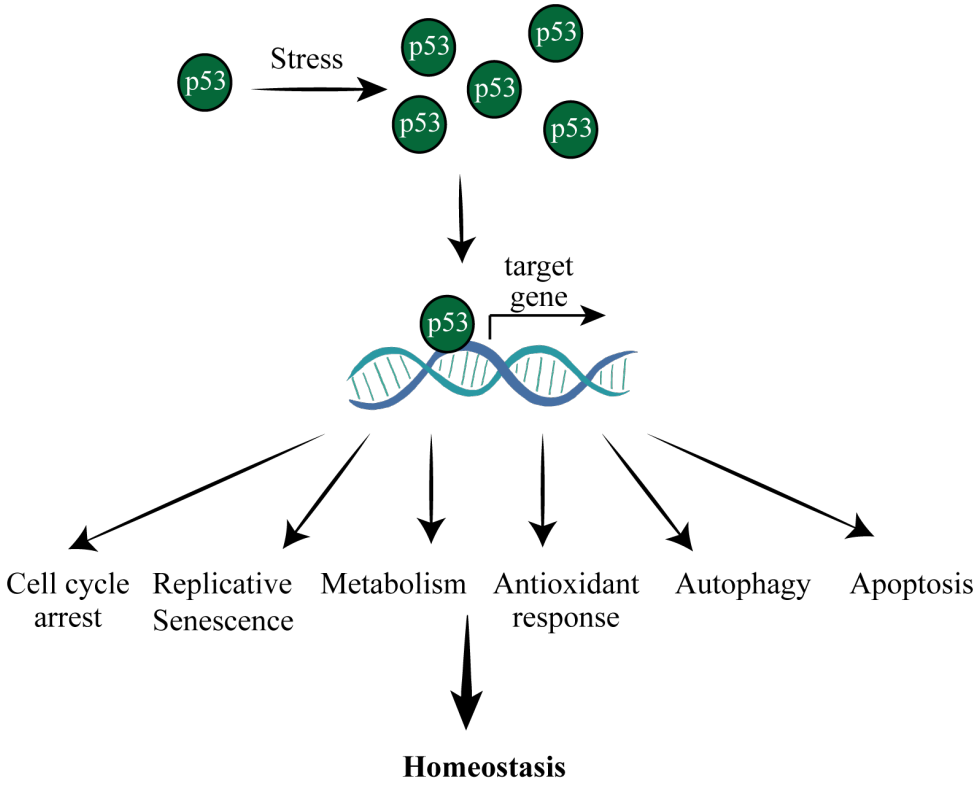

Figure 1-1- p53 as a multifaceted tumour suppressor.
The p53 transcription factor is stabilised and activated in response to cellular stresses, such as accumulation of DNA damage. The association of p53 with response elements in the genome allows transcription of target genes and subsequent induction of cellular processes. These include tumour-suppressive functions, such as the control of cell cycle arrest, replicative senescence and apoptosis. Additionally, other non-canonical functions of p53 have recently been identified, such as the control of autophagy, antioxidation and cellular metabolism.

The best characterised cellular processes regulated by p53, often referred to as its canonical roles, are the induction of cell cycle arrest, apoptosis and senescence (Di Micco et al., 2006; Jimenez et al., 2000; Kastan et al., 1991). Additionally, several non-canonical roles for p53 have emerged over the years, likely reflecting the broad range of target genes regulated by p53. These include, but are not limited to, modulation of autophagy, cellular metabolism and antioxidant responses (Bensaad et al., 2006; Crighton et al., 2006; Sablina et al., 2005). Although the mechanism by which one of these responses is selected is not completely clear, the outcome of p53 stabilisation seems to be fine-tuned according to the cell type, microenvironmental cues, and the type and extent of stress (Kastenhuber and Lowe, 2017). In response to spontaneous mutagenesis, p53 stabilisation is often associated with induction of cell cycle arrest, with concomitant activation of pathways that promote DNA repair. When the damage is beyond repair, as is the case for sustained oncogenic signalling, p53 seems to favour senescence or apoptosis. Either way, p53 activation in response to DNA damage ultimately protects genomic integrity, ensuring that DNA abnormalities are not carried over to daughter cells, thus suppressing tumourigenesis.

1.2 p53 domains and mutations

p53 has a modular protein domain organisation, characteristic of transcription factors (TFs). The N-terminus contains two acidic, tandem transactivation domains (TADs), TAD1 and TAD2, spanning amino acid residues 1-40 and 40-60 respectively. These domains are independently capable of mediating the start of transcription at target sites by recruiting histone-modifying enzymes, co-activators and members of the transcription machinery (Sullivan et al., 2018). There is a proline-rich domain (PRD) adjacent to these, spanning residues 60-95, with a structural but essential role in p53-mediated responses (Toledo et al., 2007; Walker and Levine, 1996). These are followed by a core region, within residues 100-300, comprising the evolutionary conserved DNA-binding domain (DBD), which is responsible for specific binding to DNA response elements (Bargonetti et al., 1993, 1991; Kern et al., 1991). Adjacent to this an oligomerisation domain (OD), ranging from residues 325-356, allows formation of p53 tetramers; the conformation that is required for p53-mediated responses (Clore et al., 1995). Finally, p53 contains a basic, lysine-rich C-terminal domain (CTD), between residues 369-393, which binds DNA in a non-specific manner to promote p53's DNA sliding and homing to response elements (Terakawa et al., 2012).

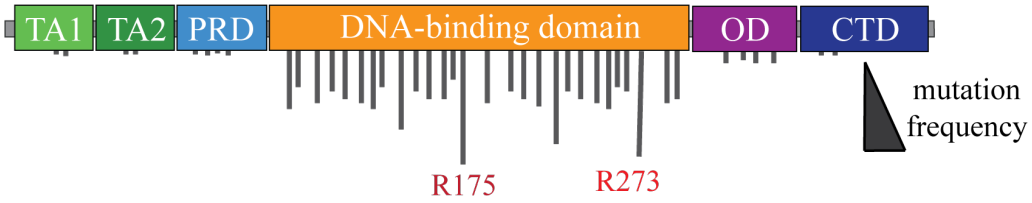

Figure 1-2- p53 is a modular transcription factor and most of the mutations in p53 occur in the DNA-binding domain.
p53 is a multidomain transcription factor. The transactivation domains 1 and 2 (TA1 and TA2) are responsible for starting transcription at target genes via recruitment of transcriptional machinery. The proline-rich domain (PRD) is thought to have a structural role. The DNA-binding domain dictates the association of p53 with DNA response elements in a sequence-specific manner. The oligomerisation domain (OD) drives formation of p53 tetramers. The C-terminal domain (CTD) binds DNA in a non-specific manner and allows p53 homing to response elements. Even though mutations in every p53 domain have been identified in humans, single amino acid substitutions within the DNA-binding domain are the most prevalent. The arginine located at 175 and 273 are mutated at such frequency in human cancers that they are referred to as mutational hotspots.

TP53 is the most frequently mutated gene in human cancers. Germline mutations in p53 are known to cause Li-Fraumeni syndrome (LFS), a hereditary predisposition to cancer in a variety of organs, such as breast, pancreas, lung and brain (Malkin 1990). While p53 can be lost by deletion, around 40% of all cancers acquire single amino acid substitutions within the p53 DBD. Within this domain, 6 residues are mutated so frequently that they are referred to as “mutational hotspots” (Olivier et al., 2010). Mutations in the DBD often give rise to full length proteins, termed mutant p53 (mutp53), which fail to activate p53-mediated transcription by either being unable to engage DNA (contact mutants), or by acquiring conformational changes that impair recognition of p53 response elements (conformational mutants). Examples of mutational hotpots from these 2 categories are R273H and R175H, respectively. Furthermore, around 60% of human cancers with mutations in one TP53 allele display loss-of-heterozygosity, where the remaining functional allele is lost (Baker et al., 1990; Olivier et al., 2010), reinforcing the selective pressure for p53 loss in tumour progression.

1.3 Stabilisation of mutp53 in cancer

Although the observation that mutp53s are expressed at high levels in tumour cells (Rodrigues et al., 1990) led to the assumption that mutp53 is inherently stable, this has been proven not to be the case. For instance, healthy tissue in mutp53 knock-in mice display low levels of mutp53 expression (Lang et al., 2004; Olive et al., 2004), indicative of the requirements of secondary events to stabilise the protein during tumourigenesis. As for p53wt, levels of mutp53 in the cell are regulated by the ubiquitin ligase MDM2, through binding to the N-terminus of mutp53, leading to its polyubiquitylation and proteasomal degradation (Terzian et al., 2008). Accordingly, stimuli that are supposed to stabilise p53wt, such as DNA damage resulting from oncogenic signalling, lead to post-translational

modification (PTM) of mutp53 and weaken its association with MDM2, preventing its degradation (Frum et al., 2016). Although accumulation of p53wt would result in drastic cytotoxicity, mutp53 is tolerated because it fails to activate tumour suppressive mechanisms. Also, MDM2 is a p53wt target and as such, mutp53 fails to activate its transcription, disrupting a negative feedback loop that would otherwise contribute to keeping the levels of mutp53 in check (Midgley and Lane, 1997).

Mutp53 stabilisation depends on its interaction with members of the heat-shock family of chaperones, in particular HSP90. Binding of HSP90 to a mutp53-MDM2 complex protects mutp53 from polyubiquitination, thereby contributing to its accumulation (Peng et al., 2001). Although HSP90 can interact with p53wt in a transient manner, its association with mutp53 in cancer cells is stable and a number of pathways were shown to contribute to this. For instance, HSP90 levels are increased upon oxidative stress, due to activation of the TF HSF1 (Ahn, 2003). Additionally, geranylgeranylation of RhoA via the mevalonate pathway (MVP) can sustain HSP90-dependent mutp53 stabilisation (Ingallina et al., 2018). As HSF1, RhoA and MVP are often hyper-activated during tumourigenesis, their effect on mutp53 stabilisation is likely to be relevant and might explain the high levels at which mutp53 accumulate in cancer cells. Furthermore, these pathways were previously shown to be upregulated by mutp53, thus raising the possibility for a feedback loop allowing mutp53 to, once stabilised, sustain its own expression (Freed-Pastor et al., 2012; Li et al., 2014; Timpson et al., 2011b).

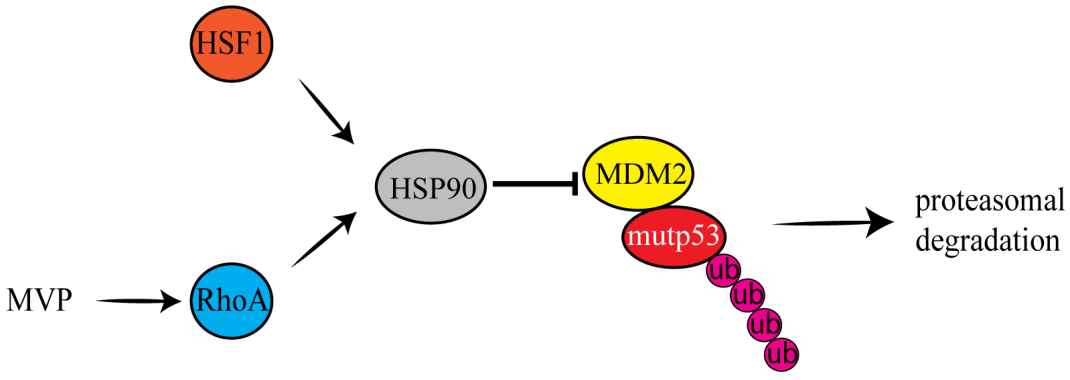

Figure 1-3- HSP90 stabilises mutp53 by preventing its association with MDM2 and its consequent proteasomal degradation.
Expression of mutp53 in cells is influenced by MDM2, an ubiquitin-ligase that tags mutp53 for proteasomal degradation. Mutp53 polyubiquitination and degradation is opposed by its association with heat-shock chaperones (e.g. HSP90). Levels of HSP90 and its ability to associate with mutp53 depend on HSF1 and the MVP-RhoA axis respectively.

1.4 Mechanisms of mutp53's action

Expression of mutp53 is associated with poor prognosis in a variety of cancer types (Freed-Pastor and Prives, 2012). Primarily, this is likely to be the result of loss of p53wt function in mutant forms of the protein, due to the key role for the DBD in p53-mediated tumour suppression. Nonetheless, this is not the only mechanism through which mutp53s act. In situations where the functional allele of p53 is not lost, mutp53 may form tetrameric complexes with p53wt, keeping the functional protein away from its response element and, therefore, inhibiting its function via a dominant-negative mechanism (Willis et al., 2004). Finally, mutp53 can also acquire functions distinct from the wild-type protein, thereby modulating cellular responses in gain-of-function mechanisms.

The mechanisms by which mutp53s exert gain-of-function phenotype mostly involve their stable interaction with varied cellular partners, and modulation of their functions. The majority of mutant p53 binding partners are TFs. However, many reports have identified other types of mutp53-binding partners, and not surprisingly most of these reside in the nucleus. Although there is some evidence that mutp53 may directly bind to DNA in a rather specific manner (Göhler et al., 2005), this hypothesis remains to be further investigated. Importantly, these mechanisms are not mutually exclusive and require cellular accumulation of mutp53.

Mutp53 can physically associate with a number of TFs to transactivate their target genes. This function is consistent with the intact TADs of mutp53, leading to the recruitment of transcription activators p300 to the RE of these genes and transcription initiation (Valenti et al., 2011). Many prominent TFs interact with mutp53 in this manner, including NF-Y, YAP, SREBP-2, Sp1 and VDR (Di Agostino et al., 2016, 2006; Freed-Pastor et al., 2012; Sorrentino et al., 2014; Stambolsky et al., 2010; Tocci et al., 2019; Vogiatzi et al., 2016).

mutp53 can also interact with other TFs of the p53-family, such as p63 and p73. As opposed to the role of mutp53 in transactivating response elements of other TFs, the association of mutp53 with members of its own family mostly leads to transcriptional repression of their target genes, likely by forming tetrameric forms with these and preventing their homing to their specific response elements (Strano et al., 2002).

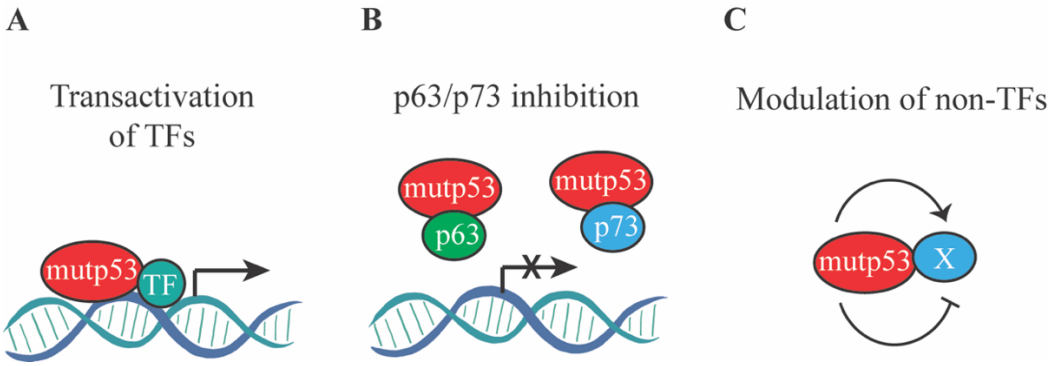

Figure 1-4- Mechanisms of mutp53's GOF.
In addition to dominant negative regulation of p53-wild-type proteins, mutp53 may acquire novel functions through a set of mechanisms. These include: (A) interaction of mutp53 with certain transcription factors (TFs) and the transactivation of their target genes; (B) oligomerisation of mutp53 with members of the p53 family p63 and p73, thereby preventing their homing to response elements and inhibiting their transactivating activities; (C) association of mutp53 with non-transcription factors and modulation of their cellular activity.

1.5 mutp53 gain-of-function in cancer

The high accumulation of mutant forms of p53 in cancer cells (Rodrigues et al., 1990), as well as the ability of these to promote tumourigenesis when over-expressed in a p53-null background (Wolf et al., 1984), led to p53 being initially classified as an oncogene. This was proven to be wrong a decade later, with seminal work from Bradley lab reporting that p53 knock-out mice are prone to tumourigenesis (Donehower et al., 1992). However, those early observations were likely to be the first hints of gain-of-function (GOF) for mutp53 in cancer; a postulate that was experimentally confirmed by the development of p53 knock-in mice. In comparison to mice lacking p53, animals engineered to express $p53^{R172H}$ or $p53^{R270H}$ (which are equivalent to the human hotspot mutants $p53^{R175H}$ and $p53^{R273H}$ respectively) display a more diverse tumour spectrum and, perhaps more importantly, more metastatic tumours (Lang et al., 2004; Olive et al., 2004). Consistently, LFS patients that carry mutp53 alleles present a prognosis poorer than patients with p53 loss, indicating the likelihood of mutp53 GOF to be manifest in humans (Malkin et al., 1990). Even though the phenotypes resulting from mutp53 expression are diverse and reflect the cellular context in which these mutants occur (Freed-Pastor and Prives, 2012), mutp53 may influence multiple, if not all, stages of carcinogenesis.

1.5.1 Genomic instability and tumour growth

Carcinogenesis occurs through accumulation of deleterious mutations. Genomic instability is key for this to occur, as the rate of spontaneous mutagenesis for a normal cell is low (Hanahan and Weinberg, 2000). In contrast to the key role of p53 as the "guardian of the genome", mutp53 can interfere with and impair genome integrity processes. This is

consistent with studies highlighting chromosomal rearrangements and genomic abnormalities as a result of mutp53 expression (Mackay et al., 2018). The best characterised mechanism through which this occurs involves modulation of ataxia-telangiectasia mutated (ATM), a DDR transducer that is activated in response to DNA double-stranded breaks. This is achieved by binding of mutp53 to the nuclease Mre11, preventing this protein from forming a complex required for ATM activation and G2-M checkpoint. Through this mechanism, mutp53 may increase the rate of intrachromosomal translocations in the cell, driving genomic instability (Song et al., 2007). Speculatively, such phenotype is likely to be selected for during the early phases of tumour progression and may allow mutp53 to contribute to a higher mutational load, therefore driving carcinogenesis.

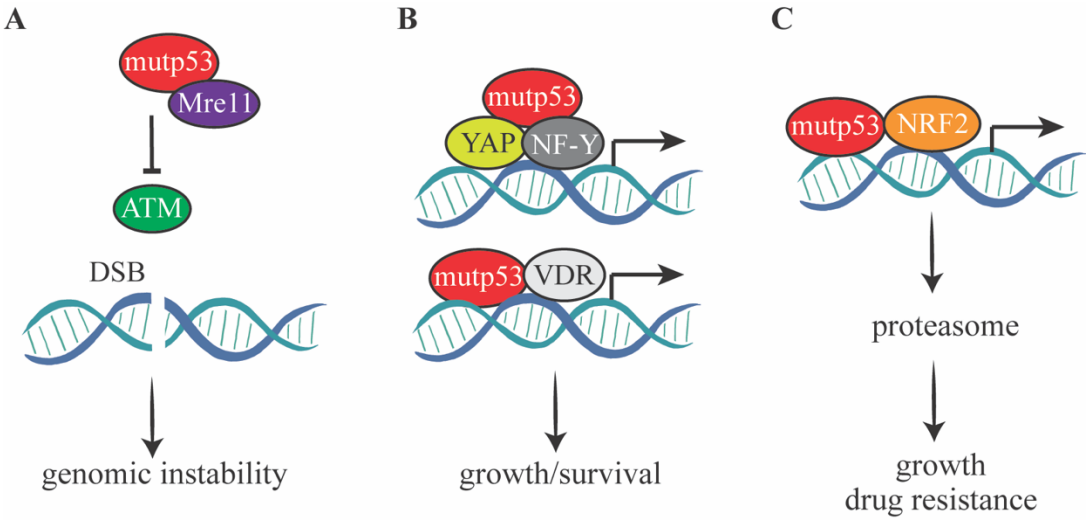

Figure 1-5- mutp53 promotes genomic instability, tumour growth and drug resistance.
(A) mutp53 drives genomic instability by increasing the rate of intrachromosomal translocations in cells. A way for this to occur is through mutp53's association with Mre11 and inhibition of ATM activation in response to DNA double-stranded breaks (DSBs). (B) mutp53 promotes tumour growth by driving expression of cell cycle and pro-survival genes, through forming complexes with transcription factors (e.g. NF-Y and VDR) in their DNA response elements. (C) mutp53 may drive detoxification and tumour growth by upregulating the proteasome machinery, through associating with the NRF2 transcription factor at response elements of proteasome genes.

Tumour growth is characterised by modulation of cell cycle progression and/or apoptosis. Mutp53s may promote tumour growth by associating with a number of TFs and transactivating target genes involved in these programs. For example, mutp53 can form a stable complex with Yap and NF-Y at RE of genes encoding for the cell cycle stimulators cyclin A, cyclin B and CDK1, thereby sustaining proliferation by potently upregulating these genes (Di Agostino et al., 2016). Similarly, mutp53 may bind to VDR and promote transcriptional activation of several pro-survival genes (Stambolsky et al., 2010). Furthermore, mutp53 can associate with the TF NRF2 at the RE of genes encoding for members of the proteasome machinery, leading to increased proteasomal degradation of

several tumour suppressors, in turn sustaining tumour cell proliferation and resistance to proteasomal inhibitors (Walerych et al., 2016). As chemotherapeutic drugs are known to cause proteolytic stress, mutp53-mediated upregulation of proteasome might allow cancer cells to cope better in such conditions, likely contributing to the clear correlations between mutp53 expression, drug resistance and tumour relapse after therapy in a variety of cancer types (Mantovani et al., 2019).

1.5.2 Tumour metabolism

Metabolic rewiring is often observed in cancer (Dang, 2012) and mutp53 was previously shown to play roles in these processes. One frequent metabolic adaptation of tumour cells is their ability to uptake large amounts of glucose and use it for aerobic glycolysis (known as the Warburg effect). Mutp53 can sustain this process firstly by stimulating glucose uptake through translocation of the glucose transporter GLUT1 to the plasma membrane, via activation of RhoA and Rock (Zhang et al., 2013), and secondly by directly inducing aerobic glycolysis, through association and inhibition of AMPK (Zhou et al., 2014).

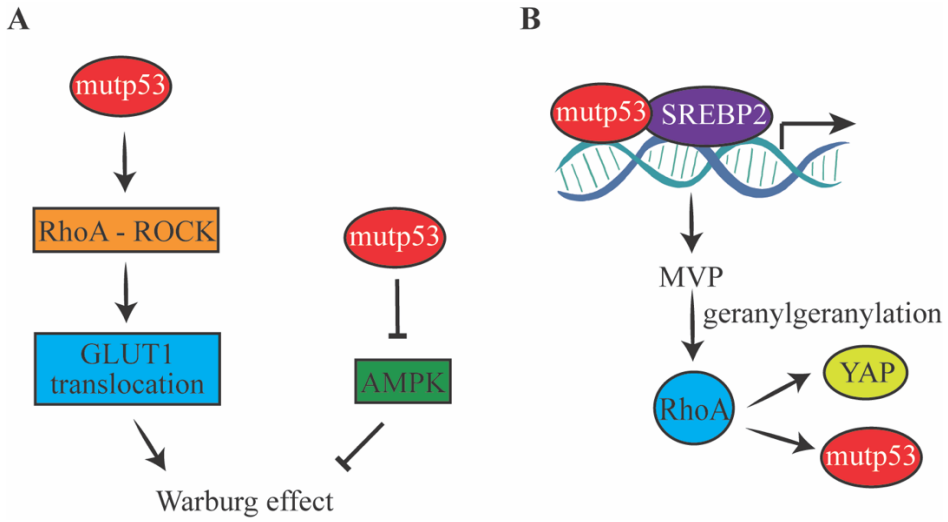

Figure 1-6- mutp53 deregulates aerobic glycolysis and lipid metabolism.
Tumour growth occurs through rewiring of cellular metabolism and mutp53 influences this. (A) Tumours often use aerobic glycolysis to produce cellular ATP, coupled with release of lactate to the extracellular milieu – the Warburg effect. mutp53 drives this phenotype via activation of RhoA-ROCK-dependent recycling of the glucose transporter GLUT1 from endosomes to the plasma membrane, thereby sustaining the uptake of glucose in cells. mutp53 may also promote the expression of several glycolytic enzymes by associating with and inhibiting the function of the energy sensor, AMPK. (B) Many tumours display rewiring of lipid metabolism. The association of mutp53 with SREBP2, a major inducer of fatty acid and cholesterol biosynthesis, drives expression of mevalonate pathway (MVP) enzymes. Downstream of this, the MVP sustains geranylgeranylation of RhoA, which in turn drives the translocation of YAP to the nucleus and HSP90-mediated mutp53 stabilisation, thus reinforcing a positive feedback loop.

Many tumours are characterised by rewiring of lipid metabolism (Munir et al., 2019). The interaction of mutp53 with SREBP2, which is a major inducer of fatty acids and cholesterol biosynthesis, led to transcriptional activation of the MVP (Freed-Pastor et al., 2012).

Downstream of mutp53, the MVP drives geranylgeranylation and activation of RhoA, which in turn promotes the translocation of YAP/TAZ to the nucleus and subsequent oncogenic signalling (Sorrentino et al., 2014). As geranylgeranylation of RhoA leads to mutp53 stabilisation (Ingallina et al., 2018), lipid rewiring by mutp53 contributes to mutp53 accumulation, thus likely driving gain-of-function mechanisms.

1.5.3 Tumour cell invasion

The best elucidated mechanism through which mutp53s promote cancer aggressiveness involves its stable association with, and inhibition of, p53-family members p63 and p73. In fact, mice with loss of p63 recapitulate the highly metastatic phenotype reported for mutp53 knock-in mice (Su et al., 2010), and depletion of p63 or p73 in p53-null cancer cell phenocopied invasiveness of cells expressing mutp53 (Muller et al., 2009; Weissmueller et al., 2014).

Mutp53-mediated inhibition of p63/p73 functions can promote tumour cell invasion by deregulating their target genes. Mutp53-dependent inhibition of p63/p73 functions in tumour cells suppressed expression of SHARP1, cyclin G2 and DICER, and/or stimulated expression of PDGFR2. As it has been reported that the rescuing of the levels of these proteins reduced invasiveness in mutp53-expressing cells (Adorno et al., 2009; Muller et al., 2014; Weissmueller et al., 2014), it is likely that modulation of these p63/p73 targets contributes to mutp53-mediated invasiveness. In particular, the loss of DICER in p63-knockout mice impairs miRNA processing and potentiates metastasis formation in vivo (Su et al., 2010), so it is likely that mutp53 promotes invasion, at least in part, by deregulating miRNA levels in cells.

The mutp53-p63 axis can also promote tumour cell invasion by modulating endocytic recycling of receptors. In particular, inhibition of p63 function by mutp53 stimulates recycling of α5β1 integrin from recycling endosomes to the plasma membrane, by promoting its association with the Rab11 effector Rab-coupling protein (RCP) (Muller et al., 2009). Through its N-terminus, RCP can associate with a number of RTKs, including EGFR and cMET (Caswell et al., 2008; Muller et al., 2013, 2009). Thus, via RCP, mutp53 stimulates the coordinated recycling of adhesion and growth factor receptors.

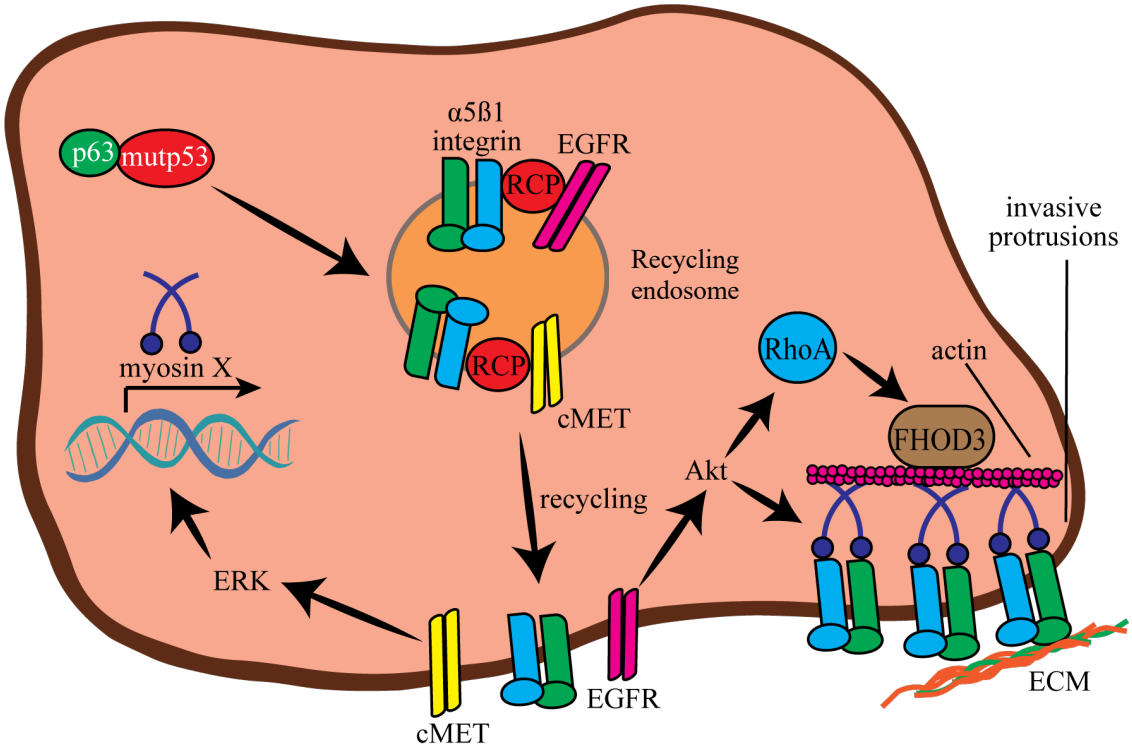

Figure 1-7- mutp53 promotes cancer cell invasion by inhibiting p63 function and stimulating receptor recycling.
Inhibition of p63 function by mutp53 stimulates the association of Rab-coupling protein (RCP) with α5β1 integrin and receptor tyrosine kinases EGFR and cMET. This promotes their recycling to the plasma membrane and activation of the Akt/PI3K and MAP kinase (MAPK) pathways. Activation of Akt drives phosphorylation and recruitment of Rac1GAP to the plasma membrane at the front of migrating cells, leading to local activation of RhoA. In turn, RhoA activates the formin FHOD3, mediating actin polymerisation to drive formation of invasive protrusions. In parallel, through activation of MAPKs and Akt respectively, mutp53 upregulates and activates myosin X, a motor protein that associates with α5β1 integrin and mediates its translocation to the tips of filopodia. This way, mutp53 modulates tumour cell-ECM adhesions and invasion.

Consistent with the trafficking of RTK influencing their signalling, mutp53 stimulation of EGFR and cMET recycling was shown to activate the Akt/PI3K and MAP kinase (MAPK) pathways respectively (Muller et al., 2013, 2009). Activation of Akt drives phosphorylation and recruitment of Rac1GAP to the plasma membrane at the front of migrating cells, leading to local activation of RhoA (Jacquemet et al., 2013; Timpson et al., 2011b). In turn, RhoA activates formin FHOD3, mediating actin polymerisation to drive formation of filopodial spike-based protrusions (Paul et al., 2015). In parallel, through activation of MAPKs and Akt respectively, mutp53 upregulates and activates myosin X, a motor protein that associates with β1 integrin (Arjonen et al., 2014). Together with the enhanced surface levels of α5β1 integrin resulting from RCP-mediated recycling, myosin X drives translocation of α5β1 integrin to the tips of filopodia, where it can associate with components of the extracellular matrix (ECM), thereby allowing mutp53 to induce the formation of tumour cell-ECM adhesion and invasion (Arjonen et al., 2014). Additionally, mutp53 was recently shown to drive invasion by upregulating ENTPD5, a uridine 5′-diphosphatase (UDPase) that resides in the endoplasmic reticulum (ER) and controls folding of N-glycosylated proteins (Vogiatzi

et al., 2016). As integrins and RTKs are often highly N-glycosylated, is it interesting to speculate whether this mechanism might contribute to the quality-control of proteins, thus sustaining the presence of a recycling pool of glycosylated receptors.

Although other pathways have been reported to cooperate with mutp53 to drive the acquisition of aggressive phenotypes, it seems that many do so, at least in part, by affecting mutp53-p63 binding. For example, Pin1, TopBP1 and SMAD2, which were shown to promote mutp53-mediated cancer cell invasion, can associate with mutp53 and form complexes with p63, stimulating such inhibition (Adorno et al., 2009; Girardini et al., 2011; Liu et al., 2011). This, again, reinforces the idea that phenotypes resulting from mutp53 expression are context dependent, and are potentially affected by the levels of multiple mutp53-binding partners in cells.

1.6 Tumour microenvironment

Tumour cells reside within a complex tumour microenvironment (TME) consisting of numerous cell types and the ECM. Reciprocal interactions between TME components, including tumour, immune, endothelial, and lymphatic cells, and cancer-associated fibroblasts (CAFs) and their deposited ECM, influence tumour growth and progression into invasive disease. Thus, metastasis formation depends on both autonomous and non-cell autonomous mechanisms.

Perhaps the first obstacle for tumour growth is the immune system. Anti-tumour immunity is largely mediated by resident $CD8^+$ cytotoxic T lymphocytes (CTL) and natural killer (NK) cells, which have the ability to bind to antigens at the tumour cell surface and promote its elimination (Binnewies et al., 2018). Thus, in order to grow, tumours may have to avoid immune surveillance. A common mechanism for avoidance of anti-tumour immunity is cancer-induced inflammation, often characterised by recruitment of immune-suppressive bone marrow-derived cells (BMDCs). Many cell types with immune-suppressive function are often present within the TME, including regulatory T-lymphocytes (T_{reg}), immature monocytes, tumour-associated macrophages, neutrophils and dendritic cells, all of which may counterbalance T cell function and subsequent anti-tumour immunity (Vinay et al., 2015).

Tumour cells can be highly metabolically active and require nutrients and oxygen from the bloodstream to survive and proliferate. Interactions within the TME may influence

endothelial cell behaviour and stimulate the vascularisation of tumours, supporting tumour growth (Hillen and Griffioen, 2007). Importantly, tumours may enter the vasculature to disseminate to other organs, making vascularisation of tumours a possible contributor to metastasis.

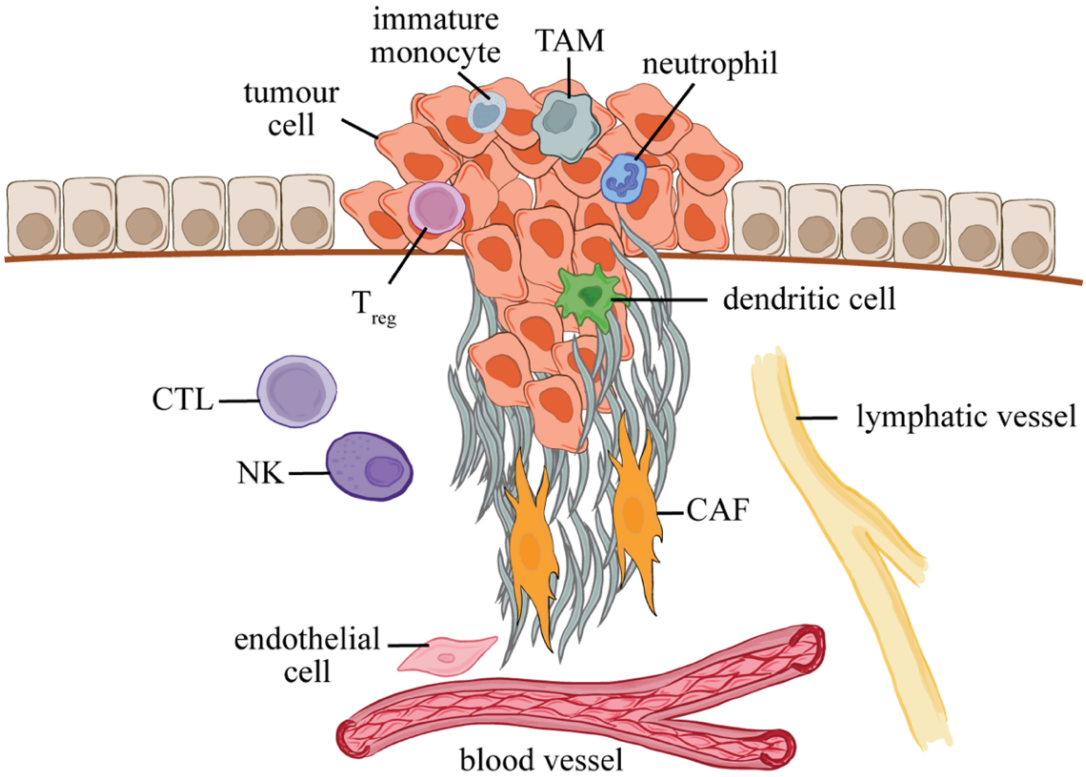

Figure 1-8- The components of the tumour microenvironment.
Tumour cells reside within a complex tumour microenvironment (TME), consisting of various cell types and ECM. The interactions between TME components, including tumour, immune, endothelial, and lymphatic cells, and CAFs and their deposited ECM, are thought to influence the way tumours grow and progress into metastatic disease. Abbreviation are as follows: CTL – cytotoxic T-lymphocyte; Treg – regulatory T-lymphocyte; NK – natural killer cell; TAM – tumour-associated macrophage; CAF - carcinoma-associated fibroblast.

In order to reach the vasculature, tumour cells must cross physical barriers posed by the ECM, such as the basement membrane outlining the epithelium and vasculature, and the rich, desmoplastic stroma that separates them. Tumour cell dissemination depends on the intrinsic invasiveness of tumour cells, as well as the existence of an invasion-permissive stroma (Levental et al., 2009). CAFs in the stroma have a major role in allowing this to occur. Furthermore, CAFs can perform a set of behaviour that may influence other TME components, contributing to the formation of a tumour-permissive microenvironment.

1.6.1 Cancer-associated fibroblasts

CAFs are an abundant cell type in the TME. Although the origin of CAFs is complex and continues to be somewhat controversial, the main source for CAFs is thought to be via

activation of tissue-resident fibroblasts by microenvironmental signals (LeBleu and Kalluri, 2018). This process shares features with fibroblast activation during tissue healing responses. However, fibroblast activation in cancer is a persistent phenomenon, because many factors that stimulate this are within the tumour secretome. Indeed, many proteins in the tumour secretome, such as TGFβ, PDGF, LIF and OSM, have been shown to promote fibroblast activation and are also known to contribute to wound healing (Albrengues et al., 2014; Midgley et al., 2013; Rajkumar et al., 2006; Scaffidi et al., 2002).

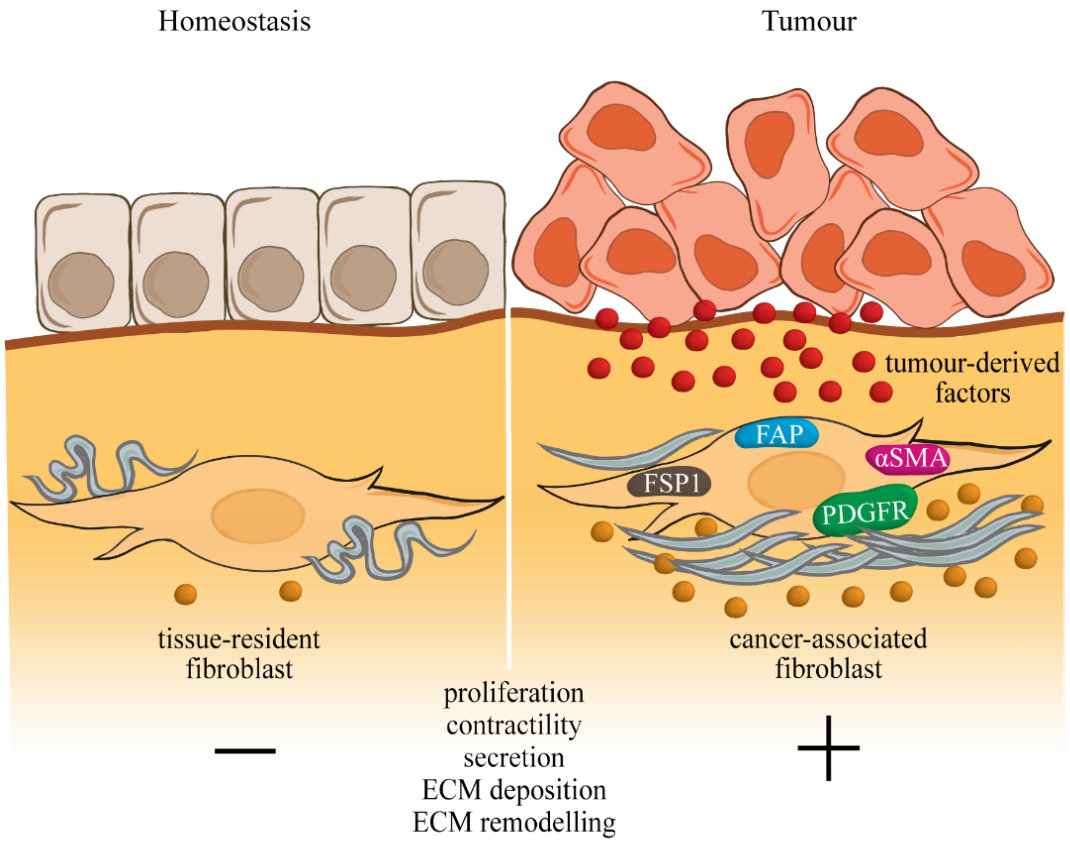

Figure 1-9- Fibroblast activation in cancer.
CAFs are an abundant cell type in the TME and may derive from the activation of tissue-resident fibroblasts by factors within the tumour secretome (e.g. TGFβ, PDGF, LIF and OSM). Activation of CAFs is often accompanied by upregulation of PDGFR1, FSP1, FAP, and/or αSMA. While resident fibroblasts are often kept in a quiescent, inactive state during homeostasis, CAFs are proliferative, contractile cells that produce a complex secretome and actively deposit and remodel the ECM.

The lack of bona fide markers for distinguishing CAFs from other fibroblasts is consistent with the observation that CAFs in the TME are heterogenous (Bu et al., 2019; Neuzillet et al., 2019). Nonetheless, activation of CAFs is often accompanied by upregulation of PDGFR1, FAP, and/or αSMA (Anderberg et al., 2009; Rønnov-Jessen et al., 1995; Teichgräber et al., 2015). Furthermore, while resident fibroblasts are kept in a quiescent, inactive state during homeostasis, CAFs are proliferative, contractile cells that produce a secretome containing copious amounts of ECM components (LeBleu and Kalluri, 2018).

1.6.2 ECM components

The desmoplastic stroma is characterised by aberrant deposition of ECM. The ECM components which constitute the bulk of the CAF secretome are the fibrillar proteins collagen I and fibronectin (De Boeck et al., 2013).

1.6.2.1 Collagen I

The collagen family of proteins comprises 28 members. A hallmark of all collagens is their triple-helix, formed by homo- or heterotrimers of collagen polypeptides. This structure is supported by the core collagenous domain which comprises the repeating motif, Gly-X-Y. Some collagens can also be modified in the extracellular space to be assembled into fibrils – termed fibrillar collagens. Collagen I is the most abundant fibrillar collagen in most healthy tissues, as well as in desmoplastic TME (Mouw et al., 2014).

The product of transcription and translation of collagen genes are the collagen α-chains. These are precursor molecules with large N- and C-terminal regions – named N- and C-propeptide respectively, and a central collagenous domain. In the ER, many residues in the newly-synthesised α-chains are hydroxylated and glycosylated (KellokumpuS et al., n.d.; Schegg et al., 2009). Such PTMs stabilise the triple-helix, which starts at the C-propeptide domains via nucleation and specific chain recognition (Bourhis et al., 2012). Additionally, the Gly-X-Y motif in the collagenous domain gives further stability to the triple-helix, with glycine being small enough to be accommodated in a packed structure that enforces steric constrains on every third amino acid (Brodsky and Persikov, 2005). Procollagen is then trafficked to the Golgi apparatus, where it can be further modified and secreted to the extracellular milieu.

Following or during secretion of procollagen, the propeptides are cleaved by collagen-specific metalloproteases, giving raise to mature collagen that can self-assemble and grow unilaterally into microfibrils (Orgel et al., 2006). Multiple microfibrils can merge and grow both longitudinally and axially, leading to formation of mature fibrils. Importantly, fibril maturation is regulated by the incorporation of collagen-binding proteins in the assembling structure, including other collagens and small leucine-rich repeat proteoglycans (SLRPs) that modulate fibril stability (Holmes et al., 2001; Zhang et al., 2006). Finally, extracellular lysyl-oxidases (LOX), transglutaminases and other cross-linking enzymes catalyse the introduction of covalent cross-links into the supramolecular structure, between and within

collagen fibrils. This last step in collagen fibrillogenesis leads to the formation of mature fibres, capable of enduring tensile force (Grenard et al., 2001; Herchenhan et al., 2015).

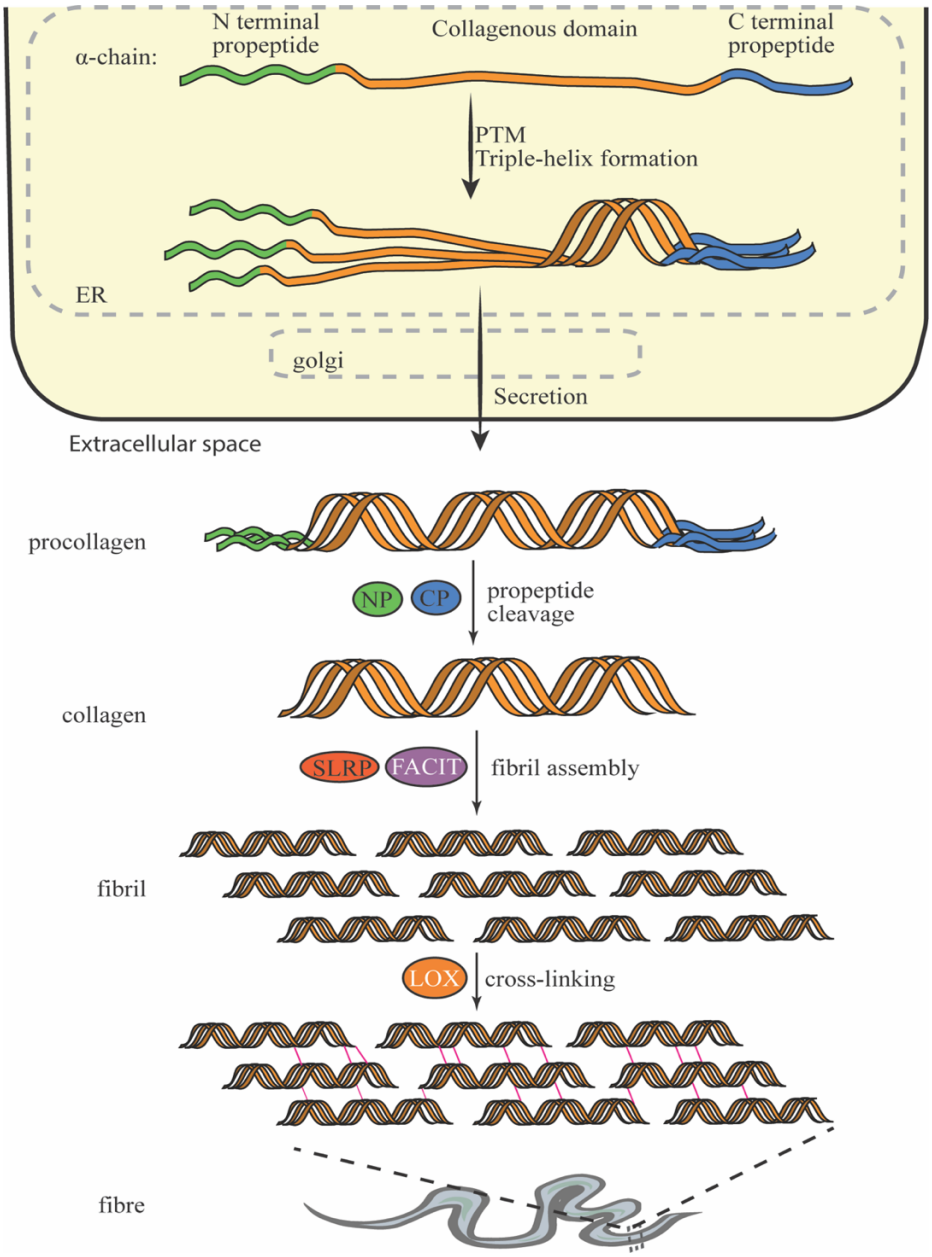

Figure 1-10- Biogenesis of fibrillar collagen.
The product of collagen genes are the collagen α-chains. These are precursor molecules with large N- and C-terminal regions – named the N- and C-propeptides respectively, and a central collagenous domain. In the endoplasmic reticulum (ER), many residues in the α-chains are hydroxylated and glycosylated. Such post-translational modifications (PTMs) stabilise the triple-helix, which starts forming at the C-propeptide domains via nucleation and specific chain recognition. Procollagen is then trafficked to the Golgi apparatus, where it can be further modified and then secreted to the extracellular milieu. Following, or during, secretion of procollagen, the propeptides are cleaved by N- and C-procollagen proteinases (NP and CP), giving raise to mature collagen that can self-assemble and grow unilaterally into microfibrils. Multiple microfibrils can merge and grow, leading to formation of mature fibrils. Fibril maturation is regulated by the incorporation of collagen-binding proteins in the assembling structure, including fibril associated collagens with interrupted triple helices (FACIT) and small leucine-rich repeat proteoglycans (SLRPs) Finally, cross-linking enzymes (e.g. lysyl-oxidase (LOX)) catalyse the introduction of covalent cross-links into the supramolecular structure, between and within collagen fibrils.

1.6.2.2 Fibronectin

The fibril-forming protein fibronectin is an obligate component of the ECM in mammals. Fibronectin is a dimeric modular glycoprotein, composed of type I, II and III repeating units that are organised into domains for interaction with several ECM components, including collagen I and other fibronectin molecules, as well as cell adhesion receptors (i.e. integrins) (Schwarzbauer and DeSimone, 2011). This way, fibronectin fibrillogenesis influences ECM maintenance and the behaviour of cells which inhabit it. Additionally, the fibronectin mRNA is subject to alternative splicing which may yield at least 20 different isoforms of the protein in humans (Schwarzbauer and DeSimone, 2011).

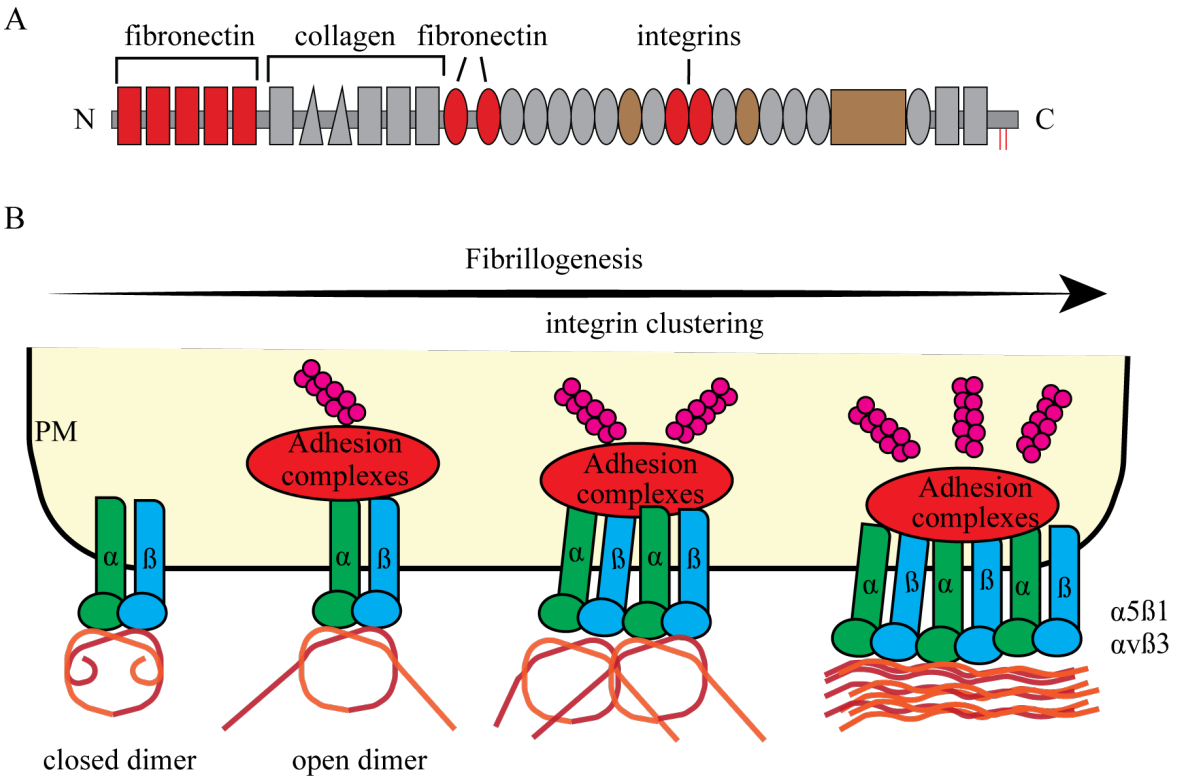

Figure 1-11- Fibronectin domains and fibrillogenesis.
(A) Fibronectin is a modular glycoprotein, composed of type I, II and III repeating units that are organised into domains for interaction with several ECM components, including collagen I and other fibronectin molecules, as well as cell adhesion receptors (i.e. integrins). Fibronectin exists as a dimer, consisting of two fibronectin molecules linked by a pair of disulphide bonds at their C-terminus (red lines). Additionally, the fibronectin mRNA is subject to alternative splicing which may yield at least 20 different isoforms of the protein in humans. Domains required for fibronectin fibrillogenesis are in red. Domains under the control of alternative splicing are in brown. (B) Upon fibronectin secretion, its binding to α5β1 or αvβ3 integrins leads to integrin activation and clustering, which promotes fibrillogenesis in multiple ways. Firstly, it contributes to local accumulation of fibronectin molecules. Secondly, integrins can transmit forces onto the fibronectin dimer and expose residues that are critical for binding to other fibronectin molecules, changing its conformation to one that favours fibrillogenesis. These forces are generated by actomyosin cables and transmitted to integrins via adhesion complexes. Finally, integrins can be translocated along actomyosin cables, stimulating fibrillogenesis by pulling on bound fibronectin.

Upon secretion of the fibronectin dimer, its fibrillogenesis is initiated by integrin binding to the RGD sequence and adjacent synergy site (Schwarzbauer and DeSimone, 2011). Binding of α5β1 (but also αvβ3) integrins to fibronectin leads to integrin activation and receptor clustering (Roca-Cusachs et al., 2009), which promotes fibrillogenesis in multiple ways. Firstly, it contributes to accumulation of fibronectin molecules in the same vicinity. Secondly, integrins can transmit forces onto the fibronectin dimer and expose residues that are critical for binding to other fibronectin molecules, changing its conformation to one that favours fibrillogenesis (Klotzsch et al., 2009). These forces are generated by actomyosin cables and transmitted to integrins via adhesion complexes. Finally, integrins can be translocated along actomyosin cables, stimulating fibrillogenesis by pulling onto bound fibronectin (Clark, 2005).

Nascent fibronectin fibrils are formed through end-to-end association of dimers, via the N-terminal residues that become exposed following the exertion of tension by integrin engagement and the cell's contractile machinery. As the matrix matures, small fibrils can then establish lateral associations, leading to longitudinal and axial growth. During growth, the matrix is irreversibly converted into a deoxycholate-insoluble form, via strong, noncovalent protein-protein interactions (Schwarzbauer and DeSimone, 2011).

1.6.2.3 CAFs are 'masters of ECM remodelling'

The ability of CAFs to deposit substantial levels of fibrillar ECM is owing to a combination of phenotypes that result from their activation. These include the secretion of copious amounts of ECM proteins and proteins involved in ECM remodelling (e.g. MMPs and FAP) and cross-linking (e.g. LOX and LH2), as well as their ability to contract. Their increased contractility is particularly relevant, as it allows CAFs to generate forces during fibrillogenesis and to align those newly-formed fibres in a direction parallel to the actomyosin cytoskeleton (Barbazán and Matic Vignjevic, 2019).

The contractile phenotype of CAFs is the result of the organisation of α-smooth muscle actin (α-SMA) in actomyosin cables and this depends on the activity of the RhoA-ROCK axis (Sanz-Moreno et al., 2011), as well as the translocation and activation of YAP into the nucleus (Calvo et al., 2013). These pathways are often hyperactivated in CAFs, thereby allowing CAFs to contract and deposit ECM. Furthermore, the increased stromal stiffness that results from ECM deposition and cross-linking is in itself a stimulus for RhoA and YAP

signalling (Handorf et al., 2015), highlighting a positive feedback-loop that ensures prolonged fibroblast activation and desmoplasia.

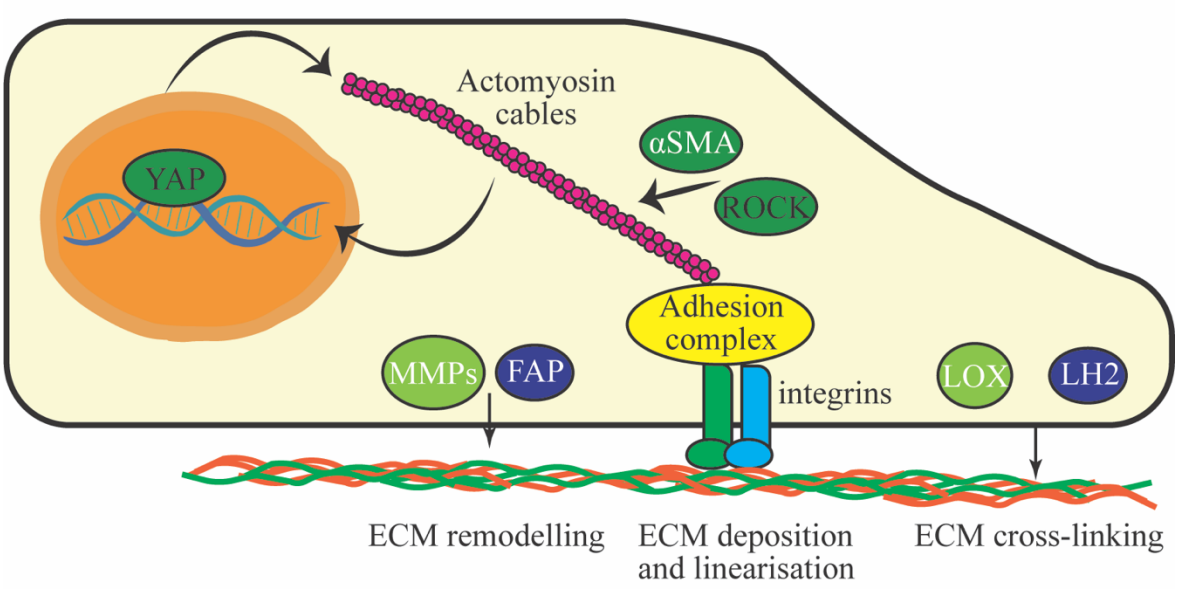

Figure 1-12- Mechanisms by which CAFs deposit/remodel ECM.
The ability of CAFs to deposit substantial levels of fibrillar ECM is owing to a combination of phenotypes that result from their activation. These include the secretion of copious amounts of ECM proteins and proteins involved in ECM remodelling (e.g. MMPs and FAP) and cross-linking (e.g. LOX and LH2), as well as their ability to contract and apply forces to ECM molecules via integrin-mediated adhesions. The contractile phenotype of CAFs is the result of the organisation of α-SMA into actomyosin cables, and this depends on the activity of the RhoA-ROCK axis and YAP. These pathways are often hyperactivated in CAFs, thereby allowing efficient CAF contraction and ECM deposition.

1.6.3 CAFs and cancer

Although a few reports have suggested that certain CAFs may inhibit carcinogenesis (Özdemir et al., 2014), most studies showed that CAFs stimulate tumour growth and progression. The mechanisms that CAFs use to impact on tumour progression are diverse, and are associated with the CAF secretome, as well as their ability to generate forces and deposit ECM.

The secretome of CAFs may affect multiple cell types in the TME, including tumour cells and those of the vasculature and immune system. Indeed, CAF-derived vascular endothelial derived growth factor (VEGF) may stimulate endothelial cells to establish new capillaries, allowing oxygenation of tumours and their growth, and indirectly stimulating immune cell infiltration (Tang et al., 2016). Also, within the CAF secretome, TGFβ, IL-6 and CCL5, to name a few, may modulate the inflammatory state of tumours, often in ways that are permissive to their grow (Cho et al., 2019; Poggi et al., 2014). Furthermore, the CAF secretome may also comprise molecules that directly affect tumour cell behaviour. For example, previous studies indicate that certain growth factors in the CAF secretome, such as

HGF and PDGF, can stimulate tumour cell growth and invasion (Ding et al., 2018; Neri et al., 2017).

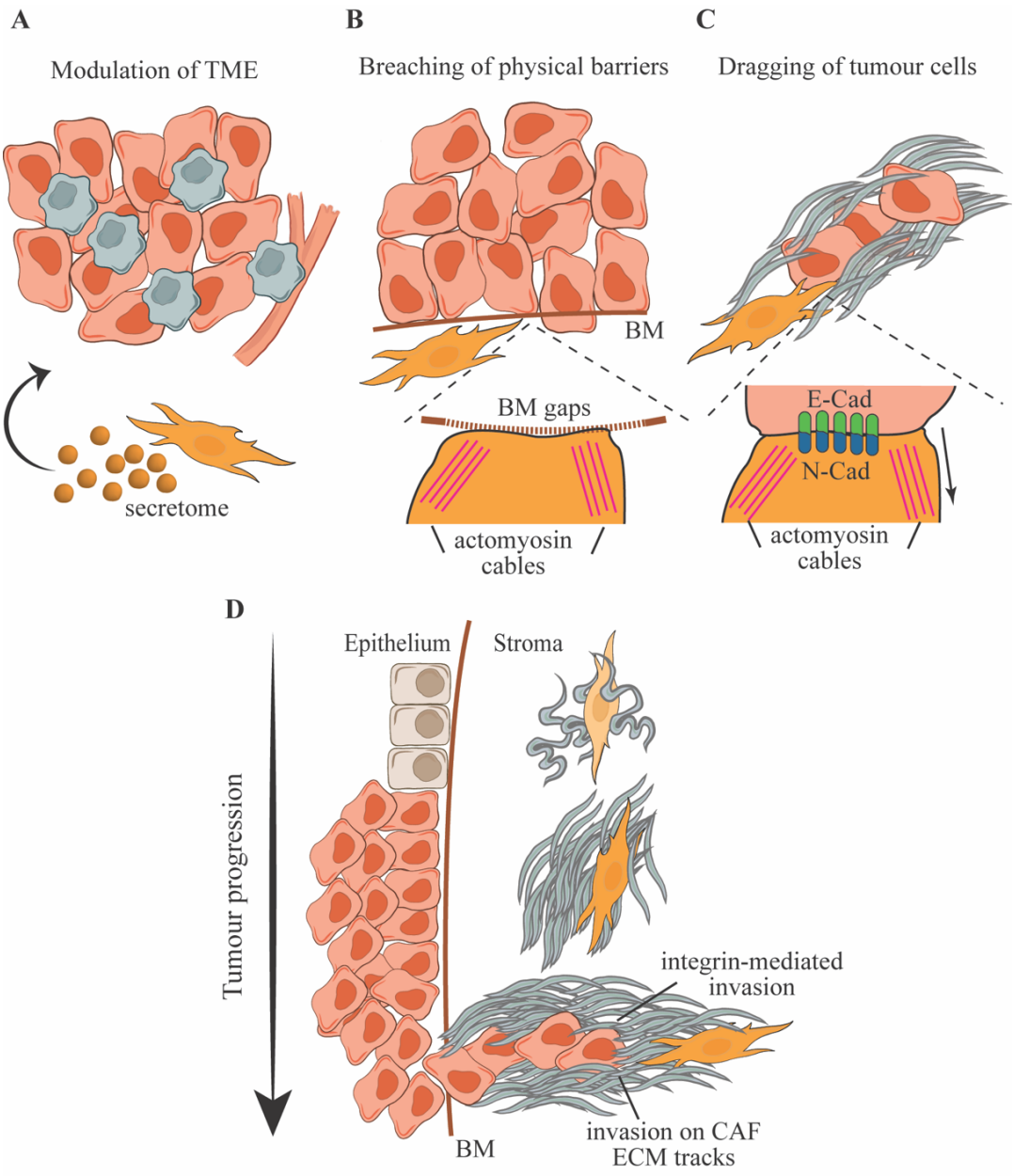

Figure 1-13- CAFs and tumour progression.
The mechanisms that CAFs use to impact on tumour progression are diverse, and are associated with the CAF secretome, as well as their ability to generate forces and deposit ECM. (A) The secretome of CAFs may affect multiple cell types in the TME. Growth factors secreted from CAFs may stimulate endothelial cells to establish new capillaries, allowing oxygenation of tumours and their growth. Cytokines within the CAF secretome may modulate the inflammatory state of tumours, often in ways that are permissive to their growth. The CAF secretome may also comprise molecules that directly affect the behaviour of tumour cells, such as their proliferation and invasion. (B) CAFs may use their contractile phenotype to modify physical barriers for the dissemination of tumour cells, like basement membranes (BM). This involves pulling and softening of the basement membrane, allowing the formation of gaps that tumour cells may use to invade through. (C) CAFs may form heterotypic adhesions with tumour cells and use their contractility to pull on fibres, thereby dragging tumour cells along the ECM and facilitating tumour invasion. (D) The progression of tumours is influenced by desmoplasia. Initial tumour growth is accompanied by activation of fibroblasts, resulting in the deposition of ECM fibres in a direction parallel to the tumour edge. During tumour progression, further ECM is deposited and linearised, contributing to the stiffening of TME. Finally, in areas of tumour cell invasion, ECM fibres organise perpendicularly to the tumour edge. Tumour cells may follow such tracks, pulling on linearised fibres to migrate towards the stroma.

In parallel to the generation of a secretome, CAFs may use their contractile phenotype to modify physical barriers for the dissemination of tumour cells, like basement membranes. This can occur in an MMP-independent manner and involves the pulling and softening of the basement membrane, allowing the formation of gaps that tumour cells may use to invade through (Glentis et al., 2017). Additionally, CAFs may form heterotypic adhesions with tumour cells and use their contractility to pull onto fibres, thereby dragging tumour cells along the ECM and facilitating tumour invasion (Labernadie et al., 2017).

The progression of tumours is influenced by the desmoplastic stroma. In mouse and humans, initial tumour growth is accompanied by activation of fibroblasts, resulting in the deposition of ECM fibres in a direction parallel to the tumour edge (Conklin et al., 2011; Levental et al., 2009). During tumour progression, further ECM is deposited and linearised, contributing to the stiffening of TME. Finally, in areas of tumour cell invasion, ECM fibres organise perpendicularly to the tumour edge (Conklin et al. 2011; Levental et al. 2009). Hypothetically, in vivo, tumour cells may follow such tracks, pulling onto linearised fibres to migrate towards the stroma.

1.7 The pre-metastatic niche

Since the proposal of the ‘seed and soil’ hypothesis by Paget in 1889 it has been thought that certain organs are more receptive to the seeding of metastases than other. Moreover, it is now thought that primary tumours release factors which increase the receptivity of certain organs to metastasis – a so-called ‘pre-metastatic niche’ (PMN). Indeed, tumour-derived factors can influence processes that allow this to occur, including vascular leakiness and the recruitment of immune-suppressive cells to create a tumour-permissive microenvironment (Peinado et al., 2017). Resident fibroblasts in these sites have also been shown to be influenced by signals from the primary tumour in a way that alters ECM dynamics to stimulate PMN formation (Erler et al., 2009).

The first solid piece of evidence supporting the existence of PMNs was provided through transplantation experiments in mice. These researchers observed that the injection of a Lewis lung carcinoma cell line, which would normally only colonise the lung, together with media conditioned by melanoma cells, led to metastasis in organs associated with melanoma dissemination, such as the kidney, spleen and intestine (Kaplan et al., 2005). In addition to this observation which moots the existence of PMNs, it also suggests that metastasis

formation is not a random process. Instead, the organs in which tumour cells colonise and outgrow are pre-determined by tumour-derived factors, supporting the concept of organotropism in metastasis.

Following this seminal study, multiple tumour-specific mechanisms that contribute to priming of the PMN have been identified. It seems that these effects are a combination of various tumour-derived factors, many of which have similar roles in the modulation of the TME. For example, tumour-derived VEGF-A may promote vascular leakiness in both the TME and the PMN (Kaplan et al., 2005; Tang et al., 2016). Cytokines and chemokines such as TGFβ and CCL2, which can be secreted by cells in the TME to stablish an immune-suppressive phenotype, may also modulate the immune composition of the PMN (Qian et al., 2011; Yan et al., 2015). Furthermore, proteins involved in remodelling and cross-linking of the stromal ECM, such as MMPs and LOX respectively, may also mediate metastasis formation by affecting ECM properties in the PMN (Erler et al., 2009; Kaplan et al., 2005).

Another tumour-derived factor that has been extensively associated with the PMN is extracellular vesicles. EVs have been shown to influence many of the aspects that mediate PMN priming, likely reflecting their ability to serve as information carriers in long-distance communication (Wortzel et al., 2019). Importantly, there is also evidence that they are determinants of organotropic metastasis (Hoshino et al., 2015).

1.8 Extracellular vesicles

From bacteria to humans, membrane vesicle release is a conserved process (Margolis and Sadovsky, 2019). Apart from secretory vesicles that are released by specialised cells, including those containing hormone and neurotransmitter cargoes, all cells can release membrane-bounded vesicles, which have been termed EVs. As they can carry a variety of cargoes, EVs can be used by cells as means of intercellular communication. This is observed in both tissue homeostasis and cancer. Cancer, however, hijacks many cellular processes and it can do so via regulation of EV release, including cargo sorting (Rajagopal and Harikumar, 2018). Thus, not only are EVs being considered as cancer biomarkers, increasing evidence suggests that they effect the behaviour of recipient cells. EVs can influence phenotypes in the TME (Li and Nabet, 2019) and, owing to their capacity in transmitting signalling in a long-range manner, it also influences the PMN (Costa-Silva et al., 2015; Hoshino et al., 2015; Peinado et al., 2012), as will be discussed later in this chapter.

1.8.1 EV classes

Despite EVs being highly heterogenous, they can largely be classified into 2 categories - microvesicles and exosomes – according to their origin. Microvesicles are vesicles derived from the outward budding and fission of the plasma membrane. In contrast, exosomes have an endosomal origin. They are intraluminal vesicles (ILVs) that form by the inward membrane budding of maturating multivesicular endosomes (MVE) which are subsequently released to the extracellular milieu by fusion of MVEs with the plasma membrane. Although exosomes are often small, ranging from 50-150 nm in diameter, microvesicles can display a broader range of sizes, from 100 to 1000 nm, which renders the evaluation of EV dimensions insufficient for distinguishing between exosomes and microvesicles (Margolis and Sadovsky, 2019).

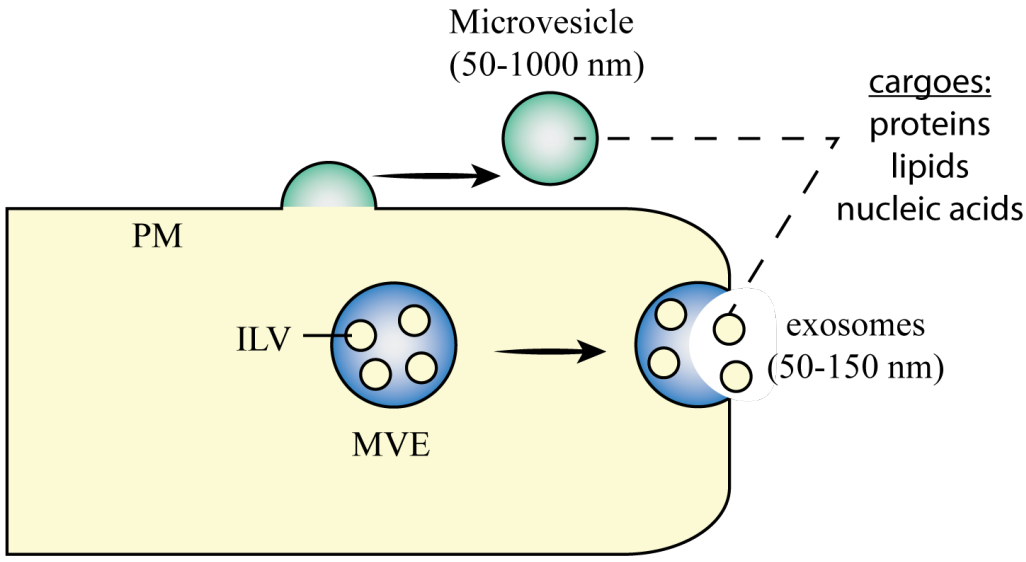

Figure 1-14- EV classes.
EVs are membrane-bound structures released by cells that may encapsulate a variety of cargoes, such as proteins, lipids and nucleic acids, thereby functioning as means for intercellular communication. Despite EVs being highly heterogeneous, they can largely be classified into 2 categories - microvesicles and exosomes – according to their origin. Microvesicles are vesicles derived from the outward budding and fission of the plasma membrane. In contrast, exosomes are intraluminal vesicles (ILVs) that form by the inward membrane budding of maturating multivesicular endosomes (MVE), which are subsequently released to the extracellular milieu by fusion of MVEs with the plasma membrane. Although exosomes are often small, ranging from 50-150 nm in diameter, microvesicles can display a broader range of sizes, from 100 to 1000 nm, which renders the evaluation of EV dimensions insufficient for distinguishing between these classes.

EV composition is likely to be cell type-specific. Both microvesicles and exosomes can encapsulate a multitude of cargoes, including nucleic acids, proteins and lipids. Although the sorting of nucleic acids to EVs is not well understood, microvesicles and exosomes may indeed carry DNA and different types of RNA, including mRNA, microRNAs and other non-coding RNAs, and these are thought to affect the transcriptome of recipient cells (Gusachenko et al., 2013). The lipid composition of EVs is now beginning to emerge, and

exosomes and microvesicles are thought to be enriched for particular lipid species which respectively reflect their endosomal or plasma membrane origin, and there is some evidence that EV-lipids may modulate recipient cell signalling (Garcia et al., 2019; Skotland et al., 2017). Finally, EVs can carry a multitude of protein cargoes with many different molecular functions, thereby having the potential to influence recipient cell post-transcriptionally (Yang et al., 2017).

Owing to their heterogeneity, a large number of protein cargoes of EVs have been identified. Despite microvesicles and exosomes originating from different cellular compartments, many of their protein cargoes overlap, which may reflect common elements to the intracellular mechanisms and sorting machineries that drive their biogenesis (Mathieu et al., 2019). EVs often include membrane organisers of the tetraspanin family, with CD63 as an exosome-specific tetraspannin - according to studies employing the most precise methods for exosome purification, whereas CD9 and CD81 are present in both exosomes and microvesicles (Zhang et al., 2018). EV cargoes can also include components of the ESCRT machinery and members of the Rab family of GTPases which, as will be discussed below, have an important role in EV biogenesis and transport respectively. Both exosomes and microvesicles can contain cell adhesion receptors, such as integrins (Zhang et al., 2018), and some microvesicles have even been shown to be associated with ECM components such as fibronectin (Chanda et al., 2019). Microvesicles are also likely to be enriched for cytosolic material, as well as cytoskeletal proteins, such as actin and tubulin (Zhang et al., 2018).

1.8.2 EV production

EV biogenesis starts with clustering of lipids and membrane-associated proteins in specific microdomains of the plasma membrane, for microvesicles, or of the limiting membrane of MVE for exosomes. These microdomains are also likely to participate in the recruitment of soluble cargoes, such as cytosolic proteins and nucleic acids. Then, membrane rearrangements promote membrane budding and fission at the cell surface for EV release, or at the limiting membrane of MVE for ILV formation (Yáñez-Mó et al., 2015).

1.8.2.1 Exosome production

Biogenesis

The biogenesis of exosomes is fairly well understood and largely depends on the endosomal sorting complexes required for transport (ESCRT) machinery. (Colombo et al., 2013). Subunits of the ESCRT machinery act sequentially to modulate membrane shape and

scission. ESCRT-0 and ESCRT-1 subunits cluster ubiquitinated transmembrane cargoes on microdomains of the limiting MVE membrane. Together with ESCRT-2, they recruit ESCRT-3 to the assembly to execute budding and fission of the microdomain, leading to ILV formation (Colombo et al., 2013; Wollert and Hurley, 2010). This canonical pathway for exosome biogenesis can be influenced by syntenin. Through binding to the cytosolic domain of syndecan-1, syntenin can recruit the ESCRT-accessory protein Alix, which in turn bridge syntenin-associated cargoes to VPS32, a member of the ESCRT-3 subunit (Baietti et al., 2012).

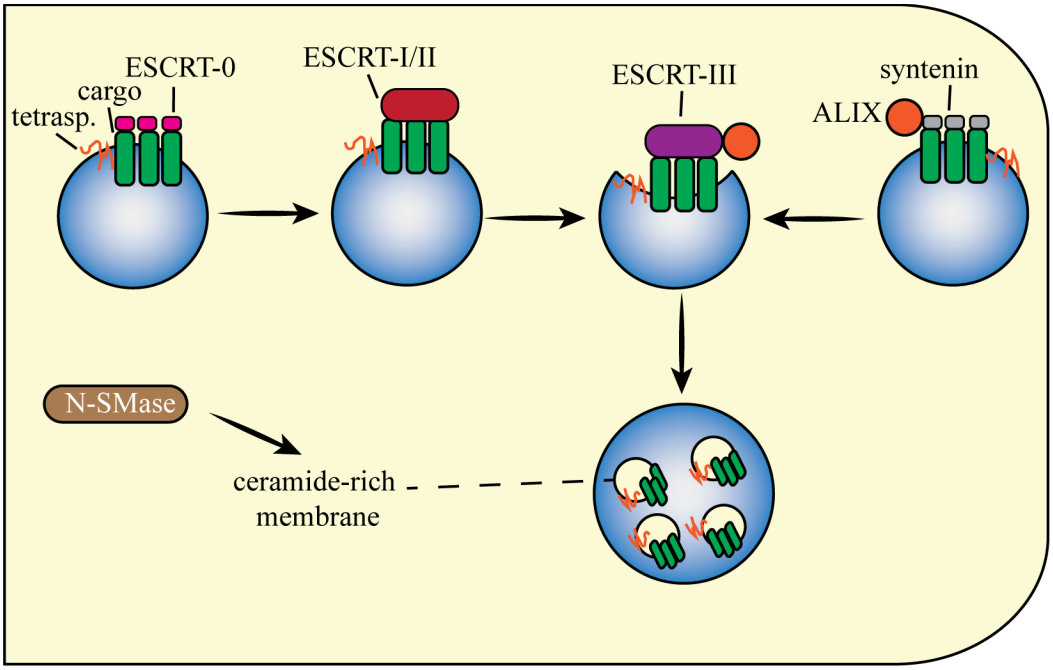

Figure 1-15- Biogenesis of exosomes.
The biogenesis of exosomes mostly occurs through endosomal sorting complexes required for transport (ESCRT)-mediated membrane remodelling and scission. ESCRT-0 and ESCRT-1 subunits cluster ubiquitinated transmembrane cargoes on microdomains of the limiting MVE membrane. Together with ESCRT-2, they recruit ESCRT-3 to the assembly to execute budding and fission of the microdomain, leading to ILV formation. The Syndecan-binding protein, syntenin, may also promote ILV biogenesis, by recruiting the ESCRT-accessory protein, Alix, which in turn bridges syntenin-associated cargoes to VPS32, a member of the ESCRT-3 subunit. The synthesis of ceramide in the limiting membrane of MVE, catalysed by neutral type II sphingomyelinases, was previously shown to promote membrane budding and ILV biogenesis. Proteins of the tetraspanin (tetrasp.) family may also mediate ILV biogenesis, likely by having a structure that induces membrane curvature and contributing to the formation of budding microdomains.

Despite the importance of the ESCRT machinery for ILV formation, other pathways have also shown to influence exosome biogenesis. This is the case for the synthesis of ceramide in the limiting membrane of MVE, catalysed by neutral type II sphingomyelinases, which was previously shown to promote membrane budding and ILV biogenesis (Trajkovic et al., 2008). Proteins of the tetraspanin family may also mediate ILV biogenesis, likely by having a structure that induces membrane curvature (Zimmerman et al., 2016), thus contributing to the formation of budding microdomains. In support of this, loss of CD9 and CD81 was previously shown to modulate the levels of various cargoes in exosomes, and other studies

demonstrated that loss of CD63 has an impact on both cargo sorting and exosome release in various cell types (Margolis and Sadovsky, 2019). Additionally, chaperones such as HSP70 and HSP90 might regulate EV biogenesis, by modulating sorting of cytosolic proteins to budding microdomains of the MVE limiting membrane (Lancaster and Febbraio, 2005; Lauwers et al., 2018).

Avoiding degradation

As MVEs are classically fated for lysosomal degradation, mechanisms that prevent this outcome are likely in place in MVEs destined for secretion. This is in line with previous studies showing that the inhibition of endosome acidification is a trigger for EV release, presumably by re-routing MVE to the plasma membrane (Villarroya-Beltri et al., 2016). While this aspect of exosome biogenesis is still a mystery, an attractive hypothesis in the field is that ESCRT-dependent mechanisms of cargo sorting lead to MVEs that can follow either route, while ESCRT-independent cargo sorting is exclusive for those that will produce exosomes (van Niel et al., 2018). Consistent with this hypothesis, syntenin function seems to be restricted to MVEs that result in exosomes. Furthermore, overexpression of tetraspanin-6, which recruits and physically interacts with syntenin in MVE, impairs lysosomal function whilst upregulating exosome release (Guix et al., 2017). This is also supported by observations that the level of ubiquitination of certain cargoes, which might influence their affinity to ESCRT-0 and -1 complexes, dictated whether they were degraded or released in exosomes (Buschow et al., 2009).

The endosomal and autophagy pathways can also converge, due to fusion of MVEs with the autophagosome. There are many reports in which modulation of autophagy has been shown to influence EV release. For example, caveolin has an inhibitory role on autophagosome formation, whereas modulation of caveolin function by prion protein (PrP) potentiates EV release (Dias et al., 2016). Thus, exosome production is likely to be influenced by levels of autophagy in cells.

Transport

Once matured, the transport of MVEs towards the lysosome for degradation, or the plasma membrane for exosome release, occurs through engagement of MVEs with microtubules and associated motor proteins. As membrane trafficking events, these processes are regulated by members of the Rab family of small GTPases. Trafficking of MVE to the lysosome is mediated by Rab7 and its associated effectors, and this is mediated through retrograde transport on microtubules (Guerra and Bucci, 2016). In contrast, targeting to the plasma

membrane for exosome release is mediated by Rab27a and Rab27b and their effector proteins synaptogmin-like protein 4 and exophilin 5 respectively. Rab27b acts on the antegrade transport of MVB and both Rab27s mediate the docking of MVE to the plasma membrane (Ostrowski et al., 2010).

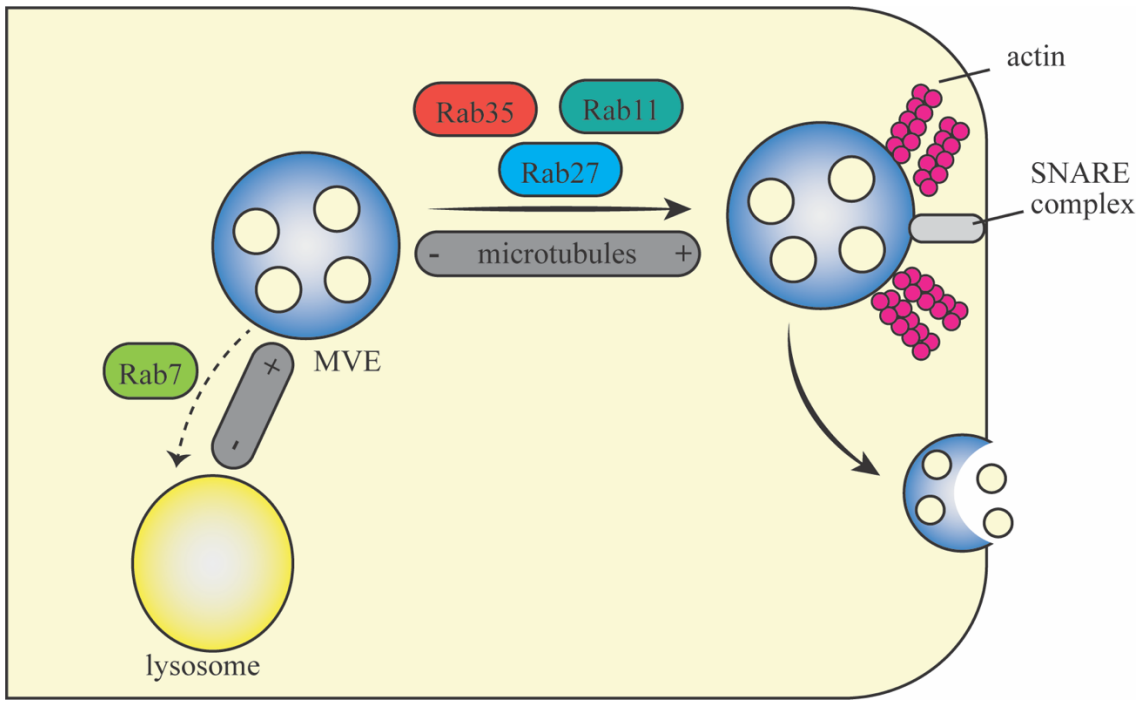

Figure 1-16- Transport of MVE and exosome release.
The transport of MVEs towards the lysosome for degradation, or the plasma membrane for exosome release, occurs through engagement of MVEs with microtubules and associated motor proteins. As membrane trafficking events, these processes are regulated by members of the Rab family of small GTPases. Trafficking of MVEs to the lysosome is mediated by Rab7 and occurs through retrograde transport on microtubules. For exosome release, anterograde transport of MVEs to the plasma membrane and their subsequent docking at this site is largely mediated by Rab27a and Rab27b and, to a lesser extent, Rab11 and Rab35. The final step in exosome production is the fusion of the limiting MVE membrane with the plasma membrane, leading to exosome release. This process is mediated by the SNARE machinery and is likely to also involve rearrangements in the actin cytoskeleton.

Although several studies have demonstrated that Rab27a and Rab27b are required for exosome production, the GTPases are not ubiquitously expressed, which may indicate that other GTPases mediate MVE trafficking to the plasma membrane. Indeed, while their mechanisms of actions are not clear, other Rab family members, such as Rab35 and Rab11, have previously been shown to mediate transport and docking of MVE to the plasma membrane in some cell types (Hsu et al., 2010; Koles et al., 2012; Messenger et al., 2018).

Release

The final step in exosome production is the fusion of the limiting MVE membrane with the plasma membrane, with concomitant exosome release. As a membrane fusion event, this process is mediated by SNARE and synaptotagmin family members, and actin. A SNARE

complex known to be involved in the exocytosis of conventional lysosomes includes VAMP7, syntaxin7 and synaptotagmin7, and exosome release in some cell lines has been shown to be dependent on these proteins (Fader et al., 2009). However, some studies have provided evidence for exosome release being independent of these proteins in other cell types (Proux-Gillardeaux et al., 2007), which is a reason to believe that other SNARE proteins might participate in this fusion event. The SNARE protein SNAP23, for example, has been shown to mediate exosome release in a number of human tumour cell lines (Wei et al., 2017). In humans and C. elegans, exosome release can be modulated by the SNARE proteins syntaxin-1 and syntaxin-5 respectively (Hyenne et al., 2015; Koles and Budnik, 2012). Thus, this aspect of exosome release is complex, and different SNARE and SNARE-associated proteins execute this process depending on the cell type and biologic context.

1.8.2.2 Microvesicle production

Biogenesis

The machinery responsible for microvesicle biogenesis has only recently started to be revealed. Microvesicle biogenesis seems to comprise rearrangements of lipid and protein elements within the plasma membrane, as well as modulation of local Ca^{2+} levels (Minciacchi et al., 2015). Ca^{2+} within those domains activates Ca^{2+}- dependent enzymatic machineries, including aminophospholipid translocases and scramblases that drive translocation of phosphatidylserine and phosphatidylethanolamine from the inner to the outer leaflet of the plasma membrane (Al-Nedawi et al., 2008). Such phospholipid translocation may lead to bending of the membrane and subsequent association with the actomyosin cytoskeleton, leading to membrane budding and microvesicle biogenesis (Al-Nedawi et al., 2008). Accordingly, the actomyosin regulators RhoA and ROCK have been shown to stimulate microvesicle biogenesis in tumour cells (Li et al., 2012). Furthermore, cholesterol is often abundant in microvesicles, and there is some evidence that it might promote microvesicle biogenesis, by inducing lipid raft formation (Pollet et al., 2018).

Release

Upon formation, the release of microvesicles is completed by their fission from the plasma membrane. This step is also likely to involve the actomyosin cytoskeleton, as modulation of the actin regulators Arf6, Arf1 and cdc42 have been shown to influence the fission of microvesicles from the plasma membrane (Antonyak et al., 2012; Muralidharan-Chari et al., 2009; Schlienger et al., 2014). Additionally, some of the factors that mediate exosome biogenesis have also been shown to modulate fission of microvesicles. For instance, a rise

in levels of ceramide, mediated by acidic sphingomyelinases, can promote membrane bending and microvesicle release from glial cells (Bianco et al., 2009). Likewise, the ESCRT-I complex members TSG101 and ESCRT-III associated protein VPS4 have been reported to be required for the release of certain EVs (Nabhan et al., 2012), and the MVE-to-plasma membrane trafficking regulators Rab27a and Rab27b have been shown to mediate shedding of EVs from the plasma membrane (van Niel et al., 2018). Thus, modulation of these pathways is likely to affect the biogenesis and/or release of both microvesicles and exosomes.

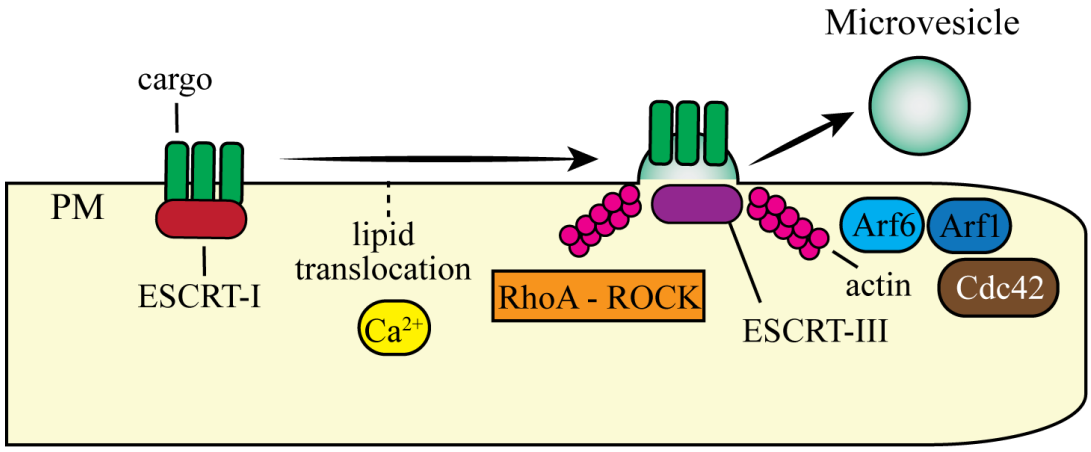

Figure 1-17- Microvesicle production.
EV biogenesis starts with clustering of lipids and membrane-associated proteins in specific microdomains of the plasma membrane, as well as modulation of local Ca^{2+} levels. Ca^{2+} within those domains activates aminophospholipid translocases and scramblases that drive translocation of phosphatidylserine and phosphatidylethanolamine from the inner to the outer leaflet of the plasma membrane, leading to membrane bending and subsequent association with the actomyosin cytoskeleton, in a RhoA-ROCK-dependent manner. The release of microvesicles is completed by their fission from the plasma membrane. This step is also likely to require engagement with the actomyosin cytoskeleton, as modulation of the actin regulators Arf6, Arf1 and cdc42 were shown to influence the fission of microvesicles from the plasma membrane. In certain cell types, a rise in levels of ceramide, mediated by acidic sphingomyelinases, can promote membrane bending and microvesicle release. Likewise, the ESCRT-I complex members, TSG101 and ESCRT-III associated protein VPS4 have been reported to be required for the release of certain microvesicles.

1.8.3 EVs and recipient cells

Once in the extracellular milieu, EVs may come into contact with recipient cells. The intercellular communication mediated by EVs is likely to require their docking with the plasma membrane of recipient cells. An important aspect to consider is that EVs may dock to the plasma membrane of other cells, as well as of the cell that released them. This way, EVs can modulate both paracrine and autocrine signalling (Matsumoto et al., 2017). The docking of EVs to recipient cells seems to occur through interaction between molecules at the EV surface with those on the cell surface. There is evidence for some degree of specificity to the docking of EVs with recipient cells, and a number of factors have been shown to mediate, and to define the specificity of, these interactions.

The best understood mechanisms for EV docking involve interactions with integrins on the EV surface. EV-associated integrins can bind to adhesion molecules on recipient cells, such as intercellular adhesion molecules (ICAMs), thereby favouring their docking (Morelli, 2004). As will be discussed later in this chapter, experiments in mice have demonstrated that different integrin heterodimers on EVs can modulate their accumulation in specific organs, further reinforcing the hypothesis that EV-associated adhesion molecules play a role in the binding and recognition of EVs by recipient cells (Hoshino et al., 2015). Additionally, the interaction of integrins on both EV and recipient cell membrane with fibronectin in the ECM may also mediate this process, with ECM favouring their docking by retaining EVs in close proximity to the cell (Purushothaman et al., 2016). Furthermore, EV-associated tetraspannins have also been shown to mediate docking and uptake of EVs to recipient cells (Nazarenko et al., 2010), possibly by interacting with integrins in tetraspannin-enriched microdomains.

Docking of EVs to recipient cells is also likely to depend on their lipid composition. In this context, the level of phosphatidylserine in EVs can determine the amount of specific lipid-binding proteins in EVs, including galectin 5, a lectin that can induce EV docking to macrophages (Barres et al., 2010). As galectins have been identified in EVs from cancer cell lines (Klibi et al., 2009), it is interesting to speculate whether these mechanisms are in place for uptake of EVs released by cancer cells.

Upon docking to recipient cells, EVs may transmit information by acting at the cell surface, without transferring their content. This mechanism is particularly relevant for immune-cell modulation, as EVs may contain major histocompatibility complex peptides that can bind to T-cell receptors on the surface of T-lymphocytes (Admyre et al., 2003; Testa et al., 2010). For EVs that transfer their content to cells, this can occur via EV fusion with the plasma membrane, through a mechanism that is largely unknown, or via EV internalisation.

For EVs that are internalised, several well-described pathways were shown to facilitate this, including clathrin-dependent endocytosis (i.e. receptor-mediated endocytosis), endocytosis mediated by caveolae and lipid rafts, micropinocytosis and even phagocytosis by cells such as macrophages and monocytes. Although the factors that dictate which internalisation pathway is used remain elusive, studies suggest that EV size and composition might play a role in this (van Niel et al., 2018). Furthermore, perhaps more pertinent for the context of this work, EV uptake in certain fibroblasts was previously shown to occur through clathrin-dependent endocytosis and to be influenced by the formation of filopodia, which stimulated

the movement of single EVs toward sites of the plasma membrane where endocytosis occurs (Heusermann et al., 2016)

Internalised EVs may then follow an endocytic pathway and reach MVE in recipient cells. Once in the MVE, they may be degraded by fusion of this compartment with lysosomes, transported to the plasma membrane for re-release or, in some cases, these ILV have been suggested to fuse with the MVE's limiting membrane (termed 'back-fusion') and release their content in the cytoplasm (Tian et al., 2014). The latter is particularly significant for the intercellular delivery of nucleic acids or cytosolic components, if they are to modulate responses in recipient cells. However, the mechanisms controlling back-fusion have not yet been elucidated.

1.8.4 EVs as cancer biomarkers

There is substantial interest in exploiting EVs as cancer biomarkers. This is based on the fact that tumour-derived EVs can be purified from body fluids, such as blood and urine, and the premise that EV cargoes may reflect the composition of the donor cell.

Among the first studies that explored the utility of EVs as tumour biomarkers was the comparison of the composition of glioblastoma-EVs with those of their normal counterparts. These researchers demonstrated that EVs in the serum of glioblastoma patients contained glioblastoma-associated RNA and proteins (Skog et al., 2008). Subsequently, several reports validated these observations in multiple cancer types, by showing that EVs encapsulate cargoes that reflect the cell of origin (Kloecker et al., 2008; Soldevilla et al., 2014). Furthermore, other studies suggested that EV composition might be informative of patient prognosis in a variety of cancer types, including pancreatic and non-small cell lung cancer (Vader et al., 2014). Therefore, the correlation between EV and cell composition might be valuable for the detection and monitoring of tumours.

Early detection of cancer greatly impacts the chances for successful therapy. This is especially important for many deadly types of cancer, such as pancreatic adenocarcinoma, which are often 'silent' and may form metastasis before the patient develops symptoms. In this context, there is some evidence indicating that tumour-derived EVs may be detected in the blood stream of tumour-bearing mice prior to the tumour being fully formed (Sharma et al., 2017). However, markers that enable cancer-specific EVs to be discriminated from their

normal counterparts are still lacking which has, so far, precluded the use of EVs as early detection markers for cancer.

1.8.5 Tumour-EVs and the tumour microenvironment

As mediators of intercellular communication, it is likely that EVs from different cell types contribute to the many interactions that occur in the TME, thereby potentially shaping the way tumours grow and progress. There are, indeed, many reports in the literature that are consistent with this hypothesis. Bellow, we focus on a few examples regarding tumour-EVs.

Increasing evidence suggests that tumour-EVs may influence the behaviour of other tumour cells. For example, certain tumour-EVs have previously been shown to carry oncogenic proteins, such as EGFRvIII, to generate a transformed phenotype in recipient cells(Al-Nedawi et al., 2008). Similarly, a few studies have shown that EVs released from aggressive tumour cell lines can induce migratory phenotypes in recipient cells *in vitro*, and a study using a co-transplantation mouse model has confirmed that this type of communication can also occur in vivo (Rahman et al., 2016; Zomer et al., 2015). However, in the context of tumour-EV-induced migration, the mechanisms by which EVs may stimulate such phenotypes are not yet clear.

Tumour-EVs may also affect the behaviour of non-tumour cells in the TME, such as endothelial cells. EVs released from tumour cells overexpressing EGFR, for example, have previously been shown to transfer the receptor to recipient endothelial cells, leading to VEGF upregulation and angiogenesis (Al-Nedawi et al., 2009).

Tumour cell-EVs may also directly interact with immune cells to stimulate the formation of a tumour-permissive microenvironment. Numerous reports have demonstrated that EVs released by tumour cells can modulate the polarisation of macrophages to a tumour-permissive state (Cooks et al., 2018; Sun et al., 2019). Additionally, a recent study has demonstrated that EVs from metastatic melanoma may carry PD-L1 on their surface, directly suppressing the activity of $CD8^+$ T cells (Chen et al., 2018)

There is also evidence for fibroblasts being affected by tumour-EVs. For instance, tumour-EVs may stimulate activation of fibroblasts into CAFs by transferring activating factors, such as TGF-β and certain miRNAs (Baroni et al., 2016; Ringuette Goulet et al., 2018).

1.8.6 Tumour-EVs and the pre-metastatic niche

Over the last few years, it has become clear that EVs are key players in orchestrating the formation of PMNs. As previously mentioned, an early event in the formation of the PMN is acquisition of vascular leakiness. Indeed, previous reports showed that injection of tumour cell-EVs in mice is sufficient to induce vascular leakiness in PMNs (Hoshino et al., 2015; Peinado et al., 2012). Several in vitro studies have demonstrated that tumour-EVs may disrupt endothelial cell junctions, and this often involves transfer of certain EV cargoes, such as VEGFA and specific miRNAs (Di Modica et al., 2017; Treps et al., 2017).

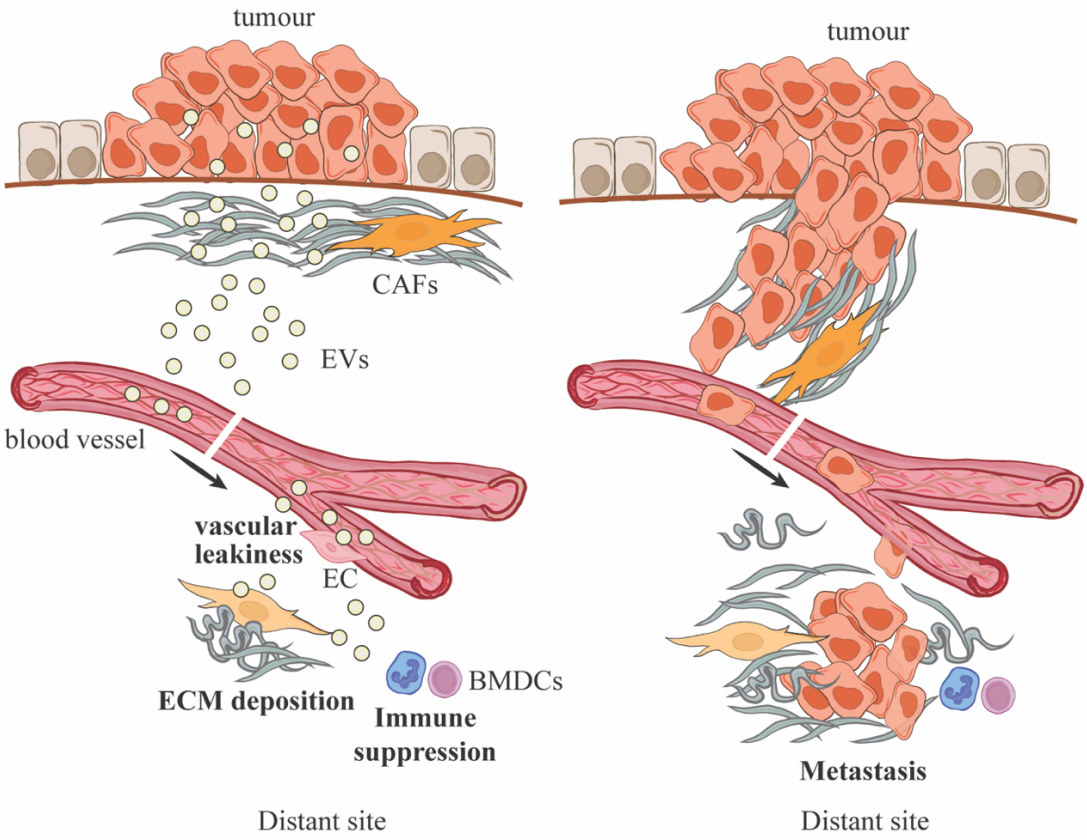

Figure 1-18- The priming of pre-metastatic niches occurs in a multistep process.
Primary tumours release factors that prime the receptivity of certain organs to metastasis – a so-called 'pre-metastatic niche' (PMN). Given that tumour-EVs may travel the circulation and affect the behaviour of cells in distant organs, they have been implicated in the establishment of PMNs. An early event in the formation of PMNs is acquisition of vascular leakiness and evidence suggest that EVs may lead to this by transferring certain growth factors and miRNAs that disrupt endothelial cell junctions. Another event in the PMN is the "education" of resident fibroblasts and modulation of ECM deposition and/or remodelling. Tumour EVs may also modulate the behaviour of resident fibroblasts in the PMN, as well as the characteristics of the ECM deposited by these cells. Finally, formation of the PMN involves recruitment of immune cells and establishment of an immune-suppressive microenvironment, and tumour-cell EVs have been shown to stimulate this by promoting the infiltration of bone marrow-derived cells (BMDCs), in part through modulating ECM deposition in distant organs.

Formation of the PMN involves recruitment of immune cells and establishment of an immune-suppressive microenvironment, and tumour-cell EVs may modulate this process. When injected into mice, EVs from highly metastatic tumour cells have been shown to

stimulate recruitment of BMDCs to both the lung and the liver PMNs, possibly leading to impairment of anti-tumour immunity (Costa-Silva et al., 2015; Hoshino et al., 2015; Peinado et al., 2012). Additionally, tumour EVs have been shown to mediate expression of TLR3 in the lung epithelium, which led to recruitment of neutrophils to the lung and PMN formation (Liu et al., 2016). Conversely, EVs released from poorly metastatic tumour cells promoted the recruitment of tumour-reactive macrophages, leading to reduced metastasis (Plebanek et al., 2017) Thus, it seems that EVs from multiple cancer types can modulate immune responses in the PMN, and that the ability of EVs to promote immune suppression may depend on the metastatic capacity of the donor cell.

A common event in the PMN is the "education" of resident cells, such as fibroblasts, and modulation of ECM deposition and/or remodelling. Tumour EVs may also modulate the behaviour of resident fibroblasts in the PMN, as well as the characteristics of ECM deposited by these cells. For instance, injection of tumour cell-EVs in mice induced fibronectin deposition in both the liver and lung PMN. In the liver, pancreatic cancer EVs that are positive for migration inhibitory factor (MIF) stimulated TGF-β secretion by Kupffer cells, leading to fibronectin deposition by neighbouring stellate cells (Costa-Silva et al., 2015). In the lung, breast cancer EVs promoted fibroblast activation and fibronectin deposition (Hoshino et al., 2015). Importantly, immune-suppressive BMDCs were found in association with these fibronectin-rich regions, indicating that ECM deposition and/or remodelling may contribute to the priming of PMNs (Costa-Silva et al., 2015; Hoshino et al., 2015).

Finally, there is also evidence that EVs play a key role in the organotropism of metastasis. As previously discussed in this chapter, adhesion molecules at the EV surface, such as integrins, may be involved in specific docking of EVs to recipient cells. Consistently, the expression of different integrin heterodimers at the surface of EVs has been shown to dictate to which organs they are targeted. In particular, α6β4 and α6β1 integrins were enriched in EVs that accumulated in the lung, while αvβ5 integrin was upregulated in EVs that end up in the liver. The pattern of internalisation of these EVs mirrored the organotropism of the donor cells, indicating that EV-associated integrins play a role in organotropic metastasis, by determining where in the body the PMN is formed (Hoshino et al., 2015).

1.9 PhD objectives

The investigation of mechanisms that drive carcinogenesis has contributed immensely to the improvement of survival in cancer patients. Still, for many cancer types the prognosis is poor and the main cause of cancer-related death is metastasis. In addition to cell-autonomous phenomena, such as the ability of cancer cells to invade the ECM, metastasis is known to be driven by non-cell autonomous mechanisms. Of the several diffusible factors that cancer cells release, EVs can drive many of the processes that contribute to metastasis formation. Not only are EVs able to transmit information between different cell types in the TME, they have the capacity to travel bloodstream as carriers of information between distant sites, and sometimes affect processes such as ECM remodelling and immune composition, thereby being involved in the priming of metastatic niches. Thus, deciphering how EVs contribute to metastasis might lead to improvement in therapy and might inform for biomarkers of metastatic disease.

In addition to playing a clear role in bypassing mechanisms of tumour suppression, many oncogenes (including mutp53s) also contribute to metastasis formation. Of the many mutp53-binding partners, its association with p63 is particularly relevant in the acquisition of invasive traits and this is, in part, achieved through deregulation of membrane trafficking processes. EVs are classically known to depend on membrane trafficking processes for their production, and this might be indicative of a possible role for mutp53 in influencing EV production and/or function. The objective of this thesis is therefore to investigate whether expression of mutp53 in cancer cells influences EV release, composition and function, with a particular interest in understanding whether EVs from mutp53-expressing cells influence non-cell autonomous processes and/or inter-organ communication in a way that might promote metastasis.

Chapter 2 Materials and methods

2.1 Materials

2.1.1 Reagents

Reagent	Supplier
0.45 µm filter	Gilson
2 % gelatin	Sigma
27-gauge needle	Becton Dickinson
4.8 µm silica microsphere	Bang Labs
96 well PCR plate	Bio-Rad
Acetonitrile	Sigma
AFM probe	Nanoworld
Agarose	Melford Laboratories
All blue protein standard	Bio-Rad
Ampicillin	Sigma
Apo-transferrin	Sigma
Ascorbic acid	Sigma
ATP	Sigma
BSA	First Link
BsmBI enzyme	NEB
$CaCl_2$	Sigma
Cell lifter	Corning
Citric acid	Sigma
Dialysed FBS	Life Technologies
DMEM	Thermo Fisher
DNA dilution buffer	NEB
DNaseI	Roche
DTT	Melford Laboratories
Dynabeads (anti-mouse)	Life Technologies
Dynabeads (streptavidin)	Life Technologies
EDTA	Sigma
EGF	Life Technologies
EGTA	Sigma
F12 ham medium	Sigma
FBS	PAA
Filtered FBS	Thermo Fisher
Formic acid	Sigma
Formvar carbon coated EM grids	Polysciences
Glucose	Sigma
Glutamine	Life Technologies
Glutaraldehyde	Sigma
Glycine	Sigma

Heavy arginine (10)	Cambridge Isotope Labs
Heavy lysine (8)	Cambridge Isotope Labs
HEPES	Life Technologies
Hydrocortisone	Sigma
Hydrogen peroxide	Sigma
IAA	Sigma
Igepal CA-630	Fluka
Insulin ActRApid	Life Technologies
Iodoacetamide	Sigma
KCl	Sigma
Lipofectamine RNAiMAX	Thermo Fisher
Low melting point agarose	Sigma
M199 medium	Sigma
Medium arginine (6)	Cambridge Isotope Labs
Medium lysine (4)	Cambridge Isotope Labs
MEM vitamins	Life Technologies
MesNa	Fluka
Methyl cellulose	Sigma
Milk powder	Marvel
Na_2CO_3	Thermo Fisher
Na_2HPO_4	Sigma
Na_3VO_4	Thermo Fisher
NaCl	Thermo Fisher
NaF	Sigma
NEBuffer 3.1	NEB
NH_4OH	Sigma
Nunc MaxiSorp plates	Thermo Fisher
NuPage MOPS running buffer	Life Technologies
NuPAGE pre-cast gel (4-12 %)	Life Technologies
NuPage sample buffer	Life Technologies
NuPage transfer buffer	Merck
Ortho-phenylenediamine	Sigma
Ortho-phosphorylethanolamine	Sigma
PBS	Thermo Fisher
PBS with calcium and magnesium	Sigma
Penicillin/streptomycin	Life Technologies
Pentobarbital	Sigma
PerfeCTa SYBR green master mix	Quantabio
PFA	EMS
Polybrene	Sigma
Primaquine	Sigma
Puromycin	Sigma
PVDF membrane	Merck
S.O.C medium	Thermo Fisher

SDS	Thermo Fisher
SILAC DMEM	Lonza
Stbl3 competent cells	Thermo Fisher
Streptavidin-HRP	GE Healthcare
Sucrose	Sigma
Sulfo-NHS-SS-biotin	Thermo Fisher
T4 DNA ligase	NEB
T4 DNA ligation buffer	NEB
T4 polynucleotide kinase	NEB
T4 polynucleotide kinase reaction buffer	NEB
Thinwall Polypropylene Tube (38.5 mL)	Beckman
Tissue culture dishes (10 and 15 cm^2)	BD Biosciences
Tissue culture plate (6 well)	Corning
Tri-iodotyronine	Sigma
Tris HCl	Melford Laboratories
Triton-X100	Sigma
Trypsin	Life Technologies
Tween-20	Sigma
Uranyl oxalate	Thermo Fisher
Urea	Sigma
Vectashield (soft set with DAPI)	Vector Labs

Table 2-1- Reagents and suppliers.

2.1.2 Solutions

Solution	Components
1% SDS lysis buffer	1% SDS (v/v), 50 mM Tris-HCl pH7.0, 0.1 M DTT
2x HBS	274 mM NaCl, 10 mM KCl, 1.4 mM Na_2HPO_4, 15 mM glucose, 42 mM HEPES, pH6.8
Antibody coating buffer	0.05 M Na_2CO_3, pH9.6
CDM extraction buffer	10 mM NH_4OH, 0.5 % Triton-X100 (v/v) in PBS with calcium and magnesium
ELISA developing buffer	0.56 mg/mL ortho-phenylenediamine, 25.4 mM Na_2HPO_4, 12.3 mM citric acid, pH5.4 with 0.003% H_2O_2
LB Broth	85mM NaCl, 1% bacto-trypton (w/v), 0.5% yeast extract (w/v)
Non-denaturing lysis buffer	50 mM Tris-HCl pH7.0, 150 mM NaCl, 10 mM NaF, 1 mM Na_3VO_4, 5 mM EDTA, 5 mM EGTA, 1.5 % Triton-X100 (v/v), 0.75 % Igepal CA-630 (v/v)
PBS-T	PBS, 0.1 % Tween-20 (v/v)
TBS-T	10 mM Tris-HCl pH7.4, 150 mM NaCl, 0.1 % Tween-20 (v/v)

Table 2-2- Solutions and their components.

2.1.3 Kits

Kit	Supplier
Amaxa Nucleofector Kit V	Lonza
QIAquick Gel Extraction Kit	QIAGEN
QIAshredder columns	QIAGEN
Reverse Transcription system	Promega
RNAeasy spin columns	QIAGEN

Table 2-3- Kits and suppliers.

2.1.4 Primers

Primer	Product, supplier, catalogue number/sequence
GAPDH	QuantiTect, QIAGEN, QT00273322
LKO.1 forward	5'-GACTATCATATGCTTACCGT-3'
Podocalyxin	QuantiTect, QIAGEN, QT00005138

Table 2-4- Primers.

2.1.5 siRNA

Target	Product, supplier, catalogue number/sequence
DGKα	ON-TARGET, Dharmacon, L-006711-00-0020
α3 Integrin	ON-TARGET, Dharmacon, L-004571-00-0010
p53	5'-GACUCCAGUGGUAAUCUACUU-3'
p63	5'-UGAACAGCAUGAACAAGCUTT-3'
Podocalyxin	ON-TARGET, Dharmacon, L-010617-00-0020
Rab27a	ON-TARGET, Dharmacon, L-004667-00-0010
Rab27b	ON-TARGET, Dharmacon, L-004228-00-0010
Rab35	ON-TARGET, Dharmacon, L-009781-00-0020
Rab35	ON-TARGET, Dharmacon, J-009781-05-0010
RCP	ON-TARGET, Dharmacon, L-015968-00-0020

Table 2-5- siRNAs.

2.1.6 Plasmids

Plasmid	Supplier
GFP-Rab35	Addgene
lentiCRISPR vector	Addgene
podocalyxin-GFP	Echard lab
podocalyxin$^{V486A/Y500A}$-GFP	Echard lab
psPAX2 packaging plasmid	Addgene
VSV-G plasmid	Addgene

Table 2-6- Plasmids and suppliers.

2.1.7 Antibodies

Antibody	Species	Application and dilution	Supplier
Actin	Rabbit	WB - 1:3000	Sigma
Alexa-fluor 488 anti-mouse	Goat	IF - 1:400	Life Technologies
Alexa-fluor 555 anti-mouse	Goat	IF - 1:400	Life Technologies
CD63	Mouse	WB - 1:1000; IF - 1:200; IEM - 1:200	Pelicluster
CD9	Rabbit	WB - 1:10000	Abcam
cMET	Goat	ELISA - 5 µg/mL	R&D Systems
DGKα	Rabbit	WB - 1:500	Protein Tech
Fibronectin	Mouse	IF - 1:100	BD Pharmingen
GFP	Rabbit	WB - 1:1000	Abcam
HSPA8	Rabbit	WB - 1:1000	Cell Signalling
α3 Integrin	Rabbit	WB - 1:1000	Abcam
β1 Integrin	Mouse	WB - 1:2000	BD Pharmingen
α5 Integrin	Mouse	ELISA - 5 µg/mL	BD Pharmingen
IRDye 680CW anti-mouse	Donkey	WB - 1:20000	LI-COR
IRDye 680CW anti-rabbit	Donkey	WB - 1:20000	LI-COR
IRDye 800CW anti-mouse	Goat	WB - 1:20000	LI-COR
IRDye 800CW anti-rabbit	Goat	WB - 1:20000	LI-COR
mouse IgG	Rabbit	IEM - 1:200	Pierce
p21	Rabbit	WB - 1:1000	Cell Signalling
p53	Mouse	WB - 1:10000	In-house antibody
p63	Rabbit	WB - 1:1000	Abcam
Paxillin	Mouse	IF - 1:100	BD Pharmingen
PODXL	Rabbit	WB - 1:1000	Abcam
Rab27	Mouse	WB - 1:1000	Abcam
RCP	Rabbit	WB - 1:1000	in-house
Tnf Receptor	Mouse	ELISA - 5 µg/mL	BD Pharmingen
TSG101	Mouse	WB - 1:1000	GeneTex

Table 2-7- Antibodies.

2.2 Methods

2.2.1 Mouse models of cancer

2.2.1.1 Autochthonous mouse model

$KP^{172}C$ (Pdx1-Cre, $Kras^{G12D/+}$, $p53^{R172H/+}$), $KP^{270}C$ (Pdx1-Cre, $Kras^{G12D/+}$, $p53^{R270H/+}$), $KP^{fl}C$ (Pdx1-Cre, $Kras^{G12D/+}$, $p53^{fl/+}$) and KC (Pdx1-Cre, $Kras^{G12D/+}$) mice of mixed FVB/Bl6 background are as previously described (Hingorani et al., 2005; Morton et al., 2010). At approximately 12 weeks of age, when metastases were not apparent, mice were culled and liver and lung ECM was visualised *ex vivo,* as described in 2.2.1.3 (bellow). Tumour growth was assessed by gross pathology and confirmed by histology. All animal experiments were performed under UK Home Office licence and approved by the University of Glasgow Animal Welfare and Ethical Review Board.

2.2.1.2 Xenograft mouse model

For xenograft experiments, 1×10^6 H1299 cells were subcutaneously injected into 8-week-female CD1 nude mice. Subcutaneous tumours were measured by callipers three times a week until they reached a size endpoint of 8 mm in diameter. Mice were culled once tumours reached the defined size endpoint and lung ECM was visualised *ex vivo,* as described in 2.2.1.3. All xenografts experiments were performed under UK Home Office licence and approved by the University of Glasgow Animal Welfare and Ethical Review Board.

2.2.1.3 Second harmonic generation microscopy of lung and liver

Mice were sacrificed by intraperitoneal injection of pentobarbital and lungs were inflated with 2% low melting point agarose and visualised by second harmonic generation (SHG) microscopy. Briefly, a small incision was performed in the trachea and liquid agarose was injected with a blunted syringe needle. Mice were then left on ice for 10 minutes to allow agarose to solidify in lungs. Lungs were dissected and sliced using a vibratome for downstream analysis (Campden Instruments 5100mz). Fresh lung slices were imaged using a Trimscope multiphoton microscope (Lavision) to visualise fibrillar collagen in the lung parenchyma by SHG microscopy. For the visualisation of perivascular/peribronchial areas, lung slices were fixed in 4% PFA and imaged using an LSM 880 NLO multiphoton microscope (Zeiss).

For the animals in which liver ECM was examined, we dissected the liver and imaged fibrillar collagen in the liver capsule by SHG microscopy, using a Trimscope multiphoton microscope (Lavision).

2.2.2 Cell culture

2.2.2.1 Cancer cell lines

H1299 ($p53^{-/-}$ and $p53^{R273H/R175H}$) and MDA-MB-231 cells (ATCC) were cultured in Dulbecco's modified Eagle medium supplemented with 10% foetal bovine serum (FBS), 1 mM L-glutamine, 100 μg/mL streptomycin and 100 U/mL penicillin, here referred to as complete media, and incubated at 37°C in 10% CO_2. Cells were passaged by washing with PBS, followed by a 3-minute incubation in 0.25 % trypsin to detach cells from plates, with trypsin being quenched using complete media. Cell lines were routinely tested for mycoplasma contamination.

2.2.2.2 Immortalised cell lines

Telomerase-immortalised human dermal fibroblasts (TIFs, in house, Beatson Institute) and HEK 293T cells (ATCC) were cultured in complete media and incubated at 37°C in 10% CO_2. Cells were passaged by washing with PBS followed by a 3-minute incubation in 0.25% trypsin to detach cells from plates. The trypsin was quenched using complete media. Cell lines were routinely tested for mycoplasma contamination.

2.2.2.3 Patient-derived cell lines (PDCLs)

The three PDCLs were previously generated by the Biankin lab (Bailey et al., 2016). They were cultured in M199/F12 HAM medium supplemented with 7.5% filtered FBS, 15 mM HEPES, 2 mM L-glutamine, 20 ng/mL EGF, 40 ng/mL hydrocortisone, 5 ng/mL apo-Transferrin, 0.2 IU/mL Insulin ActRApid, 0.06% glucose, 0.5 pg/mL Tri-iodotyronine, 1x MEM vitamins and 2 g/mL Ortho-phosphoryl ethanolamine and were incubated at 37°C in 5% CO_2. Cells were passaged by washing with PBS followed by a 3-minute incubation in 0.25 % trypsin to detach cells from plates. The trypsin was quenched using the culture media described above. Experiments using these cell lines were done in collaboration with Peter Bailey and Giuseppina Caligiuri, Beatson Institute.

2.2.2.4 Transient transfection

H1299 cells were transfected with 2 μg of expression constructs containing podocalyxin-GFP, podocalyxin$^{V486A/Y500A}$-GFP (kindly gifted from the Echard lab, Institute Pasteur, Paris, France) or GFP, using the AMAXA system with Solution V and X-001 nucleofection protocol, as per manufacturer's instructions.

H1299 cells were transfected with siRNA targeting RCP, DGKα, PODXL, Rab35, Rab27a, Rab27b, ITGA3, or non-targeting siRNA, at a concentration of 5 nM, using the AMAXA system with Solution V and X-001 nucleofection protocol, as per manufacturer's instructions.

PDCLs were transfected with siRNA targeting p53 or a non-targeting siRNA, at a concentration of 5 nM, using lipofectamine RNAiMAX, according to the manufacturer's instructions.

One nucleofection reaction was conducted per 80% confluent 15cm^2 cell culture dish and transfected cells were seeded in new 15 cm^2 dishes for downstream experiments. Details of siRNAs and plasmids used are in Tables 2-5 and 2-6 respectively.

2.2.2.5 CRISPR

The guide RNA (gRNA) sequences used were 5'-GTAGCGAACGTGTCCGGCGT-3' as non-targeting control, 5'-TTGTCAACGTCAAGCGGTGG-3' against Rab35, and 5'-GTGAGGTTCAGGACGAGCTG-3' against podocalyxin. These sequences were cloned into lentiCRISPR vector, previously established by the Zhang lab (Shalem et al., 2014). For this, 5 μg of lentiCRISPR vector were digested with 20 units of BsmBI enzyme in buffer 3.1 in a volume of 50 μL, for 2 hours at 37°C. The digested plasmid was then run on agarose gel and purified using QIAquick Gel Extraction Kit as per the manufacturer's instructions. 1 μg of each pair of gRNA oligos was then phosphorylated and annealed with 1mM ATP and 5 units of T4 polynucleotide kinase, in T4 polynucleotide kinase reaction buffer, for 30 minutes at 37°C, followed by a step of 5 minutes at 95°C and a ramp down to 25°C (5°C/minute). The phosphorylated and annealed sgRNAs were then diluted at 1:200 in ddH_2O. Finally, we performed a ligation reaction between 1 μL of phosphorylated and annealed sgRNA and 50 ng of digested lentiCRISPR vector, using 1 μL of T4 DNA ligase in DNA dilution buffer, DNA ligation buffer. As a negative control, we set up a ligation reaction with the digested lentiCRISPR vector in the absence of gRNA oligos.

For the propagation of these constructs, we transformed stbl3 competent cells. Briefly, 1 µL ligation reaction was added to a vial of competent cells. After gently mixing, cells were incubated on ice for 30 minutes, heat-shocked for 45 seconds at 42°C and returned to ice for 2 minutes. 250 µL of S.O.C medium was added to each vial, which were then cultured at 37°C, for 1 hour in a shaking incubator. 100 µL of each transformation was spread onto ampicillin-containing agar plates and incubated overnight at 37°C. From each transformation plate, several colonies were picked and grown overnight in ampicillin-containing LB broth, at 37°C in a shaking incubator. Pellets were maxiprepped and sequenced using the LKO.1 forward primer, by the Molecular Technology Service, CR-UK Beatson Institute, Glasgow. Workbench software was used to analyse the sequences and to confirm that the constructs contained the desired guide sequences.

For the production of lentivirus encoding Cas9 and the respective gRNAs, HEK 293T cells were used as a packing cell line and were transfected as follows. 10 µg lentiCRISPR plasmid, 7.5 µg psPAX2 packaging plasmid and 4 µg VSV-G plasmid, were incubated with 120 mM of $CaCl_2$ in HBS buffer, for 30 minutes at 37°C. This mixture was then added to the media of HEK 293T cells (50% confluent 10 cm^2 dish) and left overnight at 37°C. The following day, culture media was replenished with fresh media.

48 hours after transfection, the supernatant from HEK 293T cells was replaced with fresh media and passed through a 0.45 µm filter. Subsequently, the supernatant was supplemented with 4 µg/mL Polybrene and added onto a 10 cm^2 dish of 50% confluent target H1299-$p53^{R273H}$ cells. 24 hours later, the new supernatant from HEK 293T cells was passed through a 0.45 µm filter, supplemented with 4 µg/mL Polybrene and used to transduce target cells as above. After 24 hours of culture, the virus-containing media was removed and replenished with media containing puromycin 2.5 µg/mL, which was replenished every 2 days for a period of 2 weeks. The loss of podocalyxin or Rab35 in target cells was confirmed using western blotting and cryofreezing was conducted for long term storage of CRISPR cell lines. These cells lines were established with Louise Mitchell, CRUK Beatson Institute.

2.2.2.6 Condition media (CM) assays

H1299 $p53^{-/-}$ and $p53^{R273H}$ cells were seeded at a density of $1x10^6$ cells per 15 cm^2 culture dish and grown to 90 % confluency over 72 hours. CM was then collected and subjected to differential centrifugation at 300 g for 10 minutes, 2000 g for 10 minutes and 10,000 g for 30 minutes to remove live cells, dead cells and cell debris respectively. The supernatant was

collected and used to treat recipient H1299 $p53^{-/-}$ cells for 72 hours. Recipient cells were than reseeded in 6 well plates and cultured for 24 hours, upon reaching confluency and being ready to use in cell migration experiments.

2.2.2.7 Cell-derived matrix (CDM) generation

Telomerase-immortalised human dermal fibroblasts (TIFs) were cultured in the presence of purified exosomes for 72 hours. To produce de-cellularised CDM, 0.2% gelatine-coated tissue cultureware was cross-linked with 1% glutaraldehyde for 30 minutes, quenched in 1 M glycine for 20 minutes, and equilibrated in DMEM containing 10% FBS. EV-treated TIFs were detached with trypsin and re-plated at near confluence (~2×10^4 cells/cm^2) and grown for 8 days in complete media supplemented with 50 µg/mL ascorbic acid. Matrices were denuded of living cells by incubation with CDM extraction buffer, and DNA residue was removed by incubation with DNaseI. CDMs were stored at 4°C or used immediately in further experiments.

2.2.2.8 Collagen organotypic assay

Collagen plugs were generated from rat tail derived collagen 1 and pre-conditioned with fibroblasts (TIFs). Cells were seeded in DMEM supplemented with 10% FBS and allowed to contract the plug for 2 days. 4×10^4 H1299 cells were then plated on top of these plugs and cultured for 2 days. Plugs were then transferred to a metal grid and cultured with full DMEM for 1 week. For the co-culture experiment with H1299 $p53^{-/-}$ and H1299 $p53^{R273H}$ cells, plugs containing each of the cell lines were bathed in the same culture media, allowing diffusible factors to operate. Plugs were then fixed in 4% paraformaldehyde before paraffin embedding. 4 µm sections were then cut and stained using haematoxylin and eosin. The distance between the cells and the top of the plug was measured for each cell in the field of views that were acquired using a brightfield microscope.

For plugs that were used to assess collagen organisation, they were visualised by SHG microscopy after the contraction phase, in the absence of tumour cells, using a Trimscope multiphoton microscope (Lavision).

2.2.3 Extracellular vesicle (EV) preparations

2.2.3.1 EV collection

EV-free media was prepared by ultracentrifugation at 100,000g for 16 hours at 4°C and collection of the supernatant. Cells were then cultured in complete media for 24 hours and cultured for 48 hours in EV-free media. CM was collected and centrifuged to remove live cells (300g), dead cells (2000g) and finally to remove cell debris and larger lipid membrane fragments (10,000g). EVs were then pelleted in thinwall polypropylene tubes by a spin at 100,000g, using an ultracentrifuge (Beckman coulter) with a SW32 rotor. The pellet was washed in PBS before a final centrifugation at 100,000 g, after which EVs were resuspended in 200µl of PBS and used on the same day, or stored at 4°C until the next day. All centrifugation steps were performed at 4°C.

When incubating recipient cells (H1299 or TIFs) with EVs, we routinely added these to the medium at a concentration of approx. 1×10^9 particles/ml and culture cell in EV-containing medium for 72 hours. Cells were then washed in PBS, reseeded and used for further experiments.

2.2.3.2 Sucrose density gradient

For sucrose density gradient centrifugation, EV pellets were mixed with 1 mL of a 2.5 M solution of sucrose at the bottom of a 12 mL centrifugation tube. EVs were overlaid with 11 layers of sucrose decreasing in concentration (from 2 to 0.4 M sucrose using 20 nM HEPES as diluent). The gradient was centrifuged at 200,000 g overnight using a SW40 rotor. EVs were collected from each gradient fraction by a final centrifugation in PBS at 100,000 g. Pellets were resuspended in 50 ul PBS.

2.2.3.3 Nanoparticle tracking analysis

Nanoparticle tracking analysis was carried out using the NanoSight LM10 instrument (Malvern) according to the manufacturer's instructions. EVs collected by ultracentrifugation (200 µL final volume) were diluted 1:30 in filtered PBS before being introduced into the instrument for measurement.

2.2.3.4 Transmission electron microscopy

EVs were collected and fixed in 2 % paraformaldehyde. Subsequently, 5 µl of fixed EVs were adsorbed onto Formvar carbon coated EM grids overnight at 4°C. Grids were washed with 100 µl PBS and treated with 1 % glutaraldehyde for 5 min. This was followed by eight washes with distilled water. EVs were visualised by negative staining, grids were incubated with uranyl oxalate for 5 minutes and subsequently methyl cellulose-UA for 10 minutes at 4°C. Air dried grids were imaged on the transmission electron microscope FEI Tecnai T20 running at 200 kV using Olympus Soft Imaging System software.

For immunogold staining of CD63, adsorbed EVs were subject to four blocking washes with PBS/50 mM glycine after initial adsorption onto grids. A second blocking step was then carried out using PBS/5 % BSA for 10 minutes. EVs were then exposed to CD63 primary antibody or mouse IgG1 isotype control antibody and incubated in 1% BSA for 30 minutes. Grids were washed in 0.1 % BSA in PBS six times, 5 minutes each. Grids were then incubated with anti-mouse 10 nm protein A-gold conjugate secondary antibodies for 30 minutes following eight PBS washes. From here onwards, fixation and negative staining protocol was performed as described in the paragraph above. Acquired Images were analysed using ImageJ to determine EV size. Experiment conducted by Margaret Mullin and Nikki Heath, at the University of Glasgow and the Beatson Institute.

2.2.4 Migration assays

2.2.4.1 Scratch-wound assay

Cells were seeded in 6 well plates at a density of $4x10^5$ cells/well and cultured for 24 hours until reaching around 90% confluency. At that time, a scratch-wound was performed using a p200 tip. Cells were washed with culture media and fed with fresh media. Cell plates were introduced into a 5% CO2 chamber and imaged every 10 minutes for 16 hours using a Nikon time-lapse Z6011, CoolSNAP HQ camera (photometrics) and metamorph software (molecular devices). Cell tracking was performed using imageJ and parameters of migration calculated using Chemotaxis plugin.

2.2.4.2 Random migration

Fibroblasts were seeded in 6 well plates at a density of $5x10^4$ cells/well and cultured for 24 hours. Cell plates were introduced in a 5% CO_2 chamber and imaged every 10 minutes for 16 hours using a Nikon time-lapse Z6011, CoolSNAP HQ camera (photometrics) and

metamorph software (molecular devices). Cell tracking was performed using imageJ and parameters of migration calculated using Chemotaxis plugin.

2.2.4.3 Migration on CDM

MDAMB231 cells were seeded onto de-cellularised CDM at a density of $8x10^4$ cells/well in a 6-well plate. Cells were allowed to attach for 4 hours and then the plate was introduced in a 5% CO2 chamber and imaged every 10 minutes for 16 hours using a Nikon time-lapse Z6011, CoolSNAP HQ camera (photometrics) and metamorph software (molecular devices). Cell tracking was performed using imageJ and parameters of migration calculated using Chemotaxis plugin.

2.2.5 Quantitative reverse transcription PCR

2.2.5.1 RNA extraction

H1299 cells were seeded in 6 well plates and cultured for 24 hours until cells had reached around 70% confluency. Cells were washed twice with ice-cold PBS and put on ice before RNA extraction using RNAeasy spin columns according to manufacturer's instructions. The concentration and quality of RNA extracted was quantified using the nanodrop system.

2.2.5.2 cDNA synthesis

cDNA was synthesised using Promega Reverse Transcription system following manufacturer's instructions. Samples were subjected to the following cycle protocol: annealing 25 °C for 5 minutes, extension 42 °C for 60 minutes and inactivation 70 °C for 5 minutes. The resulting cDNA was stored at – 20°C until further use.

2.2.5.3 Quantitative PCR

1 µl of synthesised cDNA in 7 µl H_20 was analysed in a quantitative PCR (qPCR) reaction using 10 µl PerfeCTa SYBR green master mix and 2 µl QuantiTect primers for podocalyxin or GAPDH (housekeeping gene), according to manufacturer's instructions. Samples were loaded into a Biorad 96 well plate in triplicates. Quantitative PCR was run on the Biorad C1000 thermal cycler. DNA was denatured at 95 °C for 5 minutes. This was then followed for 40 cycles of denaturation at 95 °C for 30 seconds, annealing at 60 °C for 30 seconds and extension at 72 °C for 30 seconds. A final step of extension was performed for 5 minutes at 72 °C. Data was analysed using Biorad software using Ct cycle values. Levels of

podocalyxin expression were compared between cell lines using the ΔΔCt method and GAPDH as a sample control.

2.2.6 SILAC proteomics

H1299 cells ($p53^{-/-}$ or $p53^{R273H}$) were cultured in Single Isotope Labelling by Amino acids in Culture (SILAC) DMEM with 10% dialysed FBS, 1 mM L-glutamine, 100 µg/ml streptomycin, 100 U/ml penicillin and 1:1000 amino acid isotopes (heavy: $lysine^{8}$, $arginine^{10}$ or medium: $lysine^{4}$, $arginine^{6}$). $p53^{-/-}$ cells were labelled with heavy amino acid isotopes and $p53^{R273H}$ cells were labelled with medium amino acid isotopes. Once amino acid isotopes were fully incorporated, $p53^{-/-}$ and $p53^{R273H}$ cells were seeded for EV collection. After collection of the conditioned medium, both conditions were merged prior to processing to minimize technical errors. The final EV pellet was re-suspended in 6M urea for mass spectrometry analysis. During mass spectrometry analysis, proteins detected in EV from H1299-$p53^{-/-}$ and H1299-^{R273H} could be distinguished from one another in the sample due to the different amino acid isotope labelling.

EV proteins were reduced (10 mM dithiothreitol), alkylated (55 mM iodoacetamide) and digested (Lys C and trypsin). Peptides were cleaned using stage tips and re-dissolved in 5 % acetonitrile/0.25 % formic acid. Protein samples were then applied on the Orbitrap Elite (LC-MS). Data was searched and quantified against Swissprot (Human) database using MaxQuant software. Mass spectrometry experiments were performed in collaboration with Sara Zanivan, David Sumpton and Nikki Heath, from The CRUK Beatson Institute. Dataset in appendix I.

2.2.7 Western blotting

Cell culture media was removed from cells, which were then washed in ice-cold PBS and lysed on ice in 50 mM tris/1 % SDS lysis buffer. Cells were scraped and homogenised using Qia-shredder columns. Cell lysate was then mixed in NuPage sample buffer and boiled for 5 minutes at 95 °C.

To resolve proteins by electrophoresis, samples were loaded into a NuPage pre-cast gel (4-12 %) alongside a protein ladder. Gels were ran using NuPage MOPS running buffer at 150 V for 2 hours. Proteins were then transferred from the gel onto methanol activated PVDF membrane in NuPage transfer buffer at 120 V for 90 minutes. The membrane was blocked using 5 % Milk or 3 % BSA in TBS-T for one hour at room temperature under agitation.

Primary antibodies were then applied to the membrane in 1 % milk/BSA in TBS-T overnight at 4 °C under agitation.

Membranes were washed 3 times with TBS-T, every 10 minutes, before secondary Licor infra-red fluorescent antibodies of the appropriate species were applied for 30 minutes, at room temperature. Three more TBS-T washes were carried out and the membrane was transferred to distilled water before the Licor Odyssey system was used to expose the blots and visualise protein bands.

2.2.8 Immunoprecipitation

H1299 cells were transfected with GFP-Rab35, podocalyxin-GFP or podocalyxinV486A/Y500A-GFP as in 2.2.2.4, cultured for 48 hours and lysed in non-denaturing lysis buffer. Lysates were passed through a 27-gauge needle three times before being clarified by centrifugation at 10,000 x g for 10 minutes at 4 °C. Magnetic beads conjugated to sheep anti-mouse IgG were bound to anti-GFP antibody. Conjugated beads were then incubated with lysates for 2 hours at 4 °C whilst being subjected to constant rotation. The beads were then washed in lysis buffer and immunoprecipitated proteins were eluted at 95ºC for 10 minutes in NuPage sample buffer. Proteins were resolved by SDS-PAGE and analysed by Western blotting.

2.2.9 Surface biotinylating assay

H1299 cells were labelled with the membrane-impermeable reagent sulfo-NHS-SS-biotin (0.2 mg/mL in PBS) on ice for 30 minutes. Cells were then washed with ice-cold PBS and lysed in non-denaturing lysis buffer. Lysates were passed through a 27-gauge needle three times before being clarified by centrifugation at 10,000 x g for 10 minutes at 4 °C. Biotinylated proteins were than precipitated using streptavidin-conjugated beads. The levels of podocalyxin associated to the labelled (surface) and input (total) fractions were assessed by western blotting.

2.2.10 Internalisation assay

Recipient H1299-p53$^{-/-}$ cells were cultured in the presence of purified EVs for 72 h. Following this, cells were trypsinised and washed to remove EVs, re-plated and grown for 48 h to achieve a confluence of 80–90%. Cells were incubated in serum-free DMEM, transferred to ice, washed twice in ice-cold PBS and surface-labelled at 4ºC with 0.2 mg/mL

sulfo-NHS-SS-biotin (Pierce) in PBS for 30 min. Cells were washed with ice-cold PBS, replenished with serum-free medium with the recycling inhibitor primaquine (0.6 mM), and shifted to 37ºC for the stated times to allow internalisation of tracer. After washing cells with ice-cold PBS, the biotin remaining at the surface was reduced for 1 hour in 20 mM MesNa, and quenched in 20 mM IAA for 10 minutes, at 4 °C. Cells were then washed using ice-cold PBS and lysed in non-denaturing lysis buffer. Lysates were passed through a 27-gauge needle three times before being clarified by centrifugation at 10,000 x g for 10 minutes at 4°C.

Internalised/biotinylated α5β1, cMET and TfnR were then quantified by capture-ELISA as follows. In the previous day, Maxisorp plates were coated with antibodies recognising human α5 integrin, cMET or TfnR in antibody coating buffer, and incubated overnight at 4°C. Plates were then washed with PBS-T and blocked with 5% BSA in PBS-T, for 1 hour at room temperature. Following another wash in PBS-T, the antibody-coated plates were incubated with cell lysates, overnight at 4°C. Plates were washed again in PBS-T and incubated with streptavidin-HRP in 0.1% BSA PBS-T, for 1 hour at 4°C. A final wash in PBS-T was performed and plates were incubated with ELISA developing reagent, for 10-15 minutes at room temperature. The reaction was stopped with 8 M sulfuric acid and absorbance at 490 nm was determined. We determined the level of internalisation of each receptor (i.e. protected from MesNa reduction and therefore biotinylated) as a percentage of the total surface biotinylated pool of the approapriate receptor.

2.2.11 Recycling assay

Recipient cells were cultured in the presence of purified EVs for 72 h. Following this, cells were trypsinised and washed to remove EVs, re-plated and grown for 48 h to achieve a confluence of 80–90% prior to conducting receptor recycling assays. H1299-p53$^{-/-}$ cells were incubated in serum-free media, transferred to ice, washed twice in cold PBS and surface-labelled at 4ºC with 0.2 mg/mL sulfo-NHS-SS-biotin in PBS for 30 minutes. Cells were transferred to serum-free DMEM for 30 minutes at 37 °C to allow internalisation of tracer. Cells were returned to ice, washed with ice-cold PBS and biotin was removed from proteins remaining at the cell surface by performing a reduction with 20 mM MesNa at 4 °C for 1 hour.

The internalised fraction was then chased from the cells by returning them to 37 °C in serum-free DMEM. At the indicated times, cells were returned to ice and biotin removed from

recycled proteins by a second reduction with 20 mM MesNa for 1 hour, followed by 10 minutes of quenching with 20 mM IAA, at 4 °C. The DGK inhibitor (R59022) or DMSO control were added as the receptor internalised and were maintained during the subsequent recycling period.

Biotinylated α5β1, cMET and TfnR were then determined by capture-ELISA as in 2.12. The % of recycling was calculated by subtracting the absorbance obtained upon the second reduction with MesNa from the absorbance of the internal pool (obtained upon the first reduction with MesNa), followed by dividing this value by the absorbance of the internal pool.

2.2.12 Immunofluorescence

Cells or decellularized CDMs were fixed in 4 % paraformaldehyde in PBS for 8 minutes and permeabilised with 0.2 % triton-X100 in PBS for 10 minutes. Cells were washed twice with PBS and blocked using 1 % BSA in PBS.

The primary antibody was applied to cells in 1 % BSA/PBS for 1 hour. After 3 washes in PBS, the Alexa-conjugated secondary antibodies were incubated for 45 minutes in 1% BSA in PBS. After 3 washes with PBS, soft set Vectashield with DAPI was used to mount samples. Samples were then visualised by confocal microscopy using Olympus Fluoview FV1000.

2.2.13 GLCM analysis of ECM organisation

Using image sets generated by second harmonic and immunofluorescence imaging, the structure and organisation of the ECM was analysed by applying grey level co-occurrence matrix (GLCM) analysis, a second-order statistical method. Briefly, the intensity of each pixel containing collagen signal is compared to the neighbouring pixels (up to 100 pixels away, corresponding to 100 μm) and a 2D histogram of intensity occurrences compiled, from which statistical parameters of the intensity distribution are calculated such as correlation, homogeneity, contrast and entropy. This has the advantage of removing bias introduced by varying total amounts of signal, changes in the image acquisition and/or signal strength as compared to direct measurements from the raw image data. A bi-exponential model is applied to the correlation decay data and the fit parameters are used to calculate a weighted mean decay distance that serves as a parameterisation metric between sample conditions.

2.2.14 Atomic force microscopy

The mechanical properties of the cell-derived matrix were carried out with an Atomic Force Microscope Nanowizard II (JPK Instruments) mounted on an inverted optical microscope (Zeiss Observe) with a cell heater attachment. Force indentation measurements were carried out using an AFM probe attached with a 4.8 μm silica microsphere. Thermal calibrations were performed to determine the spring constant of each cantilever before use. Force spectroscopy measurements were performed on 50 randomised locations on each sample by applying a 3 nN force indentation. The Hertzian spherical model was applied to the approach force–distance curves to deduce the elastic modulus of the ECM using an in-house algorithm written in R.

The adhesive properties of the ECM were estimated through analysing the energy required to remove the probe from the matrix, which is the total areas of adhesion peaks in the retraction force–distance curves (JPK data analysis software). These experiments were performed in collaboration with Huabing Yin and Laura Charlton, University of Glasgow.

2.2.15 Statistics

Statistical analysis was performed on all relevant experiments. To compare two data-sets unpaired t-tests were performed if the data were normally distributed, or a Mann-Whitney test if the data were not normally distributed. To compare more than two data sets, ANOVA tests were used if the data were normally distributed, and a Kruskal-Wallis test if the data were not normally distributed. Statistical significance is annotated within the figures and the associated p-values are indicated in each figure legend, with $p<0.05$ considered as significant.

Chapter 3 A novel non-cell autonomous gain-of-function of mutp53

(This chapter features work relating to Novo et al. (2018) – Appendix II).

3.1 Introduction

Wild-type p53 function is often lost in human cancers. This is frequently driven by point mutations in 'hotspot' residues within the DNA binding domain of p53 that lead to the expression of full-length mutants with abrogated wild-type p53 function (Petitjean et al., 2007). Mutp53s are not, however, phenotypically silent, as they can interact with cellular proteins and/or directly with DNA to drive transcriptional and non-transcriptional changes in the cells which express them (Freed-Pastor et al., 2012; Jordan et al., 2008; Strano et al., 2002). This, along with the fact that mutp53s are often stable in human cancers, gives rise to an aberrantly expressed oncogene that influences a multitude of signalling pathways. As a consequence, mutp53-expressing cancers often display gain-of-function (GOF) phenotypes that render them more aggressive than the ones driven solely by p53 loss (Lang et al., 2004; Morton et al., 2010; Olive et al., 2004). This occurs, in part, through a cell autonomous mechanism in which mutp53s, by interacting with p63 and blocking its functions, activates integrin recycling in cancer cells to promote invasive migration (Muller et al., 2014, 2009).

Nonetheless, tumour progression does not depend solely on cell autonomous mechanisms. Tumours are often composed by multiple clonal populations of cancer cells within a complex microenvironment, allowing intercellular communication to occur through diffusible factors. Among these diffusible factors are EVs. In addition to cancer cell-derived EVs being considered to be potential cancer biomarkers, it is now clear that they can modulate responses in non-tumour cells to influence multiple aspects of tumour progression, including modulation of anti-tumour immunity (Wolfers et al., 2001), reprogramming of microenvironments to foster tumour progression (Baglio et al., 2017; Cooks et al., 2018; Webber et al., 2015), and priming of metastatic niches (Costa-Silva et al., 2015; Peinado et al., 2012; Zhang et al., 2017). Moreover, a few studies have now indicated that EVs can mediate communication between different cancer cells, allowing for transfer of migratory and invasive traits (O'Brien et al., 2013; Rahman et al., 2016; Tang et al., 2018). However, despite studies outlining how certain oncogenic proteins and microRNAs might be transferred between cells through EVs, the molecular mechanisms that mediate the non-cell

autonomous effects of EVs in tumour progression, as well as the role of oncogenic pathways in the release of metastasis-promoting EVs, remain elusive.

In this chapter, we sought to identify non-cell autonomous mechanisms of cancer aggressiveness, by taking advantage of a well characterised cell autonomous GOF of mutp53s, i.e. their ability to promote cancer cell migration and invasion. In particular, we explored whether mutp53-expressing cancer cells can transfer aggressive traits to other cells through the release of EVs. Furthermore, we evaluated the effect of mutp53's expression on the release of EVs and their physical properties. Subsequently, we explored whether mutp53s control EV composition and, if so, whether composition imbues EVs with the ability to transfer phenotypic traits. Finally, we describe a signalling pathway that allows recipient cells to respond to EVs.

3.2 Results

3.2.1 mutp53 promotes release of pro-invasive factors

'Organotypic' plugs of native type I collagen in which the ECM has been conditioned for several days by human fibroblasts provide an excellent model for assessing cancer cell invasiveness in complex microenvironments (Figure 3-1 A) (Timpson et al., 2011a). When plated onto organotypic plugs, pre-conditioned by telomerase-immortalised human fibroblasts (TIFs), H1299 non-small cell lung carcinoma cells (which do not express p53 - H1299-p53$^{-/-}$) were poorly invasive, with most cells residing in the upper portion of the plug 10 days after seeding. By contrast, isogenic H1299 cells expressing p53^{R273H}, a mutant form of p53 described to have GOF, invaded extensively into organotypic plugs (Figure 3-1 B). This is consistent with the well-established cell autonomous role of mutp53s in driving cancer cell invasion (Muller et al., 2014, 2009; Timpson et al., 2011b).

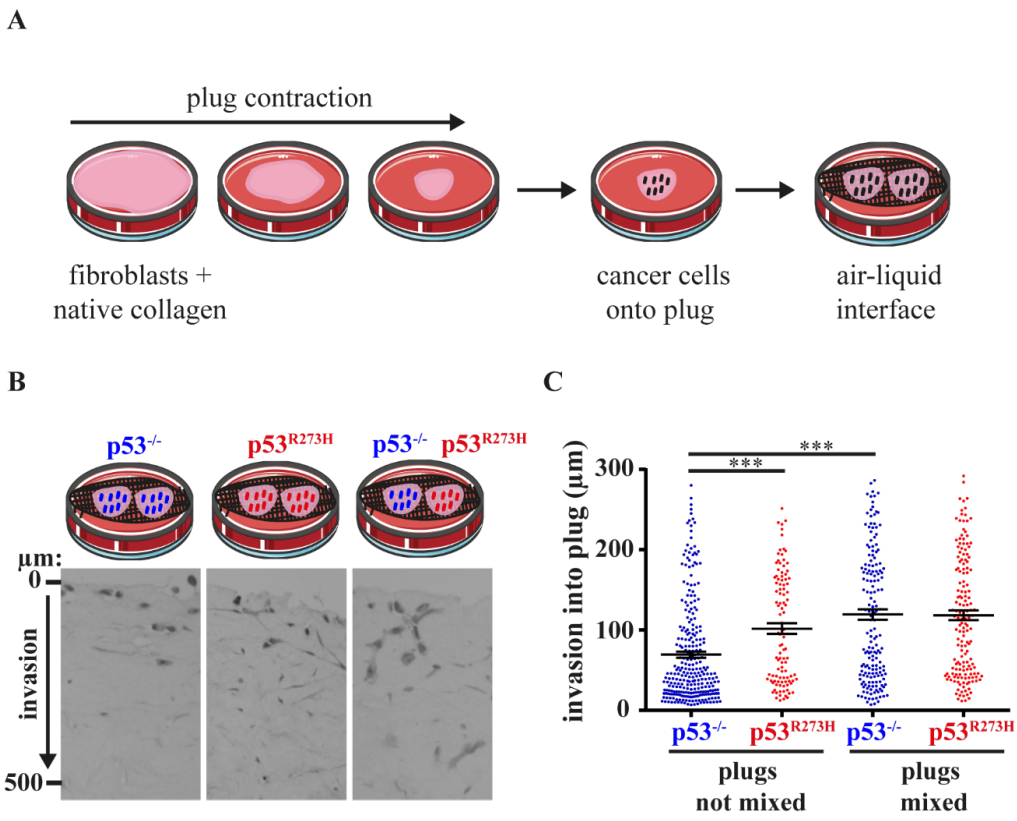

Figure 3-1- mutp53 promotes release of diffusible factors to foster tumour cell invasion in an organotypic microenvironment.
(A) Schematic with protocol of organotypic invasion assay. (B) Organotypic plugs were generated allowing collagen to polymerise in the presence of telomerase-immortalised human dermal fibroblasts (TIFs). TIF-containing plugs were conditioned for 2 days to allow TIFs to deposit and remodel the ECM. Plugs were overlaid with H1299-p53$^{-/-}$ (left panel), or H1299-p53^{R273H} (middle panel) cells and placed onto grids in independent culture dishes containing medium. In the right panel, plugs which were overlaid with H1299-p53$^{-/-}$ were placed onto grids in the same culture dish as those overlaid with H1299-p53^{R273H} cells, thus allowing the possibility of exchange of factors between plugs. Tumour cells were allowed to invade for 10 days, followed by fixation and H&E staining. The distance between each tumour cell and the top of the plug was determined and plotted in C. Bars are mean ± SEM, n= 8 plugs; *** p <0.001 Mann–Whitney test.

Pro-invasive oncogenic pathways can also operate in a non-cell autonomous fashion via diffusible factors. To test whether mutp53 promotes release of pro-invasive factors, we placed organotypic plugs containing H1299-p53^{R273H} cells in the same Petri dish as plugs with H1299-p53$^{-/-}$ cells. When cultured in this way, H1299-p53$^{-/-}$ cells displayed invasive behaviour that was indistinguishable from H1299-p53^{R273H} cells (Figure 3-1 B, C). These data indicate that mutp53's invasive gain-of-function may be transferred to other cells via diffusible factors.

3.2.2 mutp53 promotes release of EV-associated, pro-migratory factors

In addition to their increased invasiveness, mutp53-expressing cells migrate faster and more erratically on 2D substrates than their p53-null counterparts (Muller et al., 2014, 2009). Indeed, persistence and forward migration index (FMI) of H1299 cells migrating into scratch-wounds was suppressed by expression of mutp53 (Figure 3-2A - C). To represent these changes graphically, we calculated the differences between the persistence and FMI of mutp53-expressing and p53 null cells—these we term the ΔPersistence and ΔFMI—and plotted them as x and y coordinates, respectively (Figure 3-2D).

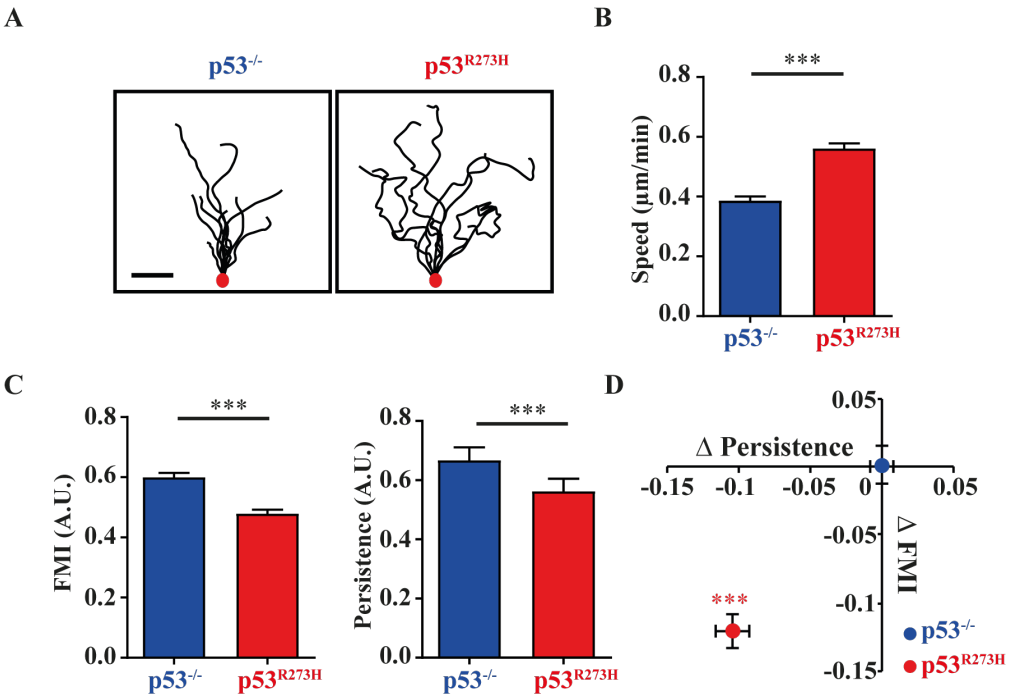

Figure 3-2- mutp53 supresses the forward migration index and persistence of H1299 cells.
Confluent monolayers of H1299-p53$^{-/-}$ or H1299-p53^{R273H} cells were wounded with a pipette tip and their migration into these scratch-wounds was monitored by time-lapse microscopy followed by cell tracking. Representative tracks are displayed in (a). Bar, 100 µm. The speed (B), persistence and forward migration index (FMI) (C) of migration into scratch-wounds was determined using cell tracking software. The differences between the migratory persistence and FMI (the Δ Persistence & Δ FMI respectively) of H1299-p53^{R273H} and H1299-p53$^{-/-}$ cells were calculated and are represented graphically in (D). Values are mean ± SEM; *** $p<0.001$ Mann-Whitney test. Experiment conducted by Nikki Heath, the Beatson Institute.

We then used this approach to investigate whether mutp53's migratory gain-of-function can be transferred to other cells via diffusible factors. We pre-treated recipient H1299-p53$^{-/-}$ cells with media conditioned by donor H1299-p53$^{-/-}$ cells (p53$^{-/-}$-CM) or H1299-p53^{R273H} cells (p53^{R273H}-CM) and evaluated their migration into scratch-wounds. Recipient cells pre-treated with p53$^{-/-}$-CM migrated indistinguishably from untreated H1299-p53$^{-/-}$ (Figure 3-3 A). By contrast, p53^{R273H}-CM suppressed the migratory persistence and FMI of H1299-p53$^{-/-}$ recipient cells to a similar extent as mutp53 expression did in cancer cells (Figure 3-3A), indicating that mutp53's migratory gain-of-function can be transferred to recipient cells via diffusible factors.

Expression of mutp53 in cancer cells modulates membrane trafficking. This, together with previous reports of non-cell autonomous mechanisms of cancer aggressiveness being mediated by cancer cell-derived EVs, led us to investigate the requirement of EVs for transfer of mutp53's migratory phenotype. Indeed, depletion of EVs by centrifugation completely opposed the ability of p53^{R273H}-CM to suppress the migratory persistence and FMI of recipient H1299-p53$^{-/-}$ cells into scratch-wounds (Figure 3-3 B). These data suggest that the diffusible factor(s) responsible for transfer of mutp53's migratory gain-of-function are associated with EVs.

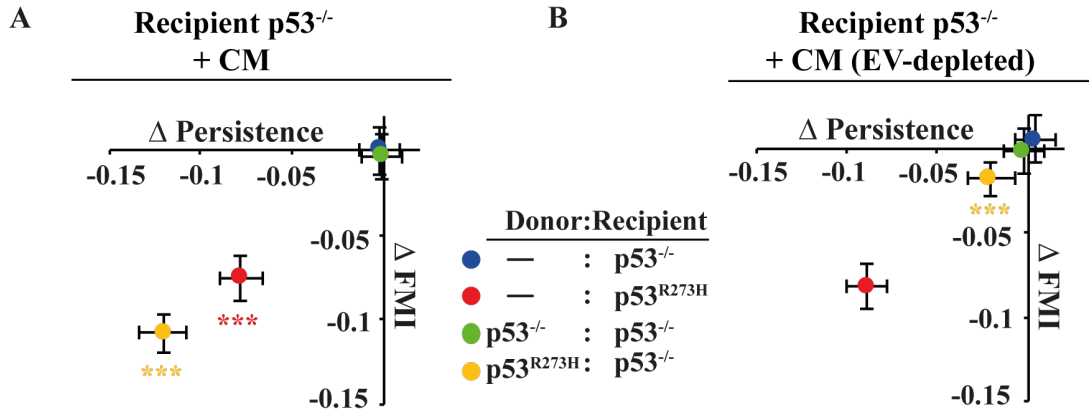

Figure 3-3- Media conditioned by mutp53-expressing tumour cells promotes cell migration in p53$^{-/-}$ cells. (A) Conditioned medium (CM) was collected from H1299-p53$^{-/-}$ and H1299-p53^{R273H} 'donor' cells and then placed onto H1299-p53$^{-/-}$ 'recipient' cells for 72 hr. Recipient cells were then replated, grown to confluence and wounded, and the Δ Persistence and Δ FMI of migration into scratch-wounds determined as for (Figure 3-2D). Values are mean ± SEM; ***yellow versus green and ***red versus blue in (B) is $p<0.001$, Mann-Whitney test. (B) CM was collected from H1299-p53$^{-/-}$ and H1299-p53^{R273H} 'donor' cells, depleted of EVs by centrifugation at 100,000 g for 70 min, and then placed onto H1299-p53$^{-/-}$ 'recipient' cells for 72 hr. Recipient cells were then replated, grown to confluence and wounded, and the Δ Persistence and Δ FMI of migration into scratch-wounds determined as for (Figure 3-2D). Values are mean ± SEM; ***yellow versus green in (A) is $p<0.001$, Mann-Whitney test. Experiment conducted by Nikki Heath, the Beatson Institute.

3.2.3 mutp53 does not influence EV production

Following the observation that depleting EVs from p53^{R273H}-CM abolished the transfer of migratory characteristics, we sought to determine whether mutp53 influences EV production and/or release. To do this, we collected EVs by differential centrifugation of p53$^{-/-}$- or p53^{R273H}-CM (Figure 3-4 A) and compared these EV preparations using Nanoparticle tracking analysis (NTA) (Figure 3-4 B) and Transmission Electron Microscopy (TEM) (Figure 3-4 C). These showed that neither number nor size of EVs was significantly different between p53$^{-/-}$- and p53^{R273H}-EV, with the average diameter of EVs detected by NTA and TEM being approximately 150 and 200 nm respectively. Notably, both analyses revealed that over 50% of EVs in both preparations were smaller than 200 nm in diameter, which is consistent with the size that is canonically attributed to exosomes.

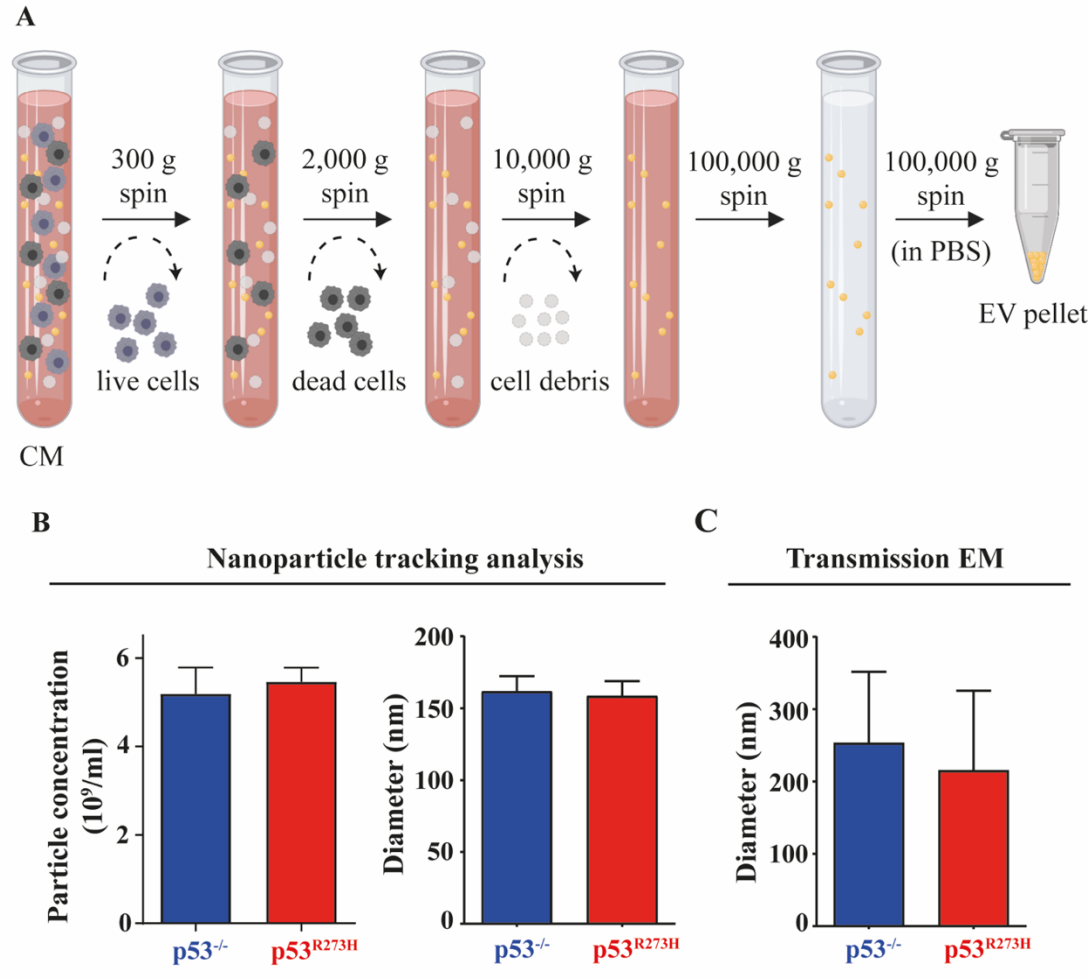

Figure 3-4- mutp53 does not influence the number nor size of EVs released by tumour cells.
(A) Schematic with protocol for collection of EVs. Conditioned medium was collected and centrifuged to remove live cells (300g), dead cells (2000g) and finally to remove cell debris and larger lipid membrane fragments (10,000g). EVs were then pelleted at a 100,000g. The pellet was washed in PBS before a final pelleting centrifugation at 100,000 g, after which EVs were re-suspended in PBS. (B) EVs were purified from H1299-p53$^{-/-}$ and H1299- p53^{R273H}-CM using differential centrifugation and the particle concentration and average particle diameter of this material were determined using Nanosight particle tracking. In (C), the average diameter of EVs in those preparations was determined using transmission electron microscopy (TEM). Values are mean ± SEM.

We then used western blotting to evaluate the expression of a panel of EV markers in our preparations. This revealed that p53$^{-/-}$- and p53^{R273H}-EV express similar levels of EV markers, including the tetraspannin CD63, which is strongly enriched in late endosomes and exosomes (Escola et al., 1998) (Figure 3-5 A). Accordingly, immunogold EM indicated that the majority of EVs from H1299 cells were CD63 positive and this was not altered by their p53 status (Figure 3-5 B). Taken together, these data indicate that mutp53 expression in cancer cells does not influence EV number or size, nor the levels of EV markers in EV preparations, thus suggesting that mutp53 does not regulate EV production per se.

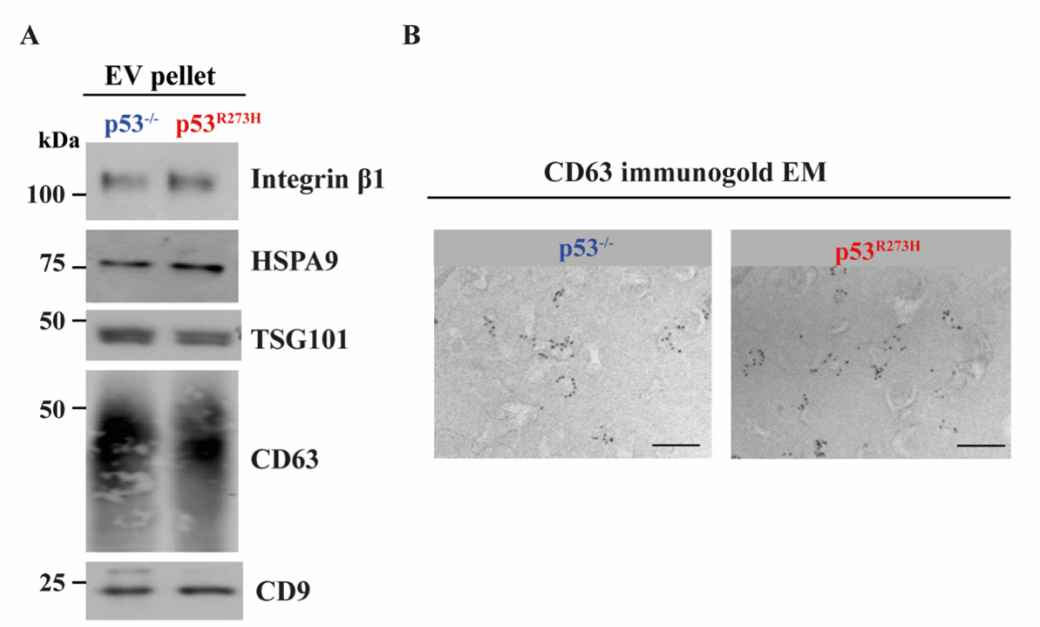

Figure 3-5- mutp53 does not influence expression of EV markers in EVs released by tumour cells.
(A) EVs from H1299-p53$^{-/-}$ and H1299- p53^{R273H} were purified by differential centrifugation and analysed by western blotting for the presence of established EV markers. (B) EVs from H1299-p53-/- and H1299-p53R273H were purified by differential centrifugation, fixed, adsorbed onto nitrocellulose-coated Formvar grids, negatively stained and labelled with anti-CD63 conjugated to 10 nm gold particles before visualisation by TEM. Bar 200 nm.

3.2.4 mutp53-EVs influence recipient cell migration

Despite the similarities found between EVs released by p53$^{-/-}$- and mutp53-expressing cells, we examined whether EVs are sufficient to mediate intercellular transfer of mutp53's migratory gain-of-function. To this end, we pre-incubated recipient H1299-p53$^{-/-}$ cells with EVs collected from donor H1299 cells expressing either of two mutp53s, p53^{R273H} or p53^{R175H} (p53^{R273H}- or p53^{R175H}-EV respectively, and referred to as mutp53-EVs), and from p53 null H1299 cells (p53$^{-/-}$-EV) and evaluated their migration into scratch-wounds (Figure 3-6 A). Strikingly, p53^{R273H}- and p53^{R175H}-EV evoked a phenotype associated with mutant p53's migratory gain-of-function (i.e. suppression of migratory persistence and FMI and

increased migration speed) in recipient cells, whereas p53$^{-/-}$-EV were ineffective in this regard (Figure 3-6 B). This indicates that mutp53's migratory gain-of-function can be transferred to recipient cells through EVs.

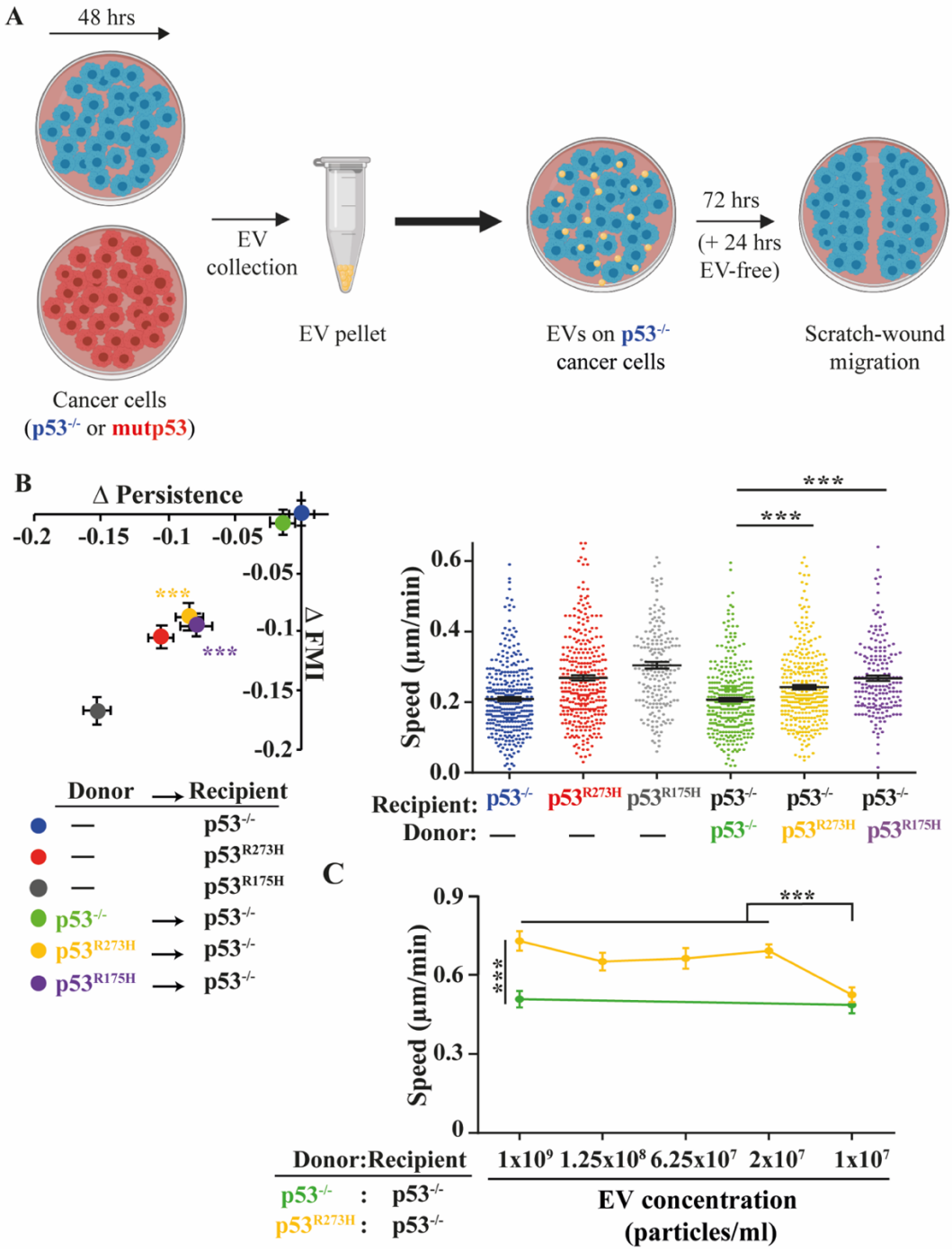

Figure 3-6- mutp53-EVs induce migration in p53$^{-/-}$ tumour cells.
(A) Schematic with protocol for assessing the effect of EVs on cell migration. (B) H1299-p53$^{-/-}$, H1299-p53^{R273H} or H1299-p53^{R175H} 'recipient' cells were pre-treated with EVs collected from H1299-p53$^{-/-}$, H1299-p53^{R273H} or H1299-p53^{R175H} donor cells, or were left untreated as indicated. Cells were then re-plated and the speed, Δ Persistence and Δ FMI of migration into scratch-wounds determined as for (Figure 3-2D). Values are mean ± SEM; n > 195 cells from three individual experiments; *** in the right panel, and ***yellow vs green and *** purple vs green in the left panel are p<0.001, Mann–Whitney. (C) EVs from donor H1299-p53$^{-/-}$, or H1299-p53^{R273H} were adjusted to the indicated concentrations and then incubated with recipient H1299-p53$^{-/-}$ cells for 72 hr. Recipient cells were re-plated and grown to confluence for 24hr. Cells were wounded with a pipette tip and their speed of migration was determined using time lapse microscopy and cell tracking. Values are mean ± SEM. *** are p<0.001, Mann–Whitney. n > 100 cells from 3 individual experiments.

We then performed titration experiments to determine the minimal concentration of $p53^{R273H}$-EV required for modulating migration in recipient H1299-$p53^{-/-}$ cells, which was $2x10^7$ EV/mL (Figure 3-6 C). Thus, the concentration of EV which accumulate in the medium bathing mutant p53-expressing cells over 72 hours (approximately $1x10^9$ EV/mL) is 100-fold more than is required to generate a migratory phenotype in recipient cells.

Mutations in the DNA-binding domain of p53, such as $p53^{R273H}$ and $p53^{R175H}$, are known to lead to loss of tumour-suppressive functions. However, some reports have suggested that mutp53s may retain and/or exaggerate other aspects of $p53^{wt}$ function (Como and Prives, 1998; Jordan et al., 2008). This raised the possibility that not only mutp53, but also $p53^{wt}$ expression in donor cells, could drive migration in recipient cells. Thus, we used a tetON-inducible system to express $p53^{wt}$ in H1299 cells (Figure 3-7 A). EVs released by H1299 cells induced to express $p53^{wt}$ ($p53^{wt}$-EV) did not affect FMI, directionality nor speed of recipient H1299-$p53^{-/-}$ cells into scratch-wounds (Figure 3-7 B), indicating that mutp53's ability to drive transfer of migratory characteristics is, indeed, a gain-of-function.

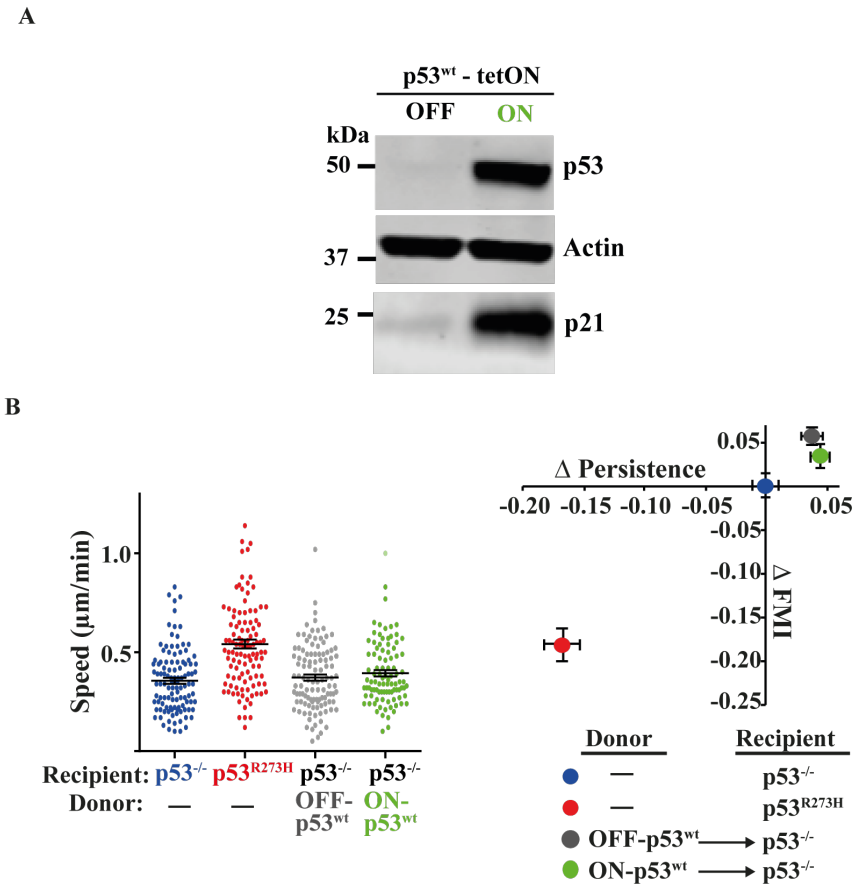

Figure 3-7- $p53^{wt}$ does not drive production of phenotype-altering EVs.
(A) H1299-p53tetON cells were incubated in the presence or absence of doxycycline and induction of wild-type p53 was confirmed by western blotting. (B) EVs from these cells were incubated with recipient H1299-$p53^{-/-}$ cells, the cells re-plated and the speed, ΔPersistence and ΔFMI of migration into scratch-wounds determined as for (Figure 3-2D). Values are mean ± SEM; n > 110 cells; *** are $p < 0.001$, Mann-Whitney.

3.2.5 mutp53-EVs promote receptor recycling in recipient cells

Integrin internalisation and recycling are crucial for cell migration. Accordingly, previous studies showed that expression of mutp53s with pro-migratory gain-of-functions in cancer cells stimulate recycling of α5β1 integrin and RTKs (Muller et al., 2014, 2009; Rainero et al., 2012). Thus, we assessed the rates of internalisation and recycling of a number of receptors in recipient H1299-p53$^{-/-}$ cells which had been pre-treated with different EV preparations. Recipient cells pre-incubated with p53$^{-/-}$- or p53^{R273H}-EV displayed similar rates of internalisation for α5β1, cMET and TfnR (Figure 3-8 A). However, the rates at which the internalised fraction of these receptors returned to the plasma membrane were strongly increased in recipient cells which had been pre-incubated with p53^{R175H}- or p53^{R273H}-EV, whilst pre-incubation with p53$^{-/-}$-EV was ineffective in this regard (Figure 3-8 B). These data show that EVs released by mutp53-expressing cells enhance receptor recycling, but not internalisation, in recipient cells.

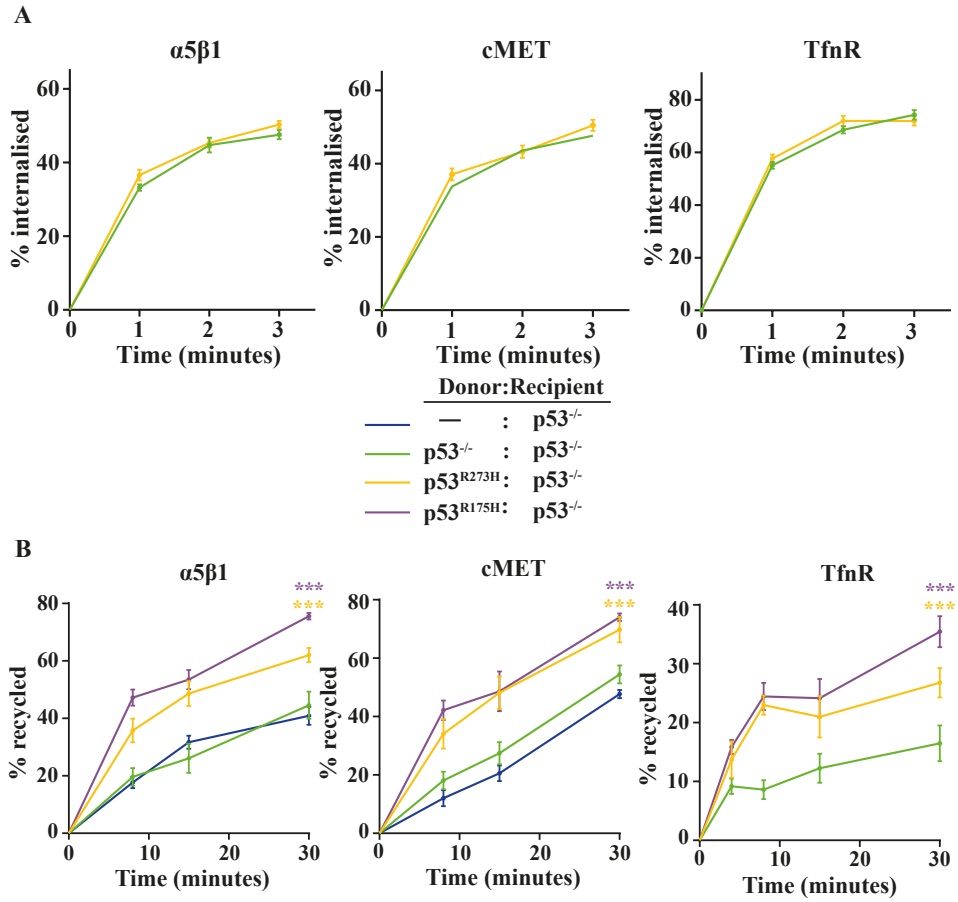

Figure 3-8- mutp53-EVs promote receptor recycling (but not internalisation) in p53$^{-/-}$ cells.
(A) H1299-p53$^{-/-}$ recipient cells were pre-treated for 72 hours with EVs collected from H1299-p53$^{-/-}$ or H1299-p53^{R273H} donor cells. Cells were reseeded and culture for a further 72 hours. Internalisation of α5β1integrin, cMET and TfnR was determined in the presence of 0.6mM primaquine. Values are mean ± SEM; n=2. (B) H1299-p53$^{-/-}$ recipient cells were pre-treated for 72 hours with EVs collected from H1299-p53$^{-/-}$, H1299-p53^{R273H} or H1299-p53^{R175H} donor cells, or were left untreated. Cells were reseeded and culture for a further 72 hours. Recycling of integrin α5β1, cMET and TfnR was determined. Values are mean ± SEM; n=3; ***yellow versus green and ***purple versuss green in the left panel are p<0.001, ANOVA.

In cancer cells, mutp53-mediated receptor recycling occurs through an RCP and DGKα-dependent pathway (Muller et al., 2009; Rainero et al., 2012). We, therefore, assessed whether EV-mediated receptor recycling in recipient cells was dependent on DGKα. We pre-incubated recipient H1299-p53$^{-/-}$ cells with p53^{R273H}-EV and measured their rates of recycling for α5β1 and cMET in the presence of R59022, an inhibitor of DGKα. DGKα inhibition in recipient cells opposed the ability of p53^{R273H}-EV to enhance receptor recycling (Figure 3-9), indicating that EVs released by mutp53-expressing activate DGKα-dependent recycling of receptors in recipient cells.

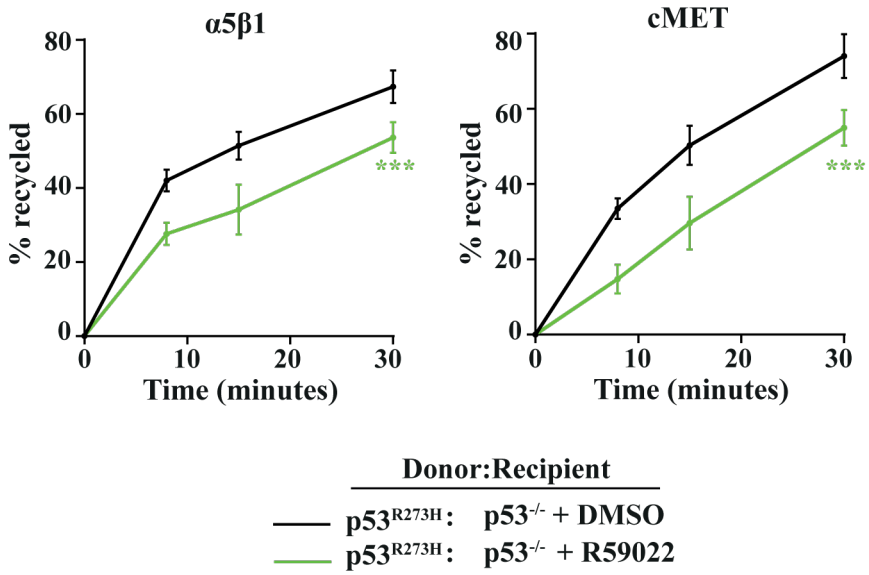

Figure 3-9- mutp53-EV-mediated receptor recycling in p53$^{-/-}$ cells depends on DGKα function. H1299-p53$^{-/-}$ recipient cells were pre-treated for 72 hours with EVs collected from H1299-p53$^{-/-}$ or H1299-p53^{R273H}. Recipient cells were then trypsinised and re-plated. Seventy-two hours following re-plating, recycling of integrin α5β1, cMET and TfnR was determined in the presence of R59022 (10 μM) or DMSO control as indicated. Values are mean ± SEM, n=3; ***green versus black are p<0.001, ANOVA.

3.2.6 Recipient cells require RCP and DGKα-dependent signalling to respond to mutp53-EVs

The migratory and invasive behaviour of mutp53-expressing cells depends on RCP- and DGKα-mediated α5β1 integrin recycling. Thus, we sought to test whether the transfer of mutp53's migratory phenotype depends on such a pathway. Addition of R59022 to, or knock-down of RCP in, recipient cells (Figure 3-10 A) completely abolished the ability of p53^{R273H}-EV to influence cell migration into scratch-wounds (Figure 3-10 B), strongly indicating that EVs released by mutp53-expressing cells evoke migratory characteristics in recipient cells by upregulating RCP- and DGKα-dependent recycling.

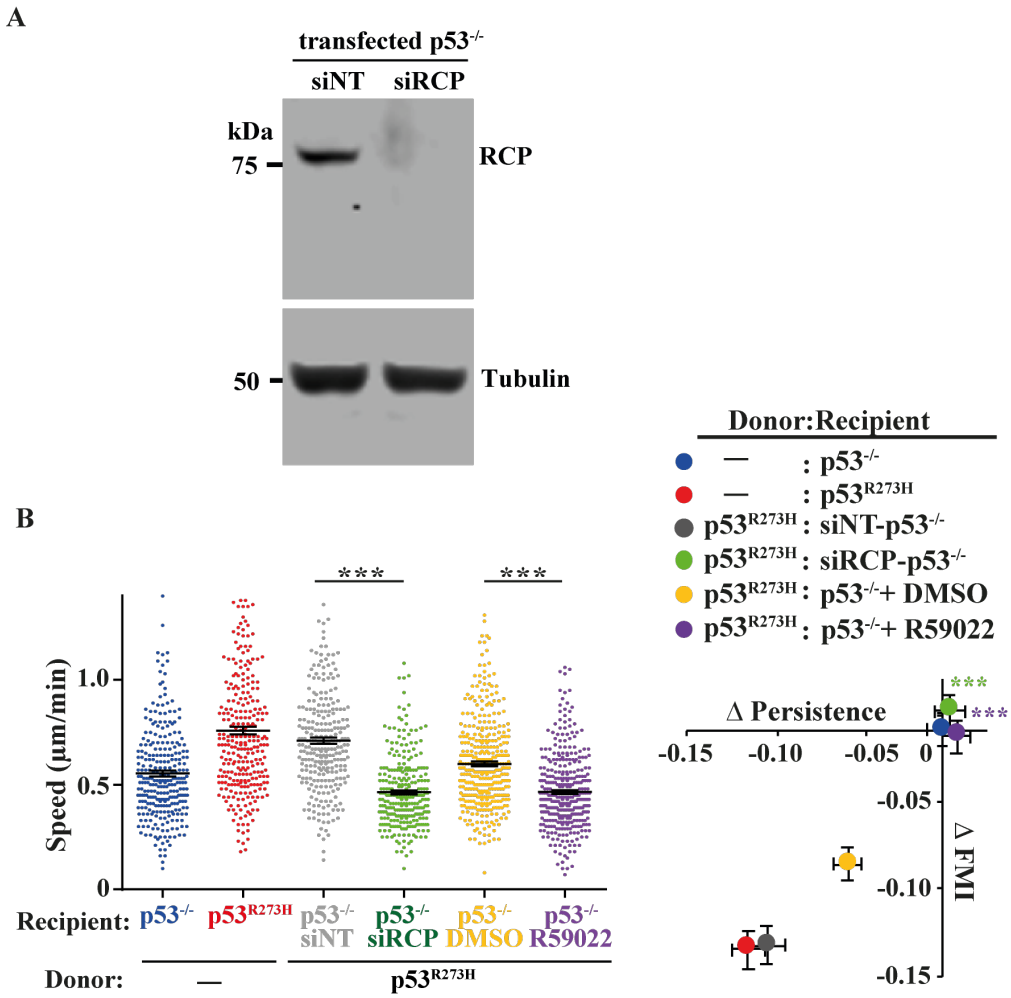

Figure 3-10- Migration mediated by mutp53-EVs depends on RCP and DGKα functions in p53$^{-/-}$ cells. (A) Validation of the knockdown of RCP in recipient H1299-p53$^{-/-}$ cells by western blotting with an antibody recognising RCP, and tubulin as loading control. (B) H1299-p53$^{-/-}$ cells recipient cells were pre-treated with EVs derived from H1299-p53^{R273H} donor cells. Recipient cells were then transfected with siRNAs targeting RCP (siRCP) or a non-targeting control (siNT), and the characteristics (ΔPersistence, ΔFMI and speed) of their migration into scratch-wounds was determined in the presence and absence of a DGK inhibitor (R59022; 10 µM) or DMSO control. Values are mean ± SEM; n > 273 cells; *** in right panel, and ***green versus black and ***purple versus yellow are $p < 0.001$, Mann-Whitney test.

3.2.7 Podocalyxin is a mutp53-regulated EV cargo

We proposed that altered EV composition might be responsible for intercellular transfer of mutp53's migratory gain-of-function. Thus, we used SILAC-based proteomics to compare the proteome of EVs released by H1299-p53^{R273H} and H1299-p53$^{-/-}$ cells which had been previously labelled with light and heavy SILAC amino acids respectively (Figure 3-11 A). Of the 428 proteins that were unambiguously identified, only 4 of these differed significantly between p53^{R273H}- and p53$^{-/-}$-EVs. Podocalyxin, a sialomucin associated with cancer aggressiveness (Wang et al., 2017), was significantly reduced in p53^{R273H}-EV (Figure 3-11 B), and the ability of mutp53s to supress EV-associated podocalyxin was confirmed by western blotting (Figure 3-11 C). Together, these data indicate that the quantity of podocalyxin in EVs is suppressed by mutp53.

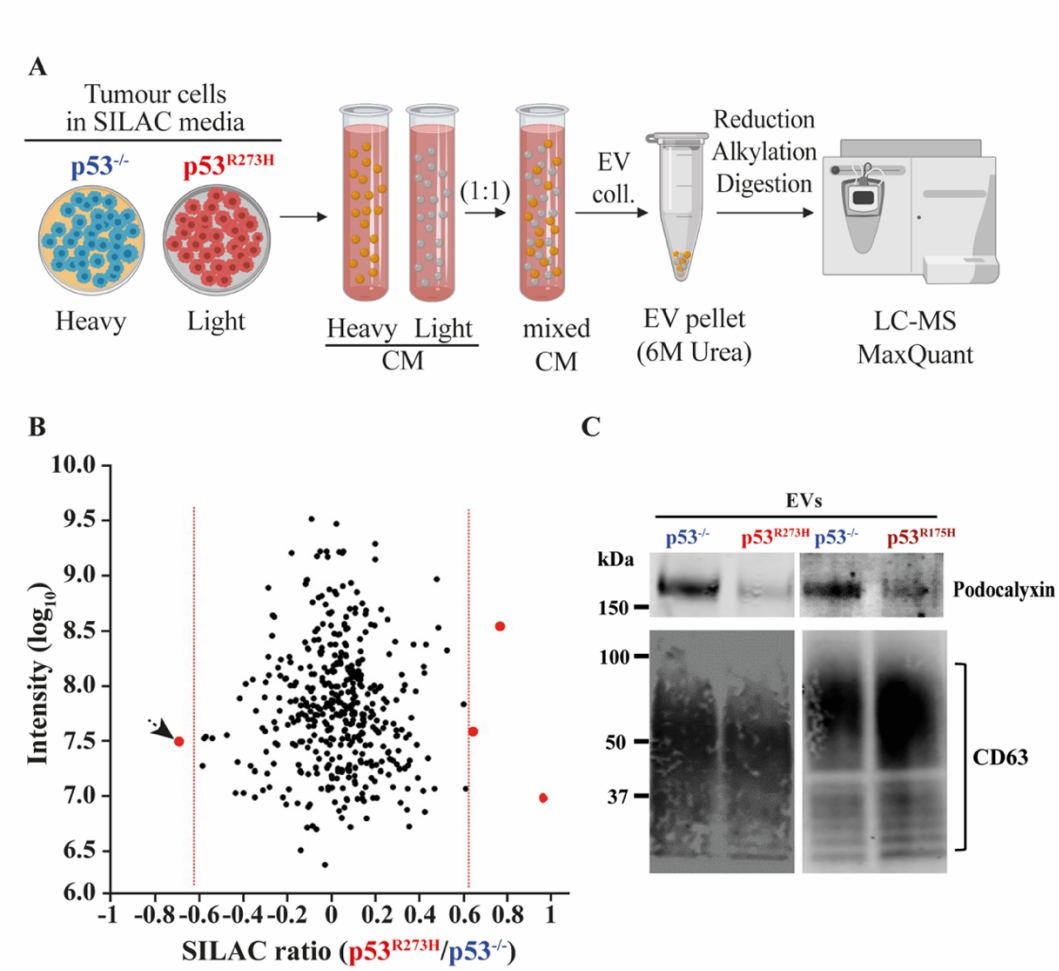

Figure 3-11- mutp53 controls EV-associated podocalyxin levels.
(A) Schematic of the protocol for analysis of EV-associated proteome by SILAC-MS. (B) H1299-p53$^{-/-}$ and H1299-p53^{R273H} cells were SILAC-labelled with heavy and light amino acids respectively. Conditioned media were collected from labelled cells, EVs purified from these using differential centrifugation, and their proteome analysed by mass spectrometry. Scatter plot indicates the SILAC ratio H1299-p53^{R273H}/H1299-p53$^{-/-}$ (Log_2 scale) of each protein identified in the EV proteome. Proteins to the left and right of the red dotted lines are significantly down and up-regulated respectively in EVs from H1299-p53^{R273H} cells (Significance B statistic test, false discovery rate of 5%, Perseus software). These data are extracted from the table presented in Appendix 1. Arrow highlights podocalyxin. (C) EVs from H1299-p53−/−, H1299-p53R273H, and H1299-p53R175H cells were analysed by western blotting with an antibody recognising podocalyxin. CD63 was used as sample control.

Although differential centrifugation-based methods are the most commonly used for EV purification from cell culture media, these approaches may yield non-EV components, such as large protein aggregates. To further establish whether podocalyxin is integrally associated with EVs (and not present as a protein aggregate or other contaminant), we performed sucrose density gradients of p53$^{-/-}$- and p53^{R273H}-EV preparations, collected fractions with increasing density from these gradients, and evaluated the quantity of podocalyxin and the EV marker CD63 in these fractions by western blotting (Figure 3-12 A). Podocalyxin precisely co-migrated with CD63 at a density of 1.1 – 1.15 g/mL (consistent with the established density of exosomes (Gupta et al., 2018)), indicating that it is integrally associated with EV (Figure 3-12 B). Furthermore, the fact that CD63 is considered to be an exosomal marker indicates the likelihood of podocalyxin being associated with exosomes.

Importantly, podocalyxin levels in CD63-positive fractions were decreased in p53^{R273H}-EV by comparison with p53$^{-/-}$-EV, emphasizing the role of mutp53 in suppressing EV-associated podocalyxin levels.

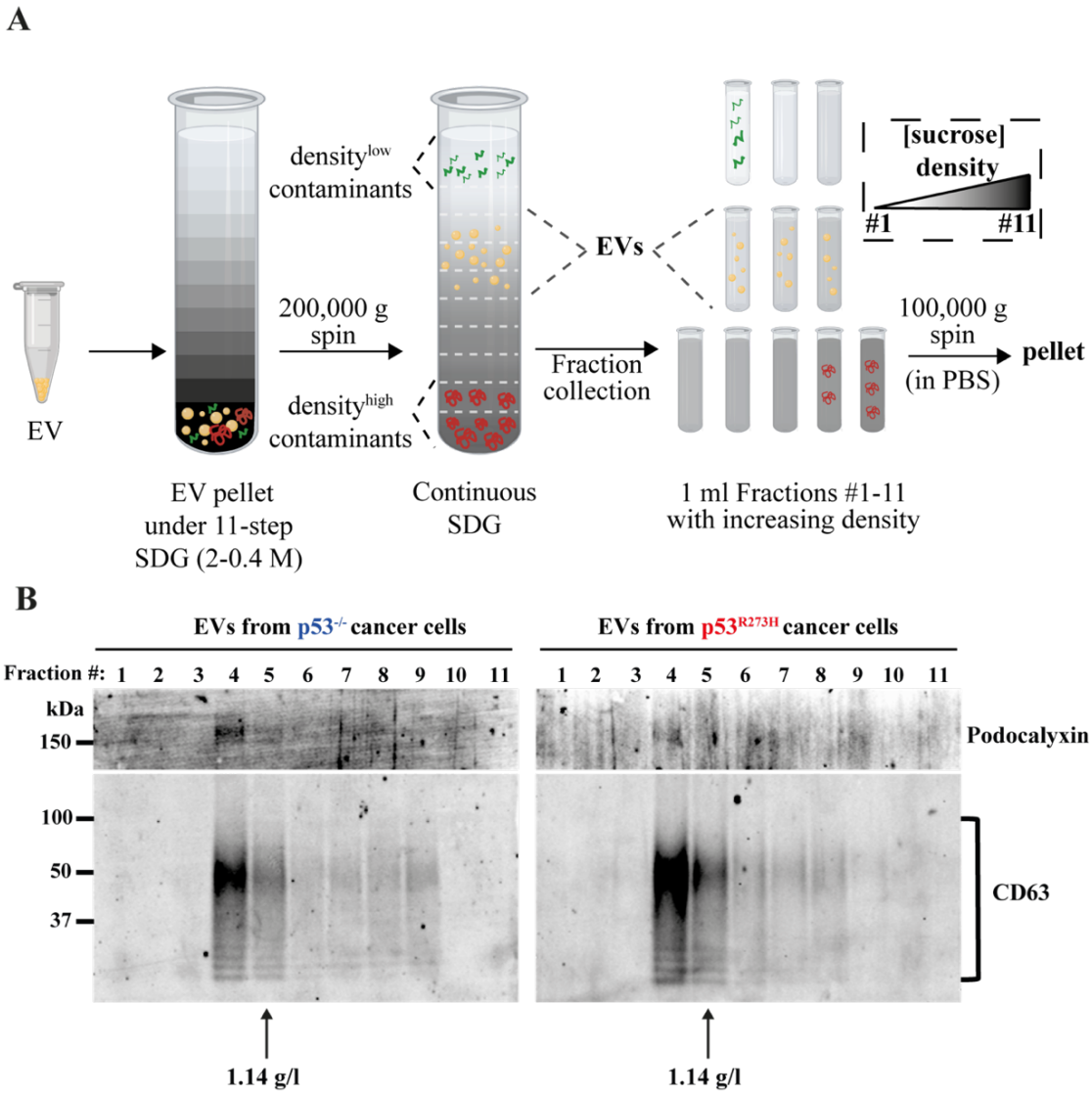

Figure 3-12- EV-associated podocalyxin co-sediments with the EV marker CD63 in sucrose density gradients (SDGs)
(A) Schematic with SDG protocol. (B) EVs were collected by differential centrifugation of media conditioned by H1299-p53$^{-/-}$ and H1299-p53^{R273H} cells and characterised using sucrose density gradient centrifugation followed by western blotting for PODXL and the EV marker, CD63.

3.2.8 mutp53 suppresses podocalyxin expression in cancer cells

Our observation that podocalyxin was suppressed in EVs released by mutp53-expressing cells led us to investigate whether mutp53s regulate podocalyxin expression at the cellular level. To this end, we assessed podocalyxin levels in lysates from H1299 cells with different p53 status. qPCR and western blotting analyses showed respectively that podocalyxin mRNA and protein levels in cancer cells were suppressed by expression of mutp53s (Figure 3-13 A, B). By contrast, induction of p53^{wt} did not affect podocalyxin levels in H1299 cells

(Figure 3-13 C), suggesting that the ability to regulate podocalyxin expression is a gain-of-function for mutp53s.

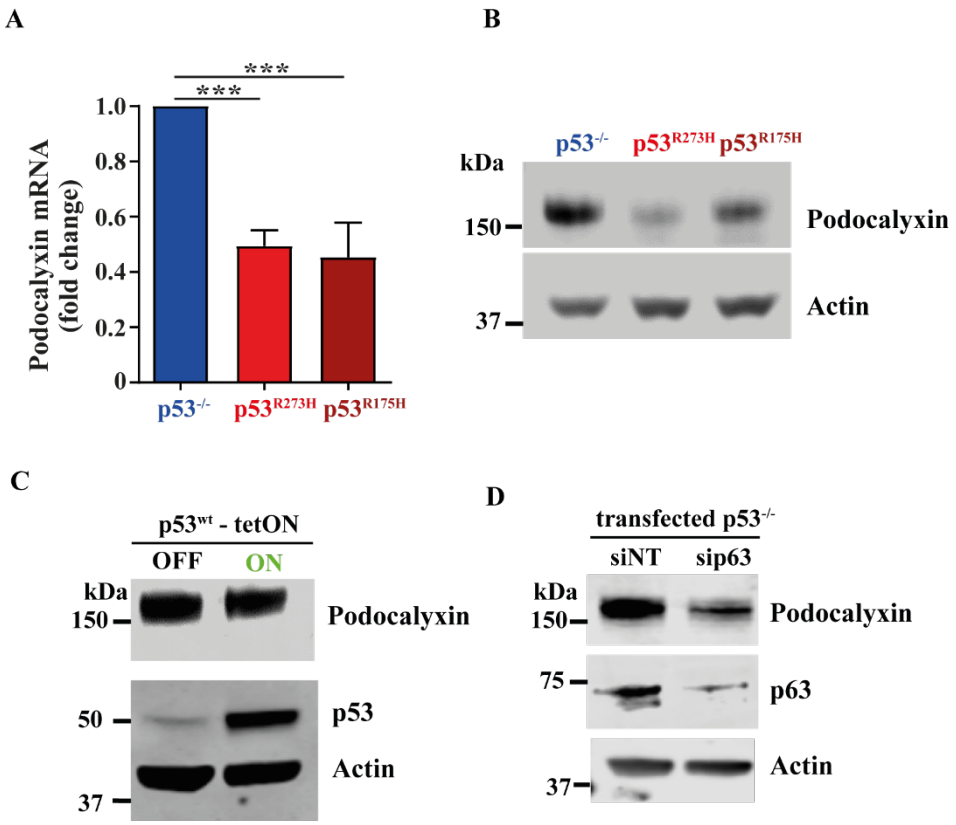

Figure 3-13- mutp53-p63 axis control cellular podocalyxin levels.
(A) H1299-p53$^{-/-}$, H1299-p53^{R273H} and H1299-p53^{R175H} cells were lysed and assayed for the levels of mRNA encoding podocalyxin using qPCR. Values are mean ± SEM, n = 3; *** is $p < 0.001$ unpaired t-test (B) H1299-p53$^{-/-}$, H1299-p53^{R273H} and H1299-p53^{R175H} cells were lysed and assayed for the levels of podocalyxin protein by western blotting with an antibody recognising podocalyxin. Actin was used as load control. n=3 (C) H1299-p53tetON cells were incubated in the presence or absence of doxycycline and cellular levels of wild-type p53 and podocalyxin were determined by western blotting using antibodies specific for these proteins. Actin was used as loading control. n=3 (D) H1299-p53$^{-/-}$ cells were transfected with siRNAs targeting p63 (sip63) or a non-targeting control (siNT). 48 hr following transfection, the levels of podocalyxin and p63 were determined by Western blotting. Actin was used as loading control. n=2

We and others have previously shown that mutant p53s exert migratory GOF by associating with and inhibiting p63 (Muller et al., 2014, 2009). Therefore, we knocked-down p63 in H1299-p53$^{-/-}$ cells and found that this suppressed cellular podocalyxin levels to a similar extent as did expression of mutp53s (Figure 3-13 D). This suggests that podocalyxin expression is under the control of p63 and mutp53 likely suppresses podocalyxin levels in cells by interfering with p63 function.

3.2.9 Podocalyxin levels in EVs dictate the intercellular transfer of mutp53's GOF phenotype

To investigate whether suppression of EV-associated podocalyxin underpins the transfer of mutant p53's GOF phenotypes, we increased podocalyxin levels in p53^{R273H}-EV by

expressing podocalyxin-GFP in H1299-p53^{R273H} (Figure 3-14 A). This did not influence the quantity nor size of p53^{R273H}-EV (Figure 3-15 A, B). Nonetheless, we assessed the ability of these EVs to affect migration of recipient cells. Over-expression of podocalyxin-GFP in H1299-p53^{R273H} cells significantly impaired the ability of p53^{R273H}-EV to affect the FMI, directionality, and migration speed of recipient H1299-p53$^{-/-}$ cells into scratch-wounds (Figure 3-16 B). Likewise, EVs purified from podocalyxin-GFP overexpressing H1299-p53$^{-/-}$ cells were ineffective in driving α5β1 and cMET recycling in recipient cells (Figure 3-17).

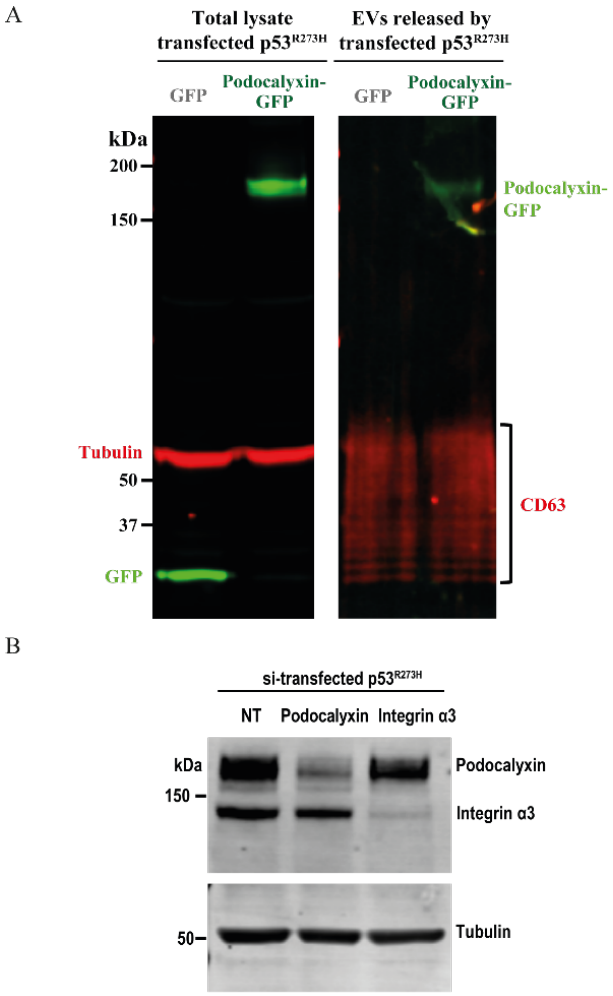

Figure 3-14- Manipulation of levels of EV-associated cargoes.
(A) H1299-p53^{R273H} cells were transfected with podocalyxin-GFP or GFP. Conditioned media was collected from these cells and EVs purified from these using differential centrifugation. The levels of podocalyxin- GFP (green) and GFP (red) in these cells and the EVs from them were determined by western blotting. Tubulin and CD63 were used as loading controls for the cell extracts and EV preparations respectively. (B) H1299 cells were transfected with siRNA targeting podocalyxin, integrin or a non- targeting control (NT). 72 hr following transfection, cells were lysed and the levels of the indicated proteins determined by immunoblotting with tubulin as a loading control.

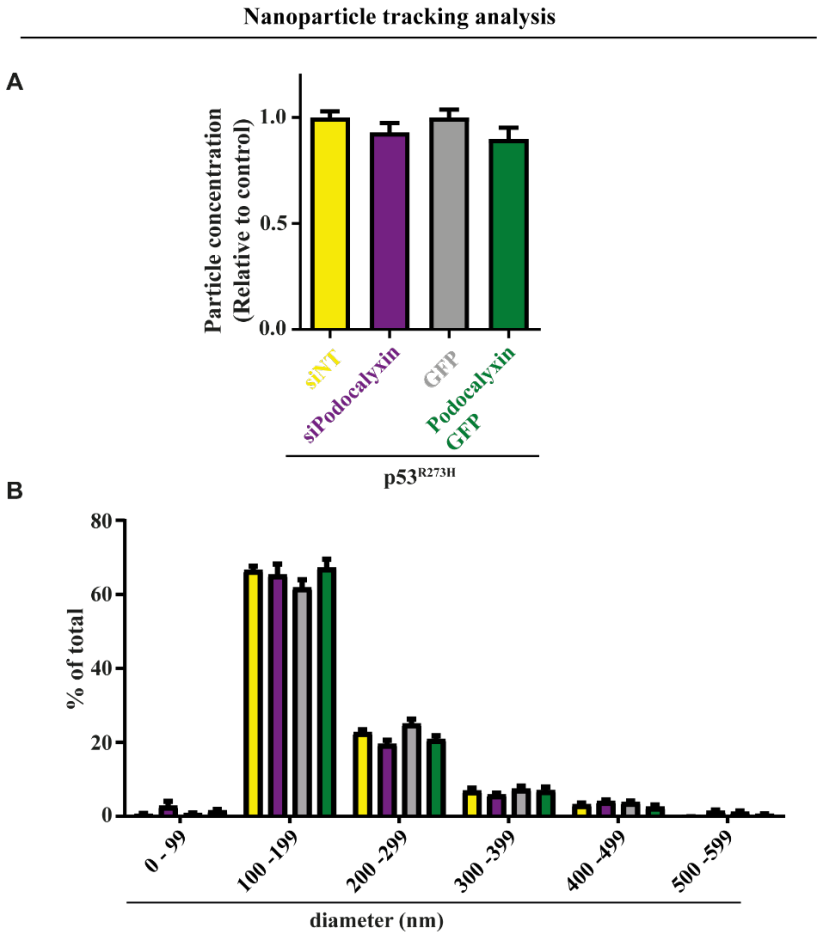

Figure 3-15- Manipulation of EV-associated podocalyxin levels do not influence EV production. H1299-p53^{R273H} cells were transfected with siRNAs targeting podocalyxin (siPodocalyxin), a non-targeting control (siNT), GFP or podocalyxin-GFP. EVs were collected from these cells by differential centrifugation and Nanosight particle tracking used to determine their particle concentration (A) and size distribution (B). Values are mean ± SEM. n=3.

In many reports, it is the presence (not the absence) of podocalyxin and other sialomucins which has been linked to cancer progression (Snyder et al., 2015). Thus, we were interested in determining the consequences of reducing podocalyxin levels in H1299 cells to levels below those effected by expression of mutp53. To this end, we collected EVs from H1299-p53^{R273H} cells in which podocalyxin had been knocked-down (Figure 3-14 B). Even though the quantity or size of p53^{R273H}-EV was not affected by loss of podocalyxin (Figure 3-15 A, B), the ability of these EVs to modulate migratory characteristics (Figure 3-16 B) and receptor recycling (Figure 3-17) in H1299-p53$^{-/-}$ cells was abolished. By contrast, knock-down of α3β1 integrin (Figure 3-14 B), the most abundant EV cargo, which was similarly expressed in p53^{R273H}- and p53$^{-/-}$-EVs, did not oppose the ability of p53^{R273H}-EV to drive migration of recipient cells (Figure 3-16 A).

Taken together, these data indicate that podocalyxin is required for EV to influence receptor recycling and migration in recipient cells, and that mutp53s maintain the levels of EV-associated podocalyxin within a range that allows this to occur.

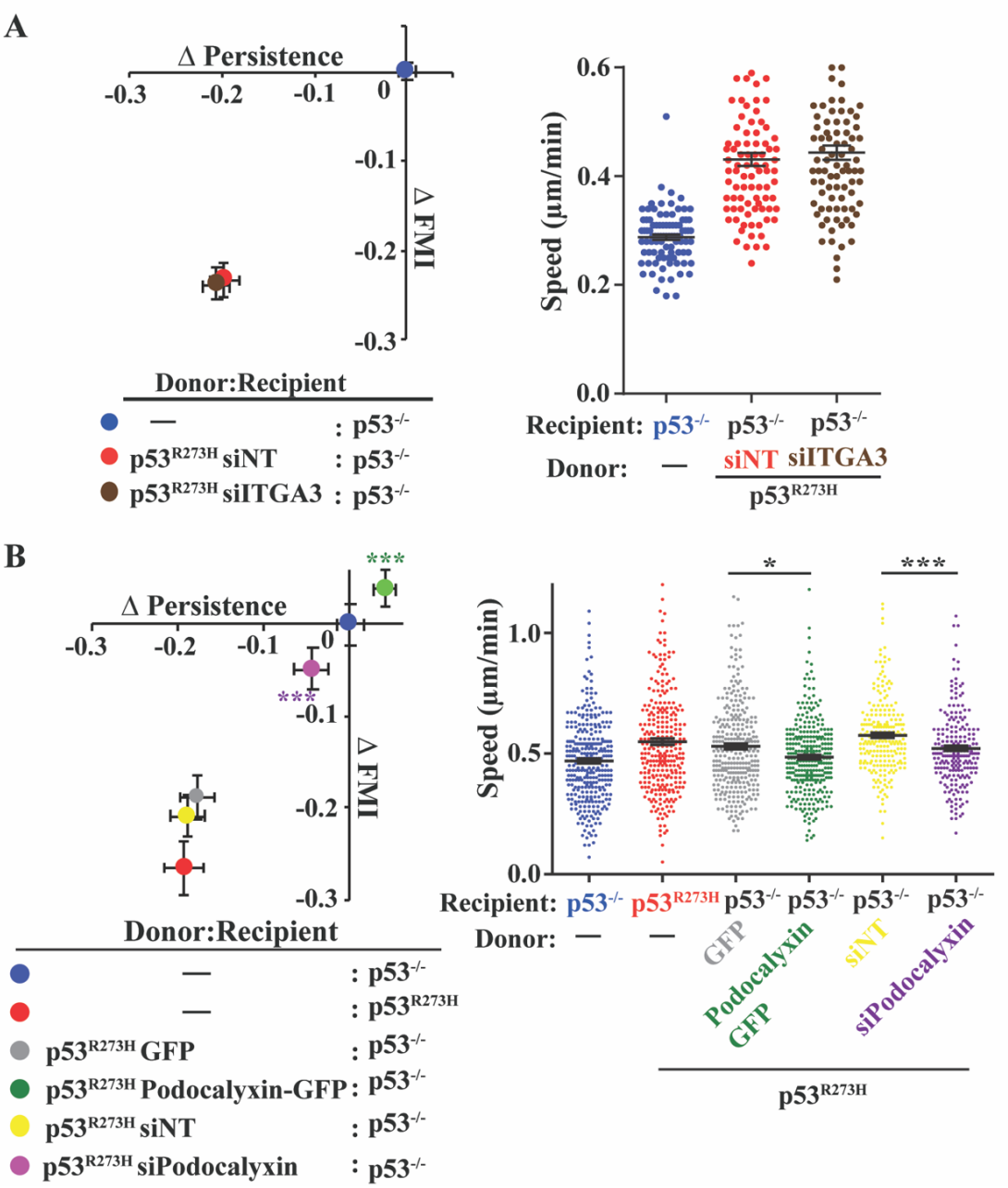

Figure 3-16- Manipulation of EV-associated podocalyxin impairs the ability of mutp53-EVs to influence migration of p53$^{-/-}$ cells.

(A) H1299-p53^{R273H} donor cells were transfected with siRNAs targeting α3 integrin (siITGA3) or a non-targeting control (siNT). EVs were collected from these donor cells by differential centrifugation and incubated with H1299-p53$^{-/-}$ recipient cells for 72 hr. Recipient cells were re-plated and characteristics of their migration into scratch-wounds determined as for Figure 3-2D n>100 cells. (B) Donor H1299-p53^{R273H} cells were transfected with GFP, or podocalyxin-GFP, siRNAs targeting podocalyxin (siPodocalyxin) or non-targeting control (siNT). EV collected from these cells were used to treat H1299-p53$^{-/-}$ recipient cells for 72 hours before the cells were re-plated and migratory characteristics of these cells into scratch-wounds were determined as for Figure 3-2D. Values are mean ± SEM. n > 317 cells; ***green versus black, and ***purple versus yellow are $p < 0.001$, Mann–Whitney test. In the right panel, *** is $p < 0.001$ and * is $p < 0.05$, Mann–Whitney.

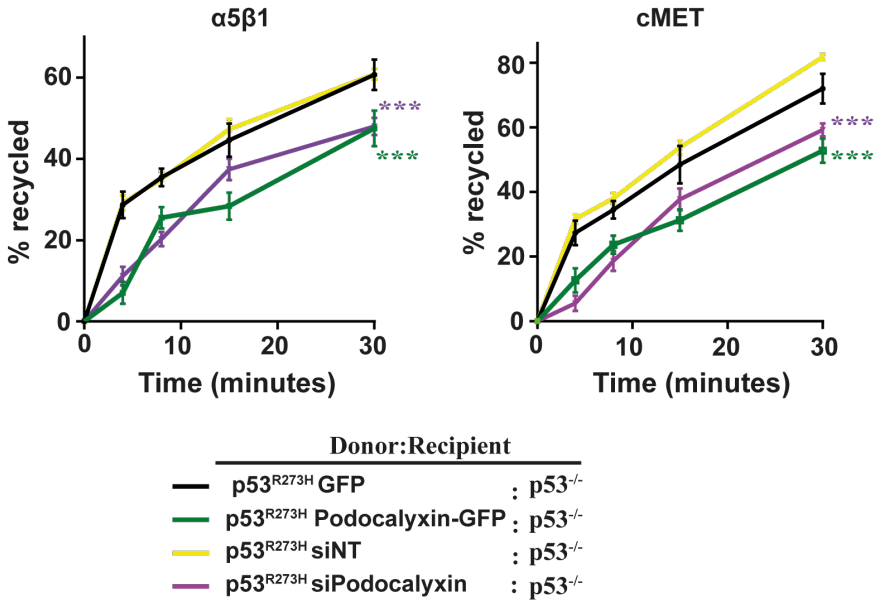

Figure 3-17- Manipulation of EV-associated podocalyxin impairs the ability of mutp53-EVs to influence receptor recycling in p53$^{-/-}$ cells.
Donor H1299-p53^{R273H} cells were transfected with GFP, or podocalyxin-GFP, siRNAs targeting podocalyxin (siPodocalyxin) or non-targeting control (siNT). EVs collected from these cells were used to treat H1299-p53$^{-/-}$ recipient cells for 72 hours before the cells were re-plated and recycling rates of α5β1 and cMET were determined. Values are mean ± SEM; n=3; ***green versus black, and ***purple versus yellow are $p < 0.001$, Mann–Whitney test.

3.2.10 Rab35 interacts with podocalyxin to drive its sorting to the plasma membrane

In polarised epithelial cells, podocalyxin binds to the small GTPase Rab35 and this association controls podocalyxin trafficking to the plasma membrane (Klinkert et al., 2016). This led us to investigate whether podocalyxin interacts with Rab35 in cancer cells. We transfected H1299 cells (p53$^{-/-}$ or p53^{R273H}) with GFP-Rab35 and assessed its co-immunoprecipitation with podocalyxin using western blotting (Figure 3-18). Rab35 and podocalyxin co-immunoprecipitated to an extent that is commensurate with the expression levels of podocalyxin in p53$^{-/-}$ and mutp53-expressing cells, indicating that podocalyxin and Rab35 interact in cancer cells.

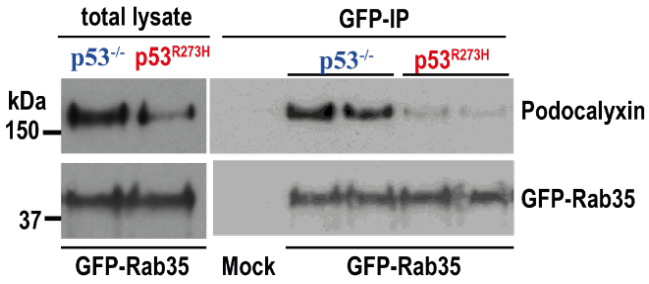

Figure 3-18- Podocalyxin co-immunoprecipitates with Rab35.
H1299 (p53$^{-/-}$ or p53^{R273H}) cells were transfected with GFP-Rab35 or mock transfected (no plasmid). GFP-tagged proteins were immunoprecipitated using an antibody recognising GFP conjugated to magnetic beads. Rab35 and podocalyxin were detected in the lysates (total) and immunoprecipitates (GFP-IP) using western blotting; n=3

Rab35 has previously been shown to drive sorting of podocalyxin to the plasma membrane (Klinkert et al., 2016; Mrozowska and Fukuda, 2016). Thus, we used cell surface biotinylation followed by streptavidin pulldown and western blotting approaches to investigate whether Rab35 controls levels of plasma membrane-exposed podocalyxin in mutp53-expressing cancer cells (Figure 3-19 A, B). Whilst knockdown of Rab35 in H1299-p53^{R273H} cells (using SMARTPool siRNAs, an individual siRNA oligo or CRISPR gene editing) did not significantly affect the total levels of cellular podocalyxin, it drastically reduced podocalyxin expression at the cell surface, indicating that Rab35 drives podocalyxin sorting to the plasma membrane in mutp53-expressing cells.

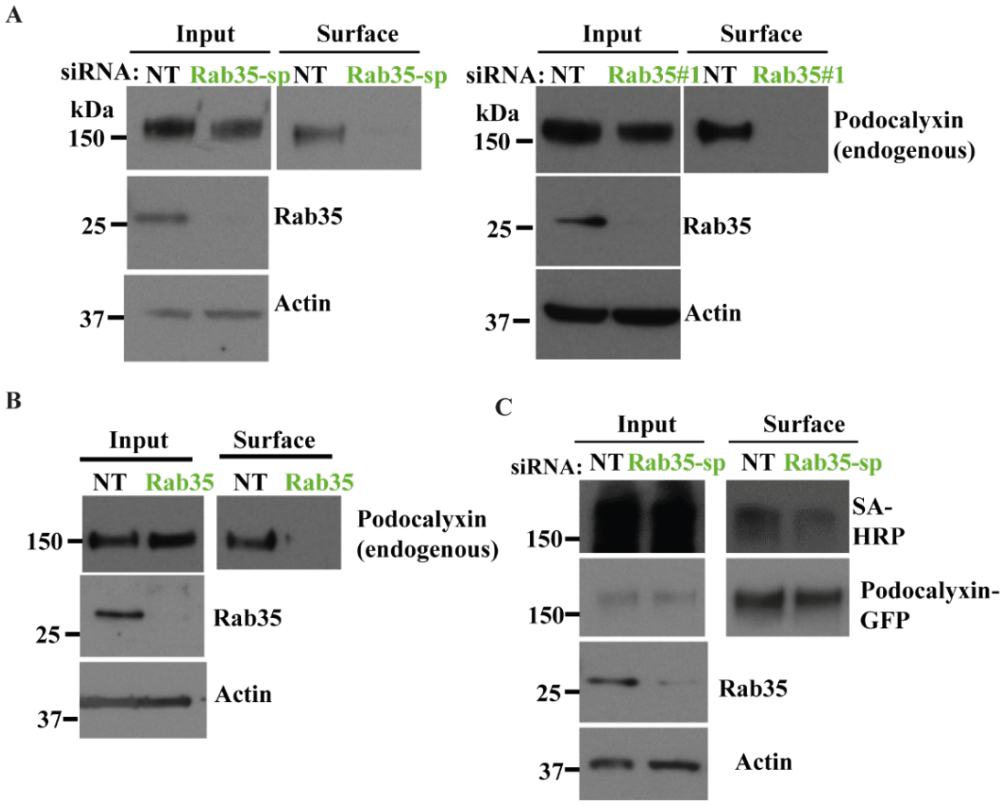

Figure 3-19- Rab35 promotes podocalyxin sorting to the cell surface.
(A) H1299-p53^{R273H} cells were transfected with siRNAs targeting Rab35 (SMARTPool (Rab35-sp) or an individual siRNA (Rab35#1)) or a non-targeting control (NT). Cell surface proteins were labelled with NHS-Biotin at 4 °C and precipitated using streptavidin beads. Labelled (surface) and total (input) podocalyxin were then visualised by western blotting with actin as sample control. n=3. (B) H1299 cells in which Rab35 had been disrupted by CRISPR or non-targeting control (NT) were used. Cells were then treated with sulfo-NHS-Biotin at 4^{0}C to label proteins exposed at the plasma membrane. Labelled cells were lysed, and labelled proteins precipitated using streptavidin beads. Podocalyxin levels in labelled surface (surface) and total (input) then visualised by western blotting with antibodies recognising podocalyxin. Actin was used as loading control. n=2 (C) H1299-p53^{R273H} cells were transfected with GFP-podocalyxin in combination with SMARTPool siRNAs targeting Rab35 (Rab35-sp) or a non-targeting control (NT). Cells were then treated with sulfo-NHS-Biotin at 4^{o}C to label proteins exposed at the plasma membrane. Labelled cells were lysed, and GFP-PODXL immunoprecipitated using magnetic beads coupled to an antibody recognising GFP (GFP- IP). Biotinylated GFP-podocalyxin was then visualised by western blotting with labelled streptavidin. Actin was used as loading control.

To further investigate the role of Rab35 in podocalyxin trafficking, we knocked-down Rab35 in H1299-p53^{R273H} cells expressing podocalyxin-GFP and used immunofluorescence to

assess its colocalisation with the late endosomal/MVE marker, CD63 (Figure 3-20 A). Rab35 knockdown led to increased colocalisation between podocalyxin and CD63, suggesting that, upon Rab35 loss, podocalyxin accumulates in CD63-positive compartments.

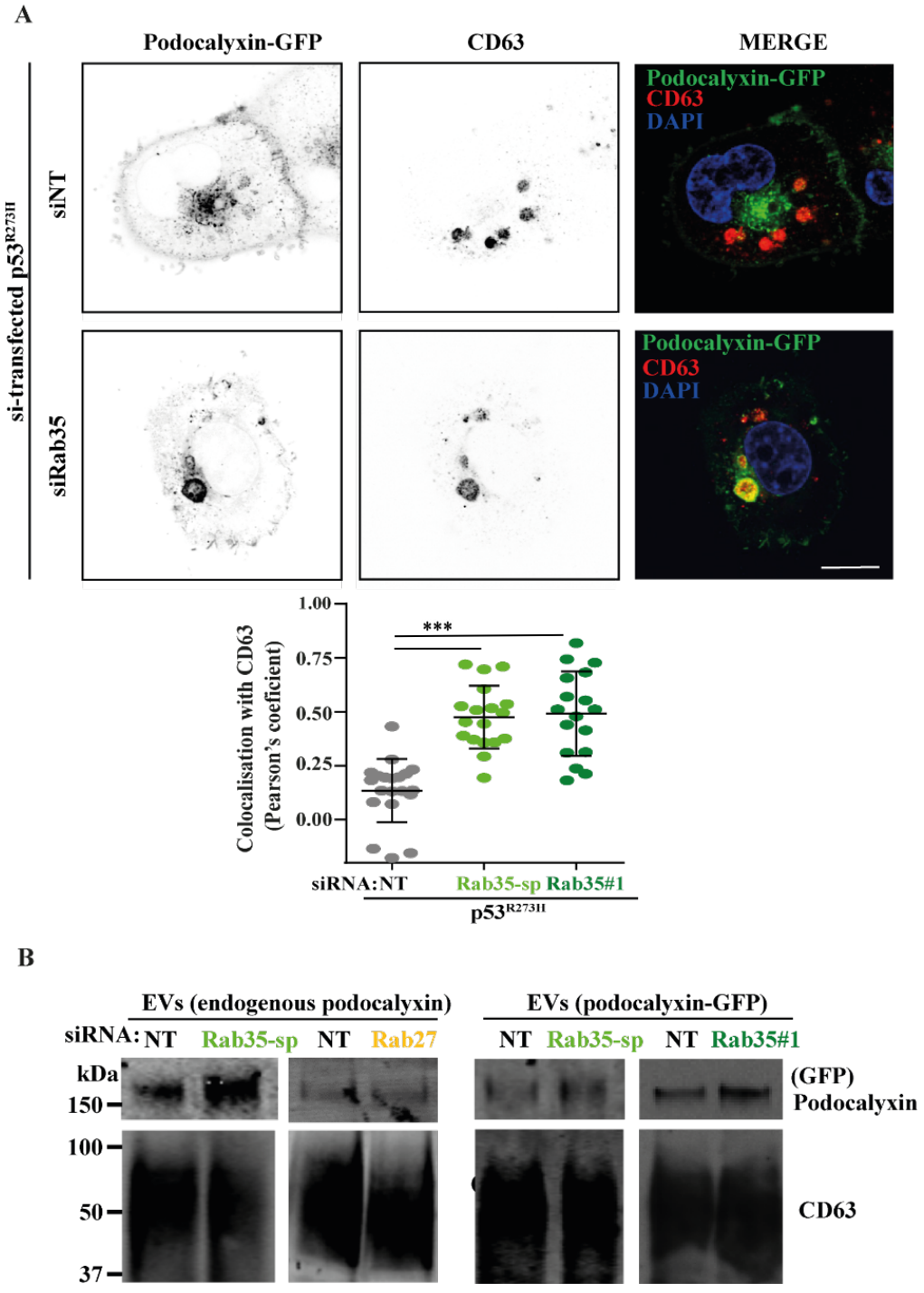

Figure 3-20- Rab35 loss in mutp53-expressing cells leads to accumulation of podocalyxin in CD63-positive organelles and in EVs.
(A) H1299-p53^{R273H} cells were transfected with siRab35-sp, siRab35#1, or siNT. Cells were fixed and podocalyxin (green) and CD63 (red) were visualised by immunofluorescence. Bar, 15 µm. ImageJ was used to quantify co localised pixels as determined by the Costes method. Values are mean ± SEM. n > 16 cells. *** is $p < 0.001$, Mann–Whitney. (B) H1299-p53^{R273H} cells were transfected with siRNAs targeting Rab35 (Rab35-sp or Rab35#1), Rab27a/Rab27b (Rab27) or a non-targeting control (NT) ± GFP-podocalyxin. EVs were purified by differential centrifugation. Western blotting was used to determine EV levels of podocalyxin and GFP-Podocalyxin with CD63 as sample control. n=3

3.2.11 Loss of podocalyxin-Rab35 interaction drives accumulation of podocalyxin in CD63-positive compartments

Mutation of residues in the juxtamembrane region of the cytoplasmic tail of podocalyxin which have previously been found to be important for podocalyxin-Rab35 association (Val496 and Tyr500), were shown to reduce co-immunoprecipitation and co-localisation between the two proteins (Klinkert et al., 2016) (Figure 3-21 A). Indeed, mutation of podocalyxin's Val496 and Tyr500 to alanine reduced both co-immunoprecipitation between Rab35 and GFP-podocalyxin in H1299-p53^{R273H} cells (Figure 3-21 B). Thus, we evaluated the colocalisation between podocalyxin$^{V486A/Y500A}$-GFP and CD63 in H1299-p53^{R273H} cells (Figure 3-22 A). This showed that podocalyxin$^{V486A/Y500A}$ colocalised more efficiently with CD63 than podocalyxin^{wt}. These data indicate that the loss of podocalyxin-Rab35 association is sufficient to oppose its delivery to the plasma membrane and thus drive podocalyxin accumulation in CD63-positive compartments.

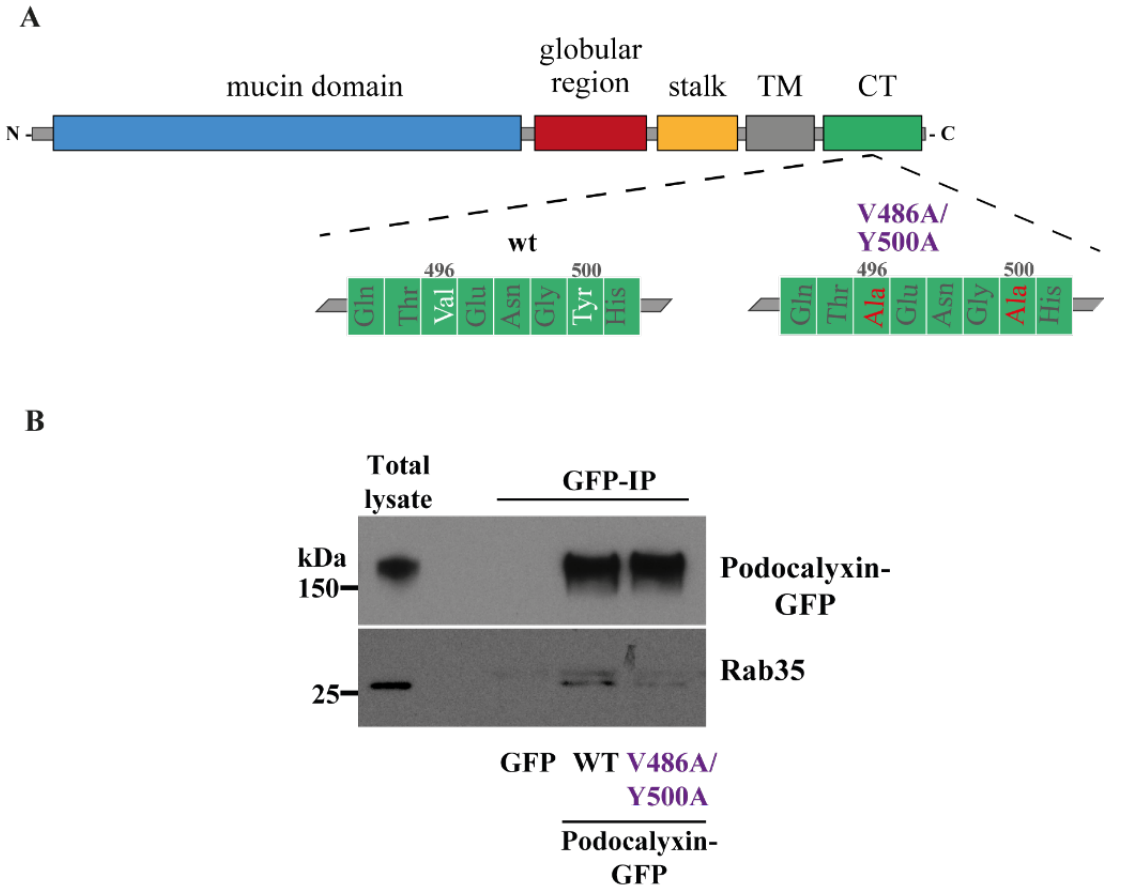

Figure 3-21 - Podocalyxin$^{V486A/Y500A}$ does not co-immunoprecipitate with Rab35.
(A) Schematic with comparison between the amino acid sequences of podocalyxin^{wt} and Podocalyxin$^{V486A/Y500A}$. (B) H1299-p53^{R273H} cells were transfected with GFP, GFP-podocalyxin or GFP-podocalyxin$^{V486A/Y500A}$. GFP-tagged proteins were immunoprecipitated using an antibody recognising GFP conjugated to magnetic beads. GFP-podocalyxin and Rab35 was detected in the lysates (total) and immunoprecipitates (GFP-IP) using western blotting; n=3

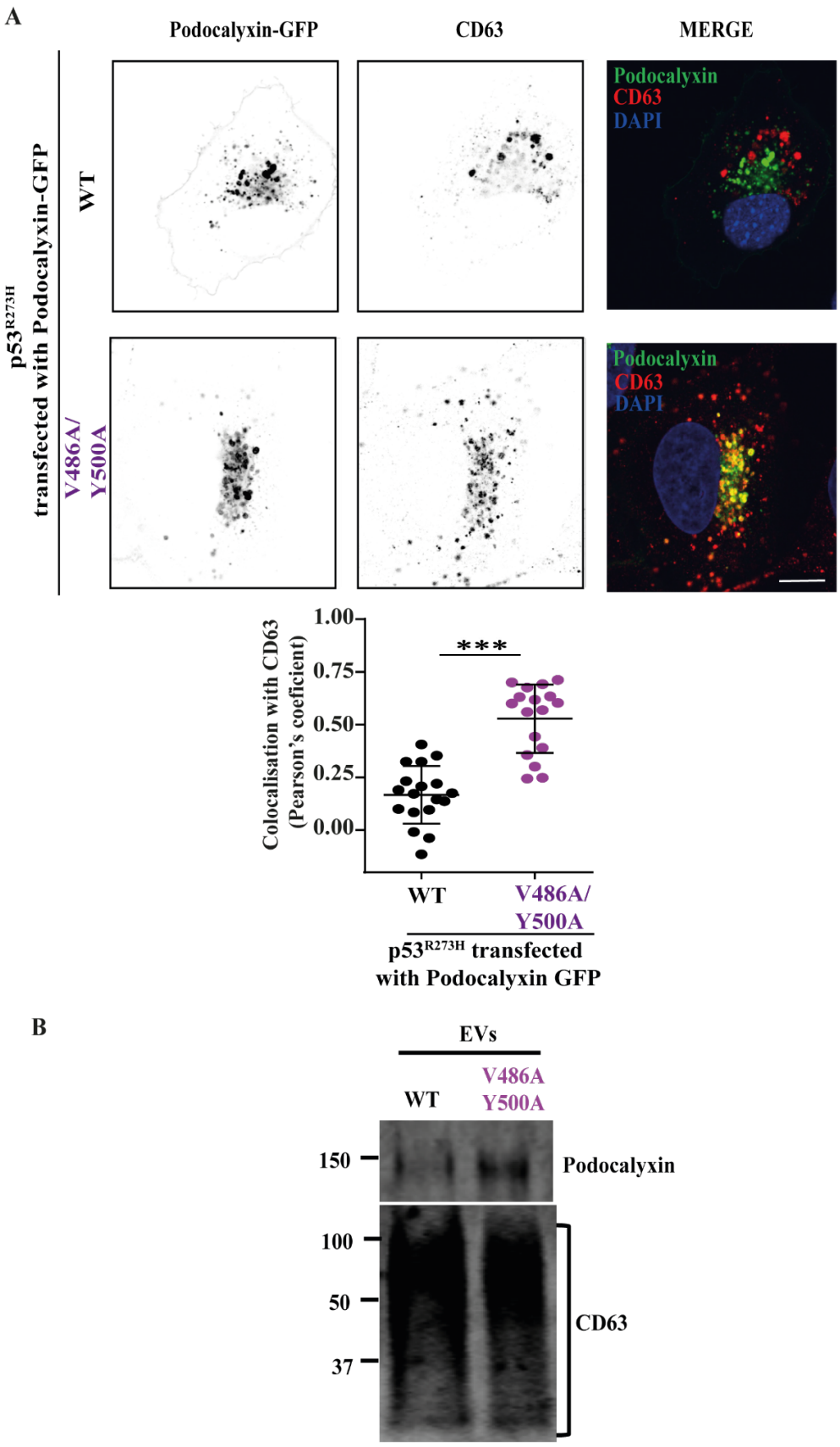

Figure 3-22- Podocalyxin$^{V486A/Y500A}$ accumulates in CD63-positive organelles and in EVs.
(A) H1299-p53^{R273H} cells were transfected with GFP-PODXL or GFP-PODXLV486A/Y500A. Cells were fixed and podocalyxin (green) and CD63 (red) were visualised by immunofluorescence. Bar, 15 µm. ImageJ was used to quantify co localised pixels as determined by the Costes method. Values are mean ± SEM. n > 16 cells. *** is $p < 0.001$, Mann–Whitney. (B) H1299-p53^{R273}H cells were transfected with GFP-podocalyxin or GFP-podocalyxin$^{V486A/Y500A}$. EVs were collected by differential centrifugation. Western blotting was used to determine EV-associated GFP-podocalyxin levels with CD63 as a sample control.

3.2.12 Loss of podocalyxin-Rab35 interaction leads to accumulation of podocalyxin in EVs

As we had demonstrated that Rab35 functions to (in particular via its ability to bind to podocalyxin) regulate podocalyxin trafficking, we were interested in evaluating the effect of Rab35 loss on the levels of EV-associated podocalyxin. To do this, we knocked down Rab35 in H1299-p53^{R273H} and collected EVs from these cells. NTA analysis showed that Rab35 loss did not affect EV number nor size (Figure 3-23 A). However, knockdown of Rab35 resulted in increased levels of podocalyxin associated with EVs (Figure 3-20 B). We then took advantage of the mutant of podocalyxin with impaired ability to bind to Rab35 to examine whether podocalyxin-Rab35 association regulates the levels of EV-associated podocalyxin. For this, we collected EVs from H1299-^{p53R273H} cells which had been transfected with podocalyxin-GFP or podocalyxin$^{V486A/Y500A}$ -GFP and compared the levels of these proteins associated with EVs. GFP-podocalyxin$^{V486A/Y500A}$ was sorted more efficiently to EVs than GFP-podocalyxin^{wt} (Figure 3-22B). These data indicate that Rab35 regulates podocalyxin levels in EVs and that this is likely to depend on its association with podocalyxin.

Because Rab27 is known to play a role in MVB dynamics and exosome release (Ostrowski et al., 2010), we also knocked down this Rab GTPase to determine whether this influences the sorting of podocalyxin to EVs. Surprisingly, combined knockdown of Rab27a and b, did not affect EV-associated podocalyxin levels (Figure 3-20 B) nor the number and size of EVs (Figure 3-23 A) released from H1299-p53^{R273H} cells. Together, these data suggest that Rab35 controls the levels of podocalyxin associated with EVs, but it does not regulate the number nor size of EVs released by H1299-^{p53R273H} cells. Furthermore, these data indicate that Rab27s do not regulate EV release from H1299 cells nor podocalyxin sorting into EVs.

3.2.13 Loss of Rab35 impairs ability of EVs to mediate intercellular transfer of mutp53's migratory GOF

As loss of Rab35 led to increased levels of EV-associated podocalyxin, we reasoned that Rab35 function in mutp53-expressing cells may be required for the production of phenotype-altering EVs. Consistently, knockdown of Rab35 opposed the ability of H1299- p53^{R273H} to release EVs capable of influencing the migration of recipient H1299$^{-/-}$ cells (Figure 3-23 B). By contrast, knock-down of Rab27a and b in donor cells, which did not influence podocalyxin sorting to EVs, did not oppose the ability of EVs released by H1299-p53^{R273H} cells to influence the migratory behaviour of recipient cells (Figure 3-23 B). Together, these

data suggest that Rab35 (but not Rab27) function is required for the production of EVs capable of transferring mutp53's migratory gain-of-function to recipient cells.

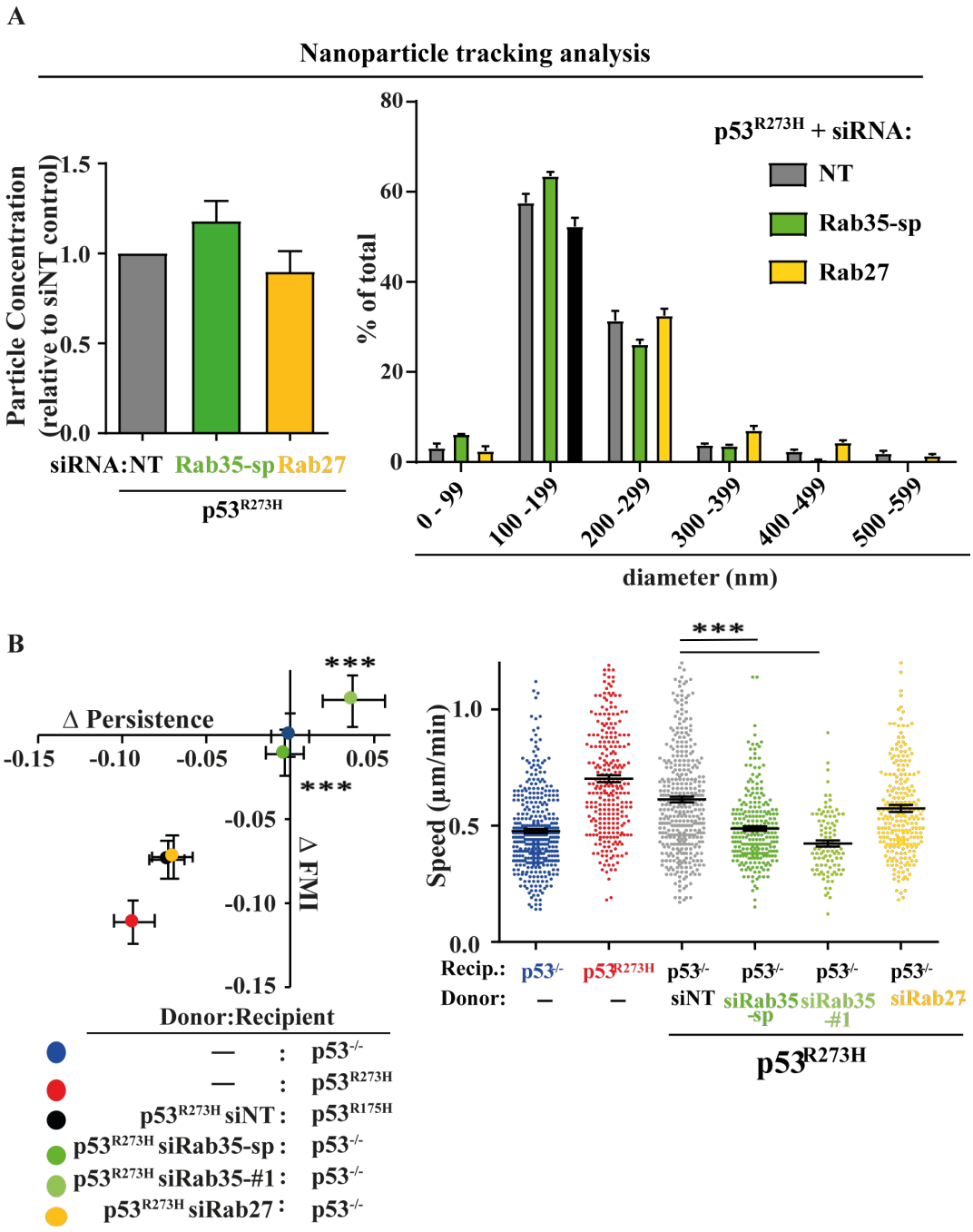

Figure 3-23- Production of phenotype-altering EVs by mutp53-expressing cells depends on Rab35. (A) H1299-p53^{R273H} cells were transfected with siRNAs targeting Rab35 (Rab35-sp or Rab35#1), Rab27a/Rab27b (Rab27) or a non-targeting control (NT) ± GFP-PODXL. EVs were purified by differential centrifugation. Nanoparticle tracking was used to characterise EVs. values are mean ± SEM, n = 6 movies from 2 individual experiments. (B) H1299-p53^{R273H} cells were transfected with siRab27, siRab35-sp, siRab35#1 or siNT. EVs collected from these cells were used to treat recipient H1299-p53$^{-/-}$ cells and the characteristics of their migration into scratch-wounds was determined. Values are mean ± SEM; n > 262 cells; for siRab35#1 n= 100 cells; ***p < 0.001, Mann–Whitney.

3.3 Discussion

Mutp53 promotes metastasis by driving cancer aggressiveness in a cell autonomous fashion. This is, in part, through a GOF mechanism in which mutp53 binds to p63 and suppress its ability to transactivate Dicer, thus resulting in loss of Dicer expression and its related anti-metastatic roles (Muller et al., 2014; Strano et al., 2002; Xu et al., 2011; Su et al., 2010). Accordingly, expression of mutp53s correlates with poor patient prognosis in a variety of cancer types, it drives metastasis in mouse models of PDAC (Hingorani et al., 2005; Morton et al., 2010; Schofield et al., 2018), and promotes invasiveness of cancer cells in 3D microenvironments (Coffill et al., 2012; Muller et al., 2014, 2013, 2009). Indeed, our observation that mutp53-expression in H1299 cells increases their ability to invade into organotypic plugs confirmed mutp53's role in the acquisition of cell autonomous invasive traits (Figure 3-1) (Timpson et al., 2011a).

Tumour progression can be also driven by non-cell autonomous mechanisms. Although some studies have shown that cancer cells can communicate with each other, through the release of diffusible factor(s), to drive cancer aggressiveness *in vivo* (Chapman et al., 2014; Inda et al., 2010; Zhang et al., 2015), the mechanisms by which specific oncogenic pathways promote this type of communication remain unclear.. Thus, we took advantage of an isogenic cell model to investigate whether mutp53s promote the release of pro-invasive factors. Strikingly, $p53^{-/-}$ and mutp53-expressing H1299 cells invaded to similar extents into plugs which were cultured in the same Petri dish (i.e. contacting the same culture media), strongly indicating that mup53 expression drives the release of factor(s) to promote invasive traits in other cancer cells (Figure 3-1) However, because the organotypic plugs contain fibroblasts whose role is to pre-condition the plug by re-modelling collagen, at this stage we are unable to determine whether the pro-invasive diffusible factor(s) exert their effects via the cancer cells or the fibroblasts. In the following chapter, we show that EVs from mutp53-expressing cancer cells do, indeed, exert their pro-invasive influence by changing integrin trafficking and ECM re-modelling in the fibroblasts. Therefore, to conclusively establish the contribution made by cancer cell-derived diffusible factor to the invasiveness of cancer cells themselves it would be necessary to evaluate the invasiveness of cancer cells in plugs depleted of fibroblasts by pre-incubation of contracted plugs with puromycin (Rath et al., 2017).

Expression of mutp53s drives fast and non-persistent migration of cancer cells on 2D substrates (Muller et al., 2009; Rainero et al., 2012). Conditioned media from donor mutp53-

expressing H1299 cells induced this type of migration in isogenic recipient $p53^{-/-}$ cells, indicating that mutp53-driven migratory traits can be transferred to other cancer cells through diffusible factors (Figure 3-3). Importantly, the pre-incubation of recipient $p53^{-/-}$ cells with EVs released from donor cells expressing mutp53s (either of the two most commonly mutated forms in human cancers – $p53^{R273H}$ and $p53^{R175H}$) was sufficient to invoke such migratory traits in them, suggesting that EVs mediate the transfer of mutp53s-induced migratory characteristics (Figure 3-6). Mutations in the DNA-binding domain of p53, such as $p53^{R273H}$ and $p53^{R175H}$, lead to loss of tumour-suppressive functions. Nonetheless, a number of studies in yeast and human cells have reported that mutp53s can still bind to certain $p53^{wt}$ responsive elements, indicating that mutp53s may maintain $p53^{wt}$ functions to a certain extent (Como and Prives, 1998; Jordan et al., 2008; Kato et al., 2003; Resnick and Inga, 2003). However, EVs released by donor H1299-$p53^{wt}$ cells did not affect the migratory traits of recipient H1299-$p53^{-/-}$, reinforcing that the non-cell autonomous role of mutp53s on cancer cell migration and invasion is, indeed, a GOF (Figure 3-7). Furthermore, the fact that H1299 cells do not express $p53^{wt}$ provides evidence that this phenotype occurs through a GOF mechanism and not through dominant-negative effects of mutp53s over $p53^{wt}$ functions, as previously described for other cancer cell lines (Willis et al., 2004).

Mutp53s drive RCP- and DGKα-mediated α5β1 integrin recycling in cancer cells. This then promotes recycling of a number of RTKs, leads to downstream Akt signalling and subsequently, phosphorylation and activation of Rac1GAP (Jacquemet et al., 2013). Consequently, it leads to a switch from Rac1 to RhoA at the cell front, driving filipodia-mediated invasion or fast and random migration in 3D or 2D substrates respectively (Jacquemet et al., 2013). We have found that mutp53-EVs potently promoted the recycling of α5β1 integrin and cMET in recipient $p53^{-/-}$ cells (Figure 3-8 B), and inhibition on DGKα in recipient cells abolished EV-mediated recycling (Figure 3-9). We also determined that inhibition of RCP or DGKα function in recipient cells impaired their ability to migrate differently when pre-incubated with mutp53-EVs (Figure 3-10B). Together, these observations indicate that mutp53s promote the release of EVs with the ability stimulate RCP- and DGKα-mediated integrin and RTK recycling in recipient cells, leading to RhoA-dependent migratory and invasive phenotypes. Interestingly, however, we found that recycling of TfR, the receptor for transferrin which was thought not to be regulated by the mutp53-RCP-DGKα pathway, was stimulated along with the other receptors (Figure 3-8 B). Previous studies from our laboratory have measured recycling of a labelled ligand for the

TfnR – ^{125}I-Tfn – and found this to be unaffected by expression of mutp53s (Muller et al., 2009). Thus, the present study suggests that mutp53 may influence the recycling of the receptor for Tfn, but not its ligand. Indeed, it has been shown that internalised Tfn and its receptor (TfnR) do not necessarily return to the plasma membrane via the same route (Mayle et al., 2012), and further studies will be necessary to determine precisely which receptor recycling routes are and are not influenced by EVs derived from mutp53-expressing cancer cells.

Activation of p53^{wt} following DNA damage has previously been shown to promote EV release in cancer cells, via a mechanism mediated by the p53 target TSAP6 (Lespagnol et al., 2008; Yu et al., 2006). Mutp53s are inefficient in transactivating p53 target genes, including TSAP6, making this target unlikely to be controlling processes through which mutp53s influence EV composition. Moreover, our studies indicate that the abundance and size distribution of EVs released by H1299 cells (Figure 3-4), and their profile of EV markers is not altered by mutp53 expression (Figure 3-5). Similar findings were reported for cells derived from mouse colorectal tumours with different p53 status (Cooks et al., 2018) and, together with our data, this is consistent with a situation in which mutp53s do not regulate EV biogenesis and/or release. Finally, titration of EVs determined that p53$^{-/-}$-EVs could not influence the migratory phenotype of recipient cells even when used at a 100-fold higher concentration than is required for p53^{R273H}-EVs to evoke increased cell migration (Figure 3-6 C), indicating the likelihood that mutp53's influence over certain EV-cargoes, and not simply altered EV production, is responsible for intercellular transfer of invasive behaviour.

SILAC-based proteomics allowed us to dissect the influence of mutp53 on the composition of EV-associated cargoes (Figure 3-11). Although previous studies reported that mutp53 expression in cancer cells had a profound effect on the cellular proteome (Polotskaia et al., 2015), we found that most of the identified proteins were indistinguishably expressed in p53$^{-/-}$- and p53^{R273H}-EVs. However, we observed that p53^{R273H}-EVs had reduced levels of podocalyxin, a sialomucin previously found in EVs collected from urine and cell cultures (Fernández et al., 2011; Hogan et al., 2014; Kwon et al., 2014). Accordingly, expression of mutp53 in cancer cells led to a reduction of podocalyxin at both mRNA and protein levels (Figure 3-13 A, B), and this was phenocopied by knock-down of p63 in p53$^{-/-}$ cells (Figure 3-13 D). Thus, it is tempting to propose a mechanism by which mutp53s interfere with p63 function to suppress podocalyxin levels in cancer cells and, as a consequence, in EVs released by these cells. A previous study demonstrated that treatment of mutp53-expressing kidney cancer cells with CP-31398, a small molecule which was shown to restore wild-type

function to mutp53s, led to reduced expression of podocalyxin (Stanhope-Baker et al., 2004). At first glance, this observation appears not to be consistent with a role for mutp53 in suppressing podocalyxin expression. A possible reason for this discrepancy may lie on CP-31398's ability to intercalate DNA and induce p53-independent cell death in a number of cancer cell lines (Rippin et al., 2002), which may imbue CP-31398 with p53-independent mechanisms of action.

Rab GTPases are key for membrane trafficking and EV release has been shown to be regulated by members of this family, including Rab27 and Rab35 (Hsu et al., 2010; Ostrowski et al., 2010). Although Rab27's role in EV release is well-characterised in a number of cell types and has been attributed to its role in the docking and fusion of vesicles with the plasma membrane (Ostrowski et al., 2010), the involvement of Rab35 in EV-release is less well-established, and has only been demonstrated in oligondrocytes (Hsu et al., 2010). However, Rab27-independent pathways for EV release have been described (Koles et al., 2012) and we have found that neither Rab27 nor Rab35 influence the quantity or size of EVs released by H1299 cells (Figure 3-23 A). Rather, we have shown that Rab35 (but not Rab27) is necessary for the intercellular transfer of mutp53's gain-of-function because it associates with podocalyxin and controls its intracellular trafficking. Specifically, Rab35 traffics podocalyxin to the plasma membrane (Figure 3-19), thus limiting the amount of podocalyxin available in late endosomes to be sorted into EVs (Figure 3-20).

Given that previous studies have highlighted transfer of certain miRNAs in EVs as the mechanism that cancer cells use to "educate" other cells into aggressive phenotypes (Tang et al., 2018), we initially proposed that podocalyxin-containing EVs might influence recipient cell phenotypes by altering gene expression. To test this, we conducted an extensive RNAseq analysis and have been completely unable to demonstrate any reproducibly altered levels of mRNAs following treatment of recipient cells with EVs from mutp53-expressing cancer cells. This implies that mutp53-EVs influence recipient cell phenotype via post-transcriptional mechanisms. Thus, it is interesting to speculate how EV-associated podocalyxin levels might influence receptor recycling in recipient cells. Podocalyxin is a glycocalyx component which, by virtue of negative charge imparted by sialylated N- and O-linked oligosaccharide residues, controls the separation of apposed lipid bilayers to promote the opening of lumens during morphogenesis, and to dictate the spacing of kidney podocytes (Doyonnas et al., 2001) Given that sialomucins would be expected to contribute to the surface charge of EVs, our data therefore suggest the possibility that EVs within a defined charge range can influence receptor trafficking by acting on membrane spacing within the

endosomal system. Thus, it would be interesting to determine whether post-translational modifications of podocalyxin, which would be expected to influence EV charge, contribute to the ability of EVs to interfere with endosomal processes. Alternatively, the level of podocalyxin in EVs might influence the levels of other cargoes. This possibility is consistent with a previous study that suggested that podocalyxin has affinity for sphingomyelin lipids and clustering of these in the plasma membrane is required for trafficking of podocalyxin to such sites (Ikenouchi et al., 2013).

Many studies have provided evidence for podocalyxin roles in carcinogenesis. In particular, it has been recently suggested that the ratio of surface/cytoplasmatic podocalyxin levels correlate with worse prognosis in many cancer types, including pancreatic, colorectal or bladder cancers (Boman et al., 2017, 2013; Kaprio et al., 2014; Saukkonen et al., 2015). We show that the maintenance of EV podocalyxin levels within a certain range is important to dissemination of invasive phenotypes, so it is interesting to speculate whether podocalyxin, by accumulating at the cell surface in aggressive cancers, is within an adequate range in MVE and EVs to allow mutp53 to influence non-cell-autonomous aggressiveness. Furthermore, as we have found that the podocalyxin content of EVs depends, not only on its expression in cancer cells, but on Rab35's capacity to dictate how much of this is sorted to EVs, it is now clear that we need to re-evaluate the role of podocalyxin in metastasis in human cancers to include analysis of how Rab35 levels and activity intersect with podocalyxin expression to dictate clinical outcomes.

Chapter 4 The effect of mutp53-EVs on ECM deposition

(This chapter features work relating to Novo et al. (2018) – Appendix II).

4.1 Introduction

Tumour progression is influenced by reciprocal interactions between tumour and stromal cells within the tumour microenvironment. Initial tumour growth is coupled with secretion of growth factors from tumour cells, some of which activate resident fibroblasts into CAFs, which feature aspects of the phenotype displayed by fibroblasts engaged in wound-healing (Augsten, 2014; Kalluri, 2016). Extracellular matrix (ECM) components, in particular fibronectin and fibrillar collagens, and ECM remodelling proteins, such as enzymes involved in collagen crosslinking (e.g. LOX) or turn-over (e.g. MMPs) are prominent amongst the CAF secretome (De Boeck et al., 2013; Tommelein et al., 2015). Through deposition and remodelling of the ECM, CAFs modulate linearisation of collagen fibres in the tumour stroma, which in turn increases stiffness to drive collective invasion of cancer cells away from the primary tumour (Levental et al., 2009). In addition to these local ECM remodelling events, primary tumours can also effect ECM deposition in distant organs through the release of factors into the circulation, and this is thought to prime PMNs for subsequent cancer cell colonisation and metastatic growth (Costa-Silva et al., 2015; Peinado et al., 2012). Although the mechanisms by which cancer cells promote ECM deposition and invasive behaviour in the stroma (via activation of fibroblasts) are well-understood, the mechanisms by which cancer cells influence the ECM in distant sites remain elusive.

ECM deposition can be regulated by endocytic trafficking of receptors for ECM ligands, such as integrins. Internalisation and recycling of α5β1 and αvβ3 integrins are known to affect deposition of fibronectin - a key ECM ligand for these integrins (Jones et al., 2009; Shi and Sottile, 2008; Varadaraj et al., 2017). As fibrillogenesis of fibronectin influences deposition of other abundant matrix proteins such as fibrillar collagens, trafficking of α5β1 integrin in fibroblasts is likely to have profound effects on ECM dynamics (Sottile and Hocking, 2002). In the previous chapter, we presented data showing that EVs released by mutp53-expressing cancer cells influence recycling of α5β1 integrin in other cancer cells. Thus, this raised the possibility that mutp53 GOF might also be transferred to non-cancer cells, such as fibroblasts and, if this were to occur, it would likely have implications for the nature of the ECM deposited by these cells.

In this chapter, we have characterised the effect of mutp53-EVs on the behaviour of fibroblasts, with particular focus on the way in which they recycle an integrin receptor for the ECM (α5β1) from endosomes to the plasma membrane, and how integrin recycling influences ECM deposition. Subsequently, we have explored in more detail the effect of EVs on the characteristics of ECM which these fibroblasts deposit/remodel, with particular regard to its organisation, physical properties and ability to support invasive migration of cancer cells. Finally, we have used autochthonous mouse models of cancer and transplantation approaches to evaluate whether expression of mutp53 in tumours affects ECM characteristics in the stroma, as well as in pre-metastatic target organs.

4.2 Results

4.2.1 mutp53-EVs influence fibroblast migration

To test whether mutp53-EVs can influence the behaviour of fibroblasts, we pre-incubated recipient telomerase-immortalised human fibroblasts (TIFs) with $p53^{R273H}$- or $p53^{R175H}$-EV, termed mutp53-EVs, or with $p53^{-/-}$-EV (Figure 4-1A).

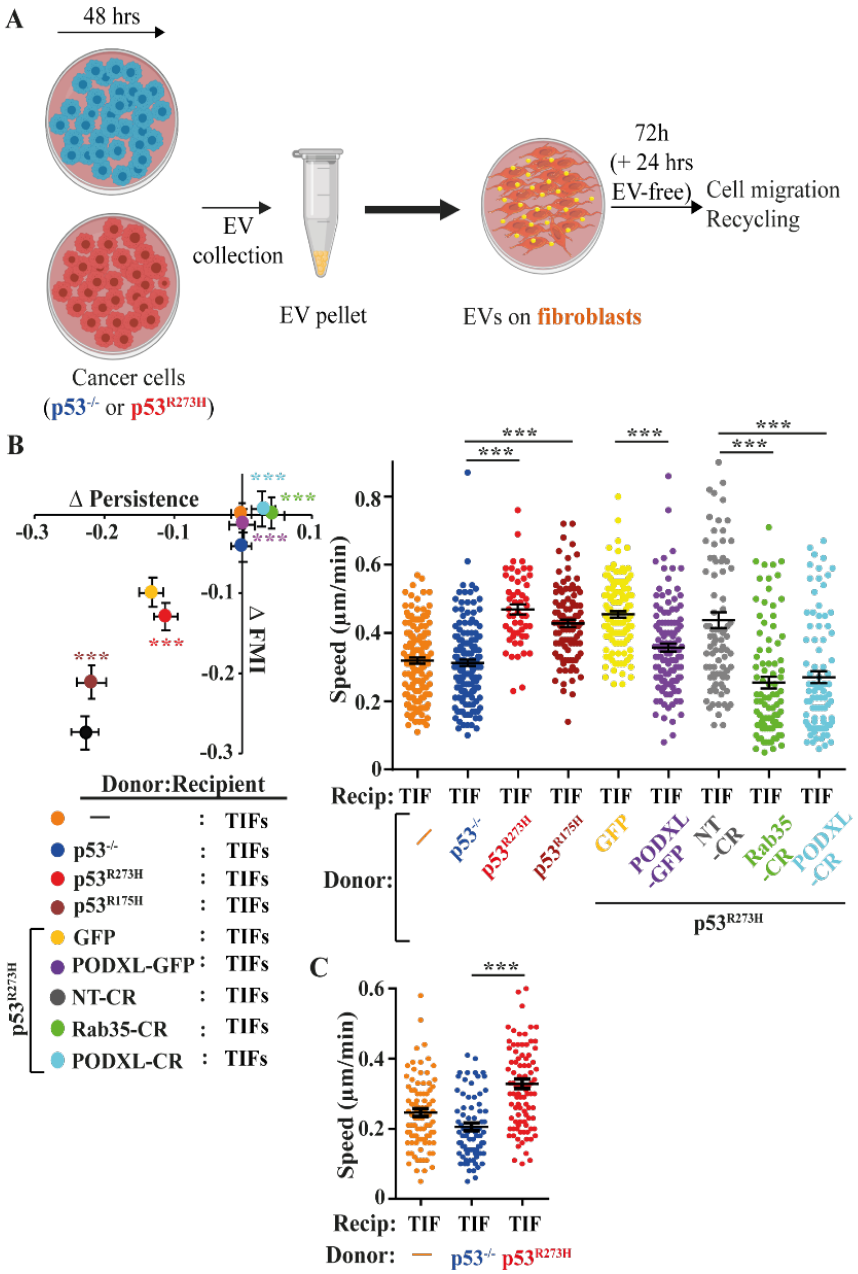

Figure 4-1- mutp53-EVs promote cell migration in fibroblasts.
(A) Protocol followed for assessing the effect of EVs on fibroblast behaviour. (B) mutp53-H1299 cells, or cells generated by CRISPR from the latter (PODXL-CR; Rab35-CR), were transfected with GFP or PODXL-GFP or were left untransfected. EVs collected from H1299-$p53^{-/-}$ and the transfected and untransfected mutant p53-expressing cells were used to treat TIFs and migration was analysed as for Figure 3-2. n = >52; ***red vs blue, ***purple vs yellow, ***green vs black, ***light blue vs black: $p < 0.001$, Mann–Whitney. *** is $p < 0.001$, Mann–Whitney. (C) TIFs were treated for 72 hr with EVs collected H1299 cells. EV-TIFs were trypsinised and then re-plated at low density onto plastic surfaces and imaged using time-lapse video microscopy. Values are mean±SEM, n>80 cell per condition, ***$p<0.001$ Mann-Whitney.

Evaluation of the migration of TIFs in scratch wounds and of these cells seeded sparsely revealed that pre-incubation of recipient TIFs with $p53^{R273H}$- or $p53^{R175H}$-EV evoked the migratory characteristics that we have associated with mutp53 GOF in tumour cells (i.e suppression of FMI and directionality, and an increase in speed) (Figure 4-1B, C). In contrast, migration of recipient TIFs which had been pre-incubated with $p53^{-/-}$-EVs was indistinguishable from untreated TIFs (Figure 4-1B, C). Importantly, manipulation of levels of podocalyxin associated with $p53^{R273H}$-EVs (by knocking-down podocalyxin, using RNAi or CRISPR, by over-expressing podocalyxin-GFP, or by knocking-down Rab35, in donor H1299-$p53^{R273H}$ cells) abrogated the ability of EVs collected from H1299-$p53^{R273H}$ cells to influence fibroblast migration (Figure 4-1B, C). Taken together, these data indicate that mutp53's migratory gain-of-function can be transferred to fibroblasts through EVs, and that the levels of EV-associated podocalyxin are critical for this to occur.

4.2.2 mutp53-EVs drive fibroblast DGKα-dependent receptor recycling

We have previously demonstrated that mutp53-EVs influence cancer cell migration by driving RCP- and DGKα-mediated integrin recycling in $p53^{-/-}$ cancer cells (Figures 3-9 and 3-10), via a mechanism that phenocopies mutp53 expression itself (Muller et al., 2009). To examine whether mutp53-EVs can promote receptor recycling in fibroblasts, we pre-incubated recipient TIFs with $p53^{R273H}$-, $p53^{R175H}$- or $p53^{-/-}$-EVs and evaluated the recycling rates of α5β1 integrin and TfnR (Figure 4-2).

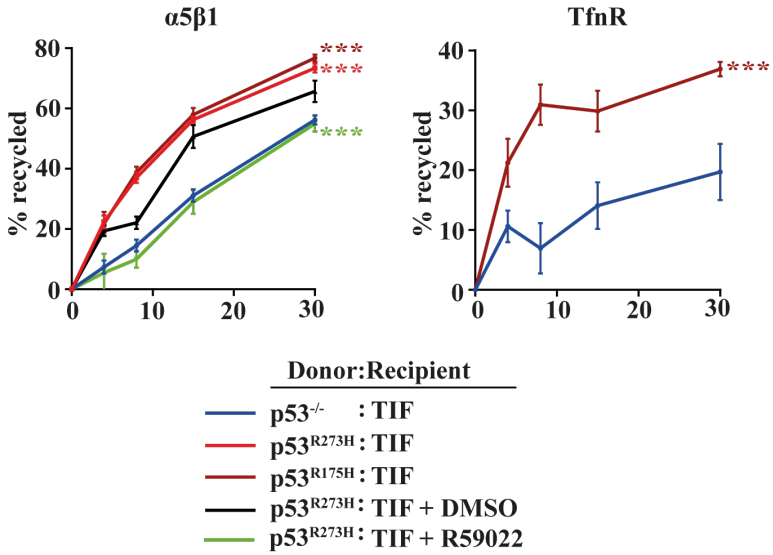

Figure 4-2- mutp53-EVs promote RCP/DGKα-dependent receptor recycling in fibroblasts.
(A) EVs were collected from mutp53-expressing R175H or R273H H1299 cells, or H1299-$p53^{-/-}$ were used to treat recipient TIFs for 72 hrs. Recipient cells were then trypsinised and re-plated. Seventy-two hours following re-plating, R59022 (10 μM) or DMSO was added to TIFs as indicated and recycling of integrin α5β1 and TfnR was determined. Mean ± SEM, n = 6. In a ***red versus blue, and ***green versus black are $p < 0.001$, ANOVA.

Pre-incubation of recipient TIFs with $p53^{R273H}$- or $p53^{R175H}$-EVs increased the recycling of these receptors by at least two-fold, while $p53^{-/-}$ EVs were ineffective in this regard. Furthermore, inhibition of DGKα in recipient cells opposed the ability of $p53^{R273H}$-EV to promote receptor recycling (Figure 4-2). These data imply that mutp53-EVs stimulate RCP/DGKα-dependent receptor recycling in fibroblasts.

4.2.3 mutp53-EVs influence the organisation of ECM deposited by fibroblasts in a DGKα-dependent manner

To test whether altered RCP/DGKα-dependent integrin trafficking influences ECM deposition (Figure 4-3A), we allowed TIFs that had been pre-incubated with $p53^{R273H}$-, $p53^{R175H}$- or $p53^{-/-}$-EVs to deposit ECM for 8 days. Cell monolayers were then de-cellularised using a buffer containing non-ionic detergents, and the remaining cell-free ECM was then analysed by immunofluorescence against fibronectin.

This showed that levels of fibronectin in the ECM were not affected by pre-incubation of TIFs with mutp53-EV. Furthermore, it showed that ECM deposited by TIFs is normally organised into bundles of largely parallel filaments, and pre-incubation of the TIFs with $p53^{-/-}$-EVs did not alter this. By contrast, pre-incubation of TIFs with $p53^{R273H}$-or $p53^{R175H}$-EVs led to a more branched, orthogonal ECM network (Figure 4-3B). To quantify this, we used grey level co-occurrence matrix (GLCM) analysis (Mohanaiah et al., 2013). This method determines the probability (intensity correlation) that pixels at increasing distances (comparison distance) from a given point can be found to have similar intensities. Thus, if an image consists mainly of long straight fibres it is possible to travel some distance in a straight line away from a given point without much alteration to intensity, and this will be reflected by long comparison distances for a given intensity correlation - i.e. a long mean decay distance. However, if an image is comprised mainly of short, orthogonally arrayed filaments then the correlation will fall more quickly as one travels away from a given point - yielding a shorter mean decay distance.

GLCM analysis showed that the intensity correlation of ECM deposited by fibroblasts treated with $p53^{R273H}$-or $p53^{R175H}$-EVs decreased more quickly with distance than it did in ECM from untreated fibroblasts or those incubated with $p53^{-/-}$-EVs. Furthermore, inhibition of DGKα (during the ECM deposition period) opposed deposition of orthogonal ECM with a short mean decay distance (Figure 4-3C). Together, these data indicate that mutp53-EVs

educate fibroblasts to deposit ECM with similar levels of fibronectin, but with increased orthogonality, and this depends on DGKα-dependent recycling in recipient cells.

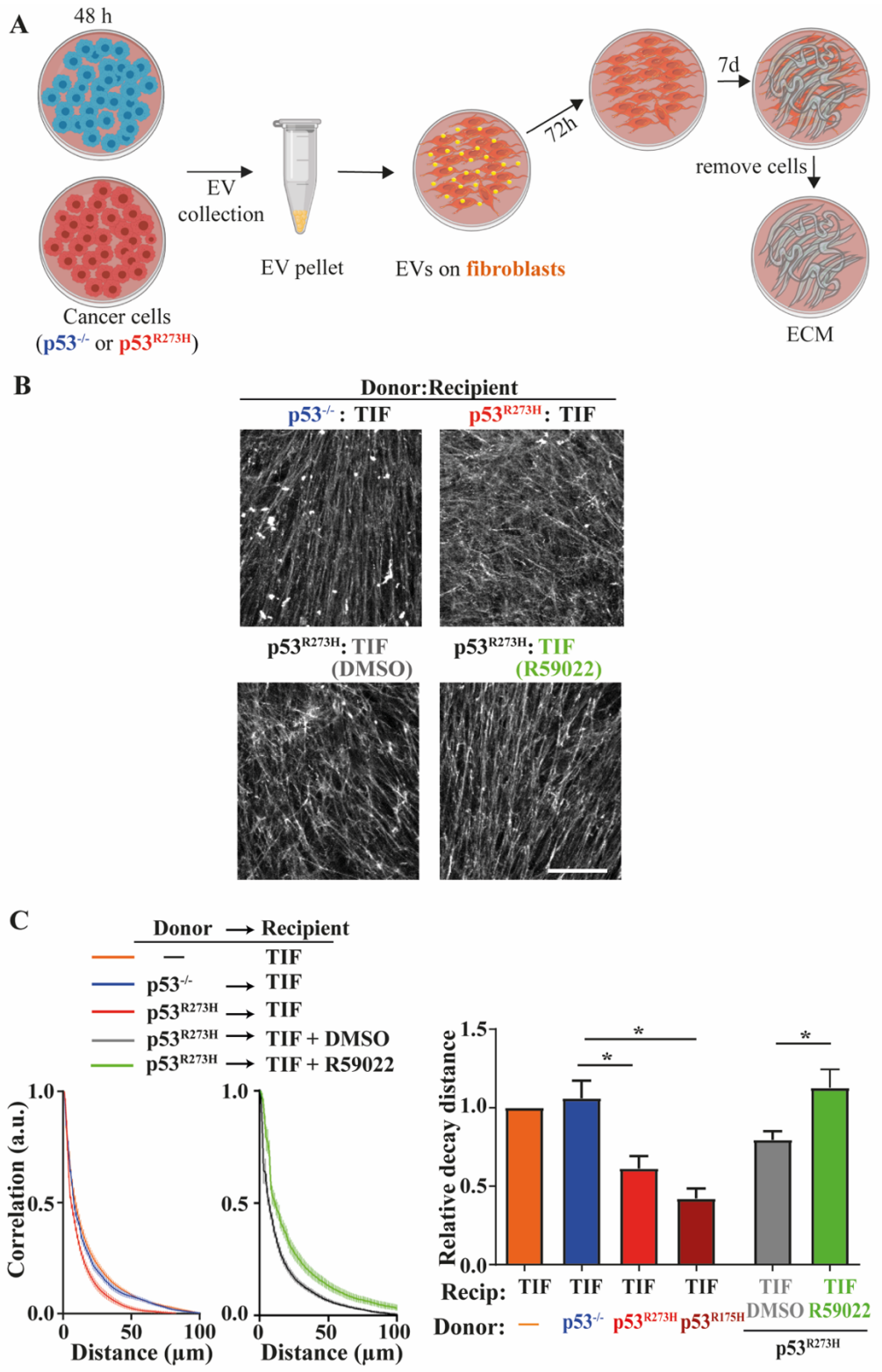

Figure 4-3- mutp53-EVs influence ECM deposition/remodelling.
(A) Protocol for evaluating the effect of EVs on fibroblast-derived ECM. (B) TIFs were incubated with EVs from H1299 ($p53^{-/-}$, $p53^{R273H}$, $p53^{R175H}$) cells or left untreated and allowed to deposit ECM in the presence and absence of R59022 (10 µM) or DMSO. ECM was then de-cellularised, stained with antibodies recognising fibronectin and image stacks were collected using confocal microscopy. Extended focus projections of these stacks are displayed, bar, 50 µm. (C) The organisation of the ECM fibres in these was determined using GLCM. The decay curves and the weighted means of the decay distances derived from these are presented in the centre and right panels of c respectively. Weighted mean ± SEM, n = 8, * is $p < 0.05$, Mann–Whitney.

4.2.4 Pre-incubation of fibroblasts with mutp53-EVs leads to deposition of ECM with reduced adhesiveness

EV-driven alterations in ECM organisation might be expected to influence its mechanical properties. To test this hypothesis, we performed atomic force microscopy (AFM) on ECM deposited by TIFs which had been pre-incubated with $p53^{R273H}$ - or $p53^{-/-}$-EVs (Figure 4-4A). This revealed that ECM deposited by fibroblasts which were pre-incubated with $p53^{R273H}$-EVs had similar stiffness to that from untreated fibroblasts and, despite observations that pre-incubation with $p53^{-/-}$-EVs encouraged the deposition of a slightly stiffer ECM (increased Young's modulus), this was not consistent with the ability of ECM deposited by $p53^{R273H}$-EVs to support increased cell migration (see Figure 4-5; below). We, therefore, continued to use AFM to determine the adhesive properties of the ECM. We attached a silica bead to the tip of the AFM cantilever, allowed this to interact with the ECM for a defined time, and then measured the energy required to remove the bead. The energy required to remove a silica bead from the ECM deposited by untreated TIFs was unchanged by pre-incubation of recipient TIFs with $p53^{-/-}$-EVs. However, pre-incubation of TIFs with $p53^{R273H}$-EVs led to a three- to four-fold reduction in energy necessary to remove a bead from the ECM deposited by these fibroblasts (Figure 4-4A). This suggests that EVs from mutant p53-expressing cancer cells induce fibroblasts to deposit an ECM with reduced stickiness.

Because of this altered adhesiveness, we assessed the adhesions formed when cancer cells interacted with these matrices. To this end, we seeded MDA-MB-231 breast cancer cells into de-cellularised ECM and visualised paxillin-positive adhesions by immunofluorescence (Figure 4-4B). Quantitative analysis of adhesion distribution showed that MDA-MB-231 cancer cells assembled significantly smaller cell-ECM adhesions when they were seeded into ECM deposited by recipient TIFs pre-incubated with $p53^{R273H}$-EVs, in comparison to those deposited by untreated or $p53^{-/-}$-EV- TIFs. Together, these data strongly indicate that mutp53-EVs educate fibroblasts in depositing/remodelling ECM with reduced adhesiveness, which influences the type of adhesion formed by cancer cells interacting with these ECMs.

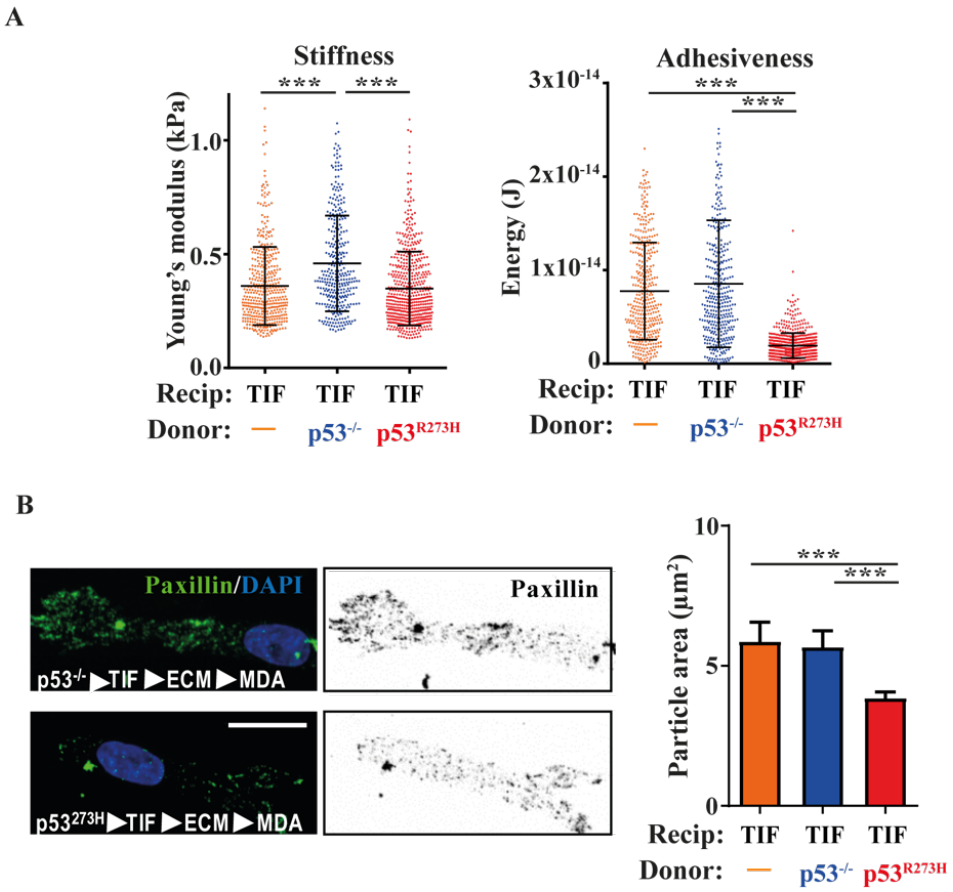

Figure 4-4- mutp53-EVs promote deposition of ECM with reduced stickiness.
(A) TIFs were treated with EVs from H1299 ($p53^{-/-}$ or $p53^{R273H}$) cells or were left untreated and allowed to deposit ECM. De-cellularised ECM was analysed using AFM. The left and right panels indicate ECM stiffness and stickiness/adhesiveness respectively. Mean ± SEM, n > 6 ECM preparations from two individual experiments *** is $p < 0.001$, Mann–Whitney. (B) MDAMB-231 cells were seeded onto de-cellularised ECM deposited by EV-treated TIFs as indicated. Cells were fixed and cell:ECM adhesions visualised by immunofluorescence suing an antibody recognising paxillin. Left panel shows representative images (bar, 20 µm). Average area of paxillin-positive particles is plotted in the right panel left. Mean ± SEM, n > 16, * is $p < 0.05$, Mann–Whitney

4.2.5 Pre-incubation of fibroblasts with mutp53-EVs leads to DGKα-dependent deposition of pro-migratory ECM

Changes in cancer cell-ECM adhesion strength is likely to affect migration of cancer cells in 3D microenvironments. To test this hypothesis, we used time-lapse microscopy to evaluate the speed in which MDA-MD-231 cells migrate through ECM deposited by EV-treated TIFs (Figure 4-5). Cell tracking analysis revealed that cancer cells migrated significantly more quickly through ECM from TIFs that had previously been incubated with $p53^{R273H}$-EVs than they did through ECM from untreated TIFs or those treated with $p53^{-/-}$-EVs (Figure 4-5). Furthermore, the ability of TIFs that had been pre-incubated with $p53^{R273H}$-EVs to deposit ECM which supported enhanced cancer cell migration was completely opposed by inhibition of DGKα (Figure 4-5). These data indicate that when incubated with mutp53-EVs, fibroblasts deposit an ECM that fosters increased cancer cell migration.

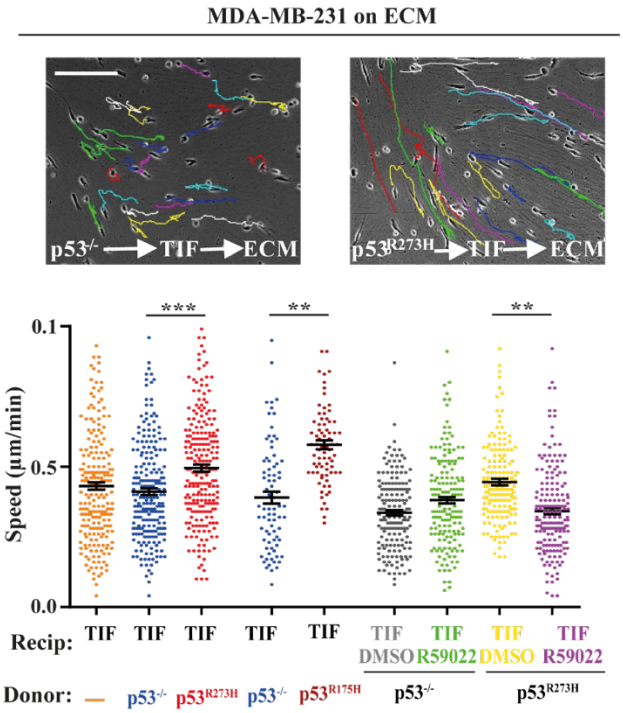

Figure 4-5- mutp53-exosomes educate fibroblasts to generate pro-migratory ECM.
TIFs were pre-treated with EVs from H1299-p53$^{-/-}$, H1299-p53^{R273H} or H1299-p53^{R175H} cells and allowed to generate ECM in the presence and absence of R59022 as for Fig. 5C. ECM was then decellularized and MDA-MB-231 breast cancer cells plated onto these. The migration of MDA-MB-231 cells through the de-cellularised ECM was recorded over a 16-hour period using time-lapse microscopy and cell tracking software. Representative tracks are indicated by the coloured lines in the top panels. Bar, 100 µm. The migration speed of the MDA-MB-231 cells was calculated and is presented in the plot. Values are mean ± SEM, n > 79 cells; **p <0.01, ***p < 0.001, Mann–Whitney.

4.2.6 Pre-incubation of fibroblasts with mutp53-EVs modulate ECM organisation in organotypic plugs

Through possessing multiple domains for interaction with other ECM components, fibronectin is known to modulates the deposition of other fibrillar proteins, such as collagen type I (Schwarzbauer and DeSimone, 2011; Sottile and Hocking, 2002). Given that the pre-incubation of fibroblasts with mutp53-EVs led to altered organisation of fibronectin fibres in decellularized ECMs, we hypothesised that mutp53-EVs may affect deposition and/or remodelling of fibrillar collagens.

To test this, we conditioned organotypic plugs with EV-treated fibroblasts and imaged fibrillar collagen in these matrices by SHG microscopy (Figure 4-6A). Pre-incubation of recipient TIFs with cancer cell-derived EVs led to an increased SHG signal in organotypic plugs (Figure 4-6C, D). However, this increase was similar whether the EVs were generated by p53$^{-/-}$ or p53^{R273H}-expressing cancer cells indicating that mutp53-expressing tumour cells do not specifically modulate the level of fibrillar collagen deposited by TIFs. Instead, GLCM analysis showed that pre-incubation of TIFs with p53^{R273H}-EV prior to seeding them into collagen plugs significantly reduced mean decay distance of fibrillar collagen within

these plugs, while p53$^{-/-}$-EVs did not alter this index of ECM organisation (Figure 4-6E). Thus, these data suggest that EVs released by mutp53-expressing cancer cells can induce fibroblasts to deposit fibrillar collagen with altered organisation.

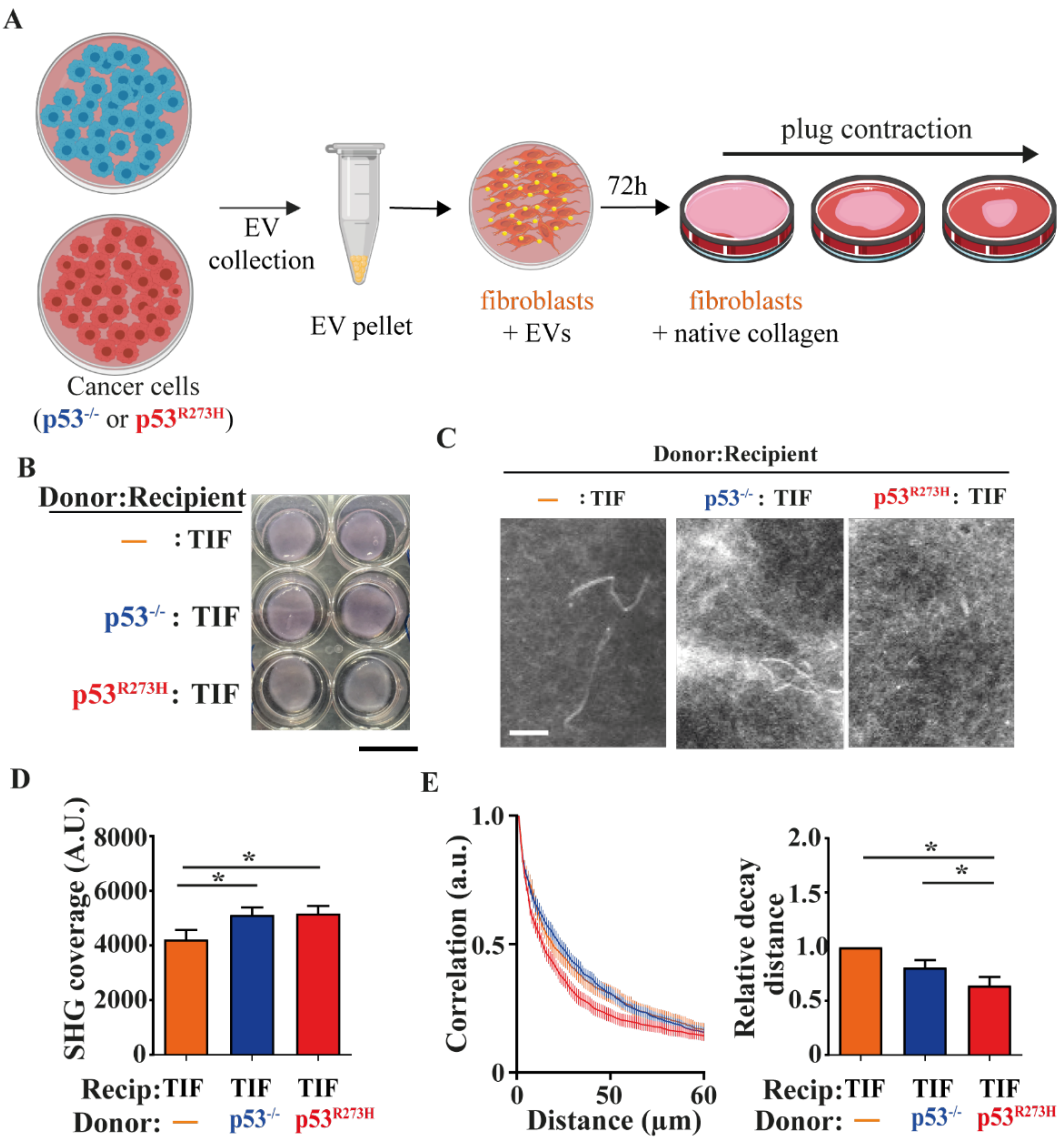

Figure 4-6- mutp53-exosomes encourage fibroblasts to produce altered ECM in "organotypic" plugs. (A) Schematic with protocol for assessing the effect of EVs in fibroblast conditioning of organotypic plugs. TIFs were incubated with EVs from H1299-p53$^{-/-}$ (p53$^{-/-}$) or H1299-p53^{R273H} (p53^{R273}) cells for 72 hrs. EV-treated TIFs were trypsinised, mixed with acid-extracted collagen and the resulting organotypic plugs allowed to polymerise and contract for 3 days. (B) Representative picture of contracted "organotypic" plugs according to the referred condition. (C) Second harmonic generation (SHG) microscopy was used to image fibrillar collagen in these matrices. Representative optical slices from these are displayed, bar, 4 µm. The coverage of the SHG signal (D) and organisation of the fibrillar collagen (E) were determined using GLCM as for Figure 4-3. The decay curves from these are presented in the left panels of (E) and the weighted means of the decay distances derived from these curves are displayed in the graph on the right. Values in (D) are mean ± SEM, n = 22 fields of view across three separate experiments. Values in (E) are weighted mean ± SEM, n = 46 fields of view across three separate experiments; * is $p < 0.05$, Mann–Whitney

4.2.7 Pre-incubation of fibroblasts with mutp53-EVs promote deposition/remodelling of pro-invasive ECM

ECM organisation is likely to affect their ability to support cancer cell invasion. To determine whether mutp53-EVs influence ECM deposition to modulate cancer cell migration in a 3D microenvironment, we pre-incubated TIFs with EVs and allowed them to pre-condition organotypic plugs, which were subsequently overlaid with H1299 cancer cells (Figure 4-7). This indicated that H1299 cells, irrespective of their p53 status, invaded efficiently into collagen plugs that had been conditioned by TIFs which were pre-incubated with $p53^{R273H}$-EV. By contrast, pre-incubation of TIFs with $p53^{-/-}$-EVs did not confer increased invasion in organotypic collagen plugs. Thus, these data emphasise that mutp53-EVs educate fibroblasts to deposit/remodel the ECM in a way which is highly supportive of cancer cell invasion.

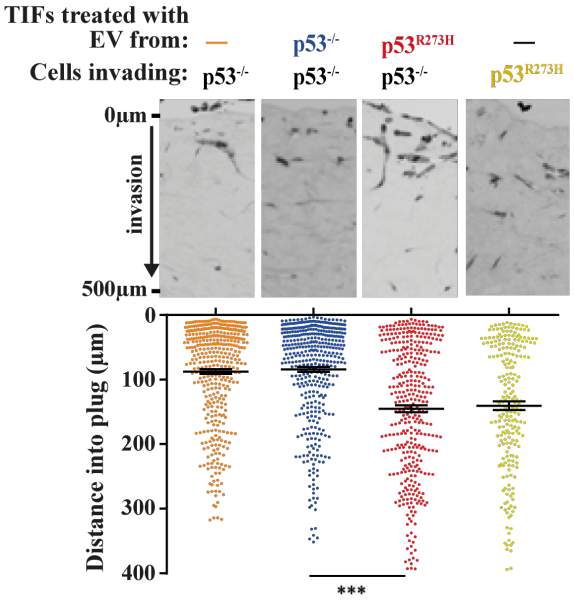

Figure 4-7- mutp53-EVs encourage fibroblasts to remodel pro-invasive ECM.
Collagen plugs were conditioned for 48 hours with untreated TIFs or with TIFs that had been pre-treated for 72 hours with EVs from H1299-$p53^{-/-}$ or H1299-$p53^{R273H}$ cells. Conditioned plugs were overlaid with H1299-$p53^{-/-}$ ($p53^{-/-}$) or H1299-$p53^{R273H}$ ($p53^{R273H}$) cells and these were allowed to invade for 10 days. Plugs were then fixed, and tumour cells visualised using H&E. The distance between each tumour cell and the top of the plug was determined using ImageJ. Bars are mean ± SEM, n > 233 cells; *** $p < 0.001$ Mann–Whitney test.

4.2.8 EVs from mutp53-expressing human PDAC promote deposition of pro-invasive ECM.

We determined whether the p53 status of human PDAC dictates the capacity of EVs from these cells to influence ECM deposition. Human PDAC may be categorised into four main subtypes, and these are termed, progenitor, immunogenic, ADEX and squamous. As the squamous subtype has the worst prognosis, is enriched for mutp53 and is thought to be driven by interference of p63 function (Bailey et al., 2016), we focussed on three patient-

derived cell lines (PDCLs) from this category. Of these, two (SQ2 and SQ3) expressed mutations that led to ablation of p53 protein expression and were considered, therefore, to be p53 null, while another (SQ1) expressed mutp53 ($p53^{M237I}$) with described GOF properties (Kang et al., 2013) (Figure 4-8A).

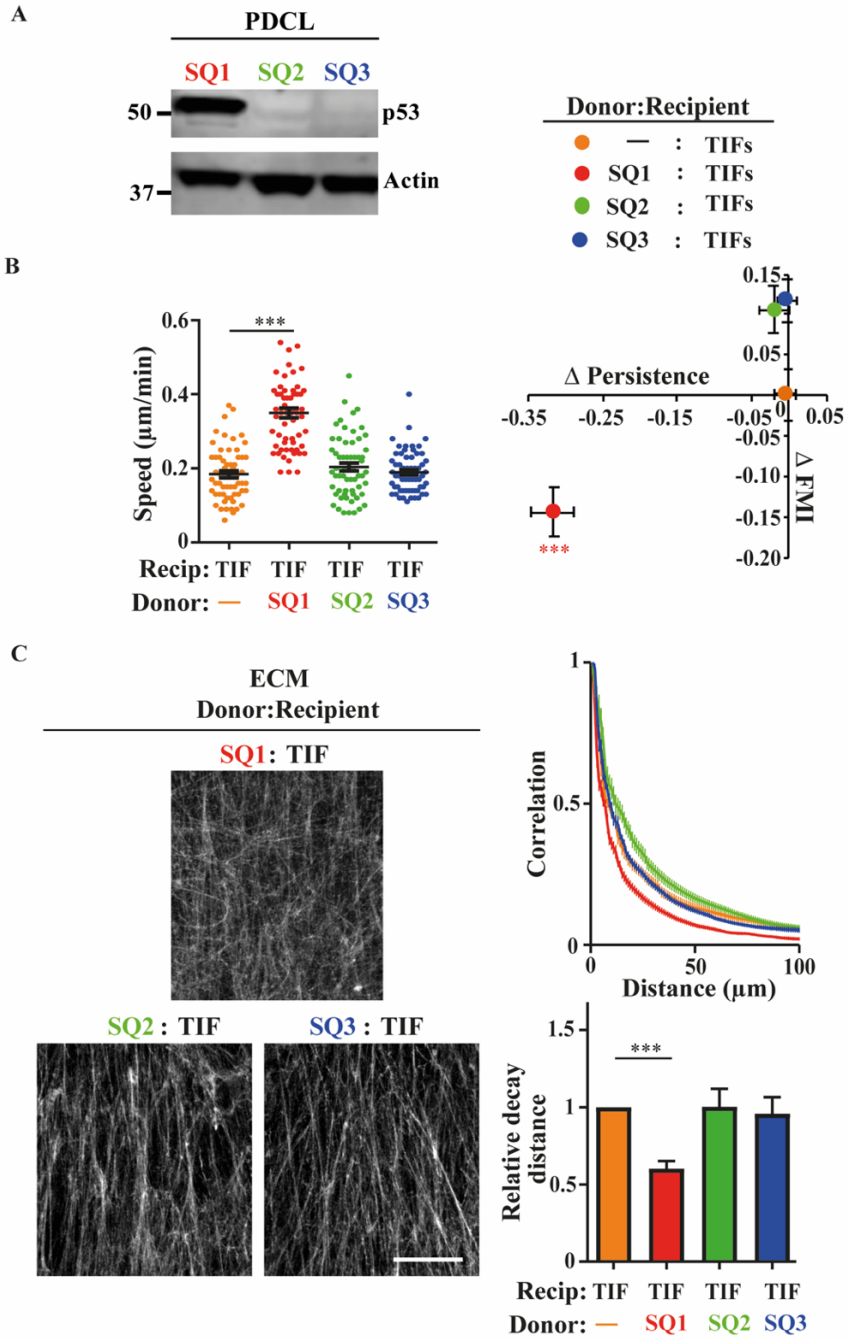

Figure 4-8- EVs released by mutp53-expressing PDCL influence ECM architecture.
(A) p53 expression in lysates from PDCLs expressing mutp53- SQ1- or null for p53 (SQ2 and SQ3) was assessed by western blot. (B) TIFs were left untreated or incubated with EVs collected from SQ1, SQ2, or SQ3 cells. TIFs were re-plated for a further 48 hrs and migratory characteristics of these cells into scratch-wounds were determined as for Figure 3-2. Values are mean ± SEM. n > 60 cells, *** is $p < 0.001$, Mann–Whitney. (C) TIFs were left untreated or incubated with EVs for 72 hours as indicated. TIFs were then re-plated and cultured for 8 days to allow deposition of ECM. ECM was de-cellularised, stained with antibodies recognising fibronectin and images collected using confocal microscopy. Extended focus projections of these stacks are displayed in the left, Bar, 50 µm. ECM organisation was determined using GLCM as for Figure 4-3. Decay curves from this are presented in the top left panel of and the weighted means of the decay distances are displayed in the bar chart. Values are weighted mean ± SEM, n > 8, *** is $p < 0.001$, Mann–Whitney.

We then isolated EVs from medium conditioned by these PDCLs (termed SQ1-, SQ2- or SQ3-EV) and incubated them with TIFs. We assessed the migration of these EV-incubated TIFs into scratch-wounds and found that only SQ1-EVs was able to increase speed and supress persistence and FMI (Figure 4-8B), as we had previously found for H1299 cells expressing mutant p53s. Furthermore, ECM deposited by fibroblasts pre-incubated with SQ1-EVs had reduced mean decay distance (Figure 4-8C) and supported invasive migration of cancer cells (Figure 4-10), while SQ2- and SQ3-EVs were inefficient in this regard.

Importantly, we found that knockdown of mutp53 in SQ1 cells, which did not significantly affect EV quantity or size (Figure 4-9B), led to increased podocalyxin levels (Figure 4-9A) and opposed the ability of EVs released by these cells to alter fibroblast migration (Figure 4-9 C) and deposition of pro-invasive ECM (Figure 4-9D, Figure 4-10). Together, these data indicate that squamous PDCL expressing mutp53 release EVs that promote deposition of misaligned, pro-invasive ECM, likely through controlling podocalyxin expression, as for H1299 cells.

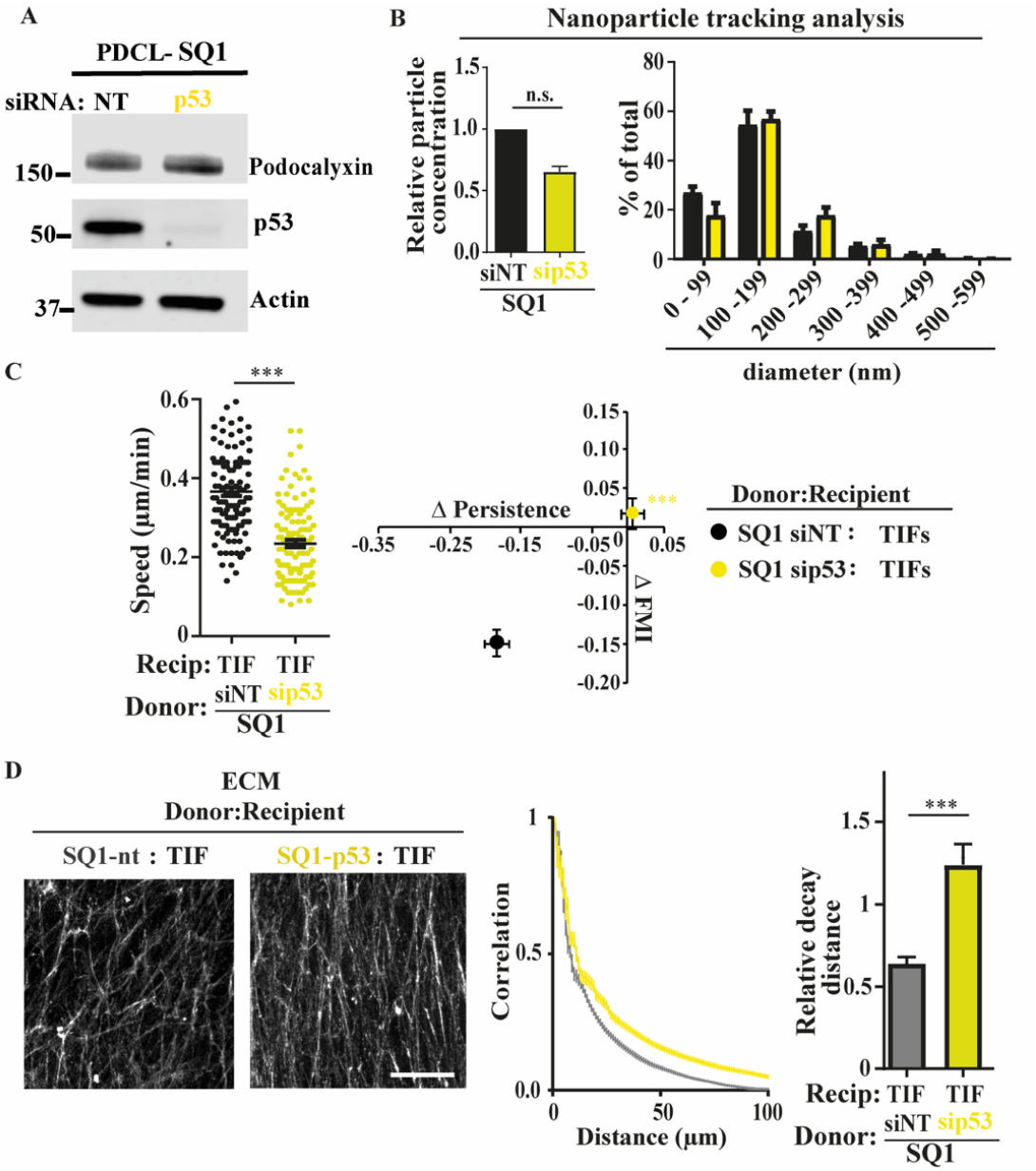

Figure 4-9- Loss of p53 in mutp53-expressing PDCL impairs their ability to produce EVs that effect fibroblast behaviour.

(A) SQ1 were transfected with siRNAs targeting p53 (si-p53), or a nontargeting control (siNT) and levels of Podocalyxin and p53 in cell lysates were assessed by western blotting, with actin as a sample control. (B) EVs were collected from the above transfected cells by differential centrifugation. Nanoparticle tracking was used to determine EV number and size distribution). Values are mean ± SEM. n = 3. (C) TIFs were incubated for 73 hrs with EVs collected from SQ1 transfected with a non-targeting siRNA (siNT) or a siRNA targeting p53 (si-p53). Recipient TIFs were re-plated for a further 48 hours and migratory characteristics of these cells into scratch-wounds were determined as for Figure 3-2. Values are mean ± SEM. n > 60 cells and *** is $p < 0.001$, Mann–Whitney. (D) TIFs were left untreated or incubated with EVs for 72 hrs as indicated. TIFs were then trypsinised, re-plated, and cultured for 8 days to allow deposition and remodelling of ECM. ECM was then de-cellularised, stained with antibodies recognising fibronectin and image stacks were collected using confocal microscopy. Extended focus projections of these stacks are displayed in the left, Bar, 50 µm. The ECM organisation was determined by GLCM as for Figure 4-3. Decay curves from this are presented in the plot on the left and the weighted means of the decay distances are displayed in the graph on the right. Values are weighted mean ± SEM, n > 8, *** is $p < 0.001$, Mann–Whitney.

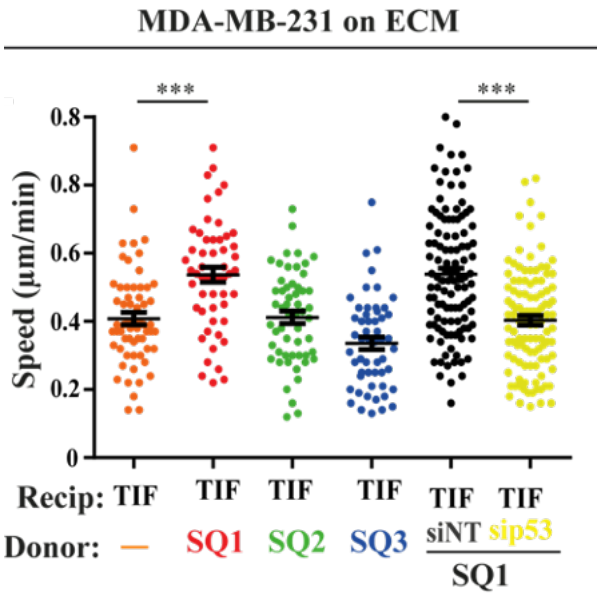

Figure 4-10- mutp53-expressing PDCLs release EVs that encourage fibroblasts to produce pro-migratory ECM.
TIFs were left untreated or incubated with EVs collected from SQ1, SQ2, or SQ3 cells or SQ1 cells transfected with a non-targeting siRNA (siNT) or a siRNA targeting p53 (sip53) for 73 hrs. After replating, TIFs were allowed to deposit ECM for 7 days. De-cellularised ECMs were prepared and MDAMB-231 breast cancer cells were plated onto these. The migration of MDA-MB-231 cells through the de-cellularised ECMs was recorded over a 16-hour period using time-lapse video microscopy and cell tracking software. The migration speed of the MDA-MB-231 cells was calculated. Values are mean ± SEM, n > 53 cells; ***p < 0.001, Mann–Whitney

4.2.9 mutp53-expressing pancreatic tumours affect ECM organisation in target organs

Following our observation that mutp53-expressing human squamous PDAC release EVs to influence fibroblastic ECM deposition/remodelling, we used mouse models of PDAC to investigate whether the p53 status of mouse primary pancreatic tumours dictates their ability to influence ECM deposition *in vivo*. To this end, we took advantage of the $KP^{172}C$ and $KP^{fl}C$ autochthonous mouse models of PDAC. In these, tumour initiation and growth is driven by expression of constitutively-active KRas (LSL-$KRas^{G12D}$) in combination with either deletion of an allele of p53 ($p53^{fl/+}$ generating $KP^{fl}C$ mice) or expression of mutp53s (LSL-$p53^{R172H}$ generating the $KP^{172}C$ mouse) under control of pancreatic-specific Cre recombinase, Pdx-Cre (Hingorani et al., 2005). Importantly, KPC tumours have previously been shown to recapitulate characteristics of the human squamous subtype (Bailey et al., 2016). We then used SHG/GLCM to visualise fibrillar collagen in primary tumours from these mice and found that the mean decay distance of collagen fibres in the stroma from KPC mice was significantly increased by comparison with the stromal regions of $KP^{fl}C$ tumours (Figure 4-11). This indicated that the expression of mutant p53 in PDAC is associated with ECM cross-linking and assembly of parallel arrays of collagen fibres in the stroma, as it was previously reported (Miller et al., 2015; Vennin et al., 2019). Furthermore, it indicates that the influence of mutant p53-expressing tumour cells on the collagen cross-

linking within the tumour itself differs markedly from the changes in the ECM organisation that we have found to be evoked by pre-treatment of fibroblasts with mut53-EVs.

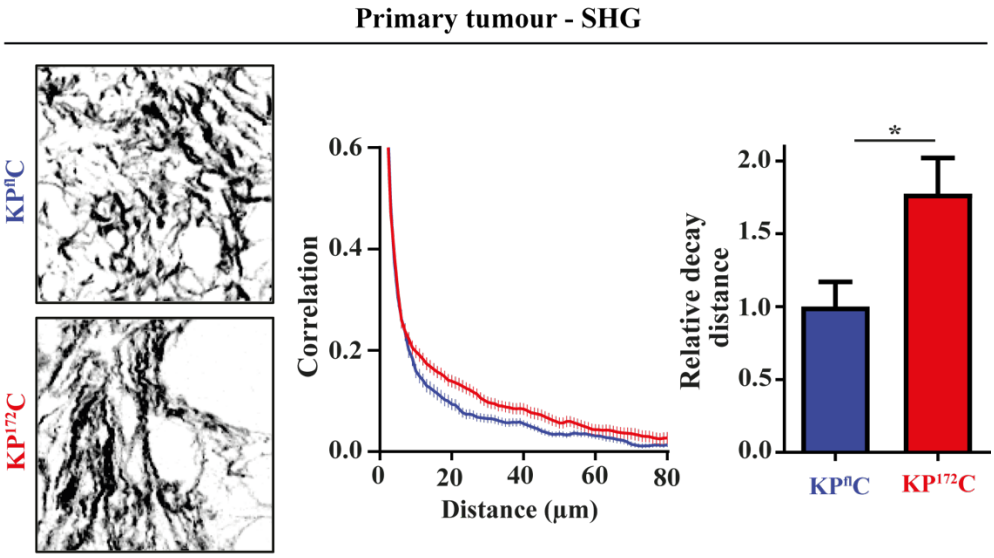

Figure 4-11- ECM of the stroma of mutp53-expressing and p53$^{-/-}$-PDAC.
(A) KP^{172}C (Pdx1-Cre;KrasG12D/+;p53R172H/+) or KP^{fl}C (Pdx1-Cre;KrasG12D/+;p53fl/+) mice were sacrificed by IP injection of pentobarbital, and the stromal regions of PDAC imaged by SHG microscopy. Representative SHG pictures of the tumour stroma are displayed on the left. Bar, 50 µm. Fibrillar collagen organisation was determined using GLCM. The decay curves from these are presented in the centre panel. Weighted means of the decay distances derived from decay curves are displayed in the right panel. Values are weighted mean ± SEM. N=4 animals per condition. * is $p<0.05$, Mann-Whitney.

We, therefore, determined whether mutant p53-expressing tumours had any influence on the ECM organisation at sites that are distant from the primary tumour. In particular, we were interested in the collagen structure in organs to which PDAC commonly metastasises, such as the lung and liver. Indeed, PDAC driven by mutant KRas in combination with mutp53 (such as the ones in KP^{172}C and KP^{270}C mice, equivalent to the human R175H and R273H respectively) metastasise to the liver and lung. On the other hand, PDAC driven by KRas in combination with p53 loss (p53$^{fl/+}$) appear with similar penetrance, but do not metastasise as efficiently (Hingorani et al., 2005; Morton et al., 2010). We thus sought to compare the ECM of the lung (parenchyma and perivascular regions) and liver capsule at an age (10-12 weeks) in which primary tumour growth was underway, but metastases were not detectable yet (Figure 4-12). As controls, we used KC mice, which only express LSL-KRas^{G12D} under control of Pdx-Cre, but the resulting tumours do not readily progress past the pre-malignant PanIN (pancreatic intraepithelial neoplasm) stage.

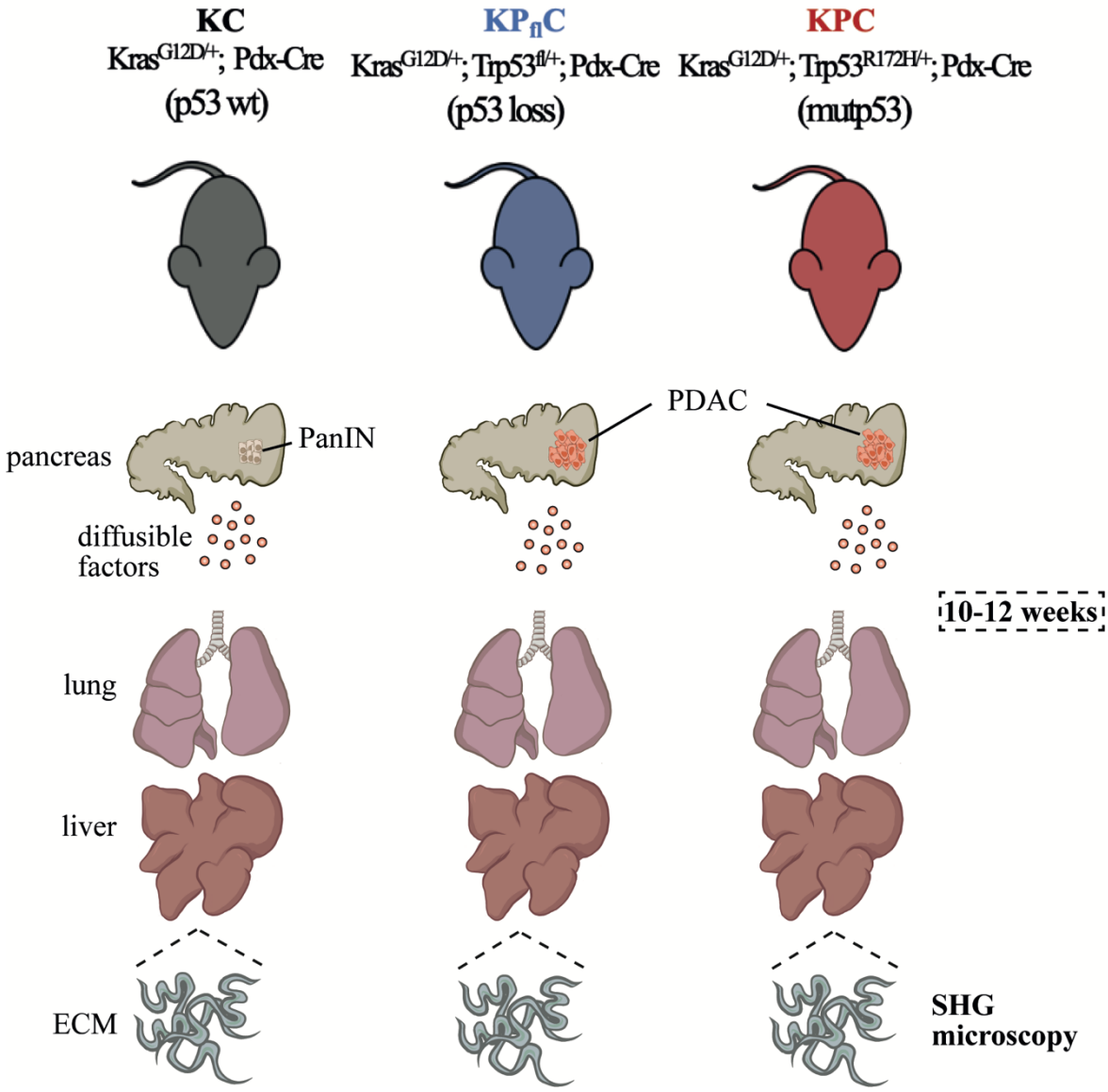

Figure 4-12- Investigating ECM architecture in the liver and lung of PDAC-bearing mice.
PDAC driven by mutant KRas in combination with mutp53 metastasise to the liver and lung. In contrast, PDAC driven by KRas in combination with p53 loss appear with similar penetrance but are poorly metastatic (Morton et al. 2010). Thus, we used SHG microscopy to visualise ECM of the lung and liver capsule at an age (10–12 weeks) in which primary tumour growth was underway, but metastases were not detectable. As controls, we used KC mice, which only express LSL-KRasG12D under control of Pdx-Cre, but the resulting tumours do not readily progress past the pre-malignant PanIN (pancreatic intraepithelial neoplasm) stage.

SHG/GLCM analysis of live precision-cut lung slices (PCLSs) and liver indicated that collagen filaments in these organs in KP^{172}C and KP^{270}C animals were shorter and misaligned, and the mean decay distance of these fibres, as assessed by GLCM analysis, was reduced by comparison with that of KC (Figures 4-13 and 4-14). By contrast, ECM organisation in the lung and liver of KP^{fl}C mice was indistinguishable from KC animals. These data highlight that alterations to ECM organisation, which we have established to be driven by the influence of p53^{R273H}- or p53^{R175H}-EVs on integrin trafficking in fibroblasts, may also be detected in target organs of animals bearing autochthonous PDAC expressing the equivalent p53 mutations, but not of animals with PDAC driven by p53 loss.

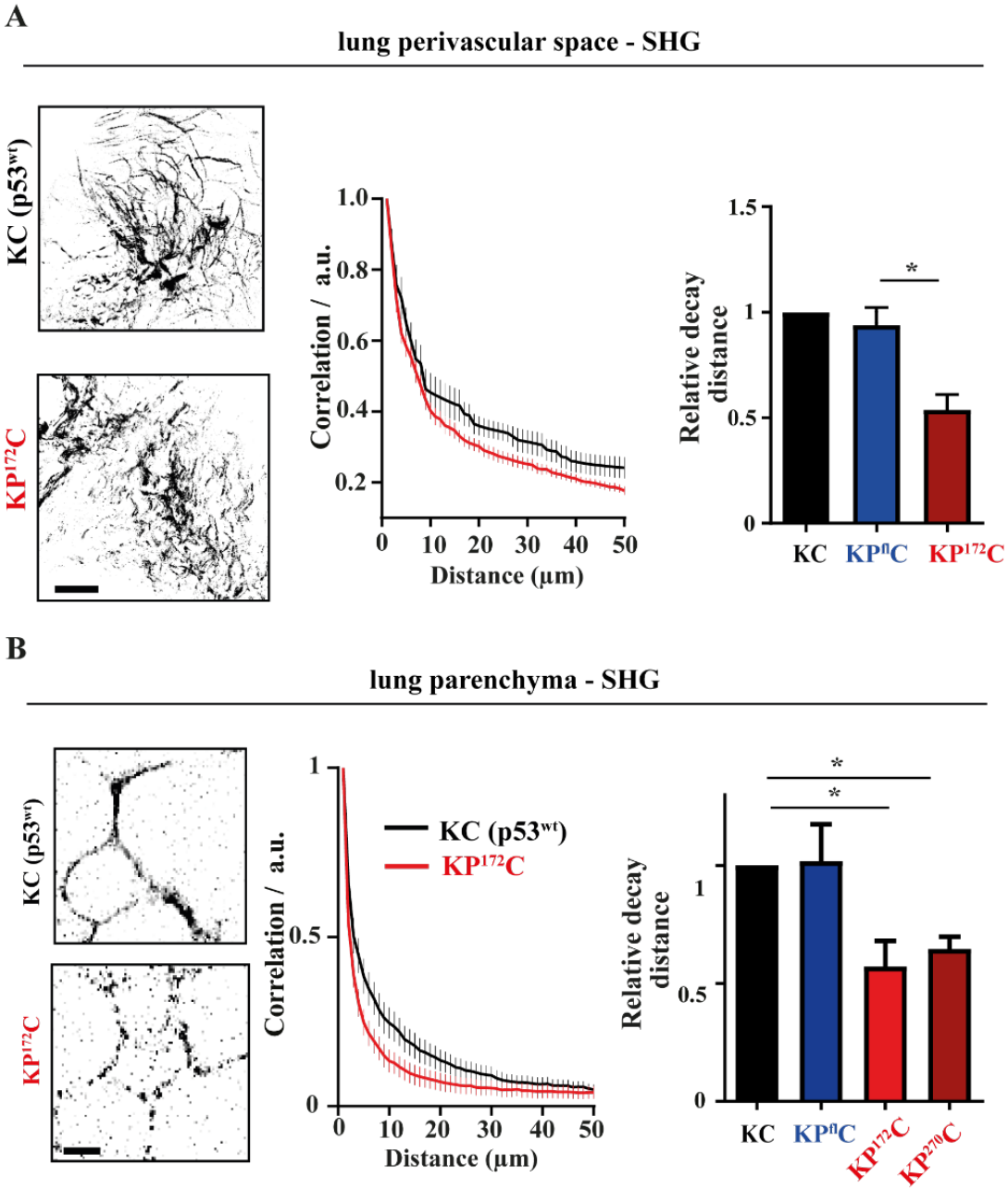

Figure 4-13- Mutant p53-expressing PDAC influences ECM architecture in the lung.
(A, B) $KP^{172}C$ (Pdx1-Cre:KrasG12D/+: p53R172H/+) or $KP^{270}C$ (Pdx1 Cre:KrasG12D/+:p53R270H/+), $KP^{fl}C$ (Pdx1-Cre:KrasG12D/+:p53fl/+) or KC (Pdx1-Cre:KrasG12D/+) mice were sacrificed by IP injection of pentobarbital, lungs were inflated with 2% low melting point agarose which was then allowed to solidify. Agarose-filled lungs were sliced using a vibratome and the perivascular (A) and parenchymal (B) regions of the lungs were imaged by SHG microscopy. Representative SHG pictures of lungs are displayed in the left. Bar in A, 25µm; bar in B, 100 µm. Fibrillar collagen organisation was determined using GLCM. The decay curves from these are presented in the centre panels. Weighted means of the decay distances derived from decay curves are displayed in the right panels. Values are weighted mean ± SEM. In A, n = 3 for KC, n =4 for $KP^{fl}C$ and n = 5 animals for KPC. * is $p < 0.05$, Mann–Whitney. In B, n > 7 lung fields from three animals per condition (except for KC, where there were 6 animals); * is $p < 0.05$, Mann–Whitney.

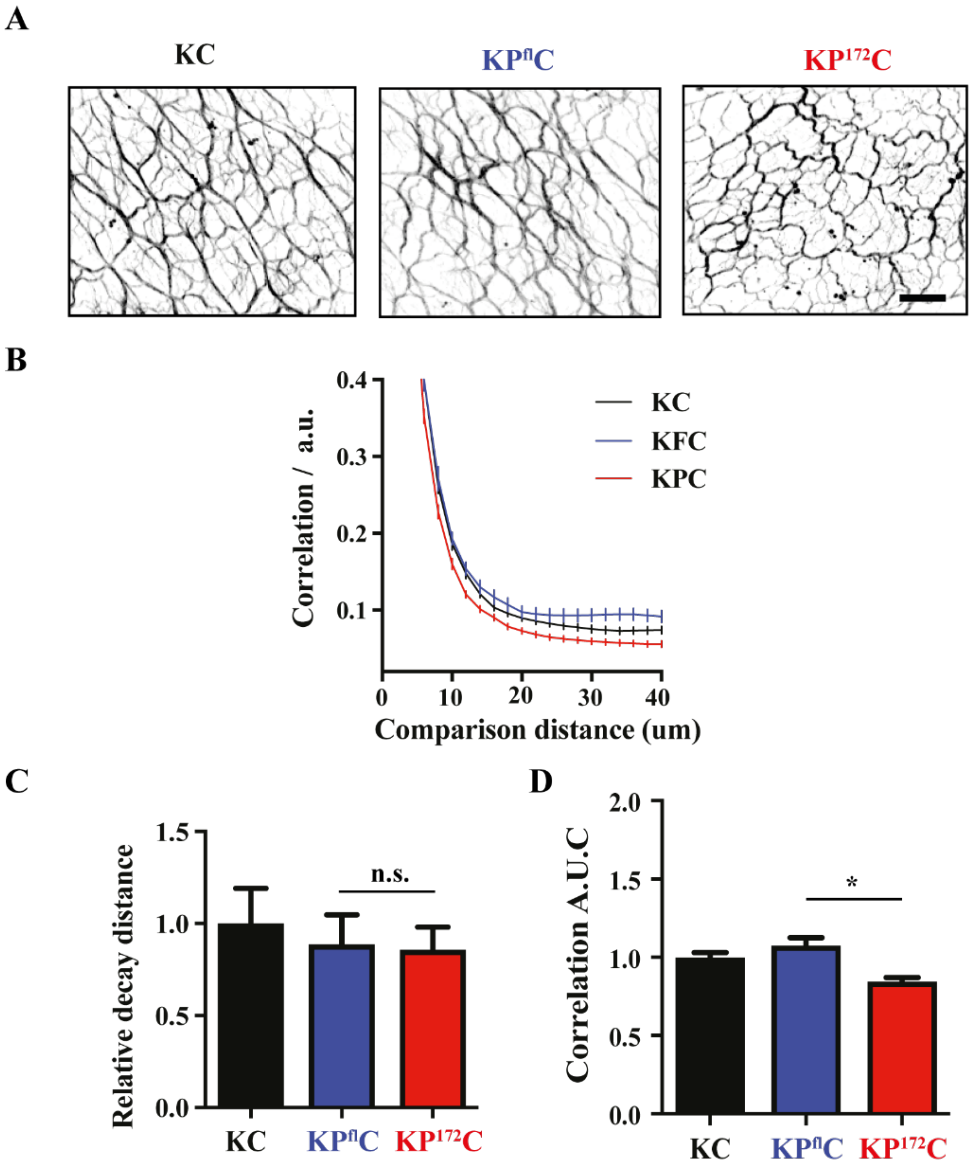

Figure 4-14- Mutant p53-expressing PDAC influences ECM architecture in the liver capsule.
(A) KP^{172}C (Pdx1-Cre:KrasG12D/+: p53R172H/+), KP^{fl}C (Pdx1-Cre:KrasG12D/+:p53fl/+) or KC (Pdx1-Cre:KrasG12D/+) mice were sacrificed by IP injection of pentobarbital, dissected and whole livers were collected in culture media and imaged by SHG microscopy. Representative pictures of liver capsule SHG are shown. (B) Fibrillar collagen organisation was determined using GLCM. The decay curves from these are presented. (C) Weighted means of the decay distances derived from decay curves. (D) Weighted Area-under-curve calculated for the decay curves. Values are weighted mean ± SEM. N=2 animals for KC, N=3 for KP^{fl}C and N=4 for KP172C. * is $p < 0.05$, ANOVA.

4.2.10 mutp53-driven subcutaneous tumours influence lung ECM organisation in a podocalyxin- and Rab35-dependent manner

We used a xenograft approach to determine whether mutp53-expressing H1299 cancer cells could influence ECM deposition *in vivo* (Figure 4-15A). We injected p53$^{-/-}$ or mutp53-expressing (p53^{R273H} or p53^{R175H}) H1299 cells subcutaneously in nude mice. We then let the tumours growth until they reached 8 mm in diameter (Figure 4-15 B) and, at this point, used SHG/GLCM to evaluate the organisation of collagen fibres in the lungs of these animals

(Figure 4-16). Xenografts of mutp53-expressing H1299 cells resulted in decreased decay distance of collagen fibres in the lung in comparison to animals injected with $p53^{-/-}$-H1299 cells or non-injected animals (Figure 4-16), thus indicating that human cancer cells can be used as subcutaneous xenografts to explore the mechanism through which mutp53-expression in tumours influence ECM deposition in distant organs.

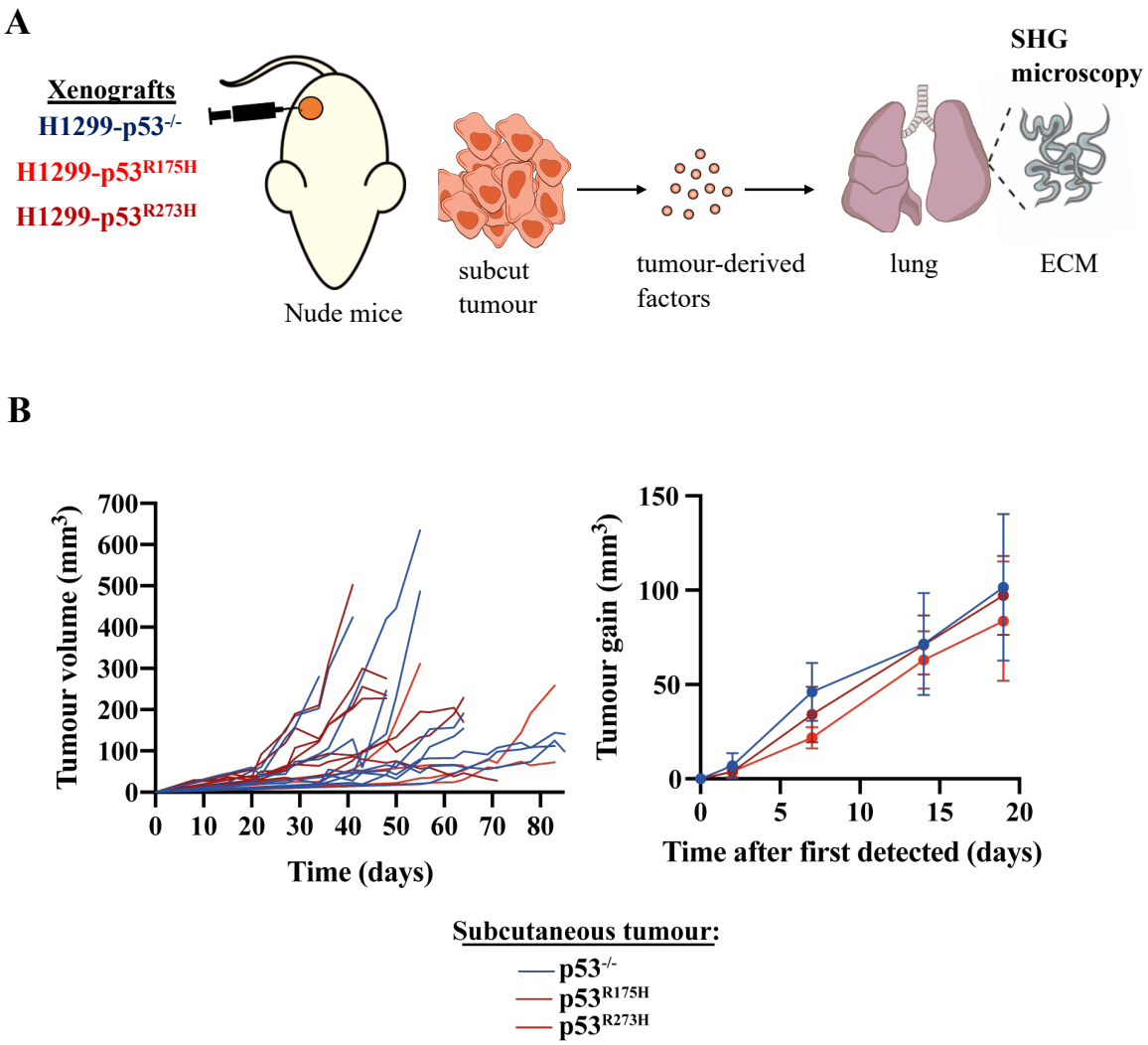

Figure 4-15- A xenograft approach for investigating the effect of mutp53 on lung ECM architecture. (A) Schematic of the xenograft model used for investigating the effect of mutp53 in lung ECM architecture. H1299-$p53^{-/-}$, H1299-$p53^{R273H}$ or H1299-$p53^{R175H}$ cells were injected subcutaneously into CD1 nude mice. Mice were monitored for tumour growth and culled when tumours reached 0.8 cm diameter. At this time, fibrillar collagen in the lung was imaged by SHG microscopy. In (B), xenograft tumour growth curves are shown on the plot in the left, and tumour gain upon first detection is shown on the right. Values are mean ± SEM.

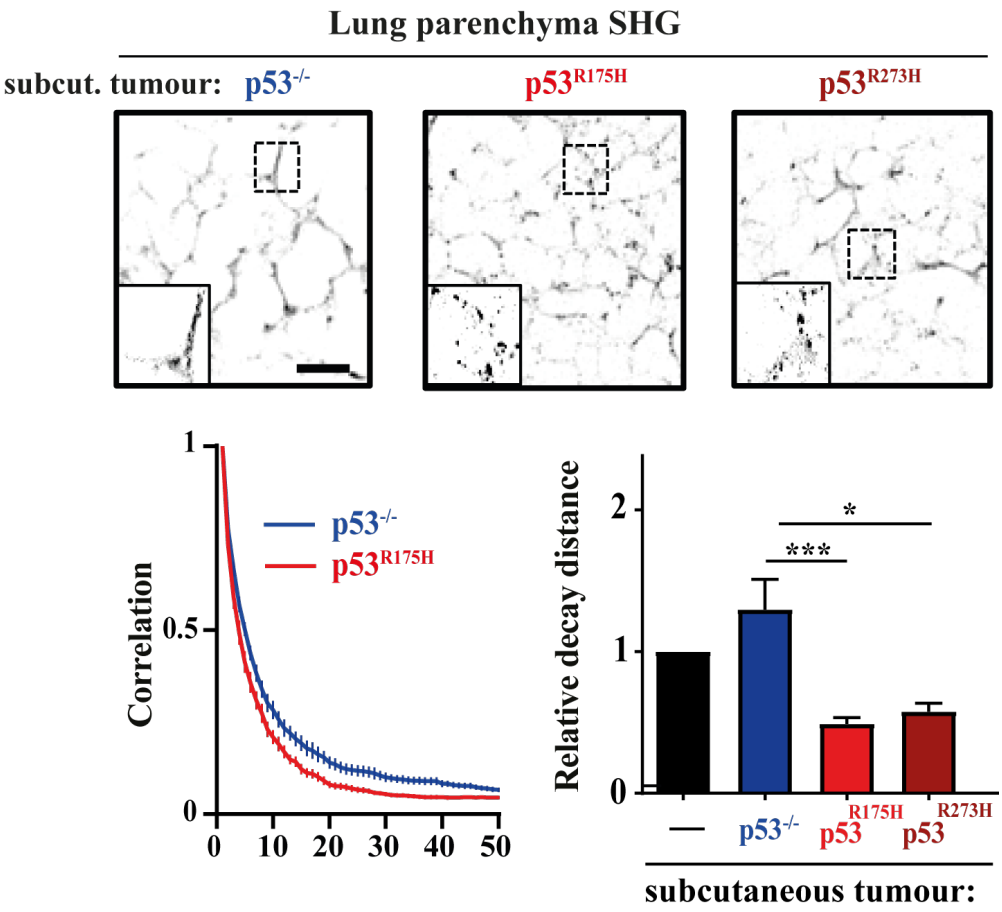

Figure 4-16- Tumour xenografts of mutp53-expressing H1299 cells influence lung ECM architecture. (A) H1299-p53$^{-/-}$, H1299-p53^{R273H} or H1299-p53^{R175H} cells were injected subcutaneously into CD1 Nude mice. Mice were monitored for tumour growth and culled when tumours reached 0.8 cm diameter. Mice were sacrificed by IP injection of pentobarbital, and lungs were inflated with 2% low melting point agarose which was then allowed to solidify. Agarose-filled lungs were sliced using a vibratome, and parenchymal regions were imaged by SHG microscopy. Representative SHG pictures of lungs from CD1 nude mice transplanted with the respective cell line are displayed on the top. Bar, 100 µm. Fibrillar collagen organisation was determined using GLCM. The decay curves from these are presented in the bottom-left panel. Weighted means of the decay distances derived from decay curves are displayed in the bottom-right panel. Values are weighted mean ± SEM; n > 4 animals per condition (except for H1299-p53R175H, where n = 3); * is $p < 0.05$, *** is $p < 0.001$, Mann–Whitney test.

We took advantage of this model to test whether regulation of the levels of podocalyxin in tumour cell-derived EVs dictate ECM organisation in the lung. We subcutaneously injected control H1299-p53R273H or H1299-p53R273H cells in which podocalyxin or Rab35 had been deleted by CRISPR into nude mice (Figure 4-17A, B). Loss of podocalyxin or Rab35 in mutp53-expressing H1299 cells impaired the ability of xenografts to modulate ECM deposition in the lung, as determined by GLCM (Figure 4-17C). Thus, these data suggest that the ability of mutant p53-expressing tumours to influence ECM deposition in distant organs depends on the levels of podocalyxin associated with EVs released by these tumours.

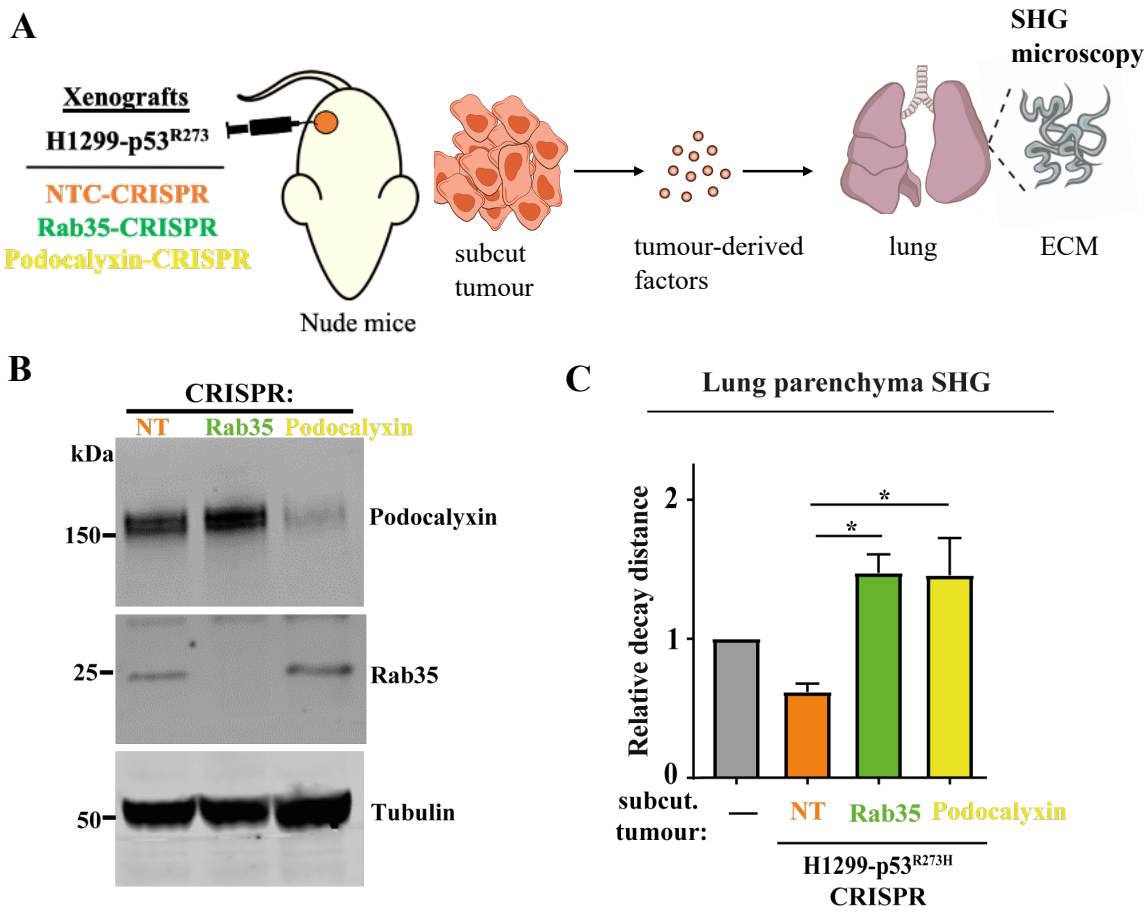

Figure 4-17- mutp53-expressing xenografts influence lung ECM architecture in a podocalyxin- and Rab35-dependent manner.
(A) Schematic of the xenograft models used for investigating whether mutp53 affects lung ECM architecture via podocalyxin and Rab35-dependent mechanisms. $p53^{R273H}$-H1299 cells in which Rab35 or podocalyxin had been disrupted by CRISPR were injected subcutaneously into CD1 Nude mice. Mice were monitored for tumour growth and culled when tumours reached 0.8 cm diameter. Mice were sacrificed by IP injection of pentobarbital, and lungs were inflated with 2% low melting point agarose which was then allowed to solidify. Agarose-filled lungs were sliced using a vibratome, and parenchymal regions were imaged by SHG microscopy. (B) The loss of podocalyxin and Rab35 in H1299-p53R273H cells was confirmed by western blotting, using tubulin as a loading control. (C) GLCM was used to analyse SHG organisation in lung. Weighted means of the decay distances derived from decay curves are displayed in the right panel. Values are weighted mean ± SEM; n > 4 animals per condition; * is $p < 0.05$, Mann–Whitney.

4.3 Discussion

In the previous chapter, we reported that mutp53-expressing H1299 cells release diffusible factors, which we subsequently demonstrated to be EVs with a defined podocalyxin level, to promote invasion of $p53^{-/-}$ cancer cells into organotypic plugs. However, fibroblasts were present within the plugs, raising the possibility that cancer cell invasion might be indirectly mediated by the effect of EVs on cells that are wild-type for p53. Thus, we tested whether fibroblasts respond to EVs. Pre-incubation of recipient TIFs with mutp53-EVs (from cancer H1299 cells, either $p53^{R273H}$ or $p53^{R175H}$-EVs) imbues them with increased migratory speed and decreased migratory FMI/persistence when they move on 2D substrates, indicating that a migratory phenotype resembling mutp53's pro-invasive gain-of-function can be transferred to fibroblasts. Furthermore, knock-down of Rab35 or podocalyxin, or overexpression of podocalyxin, in donor mutp53-expressing H1299 cells, impaired their ability to release EVs that influence migration of recipient TIFs, indicating that, as was the case for recipient cancer cells, transfer of mutp53's gain-of-function to fibroblasts requires tight regulation of EV-associated podocalyxin levels in donor mutp53-expressing cancer cells.

Previous studies have shown that directionally-erratic and rapid migration of fibroblasts on 2D substrates is associated with rapid recycling of α5β1 integrin through a pathway which depends on the Rab11 effector, RCP (Caswell et al., 2008; White et al., 2007). Moreover, it is now clear that RCP function requires the lipid kinase, DGKα which generates a source of phosphatidic acid which is necessary for the tethering and exocytosis of RCP-positive recycling vesicles (Rainero et al., 2012). Thus, the use of inhibitors of DGKα has been established as an effective pharmacological approach to opposing RCP-dependent receptor recycling. Here we show that pre-incubation of fibroblasts with mutp53-EVs activates recycling of α5β1 integrin, and inhibition of DGKα opposed this, indicating that mutp53-EVs promote recycling through the Rab11/RCP pathway in fibroblasts in much the same way as they do in $p53^{-/-}$ cancer cells. α5β1 integrin is the major receptor for fibronectin and participates in its fibrillogenesis. With this in mind, we developed quantitative approaches (GLCM analysis) to characterise the organisation of ECM deposited by mutp53-EV-treated TIFs. Treatment of fibroblasts with mutp53-EVs led to deposition of a more misaligned and branched ECM; a phenotype that depended on DGKα activity in the fibroblasts. Thus, our data are consistent with a mechanism through which mutp53-EVs modulate ECM deposition by increasing RCP- and DGKα-dependent α5β1 recycling in fibroblasts. Previous studies have shown that alteration to the trafficking of another fibronectin receptor, αvβ3 integrin in

endothelial cells leads to increased fibronectin polymerisation and deposition (Jones et al., 2009). Moreover, inhibition of caveolin-dependent α5β1 endocytosis is known to compromise fibronectin turnover in the endothelium and lead to accumulation of fibronectin (Sottile and Chandler, 2005). However, the EV-driven changes to ECM organisation described in the present study are not associated with altered levels of fibronectin.

It is interesting to consider the possible mechanisms through which increased α5β1 recycling may influence ECM organisation. One possibility is that it is the way in which fibroblasts move during the assembly and re-modelling of the ECM that is key to its organisation. Indeed, we have characterised how mutp53-EVs, via altered integrin recycling, change fibroblast migration speed and persistence. To pursue this, we have conducted some preliminary long-term time-lapse experiments to observe fibroblast movement in the confluent monolayers that they form whilst depositing ECM. This indicated that fibroblasts in a confluent monolayer normally migrate within a restricted area and this movement is directionally constrained – i.e. they tend to move backwards and forwards over an unaltering linear course. By contrast, mp53-exosome-treated fibroblasts under go much longer range and directionally adventitious movements (not shown), and this behaviour may be what leads to the more branched and disorganised ECM that they deposit. This hypothesis could be further investigated by studying in detail the relationship between ECM assembly (using fluorescently-labelled fibronectin and fibronectin-null-fluorescently-labelled TIFs, and time-lapse multiphoton microscopy), fibroblast movement and integrin trafficking in confluent monolayers and 3D organotypic plugs.

A recent study reported that fibronectin fibrillogenesis was promoted by activation of TGFβ receptor-2 (TGFβRII) and that this was dependent on Rab11 and α5β1 integrin recycling (Varadaraj et al., 2017). This is intriguing, considering first that RCP is an effector of Rab11 and second that TGFβ signalling was previously shown to potentiate mutp53-gain-of-functions (Adorno et al., 2009). However, this study relied on the use of dominant negative Rab11 (Varadaraj et al., 2017) which has a far more profound and generally disruptive influence on endosomal trafficking (and affects other processes, such as cytokinesis (Wilson et al., 2005; Yu et al., 2007)). Because we have found that gross alterations in fibronectin fibrillogenesis do not underlie the influence of mutp53-EVs on ECM organisation, we feel that it is unlikely that TFGβ receptors signal through RCP-dependent recycling – as opposed to another Rab11-regulated pathway, but further work will be needed to establish the relationship between TGFβ signalling and the function of mutp53-EVs in pro-invasive niche priming.

Our studies indicate that mutp53-EVs influence not only the organisation of the ECM, but also reduce its stickiness and stiffness, and that this correlates with decreased focal adhesion assembly in cells plated into de-cellularised matrices. It is now generally accepted that it is increased (not reduced) ECM stiffness that generates a more pro-invasive microenvironment for cancer cells. Indeed, cancer cells plated into stiff microenvironments display increased focal adhesion assembly and enhanced signalling downstream of integrin – for instance to focal adhesion kinase – which drives invasiveness (Jansen et al., 2017; Yeh et al., 2017). The level of ECM adhesiveness is also accepted to influence invasion, but the relationship between this property and cell migration is more complex that it is with stiffness. Indeed, when substrata are coated with fibronectin at moderate levels, this supports cell migration because it allows efficient assembly and disassembly of adhesions. However, on substrates coated with high concentrations of fibronectin, adhesions assembly efficiently, but cannot disassemble, and this inhibits cell migration. It is probably, therefore, that the reduced stickiness of mutp53-EV-fostered ECM allows efficient adhesion and disassembly, thus favouring invasiveness. It is also possible that alterations to ECM organisation influence the spacing and orientation of integrin-binding sites in a way that affects its adhesive properties. Indeed, a previous study reported that the strength of cell-ECM adhesions in human breast myoepithelial cells embedded in soft polyacrylamide gels functionalised with RGD peptides (a canonical ECM ligand for α5β1 and αvβ3 integrins) depends on the spacing of the RGD ligands within the gel (Oria et al., 2017). It is currently unclear why the adhesiveness of ECM is influenced by DGKα-dependent integrin trafficking in the fibroblasts that deposit it, and how this relates to its organisation. Further investigation will be aimed at addressing the mechanistic connections between these properties.

Here we show that in PDCLs derived from tumours corresponding to the squamous subtype of PDAC (Bailey et al., 2016), mutp53 influences the production of EVs capable of altering ECM deposition. We show that this is likely owing to the ability of mutp53 to suppress podocalyxin expression in these cells, in much the same way as we reported for H1299 cells in chapter 3. Moreover, the KPC mouse model used in the present study corresponds histologically to the squamous subtype of PDAC (Bailey et al., 2016). However, we have collected EVs from PDCLs corresponding to other subtypes of PDAC and found that this mechanism may not be generally applicable. Indeed, we found that EVs from the pancreatic progenitor subtype of PDAC produce EVs that profoundly influence ECM organisation irrespective of their p53 status (not shown). Mutations in TP53 are prevalent in PDAC and they are thought to be key drivers of their progression. Of the molecular subtypes of PDAC recently identified, squamous PDAC express high levels of ΔNp63, a p63 isoform that is

characteristic of squamous epithelia (Lin et al., 2014), and it is likely that ΔNp63's ability to interfere with TAp63 function accounts for the particularly poor prognosis of this category of PDAC (Bailey et al., 2016; Collisson et al., 2019). Another way in which TAp63 function may be compromised is via expression of mutp53s, which are also enriched for in squamous PDAC (Bailey et al., 2016; Collisson et al., 2019). However, in PDAC subtypes which do not express TA-p63 it is likely that mutp53 may not be able to influence podocalyxin expression. Thus, it is likely that oncogenes other than mutp53 have the potential to alter EV composition and the sorting of sialomucins into EVs so as to influence their ability to change endosomal trafficking and ECM deposition. Further work will be necessary to elucidate how the composition of EVs from PDAC subtypes other than squamous may drive the generation of pro-invasive microenvironments.

The combined expression of mutant KRas and mutp53 in the pancreatic epithelium of KPC mice drives the formation of highly invasive metastatic tumours. The ECM in the stroma of PDAC is likely to contribute to metastasis as this will define the invasiveness of the primary tumour and thus the ability of cells to reach the circulation. Previous work showed that fibrillar collagen is more aligned in the stroma of KPC tumours by comparison with those from $KP^{fl}C$ (p53 loss) mice, and we have confirmed this observation. Miller et al., showed that the increased stiffness and collagen alignment in the PDAC stroma is owing to mutp53's ability to drive increased expression of the collagen cross-linking enzyme lysyl oxidase (LOX) (Miller et al., 2015). Broadly consistent with this, a recent study characterised the effect of mutp53 on the tumour stroma, by evaluating the behaviour of CAFs isolated from KPC or $KP^{fl}C$ tumours in organotypic plugs. The authors reported that KPC-CAFs contracted the plugs more efficiently than did $KP^{fl}C$-CAFs, leading to higher levels of aligned fibrillar collagen and increased ECM stiffness which fostered cancer cell invasion and chemoresistance. Moreover, these workers showed that this was driven by the local release of factors from mutp53-expressing tumour cells, which activated NFκB signalling in the fibroblasts (Vennin et al., 2019). Clearly, the mutp53-EV-mediated influence on ECM deposition in distant organs differs from that which occurs in the stroma of the primary tumour. This is likely to be owing to the differences in the short range and long-range signals evoked by mutp53s. Thus, signals which mediate mutp53s desmoplastic phenotype in the stroma are likely to be mediated by locally-acting fibroblast-activating growth factors which dominate over any influence that EVs may have on stromal fibroblasts. By contrast, we propose that EVs can carry signals over longer distances through the circulation to foster deposition of less well-aligned tangled/orthogonal ECM that we observe to occur in the liver and lungs of animals bearing mutp53-expressing tumours.

Chapter 5 Final Discussion

Mutp53 drives metastasis in humans and mice. Here, we show that expression of mutp53 in tumour cells drives release of EVs that influence migration and membrane trafficking in other tumour cells and in fibroblasts, inducing the latter to deposit and/or remodel the ECM, in a way that did not alter its stiffness but altered its orthogonality and stickiness and ability to support tumour cell invasiveness. We also identified key players in this novel GOF of mutp53, such as suppression of podocalyxin levels in EVs that results from the combined action of the mutp53-p63 axis and Rab35. Finally, we report that ECM orthogonality can be induced by EV produced by PDCLs of mutp53-expressing PDAC, and that increased ECM orthogonality may be observed in target organs of mice bearing mutp53-expressing subcutaneous tumours and PDAC.

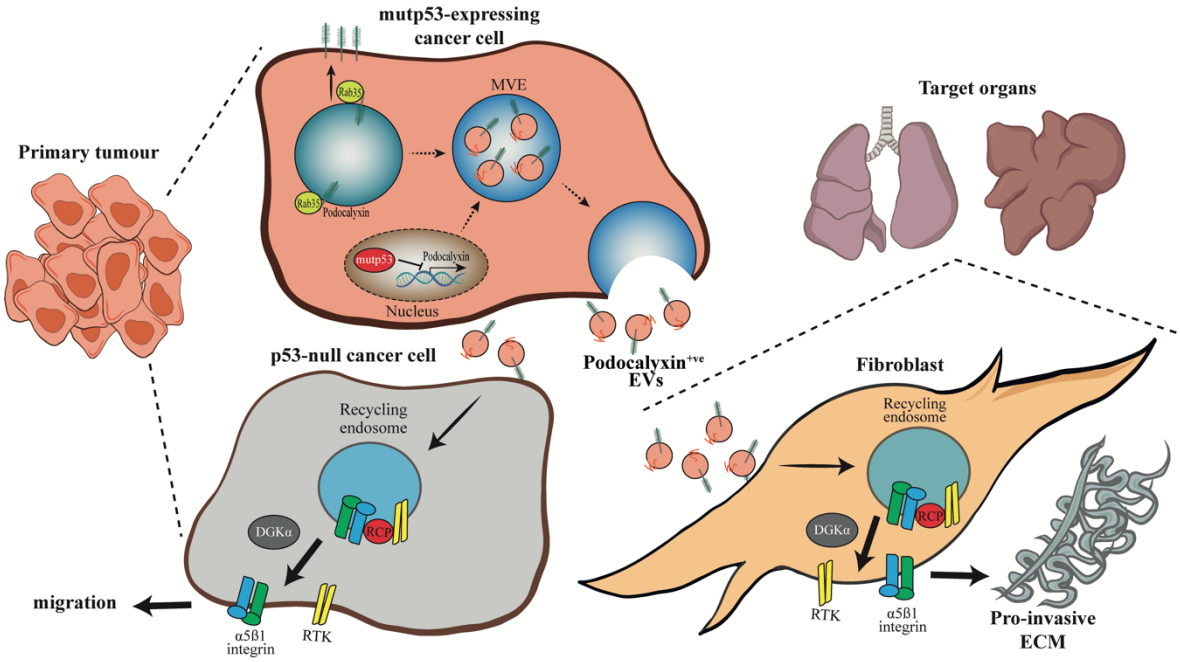

Figure 5-1- Proposed model for mutp53's gain-of-function via EVs.
mutp53-expressing cancer cells produce EVs that mediate intercellular transfer of mutp53's invasive/migratory gain-of-function by increasing RCP/DGKα-dependent receptor recycling in other cancer cells. This process depends on mutp53's ability to control expression of the sialomucin podocalyxin, and on the activity of the GTPase Rab35, a podocalyxin interactor that influences its sorting to EVs. mutp53-EVs also stimulate receptor recycling in normal fibroblasts, in turn promoting deposition of a pro-invasive ECM with characteristic orthogonal architecture. The ECM in the target organs (lung and liver) of mice possessing mutp53-expressing pancreatic tumours also displays increased orthogonal architecture which precedes metastasis, indicating that mutp53 can influence the microenvironment in distant organs in a way that may support metastatic outgrowth.

Further work will be required to explore whether the "tangled" ECM in the liver and lungs of mice bearing mutp53-expressing PDAC contributes to metastasis formation. Despite multiple lines of pre-clinical and clinical evidence indicating that invasion in the TME mostly occurs through collective cell migration in the direction of ECM fibres (reviewed in (Clark and Vignjevic, 2015), the mechanism through which tumour cells colonise distant

organs remain unclear. Thus, our observation that mutp53-EV-mediated ECM is highly permissive for tumour cell invasion may suggest a role for this ECM in promoting colonisation of disseminated tumour cells in target sites, a process that is likely to affect metastatic outgrowth. Furthermore, as we have demonstrated that the ECM fostered by mutp53-EVs affects cell-ECM adhesions, processes other than cell migration which are regulated by adhesion signalling – such as cell growth and survival - might be influenced by this type of ECM. Indeed, although the ECM fostered by mutp53-EVs did not affect tumour cell proliferation in our culture conditions, ECM remodelling in microenvironments such as the perivascular space - where tumour cells reside following extravasation - have previously been found to contribute to integrin-dependent metastatic out-growth (Albrengues et al., 2018). Because we have detected more orthogonal/tangled ECM in the perivascular space of the lung PMN, there is a possibility that, by modulating cell-ECM adhesions in vivo, mutp53-EVs might influence this or other integrin-mediated processes, thereby affecting metastasis formation. Though, this remains to be further investigated.

Another possible mechanism through which "tangled" ECM in the metastatic target organs might contribute to metastasis is through influencing recruitment of immune cell types (Amanda McFarlane, unpublished, personal communication). Notably, extensive immuno-phenotyping and time-lapse microscopy revealed that neutrophils accumulate in higher numbers and are more migratory in the lungs of KPC mice than observed in their counterparts bearing p53 null PDAC. Neutrophils in target organs are thought to promote metastasis formation by stimulating suppression of tumour-reactive lymphocytes (Leach et al., 2019). Additionally, the release of neutrophil-extracellular traps (NETs) from neutrophils has been shown to influence different aspects of metastatic outgrowth and to awaken dormant disseminated tumour cells residing in the lung. It is thought that stickiness of DNA in NETs may allow capture of tumour cells along the endothelium, promoting tumour cell extravasation (Chen, 2016) . Moreover, the proteolytic capacity of NETs may contribute to remodelling of the ECM, stimulating tumour cell invasion and growth (Park et al., 2016). Finally, a recent study has demonstrated that, during chronic inflammation, the NET components elastase and MMP9 led to remodelling of the BM, thus stimulating integrin-dependent outgrowth of dormant disseminated tumour cells (Albrengues et al., 2018). Therefore, accumulation of neutrophils in the lung is likely to contribute to the metastatic nature of the KPC model of PDAC.

Although a causal relationship between "tangled" ECM and neutrophil recruitment/function in mutp53-tumour-bearing mice remains to be demonstrated, the

ECM has previously been shown to modulate neutrophil recruitment, transmigration through the endothelium and activation. In particular, neutrophils are potently chemotactic toward the tripeptide PGP, a collagen-derived matrikine with a key role in inflammation (Akthar et al., 2015) and which is deregulated in processes such as chronic inflammation and fibrosis (O'Reilly et al., 2017). Thus, an attractive hypothesis is that the ECM fostered by mutant p53-extracellular vesicles may be more amenable to liberating chemotactic matrikines which promote neutrophil recruitment and migration. The ECM composition has also previously been shown to affect neutrophil behaviour (such as chemotaxis) and the formation of TEMs, and so there is a possibility that mutp53 expressing primary tumours might influence these processes by modulating ECM composition in metastatic target organs to prime PMNs. Some recent evidence suggests that the ECM components of the metastatic site undergo dramatical changes during metastatic outgrowth (Pearce et al., 2018). Nonetheless, the characteristics of the ECM in the PMN (i.e. prior to colonisation) are still largely unexplored. We plan to employ approaches for enrichment of ECM components from tissues, coupled with LCMS, to investigate the composition of the matrisome in PDAC-bearing mice, and to test whether expression of mutp53 in the primary tumour is able to influence this.

We have demonstrated that mutp53-EVs promote receptor recycling and migration of $p53^{-/-}$ cells. PDAC are highly heterogenous and in some cases, within the same tumour, polyclonal populations with different p53 status may co-exist (Grant et al., 2016). Furthermore, the inherent instability of mutp53 may result in heterogenous levels of mutp53 expression, a phenomenon that is described in both human and mouse tumours (Koga et al., 2001; Olive et al., 2004) Thus, our data suggest that in a tumour context, indolent tumour cells lacking mutp53 expression might acquire migratory characteristics by being 'educated' with mutp53-EVs. Speculatively, it would imply that cells lacking mutp53 might be able to invade and escape the primary tumour, and eventually reach metastatic target organs. Although it is known that metastases from mutp53-expressing tumours often display high levels of mutp53 expression, a recent study suggested that environmental cues, such as stiffness, interfere with mutp53 levels, by activating RhoA- and HSP90-mediated mutp53 stabilisation (Ingallina et al., 2018). Therefore, the expression of mutp53 is likely dynamic throughout tumour progression, rendering this hypothesis difficult to address in vivo.

PDAC is often characterised by acquisition of both mutant KRas and mutp53, and mouse models have demonstrated that these events drive PDAC initiation and invasion respectively (Morton et al., 2010). A recent study suggested that the combinatory expression of

mutant KRas and mutp53 stimulates Arf6-dependent receptor recycling in KPC cells. These workers showed that while KRas functioned in mediating translation of transcripts encoding for Arf6 and AMAP1, mutp53 activated Arf6 by upregulation PDGFR and the MVP, consequently leading to Arf6-dependent invasion and immune evasion (Hashimoto et al., 2019). Our observations that inhibition of RCP or DGKα in recipient cells completely abolished their response to mutp53-EVs is strong indication for the recycling events that drive migration and ECM remodelling occurring through Rab11, but not Arf6. Nonetheless, the interaction of mutp53 with its myriad partners, in particular those that influence mutp53-p63 inhibition, might influence the non-cell autonomous GOF for mutp53 that we have described here. Importantly, TGFβ is often present within the PDAC TME (Principe et al., 2016), and has previously been reported to drive metastasis in the KPC model(Zhong et al., 2017), which is reason for future investigation of the role of mutp53-p63-SMAD axis in the production of phenotype-altering EVs.

The deletion of podocalyxin or Rab35 in mutp53-expressing tumours impaired their ability to influence ECM deposition in distant organs. This indicates that regulation of EV-associated podocalyxin is the mechanism by which mutp53-expressing tumours mediate ECM deposition and/or remodelling in the PMN. Consistent with the fact that a large fraction of the negative charge of podocalyxin results from sialic acid residues, a recent study suggested that the amount of this sugar on EVs dictates their ability to accumulate in organs and travel through the lymphatics. These researchers injected radiolabelled EVs into mice and used PET scanning to find that at 5 minutes following injection, EVs accumulated in the liver and lung. At 72 hours, they still found EVs present in both the liver and the lung, though neuraminidase incubation (i.e. sialic acid removal) of EVs increased their accumulation in the lung and led them to travel through the lymphatics more efficiently (Royo et al., 2019). This indicates that EV charge, in particular negative charge, dictates biological function, and we believe that modulation of EV charge by podocalyxin may be important because it might act within the endosomal system of recipient cells, thereby allowing mutp53 to influence receptor recycling in a paracrine fashion and induce ECM remodelling in the PMN.

Together, the data discussed throughout this thesis highlights a non-cell autonomous mechanism that might contribute to the metastatic phenotype characteristic of many mutp53-expressing cancers. There is, indeed, a pressing need to identify mechanisms and biomarkers for metastatic disease, and our data highlights an intercellular communication pathway comprising a number of well-characterised components (including Rab35,

Podocalyxin, RCP, DGKα, collagen organisation), which may represent a panel of druggable targets and may also act as novel biomarkers to indicate the presence of metastatic tumours.

Appendices

Appendix I - EV-associated proteome Dataset

Protein name	Gene symbol	Mol. weight [kDa]	SILAC ratio	Sig.	Unique peptides
Podocalyxin	PODXL	58.64	-0.70	+	4
Ras GTPase-activating-like protein IQGAP3	IQGAP3	184.70	-0.60		2
Charged multivesicular body protein 5	CHMP5	24.57	-0.59		2
Cofilin-2	CFL2	18.74	-0.58		4
26S proteasome non-ATPase regulatory subunit 2	PSMD2	100.20	-0.56		2
Twinfilin-1	TWF1	40.28	-0.49		2
Frizzled-2;Frizzled-7	FZD2;FZD7	63.55	-0.45		2
DnaJ homolog subfamily A member 4	DNAJA4	44.80	-0.44		1
Matrilin-2	MATN2	106.84	-0.43		10
Integrin-linked protein kinase	ILK	51.42	-0.41		3
EH domain-containing protein 4	EHD4	61.17	-0.40		11
Matrix metalloproteinase-14	MMP14	65.89	-0.38		2
Charged multivesicular body protein 1b	CHMP1B	22.11	-0.37		4
Tight junction protein ZO-1	TJP1	195.46	-0.36		3
MIT domain-containing protein 1	MITD1	23.03	-0.36		2
Coronin-1C;Coronin	CORO1C	53.25	-0.36		5
Charged multivesicular body protein 1a	CHMP1A	21.70	-0.33		2
Lethal(2) giant larvae protein homolog 1	LLGL1	115.42	-0.32		2
Pituitary tumor-transforming gene 1 protein-interacting protein	PTTG1IP	20.32	-0.31		3
Connective tissue growth factor	CTGF	38.09	-0.31		4
Talin-1	TLN1	269.76	-0.31		11
BRO1 domain-containing protein BROX	BROX;C1orf58	46.48	-0.31		4
Flotillin-1	FLOT1	47.36	-0.30		4
Cofilin-1	CFL1	18.50	-0.30		8
Heat shock protein beta-1	HSPB1	22.78	-0.30		4
Centrosomal protein of 55 kDa	CEP55	54.18	-0.30		8
Elongation factor 1-beta	EEF1B2	24.76	-0.29		2
IST1 homolog	IST1	39.75	-0.28		6
Tetraspanin-4	TSPAN4	15.20	-0.28		4
Sodium-coupled neutral amino acid transporter 2	SLC38A2	56.03	-0.27		4
Neuroblast differentiation-associated protein AHNAK	AHNAK	629.09	-0.27		13
Septin-2	Sep-02	41.49	-0.27		3
40S ribosomal protein S11	RPS11	18.43	-0.27		2
Protein S100-A13	S100A13	11.47	-0.27		3
Septin-11	Sep-11	49.40	-0.26		3
Charged multivesicular body protein 4b	CHMP4B	24.95	-0.26		7

Neutral amino acid transporter A	SLC1A4	55.72	-0.25		3
Nuclear migration protein nudC	NUDC	38.24	-0.25		2
Tumor susceptibility gene 101 protein	TSG101	43.94	-0.24		6
CD63 antigen	CD63	25.64	-0.24		2
Phosphatidylinositol 4-phosphate 5-kinase type-1 alpha	PIP5K1A	62.63	-0.23		3
Tropomyosin alpha-4 chain	TPM4	28.52	-0.22		4
Platelet-activating factor acetylhydrolase IB subunit alpha	PAFAH1B1	46.64	-0.22		2
Fascin	FSCN1	54.53	-0.22		5
Ubiquitin carboxyl-terminal hydrolase 14; Ubiquitin carboxyl-terminal hydrolase	USP14	56.07	-0.21		2
Serine incorporator 1	SERINC1	50.49	-0.21		2
DnaJ homolog subfamily A member 1	DNAJA1	44.87	-0.20		7
Ras-related protein Rab-1A	RAB1A	22.68	-0.20		2
Transgelin-2	TAGLN2	22.39	-0.20		10
A-kinase anchor protein 12	AKAP12	191.48	-0.20		7
Programmed cell death protein 6	PDCD6	21.87	-0.19		4
Vimentin	VIM	53.65	-0.19		13
Vacuolar protein sorting-associated protein VTA1 homolog	VTA1	33.88	-0.19		3
Protein kinase C and casein kinase substrate in neurons protein 3	PACSIN3	48.49	-0.18		4
Adenylyl cyclase-associated protein 1	CAP1	51.90	-0.18		8
Proliferating cell nuclear antigen	PCNA	28.77	-0.18		3
EH domain-containing protein 1	EHD1	60.63	-0.18		8
DnaJ homolog subfamily A member 2	DNAJA2	45.75	-0.17		8
Peptidyl-prolyl cis-trans isomerase FKBP4	FKBP4	51.80	-0.17		6
Ras-related protein Rab-6A	RAB6A	23.59	-0.17		2
Serine incorporator 3	SERINC3	52.58	-0.17		3
ADP-ribosylation factor 6	ARF6	20.08	-0.16		4
Vacuolar protein sorting-associated protein 4B	VPS4B	49.30	-0.16		4
Destrin	DSTN	18.51	-0.16		4
40S ribosomal protein S4, X isoform	RPS4X	29.60	-0.15		3
Microtubule-associated protein RP/EB family member 1	MAPRE1	30.00	-0.15		2
Syntenin-1	SDCBP	32.44	-0.15		2
Protein HEG homolog 1	HEG1	147.46	-0.15		2
LIM and SH3 domain protein 1	LASP1	29.72	-0.15		4
Cyclin-dependent kinase 1	CDK1	34.10	-0.15		2
Methylenetetrahydrofolate dehydrogenase	MTHFD1	101.56	-0.15		6
Reticulon-4	RTN4	129.93	-0.14		2
Eukaryotic initiation factor 4A-I;Eukaryotic initiation factor 4A-II	EIF4A1;EIF4A2	46.15	-0.14		7
Heat shock 70 kDa protein 1A/1B	HSPA1A	70.05	-0.13		6
T-complex protein 1 subunit zeta	CCT6A	58.02	-0.13		5
CD151 antigen	CD151	28.30	-0.13		4

Guanine nucleotide-binding protein subunit beta-2-like 1	GNB2L1	35.08	-0.13		3
Transaldolase	TALDO1	37.54	-0.13		2
Programmed cell death 6-interacting protein	PDCD6IP	96.02	-0.12		34
40S ribosomal protein S23	RPS23	15.81	-0.12		2
CD44 antigen	CD44	81.54	-0.12		8
Elongation factor 1-gamma	EEF1G	50.12	-0.12		3
Retinoic acid-induced protein 3	GPRC5A	40.25	-0.12		2
Protein S100-A11	S100A11	11.74	-0.12		2
Guanine nucleotide-binding protein G(I)/G(S)/G(T) subunit beta-2	GNB2	37.33	-0.12		3
Endophilin-A2	SH3GL1	41.49	-0.12		4
Vinculin	VCL	123.80	-0.12		16
Vacuolar protein sorting-associated protein 35	VPS35	91.71	-0.12		4
Complement decay-accelerating factor	CD55	41.40	-0.12		3
60S acidic ribosomal protein P2	RPLP2	11.67	-0.12		2
Synaptosomal-associated protein 23; Synaptosomal-associated protein	SNAP23	23.35	-0.11		8
Sodium-dependent multivitamin transporter	SLC5A6	68.64	-0.11		5
Sulfate transporter	SLC26A2	81.66	-0.11		2
Tyrosine-protein kinase Yes	YES1	60.80	-0.11		5
E3 ubiquitin-protein ligase NEDD4-like; E3 ubiquitin-protein ligase	NEDD4L	111.93	-0.11		8
Integrin alpha-3;Integrin alpha-3 heavy chain; Integrin alpha-3 light chain	ITGA3	116.61	-0.10		20
Myelin protein zero-like protein 1	MPZL1	29.08	-0.10		6
Syntaxin-binding protein 1	STXBP1	67.57	-0.10		2
Ras-related protein Rab-8A	RAB8A	23.67	-0.10		5
5-nucleotidase	NT5E	63.37	-0.10		15
Ras-related protein Ral-A	RALA	23.57	-0.10		2
MAGUK p55 subfamily member 6	MPP6	61.12	-0.10		10
Sodium-coupled neutral amino acid transporter 1	SLC38A1	54.05	-0.09		4
Phosphatidylethanolamine-binding protein 1; Hippocampal cholinergic neurostimulating peptide	PEBP1	21.06	-0.09		4
Fermitin family homolog 2	FERMT2	77.86	-0.09		11
WD repeat-containing protein 1	WDR1	66.19	-0.09		10
Disintegrin and metalloproteinase domain-containing protein 9	ADAM9	90.56	-0.09		3
Nuclease-sensitive element-binding protein 1	YBX1	35.92	-0.09		2
Translationally-controlled tumor protein	TPT1	19.60	-0.09		4
L-lactate dehydrogenase B chain;L-lactate dehydrogenase	LDHB	36.64	-0.09		11
SLIT-ROBO Rho GTPase-activating protein 2	SRGAP2	120.88	-0.08		2
Programmed cell death protein 10	PDCD10	24.70	-0.08		4

Thioredoxin domain-containing protein 17	TXNDC17	13.94	-0.08		2
CD59 glycoprotein	CD59	14.18	-0.08		4
Alpha-soluble NSF attachment protein	NAPA	33.23	-0.08		2
Beta-2-microglobulin;Beta-2-microglobulin form pI 5.3	B2M	13.71	-0.08		3
Programmed cell death protein 5	PDCD5	14.29	-0.08		4
Ras-related protein Rab-13	RAB13	22.77	-0.08		4
Guanine nucleotide-binding protein G(I)/G(S)/G(O) subunit gamma-5	GNG5	7.32	-0.07		3
CD9 antigen	CD9	25.42	-0.07		5
Ras-related protein Rap-1b;Ras-related protein Rap-1b-like protein	RAP1B	20.83	-0.07		2
40S ribosomal protein S28	RPS28	7.84	-0.07		2
Endothelin-converting enzyme 1	ECE1	87.16	-0.06		4
Heat shock cognate 71 kDa protein	HSPA8	70.90	-0.06		19
Ras-related protein Rab-10	RAB10	22.54	-0.06		5
Phosphoglycerate kinase 1;Phosphoglycerate kinase	PGK1	44.61	-0.06		14
Nascent polypeptide-associated complex subunit alpha	NACA	205.42	-0.06		2
Choline transporter-like protein 1	SLC44A1	73.30	-0.06		4
Myoferlin	MYOF	234.71	-0.06		28
Copine-8	CPNE8	63.11	-0.06		29
Ras-related protein Rab-11B;Ras-related protein Rab-11A	RAB11B;RAB11A	24.49	-0.06		7
14-3-3 protein gamma;14-3-3 protein gamma, N-terminally processed	YWHAG	28.30	-0.06		3
Epidermal growth factor receptor	EGFR	134.28	-0.05		15
Ubiquitin carboxyl-terminal hydrolase isozyme L1	UCHL1	24.82	-0.05		6
Stress-induced-phosphoprotein 1	STIP1	62.64	-0.05		6
Catenin alpha-1	CTNNA1	100.07	-0.05		19
Poly(rC)-binding protein 1	PCBP1	37.50	-0.05		3
Ras-related protein Rab-7a	RAB7A	23.49	-0.04		11
T-complex protein 1 subunit theta	CCT8	59.62	-0.04		3
60S ribosomal protein L13a	RPL13A	23.58	-0.04		4
Axin interactor, dorsalization-associated protein	AIDA	35.02	-0.04		2
Profilin-1	PFN1	15.05	-0.04		8
Unconventional myosin-Ib	MYO1B	131.98	-0.04		16
Plastin-3	PLS3	70.81	-0.04		6
Nucleoside diphosphate kinase B;Nucleoside diphosphate kinase	NME2;NME1-NME2;NME1	30.14	-0.04		3
Transmembrane 4 L6 family member 1	TM4SF1	10.99	-0.03		1
Lactadherin;Lactadherin short form;Medin	MFGE8	43.12	-0.03		22
Membrane cofactor protein	CD46	41.36	-0.03		4
ADP-ribosylation factor 3;ADP-ribosylation factor 1	ARF3;ARF1	20.60	-0.03		2

Tyrosine-protein kinase receptor UFO	AXL	98.34	-0.03		11
N(G),N(G)-dimethylarginine dimethylaminohydrolase 2	DDAH2	29.64	-0.03		3
Myosin light polypeptide 6	MYL6	16.93	-0.03		3
Elongation factor 1-alpha 1;Putative elongation factor 1-alpha-like 3	EEF1A1;EEF1A1P5	50.14	-0.03		13
Peroxiredoxin-6	PRDX6	25.04	-0.03		3
Ras-related protein Rab-22A	RAB22A	21.86	-0.03		2
Anoctamin-6	ANO6	106.16	-0.03		3
Septin-7	Sep-07	50.68	-0.03		8
Pyruvate kinase PKM;Pyruvate kinase	PKM;PKM2	57.94	-0.02		21
Phosphoribosylaminoimidazole carboxylase	PAICS	47.08	-0.02		3
Calmodulin	CALM1;CALM2;CALM3	16.84	-0.02		7
Importin subunit alpha-1	KPNA2	57.86	-0.02		5
Ras-related protein Rap-2b	RAP2B	20.50	-0.02		3
Myosin-9	MYH9	226.53	-0.02		21
Caldesmon	CALD1	93.23	-0.02		2
Peptidyl-prolyl cis-trans isomerase A	PPIA	18.01	-0.02		6
Sodium bicarbonate cotransporter 3	SLC4A7	123.41	-0.02		9
Galectin-1	LGALS1	14.72	-0.02		4
Actin, alpha skeletal muscle; Actin, alpha cardiac muscle 1;Actin, gamma-enteric smooth muscle; Actin, aortic smooth muscle	ACTA1;ACTC1;ACTG2;ACTA2	42.05	-0.01		1
Protein eva-1 homolog B	EVA1B	18.37	-0.01		2
CD82 antigen	CD82	29.63	-0.01		3
Utrophin	UTRN	394.46	-0.01		10
Cell division cycle-associated protein 3	CDCA3	29.00	-0.01		3
Palmitoyltransferase ZDHHC5	ZDHHC5	77.54	-0.01		5
Clathrin heavy chain 1	CLTC	191.61	-0.01		12
Catenin beta-1	CTNNB1	85.50	-0.01		11
Zinc finger CCCH-type antiviral protein 1	ZC3HAV1	101.43	-0.01		3
Nucleosome assembly protein 1-like 1	NAP1L1	45.37	-0.01		2
40S ribosomal protein S3a	RPS3A	29.95	-0.01		3
Drebrin	DBN1	71.43	-0.01		5
Alpha-actinin-1	ACTN1	103.06	-0.01		10
T-complex protein 1 subunit eta	CCT7	59.37	-0.01		4
6-phosphogluconate dehydrogenase, decarboxylating	PGD	53.14	0.00		5
Syntaxin-binding protein 3	STXBP3	67.76	0.00		16
MARCKS-related protein	MARCKSL1	19.53	0.00		2
Alpha-actinin-4	ACTN4	104.85	0.00		21
Transcription factor COE2	EBF2	62.65	0.00		1
Ras GTPase-activating-like protein IQGAP1	IQGAP1	189.25	0.00		23
5-AMP-activated protein kinase catalytic subunit alpha-1	PRKAA1	64.01	0.00		2

14-3-3 protein zeta/delta	YWHAZ	27.75	0.00		10
Raftlin	RFTN1	63.15	0.00		9
Kinesin-like protein KIF23	KIF23	110.06	0.00		18
GTP-binding nuclear protein Ran	RAN	24.42	0.01		5
Protein CYR61	CYR61	42.03	0.01		14
Syndecan-4;Syndecan	SDC4	21.64	0.01		3
Integrin beta-1	ITGB1	88.41	0.01		17
Eukaryotic translation initiation factor 5A-1; Eukaryotic translation initiation factor 5A-2; Eukaryotic translation initiation factor 5A-1-like	EIF5A;EIF5A2;EIF5AL1	16.83	0.01		3
Tubulin alpha-1B chain;Tubulin alpha-1A chain;Tubulin alpha-4A chain;Tubulin alpha-3C/D chain;Tubulin alpha-3E chain	TUBA1B;TUBA1A;TUBA4A;TUBA3C;TUBA3E	50.15	0.01		3
Actin-binding protein anillin	ANLN	124.20	0.01		11
CD81 antigen	CD81	25.81	0.02		2
Butyrophilin subfamily 2 member A1;Butyrophilin subfamily 2 member A2	BTN2A1;BTN2A2	59.63	0.02		5
Protein XRP2	RP2	39.64	0.02		7
Tumor necrosis factor receptor superfamily member 6	FAS	37.73	0.02		2
Prostaglandin E synthase 3	PTGES3	18.70	0.02		3
Peripheral plasma membrane protein CASK	CASK	105.12	0.02		11
T-complex protein 1 subunit delta	CCT4	57.92	0.02		5
Guanine nucleotide-binding protein subunit alpha-11	GNA11	42.12	0.02		7
Glyceraldehyde-3-phosphate dehydrogenase	GAPDH	36.05	0.02		12
Tumor necrosis factor receptor superfamily member 10A	TNFRSF10A	50.09	0.02		2
Protein DJ-1	PARK7	19.89	0.02		3
Guanine nucleotide-binding protein G(i) subunit alpha-2	GNAI2	40.45	0.02		8
Rab GDP dissociation inhibitor beta	GDI2	50.66	0.03		13
Coactosin-like protein	COTL1	15.95	0.03		5
Leukocyte surface antigen CD47	CD47	35.21	0.03		3
Fatty acid-binding protein, epidermal	FABP5	15.16	0.03		6
Heat shock protein 105 kDa	HSPH1	96.86	0.03		6
Disintegrin and metalloproteinase domain-containing protein 10	ADAM10	84.14	0.03		8
Ras-related protein R-Ras2	RRAS2	23.40	0.03		3
Nucleophosmin	NPM1	32.58	0.03		4
Receptor-type tyrosine-protein phosphatase F	PTPRF	212.88	0.03		10
60S ribosomal protein L24	RPL24	17.78	0.03		2
Dynein light chain 2, cytoplasmic;Dynein light chain 1, cytoplasmic	DYNLL2;DYNLL1	10.35	0.03		2
Tyrosine-protein kinase JAK1	JAK1	133.28	0.03		3

Polyubiquitin-B;Ubiquitin;Ubiquitin-40S ribosomal protein S27a;Ubiquitin;40S ribosomal protein S27a;Ubiquitin-60S ribosomal protein L40;Ubiquitin;60S ribosomal protein L40;Polyubiquitin-C;Ubiquitin	UBB;RPS27A;UBC;UBA52;UBBP4	25.76	0.04		4
Monocarboxylate transporter 8	SLC16A2	59.51	0.04		2
60S ribosomal protein L15;Ribosomal protein L15	RPL15	24.15	0.04		2
Elongation factor 2	EEF2	95.34	0.04		23
Alpha-enolase	ENO1	47.17	0.04		17
78 kDa glucose-regulated protein	HSPA5	72.33	0.05		4
Triosephosphate isomerase	TPI1	30.79	0.05		11
Borealin	CDCA8	31.32	0.05		2
Protein Niban	FAM129A	103.13	0.05		6
14-3-3 protein beta/alpha;14-3-3 protein beta/alpha, N-terminally processed	YWHAB	28.08	0.05		6
Long-chain-fatty-acid--CoA ligase 4	ACSL4	79.19	0.05		7
60S ribosomal protein L4	RPL4	47.70	0.05		2
Filamin-C	FLNC	291.02	0.05		26
CD166 antigen	ALCAM	65.10	0.05		2
GTP-binding protein Rheb	RHEB	20.50	0.05		4
L-lactate dehydrogenase A chain	LDHA	36.69	0.05		10
Myristoylated alanine-rich C-kinase substrate	MARCKS	31.55	0.05		8
Annexin;Annexin A6	ANXA6	75.28	0.05		16
Cell division control protein 42 homolog	CDC42	21.26	0.05		3
Guanine nucleotide-binding protein G(I)/G(S)/G(T) subunit beta-1	GNB1	37.38	0.06		7
Transitional endoplasmic reticulum ATPase	VCP	89.32	0.06		8
Adenosylhomocysteinase	AHCY	47.72	0.06		3
60S ribosomal protein L3	RPL3	46.11	0.06		4
Disintegrin and metalloproteinase domain-containing protein 17	ADAM17	93.02	0.06		2
Ras-related protein Rab-5B	RAB5B	23.71	0.06		2
Annexin A11;Annexin	ANXA11	54.39	0.06		5
Copine-1	CPNE1	59.06	0.06		5
Disco-interacting protein 2 homolog B	DIP2B	171.49	0.06		2
Rho-related GTP-binding protein RhoG	RHOG	21.31	0.06		2
Tubulin beta chain;Tubulin beta-2B chain	TUBB;TUBB2B	49.67	0.06		2
Heat shock protein HSP 90-beta	HSP90AB1	83.26	0.06		11
RELT-like protein 1	RELL1	29.34	0.06		3
Inorganic pyrophosphatase	PPA1	32.66	0.06		4
Peroxiredoxin-1	PRDX1	22.11	0.06		8
T-complex protein 1 subunit epsilon	CCT5	59.67	0.06		8
Macrophage migration inhibitory factor	MIF	12.48	0.07		2
Ras-related protein Rab-14	RAB14	23.90	0.07		2
Catenin delta-1	CTNND1	108.17	0.07		12
Calcium-binding protein 39	CAB39	39.87	0.07		2

Hsc70-interacting protein;Putative protein FAM10A4;Putative protein FAM10A5	ST13;ST13P4;ST13P5	41.33	0.07		3
Rho GDP-dissociation inhibitor 1	ARHGDIA	23.21	0.07		4
Neutral amino acid transporter B(0)	SLC1A5	56.60	0.07		8
Rac GTPase-activating protein 1	RACGAP1	71.03	0.07		8
T-complex protein 1 subunit gamma	CCT3	60.53	0.07		6
Guanine nucleotide-binding protein G(s) subunit alpha isoforms short;Guanine nucleotide-binding protein G(s) subunit alpha isoforms XLas	GNAS	45.66	0.07		8
Sodium-dependent phosphate transporter 1	SLC20A1	73.70	0.07		2
Transferrin receptor protein 1;Transferrin receptor protein 1, serum form	TFRC	84.87	0.08		14
T-complex protein 1 subunit beta	CCT2	57.49	0.08		6
Heat shock protein HSP 90-alpha	HSP90AA1	84.66	0.08		14
Sorcin	SRI	21.68	0.08		5
Copine-3	CPNE3	60.13	0.08		10
Ras-related protein Rab-18	RAB18	22.98	0.08		5
Protein lin-7 homolog C;Protein lin-7 homolog A	LIN7C;LIN7A	21.83	0.08		5
GTPase NRas	NRAS	21.23	0.08		2
40S ribosomal protein S2	RPS2	31.32	0.08		3
Zinc transporter ZIP10	SLC39A10	94.13	0.08		7
60S ribosomal protein L13	RPL13	24.26	0.08		6
Annexin A5;Annexin	ANXA5	35.94	0.09		10
TLD domain-containing protein 1	TLDC1	50.99	0.09		6
Poliovirus receptor-related protein 2	PVRL2	51.36	0.09		4
Transforming protein RhoA	RHOA	21.77	0.09		5
Equilibrative nucleoside transporter 1	SLC29A1	50.22	0.09		3
Endoplasmin	HSP90B1	92.47	0.09		5
Plasma membrane calcium-transporting ATPase 1	ATP2B1	138.75	0.09		6
DnaJ homolog subfamily C member 5	DNAJC5	22.15	0.09		3
Disks large homolog 1	DLG1	100.45	0.09		8
Cysteine-rich and transmembrane domain-containing protein 1	CYSTM1	10.63	0.09		2
Guanine nucleotide-binding protein subunit alpha-13	GNA13	44.05	0.09		5
Guanine nucleotide-binding protein subunit beta-4	GNB4	37.57	0.09		3
Annexin A1	ANXA1	38.71	0.10		15
Folate transporter 1	SLC19A1	64.87	0.10		3
Neurogenic locus notch homolog protein 2;Notch 2 extracellular truncation;Notch 2 intracellular domain	NOTCH2	265.40	0.10		3
Vacuolar protein sorting-associated protein 28 homolog	VPS28	25.43	0.10		2
Fructose-bisphosphate aldolase A;Fructose-bisphosphate aldolase	ALDOA	39.42	0.10		12

14-3-3 protein epsilon	YWHAE	29.17	0.10		10
ADP-ribosylation factor 4	ARF4	20.51	0.11		2
Protein scribble homolog	SCRIB	174.88	0.11		17
Cytoplasmic FMR1-interacting protein 1;Cytoplasmic FMR1-interacting protein 2	CYFIP1;CYFIP2	145.18	0.11		3
Ras-related protein R-Ras	RRAS	23.48	0.11		5
Glucose-6-phosphate isomerase	GPI	63.15	0.11		6
Calreticulin	CALR	48.14	0.11		5
Plexin-B2	PLXNB2	205.12	0.11		24
Niban-like protein 1	FAM129B	84.14	0.11		12
Tyrosine-protein kinase Lyn	LYN	58.57	0.11		7
Phosphoglycerate mutase 1	PGAM1	28.80	0.11		4
Solute carrier family 2, facilitated glucose transporter member 1	SLC2A1	54.08	0.12		6
Serine/threonine-protein phosphatase PP1-gamma catalytic subunit;Serine/threonine-protein phosphatase	PPP1CC	36.98	0.12		2
Ras-related protein Rab-35	RAB35	23.03	0.12		7
Vasodilator-stimulated phosphoprotein	VASP	39.83	0.12		2
Integrin alpha-4	ITGA4	114.90	0.12		16
Guanine nucleotide-binding protein G(k) subunit alpha	GNAI3	40.53	0.12		3
F-actin-capping protein subunit alpha-1	CAPZA1	32.92	0.12		2
2,3-cyclic-nucleotide 3-phosphodiesterase	CNP	47.58	0.12		13
Annexin A4;Annexin	ANXA4	35.88	0.12		5
Radixin	RDX	68.56	0.12		8
Desmoglein-2	DSG2	122.29	0.13		5
Guanine nucleotide-binding protein G(I)/G(S)/G(O) subunit gamma-12	GNG12	8.01	0.13		5
Sodium/potassium-transporting ATPase subunit beta-1	ATP1B1	35.06	0.13		6
Vacuolar protein sorting-associated protein 4A	VPS4A	48.90	0.13		2
Plakophilin-2	PKP2	97.41	0.13		6
Ephrin type-B receptor 4	EPHB4	108.27	0.13		2
Phospholipid scramblase 1	PLSCR1	35.05	0.13		3
FERM, RhoGEF and pleckstrin domain-containing protein 1	FARP1	118.63	0.13		5
Zinc transporter ZIP6	SLC39A6	85.05	0.13		3
Golgin subfamily A member 7	GOLGA7	15.82	0.13		6
Plasminogen activator inhibitor 1	SERPINE1	45.06	0.13		2
Myosin regulatory light chain 12B; Myosin regulatory light chain 12A; Myosin regulatory light polypeptide 9;	MYL12B;MYL12A;MYL9	19.78	0.13		4
T-complex protein 1 subunit alpha	TCP1	60.34	0.13		7
Hypoxanthine-guanine phosphoribosyltransferase	HPRT1	24.58	0.13		2
Stathmin	STMN1	17.30	0.14		4

Sodium/potassium-transporting ATPase subunit beta-3	ATP1B3	31.51	0.14		7
Ribonuclease inhibitor	RNH1	49.97	0.14		2
Erythrocyte band 7 integral membrane protein	STOM	31.73	0.14		9
ADP-ribosylation factor-like protein 6-interacting protein 1	ARL6IP1	27.17	0.14		2
Ephrin type-A receptor 2	EPHA2	108.27	0.15		21
Multivesicular body subunit 12A	MVB12A	28.78	0.15		2
High affinity cationic amino acid transporter 1	SLC7A1	67.64	0.15		4
60S ribosomal protein L8	RPL8	28.02	0.15		2
Ras-related protein Ral-B	RALB	23.41	0.15		4
UDP-N-acetylhexosamine pyrophosphorylase	UAP1	58.77	0.16		9
Nicastrin	NCSTN	78.41	0.16		6
Glutathione S-transferase P	GSTP1	23.36	0.16		2
Large neutral amino acids transporter small subunit 1	SLC7A5	55.01	0.17		5
40S ribosomal protein S9	RPS9	22.59	0.17		4
MOB kinase activator 1B;MOB kinase activator 1A	MOB1B;MOB1A	25.09	0.17		3
Ras-related protein Rab-23	RAB23	26.66	0.17		4
Brain-specific angiogenesis inhibitor 1-associated protein 2-like protein 1	BAIAP2L1	56.88	0.17		3
Zinc transporter ZIP14	SLC39A14	54.21	0.17		3
Guanine nucleotide-binding protein G(i) subunit alpha-1	GNAI1	40.36	0.18		3
Urokinase-type plasminogen activator	PLAU	48.51	0.18		3
Syntaxin-4	STX4	34.18	0.18		4
14-3-3 protein eta	YWHAH	28.22	0.18		3
G protein-regulated inducer of neurite outgrowth 1	GPRIN1	102.40	0.18		2
Integrin alpha-V;Integrin alpha-V heavy chain;Integrin alpha-V light chain	ITGAV	116.04	0.18		24
Moesin	MSN	67.82	0.19		23
Sodium/potassium-transporting ATPase subunit alpha-1	ATP1A1	112.89	0.19		34
Poliovirus receptor	PVR	45.30	0.19		6
Protein FAM49B	FAM49B	36.75	0.19		5
Na(+)/H(+) exchange regulatory cofactor NHE-RF1	SLC9A3R1	38.87	0.19		2
Guanine nucleotide-binding protein G(q) subunit alpha	GNAQ	42.14	0.19		2
Formin-like protein 2	FMNL2	123.32	0.19		5
Intercellular adhesion molecule 1	ICAM1	57.83	0.20		4
Chromosome-associated kinesin KIF4A	KIF4A	139.88	0.20		6
1-phosphatidylinositol 4,5-bisphosphate phosphodiesterase beta-4	PLCB4	136.10	0.20		17
Ras-related C3 botulinum toxin substrate 1;Ras-related C3 botulinum toxin substrate 3	RAC1;RAC3	21.45	0.21		4
60S ribosomal protein L18	RPL18	21.63	0.21		3

Ezrin	EZR	69.41	0.21		14
Importin subunit beta-1	KPNB1	97.17	0.22		5
Inosine-5-monophosphate dehydrogenase 2	IMPDH2	55.80	0.22		2
Scavenger receptor class B member 1	SCARB1	56.97	0.22		3
Protein LAP2	ERBB2IP	158.30	0.22		11
Fatty acid synthase	FASN	273.42	0.23		11
Calnexin	CANX	67.57	0.23		3
Peptidyl-prolyl cis-trans isomerase FKBP1A;Peptidyl-prolyl cis-trans isomerase	FKBP1A;FKBP12-Exip2	11.95	0.24		2
Monocarboxylate transporter 1	SLC16A1	53.94	0.24		6
Ubiquitin-conjugating enzyme E2 variant 1;Ubiquitin-conjugating enzyme E2 variant 2	UBE2V1;TMEM189;UBE2V2	11.77	0.25		3
Heterogeneous nuclear ribonucleoprotein H	HNRNPH1;HNRNPH2	49.23	0.25		3
Regulator of G-protein signaling 20	RGS20	27.06	0.25		4
Chloride intracellular channel protein 4	CLIC4	28.77	0.25		7
Mitogen-activated protein kinase kinase kinase kinase 4;TRAF2 and NCK-interacting protein kinase	MAP4K4;TNIK	142.10	0.25		5
Integrin beta-5	ITGB5	88.05	0.25		5
Inactive tyrosine-protein kinase 7	PTK7	118.39	0.27		2
40S ribosomal protein S6	RPS6	28.68	0.27		4
GTPase KRas;GTPase KRas, N-terminally processed	KRAS	21.42	0.27		3
CUB domain-containing protein 1	CDCP1	92.93	0.28		15
Voltage-dependent calcium channel subunit alpha-2/delta-1	CACNA2D1	124.57	0.28		5
Collagen alpha-1(XVIII) chain;Endostatin	COL18A1	178.19	0.28		6
Exportin-2	CSE1L	110.42	0.28		2
26S protease regulatory subunit 4	PSMC1	49.18	0.28		3
Integrin alpha-6;Integrin alpha-6 heavy chain;Integrin alpha-6 light chain	ITGA6	119.47	0.29		2
Protein tweety homolog 3	TTYH3	57.54	0.29		3
Polyadenylate-binding protein 1;Polyadenylate-binding protein 3	PABPC1;PABPC3	70.67	0.30		2
Protein EFR3 homolog A	EFR3A	92.92	0.30		3
Chloride intracellular channel protein 1	CLIC1	26.92	0.31		9
Ras-related protein Rab-2A;Ras-related protein Rab-2B	RAB2A;RAB2B	23.55	0.31		6
Rho-related GTP-binding protein RhoC	RHOC	22.01	0.31		5
Plasma membrane calcium-transporting ATPase 4	ATP2B4	137.92	0.32		4
Neprilysin	MME	85.51	0.32		10
CD276 antigen	CD276	57.24	0.33		3
MAP/microtubule affinity-regulating kinase 3;Serine/threonine-protein kinase MARK1	MARK3;MARK1	84.49	0.33		2
S-adenosylmethionine synthase isoform type-2	MAT2A	43.66	0.33		3

Septin-9	Sep-09	65.40	0.33		3
MHC class I polypeptide-related sequence B	MICA;MICB	22.24	0.34		2
Heat shock 70 kDa protein 4	HSPA4	94.33	0.34		2
Plexin-A1	PLXNA1	211.06	0.34		5
CD97 antigen;CD97 antigen subunit alpha;CD97 antigen subunit beta	CD97	91.87	0.35		6
Basigin	BSG	42.20	0.36		5
Integrin alpha-5;Integrin alpha-5 heavy chain;Integrin alpha-5 light chain	ITGA5	114.54	0.37		9
Claudin domain-containing protein 1	CLDND1	28.60	0.37		2
Zinc transporter 1	SLC30A1	55.30	0.38		2
Multidrug resistance-associated protein 1	ABCC1	171.59	0.40		3
Protein-glutamine gamma-glutamyltransferase 2	TGM2	77.33	0.41		6
14-3-3 protein theta	YWHAQ	27.76	0.41		2
Lactoylglutathione lyase	GLO1	20.78	0.41		3
Histone H3.2;Histone H3.1;Histone H3.3;Histone H3.1t;Histone H3;Histone H3.3C	HIST2H3A; HIST1H3A; H3F3A;HIS T3H3;H3F3 B;H3F3C	15.39	0.42		4
ATP synthase subunit alpha, mitochondrial;ATP synthase subunit alpha	ATP5A1	59.75	0.43		2
Urokinase plasminogen activator surface receptor	PLAUR	36.98	0.45		4
Histone H4	HIST1H4A	11.37	0.47		6
Major vault protein	MVP	99.33	0.47		19
60 kDa heat shock protein, mitochondrial	HSPD1	61.05	0.51		5
Malate dehydrogenase, mitochondrial;Malate dehydrogenase	MDH2	35.50	0.59		2
Phosphatidylinositol 4-kinase alpha	PI4KA	231.32	0.60		3
Carboxypeptidase M	CPM	50.51	0.64	+	4
Basement membrane-specific heparan sulfate proteoglycan core protein;Endorepellin;LG3 peptide	HSPG2	468.83	0.76	+	32
Afadin	MLLT4	206.80	0.96	+	2

Appendix I - SILAC-based proteomic comparison of H1299-p53$^{-/-}$ and H1299-p53^{R273H} EVs.
H1299-p53-/- and H1299-p53R273H cells were SILAC-labelled with heavy (H) and light (L) amino acids respectively. Conditioned media were collected from labelled cells, exosomes purified from these using differential centrifugation, and their proteome analysed by mass spectrometry. Column F indicates the SILAC ratio of p53R273H/H1299-p53-/- EV which is calculated from reciprocal of the ratio of H/L peptides. Sig. means significant. Significance B statistic test, False discovery rate of 5%, Perseus software.

Appendix II - Novo et al., 2018

nature COMMUNICATIONS

ARTICLE

DOI: 10.1038/s41467-018-07339-y OPEN

Mutant p53s generate pro-invasive niches by influencing exosome podocalyxin levels

David Novo[1], Nikki Heath[1], Louise Mitchell[1], Giuseppina Caligiuri[2], Amanda MacFarlane[1], Dide Reijmer[1], Laura Charlton[3], John Knight[1], Monika Calka[2], Ewan McGhee[1], Emmanuel Dornier[1], David Sumpton[1], Susan Mason[1], Arnaud Echard[4], Kerstin Klinkert[4], Judith Secklehner[1,5], Flore Kruiswijk[1], Karen Vousden[1,2,7], Iain R. Macpherson[1,2], Karen Blyth[1,2], Peter Bailey[6], Huabing Yin[3], Leo M. Carlin[1,5], Jennifer Morton[1,2], Sara Zanivan[1,2] & Jim C. Norman[1,2]

Mutant p53s (mutp53) increase cancer invasiveness by upregulating Rab-coupling protein (RCP) and diacylglycerol kinase-α (DGKα)-dependent endosomal recycling. Here we report that mutp53-expressing tumour cells produce exosomes that mediate intercellular transfer of mutp53's invasive/migratory gain-of-function by increasing RCP-dependent integrin recycling in other tumour cells. This process depends on mutp53's ability to control production of the sialomucin, podocalyxin, and activity of the Rab35 GTPase which interacts with podocalyxin to influence its sorting to exosomes. Exosomes from mutp53-expressing tumour cells also influence integrin trafficking in normal fibroblasts to promote deposition of a highly pro-invasive extracellular matrix (ECM), and quantitative second harmonic generation microscopy indicates that this ECM displays a characteristic orthogonal morphology. The lung ECM of mice possessing mutp53-driven pancreatic adenocarcinomas also displays increased orthogonal characteristics which precedes metastasis, indicating that mutp53 can influence the microenvironment in distant organs in a way that can support invasive growth.

[1] Beatson Institute for Cancer Research, Glasgow G611BD Scotland, UK. [2] Institute of Cancer Sciences, University of Glasgow, Glasgow G61 1QH, UK. [3] School of Engineering, University of Glasgow, Glasgow G12 8LT, UK. [4] Membrane Traffic and Cell Division Lab, Cell Biology and Infection Department, Institut Pasteur, 25-28 rue du Dr Roux, Paris 75724, France. [5] Inflammation, Repair & Development, National Heart & Lung Institute, Imperial College London, London SW7 2AZ, UK. [6] Wolfson Wohl Cancer Research Centre, Institute of Cancer Sciences, University of Glasgow, Glasgow G611QH, UK. [7] Present address: Francis Crick Institute, 1 Midland Road, London NW1 1ST, UK. These authors contributed equally: David Novo, Nikki Heath. Correspondence and requests for materials should be addressed to J.C.N. (email: j.norman@beatson.gla.ac.uk)

Loss of wild-type p53 function is a key watershed in tumour initiation and progression. This occurs through loss of p53 expression or mutations that generate p53 proteins defective in wild-type function. A gain-of-function for mutant p53 (ref. [1]) (mutp53) first became apparent following the construction of a mouse model of Li-Fraumeni syndrome[2]. In this animal, wild-type p53 was replaced with mutp53 alleles ($p53^{R270H}$ and $p53^{R172H}$) and this led to the spontaneous growth of tumours with more aggressive phenotypes than was observed in p53 null mice. The ability of mutp53 to drive metastasis was then demonstrated using autochthonous mouse models of pancreatic cancer[3], and cells isolated from mutp53 pancreatic tumours are more invasive than their p53 null counterparts[4], indicating that mutp53's pro-metastatic gain-of-function is associated with increased cell migration[5,6].

The way in which integrin receptors for the ECM are trafficked through the endosomal pathway and returned, or recycled, to the plasma membrane is key to the migratory behaviour of cancer cells[7,8]. The Rab11 effector, Rab-coupling protein (RCP), controls integrin recycling, and it is now clear that mutant p53s can drive invasive migration by promoting RCP-dependent integrin recycling[6]. The characteristics of the tumour ECM is closely correlated with disease progression, resistance to therapy, and poor prognosis, and there is now much interest in targeting the ECM and its receptors as an anti-cancer strategy[9]. The ECM within tumours is deposited primarily by fibroblastic cells (carcinoma-associated fibroblasts (CAFs)) and this is controlled by autocrine and paracrine pathways which relay signals between malignant cells and CAFs[10]. Furthermore, ECM proteins are assembled and extensively re-modelled following secretion, and the way that integrins are trafficked through the endosomal system can control this[11,12]. Finally, secreted factors, such as lysyl oxidase, can act directly on the ECM to introduce cross-links which alter ECM organisation and stiffness in way that promotes local invasiveness[13].

The ECM of target organs also contributes to metastasis, and cells in the primary tumour can influence this by releasing factors into the circulation. For instance, lysyl oxidase not only influences the ECM of primary tumours in the breast but also primes bone marrow niches to enable metastatic seeding[14]. Primary tumours also prime metastatic niches by releasing extracellular vesicles (EVs)—such as exosomes—into the circulation. Exosomes released by melanomas can influence differentiation of bone marrow-derived stem cells to promote their mobilisation to tissues—such as the lung—where they contribute to deposition of ECM proteins[15]. More recently exosomes from pancreatic adenocarcinoma cells were shown to promote TGFβ secretion from Kupffer cells which led to fibronectin production by liver stellate cells[16]. However, despite studies outlining how certain factors, such as oncogenic proteins and microRNAs might be transmitted between cells, the molecular players that mediate the pro-metastatic effects of oncogenes are not yet clear.

Here we report that primary tumours expressing mutp53s with pro-metastatic gain-of-function can evoke pro-invasive alterations to the ECM in a metastatic target organ, and we provide the molecular details of how this occurs.

Results

Mutp53 promotes release of diffusible pro-invasive factor(s). 'Organotypic' plugs of acid-extracted type I collagen in which the ECM has been 'preconditioned' by human fibroblasts recapitulate key characteristics of the stromal microenvironment[17]. When plated onto organotypic plugs preconditioned with telomerase-immortalised human fibroblasts (TIFs), H1229 non-small cell lung carcinoma cells (which do not express p53) ($H1299\text{-}p53^{-/-}$) were poorly invasive, with most cells residing in the upper portion of the plug 10 days after plating (Fig. 1a, d). By contrast, H1299 cells expressing the conformational gain-of-function mutant of p53, $p53^{R273H}$ ($H1299\text{-}p53^{R273H}$) invaded extensively into organotypic plugs (Fig. 1b, d).

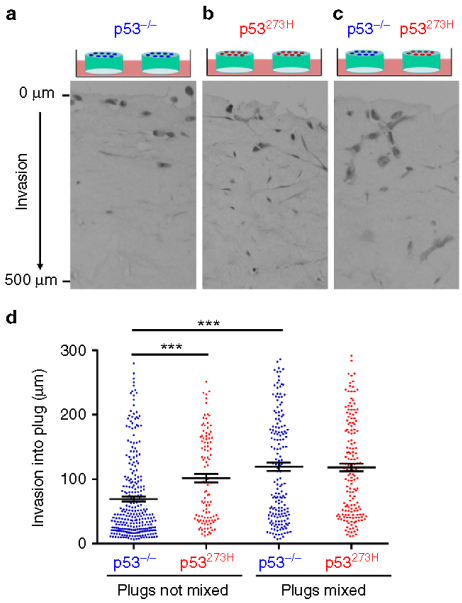

Fig. 1 Mutant p53 promotes release of diffusible factors to foster tumour cell invasion in an organotypic microenvironment. Organotypic plugs were generated allowing acid-extracted rat tail collagen to polymerise in the presence of telomerase-immortalised human dermal fibroblasts (TIFs). Fibroblast-containing plugs were conditioned for 2 days to allow TIFs to deposit and remodel the ECM. Preconditioned plugs were overlaid with $H1299\text{-}p53^{-/-}$ (**a**) or $H1299\text{-}p53^{R273H}$ (**b**) cells and placed onto grids in independent Petri dishes containing culture medium. In **c** plugs which were overlaid with $H1299\text{-}p53^{-/-}$ were placed onto grids in the same Petri dish as those overlaid with $H1299\text{-}p53^{R273H}$ cells, thus allowing the possibility of exchange of diffusible factors between plugs. Tumour cells were allowed to invade for 10 days, followed by fixation and visualisation of tumour cells with H&E. The distance between each tumour cell and the top of the plug was determined and plotted in **d**. Bars are mean ± SEM, $n = 8$ plugs; *** $p < 0.001$ Mann–Whitney test

Pro-invasive oncogenic pathways can operate in a non-cell autonomous fashion by promoting release of diffusible factors. To test whether mutp53 promotes release of pro-invasive factor(s), we placed organotypic plugs containing $H1299\text{-}p53^{R273H}$ cells in the same Petri dish as plugs plated with isogenic p53 null cells ($H1299\text{-}p53^{-/-}$) (Fig. 1c). When cultured in this way, $H1299\text{-}p53^{-/-}$ cells displayed invasive behaviour that was indistinguishable from $H1299\text{-}p53^{R273H}$ cells (Fig. 1c, d). These data indicate that the mutant p53 invasive gain-of-function phenotype may be transferred via diffusible factor(s).

Mutp53-expressing cells release exosomes to influence RCP-dependent integrin trafficking and cell migration in p53 null cells. Mutp53-expressing cells migrate faster and more erratically on 2D substrates than their p53 null counterparts[6]. Indeed,

persistence and forward migration index (FMI) of H1299 cells migrating into scratch-wounds is suppressed by expression of mutp53 (Supplementary Figure 1a–c). To represent these changes graphically, we calculated the differences between the persistence and FMI of mutp53-expressing and p53 null cells—these we term the ΔPersistence and ΔFMI—and plotted them as *x* and *y* coordinates, respectively (Supplementary Figure 1d).

Conditioned medium from H1299-p53^{R273H} donor cells significantly suppressed the migratory persistence and FMI of H1299-p53$^{-/-}$ recipient cells, and this was opposed by siRNA of p53^{R273H} in the donor cells (Supplementary Figure 1e). Moreover, depletion of exosomes by centrifugation completely opposed the ability of conditioned medium collected from H1299-p53^{R273H} cells to suppress the migratory persistence and FMI of p53$^{-/-}$ H1299 cells, indicating the likelihood that the diffusible factor(s) responsible for transfer of mutant p53's migratory gain-of-function is/are associated with exosomes (Supplementary Figure 1f).

Nanoparticle tracking, sucrose density gradient centrifugation and transmission electron microscopy (TEM) indicated that the abundance, average protein content, size distribution, and density of exosomes released by H1299 cells was not reproducibly altered by expression of mutp53 (Supplementary Figure 2a–e). Moreover, immunogold TEM indicated that the majority of EVs from H1299 cells were CD63 positive and this was not altered by expression of mutant p53 (Supplementary Figure 2f). Furthermore, a number of exosome markers (CD9, CD63, tsg101, HSPA8) did not differ between exosomes released by p53$^{-/-}$ and mutant p53-expressing cells, and p53 itself was not detectable in exosome preparations (Supplementary Figure 2g). Despite these physical similarities, we isolated exosomes from H1299 cells expressing either of two p53 mutants known to drive mutant p53's invasive gain-of-function, p53^{273H} or p53^{175H} (mutp53^{273H} or mutp53^{175H}-exosomes, respectively) and p53 null H1299 cells (termed 'p53$^{-/-}$-exosomes') and compared the ability of these to influence receptor recycling in p53 null-recipient H1299 cells. α5β1 integrin, cMET, and the transferrin receptor (TfnR) recycling was significantly increased by pre-incubation of H1299-p53$^{-/-}$ recipient cells with 'mutp53^{273H} or mutp53^{175H}, but not—p53$^{-/-}$-exosomes (Fig. 2a). Moreover, use of a DGKα inhibitor (R59022) indicated that this response was dependent on the RCP and DGKα-regulated recycling pathway previously found to be activated in mutp53-expressing cells[8]. By contrast, α5β1, cMET, and TfnR internalisation was not influenced by treatment with mutp53^{R273H}-exosomes (Supplementary Figure 3a).

To investigate the ability of exosomes to mediate intercellular transfer of mutant p53-driven migratory characteristics, we incubated p53 null recipient cells with exosomes purified from H1299 donor cells expressing either mutp53^{R273H}, mutp53^{R175H} (Fig. 2b) or wild-type p53 under control of a doxycycline-inducible promoter (H1299-p53^{tetON}) (Fig. 2c). Exosomes from donor cells that expressed mutant p53s evoked migratory characteristics associated with mutant p53's invasive gain-of-function (i.e. suppression of migratory persistence and FMI and significantly increased migration speed) in p53 null recipients, whereas exosomes from H1299 cells expressing wild-type p53 were ineffective in this regard (Fig. 2b, c). Furthermore, increased recycling (of α5β1 and TfnR) and migratory characteristics associated with mutant p53 may be passed via exosomes to A2780 cells - which express wild-type p53 (Supplementary Figure 3b). Finally, all these exosome-driven alterations to migratory behaviour were opposed by knockdown of RCP or by inhibition of DGKα in the recipient cells (Fig. 2d; Supplementary Figure 4a), but not the donor cells (Supplementary Figure 4c). Titration experiments indicated that 2×10^7 exosomes/mL were sufficient to transfer mutant p53's migratory phenotype between cells (Supplementary Figure 3c). Thus, the concentration of exosomes which accumulate in the medium bathing mutant p53-expressing cells (approx. 1×10^9 particles/mL) is 100-fold more than is required to generate a migratory phenotype in recipient cells. Moreover, these data indicate that exosomes from p53$^{-/-}$ cells cannot influence the migratory phenotype of recipient cells even when used at a 100-fold higher concentrations than is required for p53^{273H}-exosomes to evoke increased cell migration.

Taken together, these data indicate that both p53 null and mutant p53-expressing tumour cells release exosomes in similar quantities, but those from mutant p53-expressing cells upregulate RCP and DGKα-dependent receptor recycling in p53 null recipient cells to evoke migratory characteristics associated with mutant p53's invasive gain-of-function.

Mutp53 controls exosomal podocalyxin levels to drive receptor trafficking and cell migration in p53 null cells. We proposed that altered exosome composition might be responsible for intercellular transfer of mutp53's migratory gain-of-function. SILAC-based proteomics allowed comparison of exosomes purified from H1299-p53^{R273H} and H1299-p53$^{-/-}$ cells which had been labelled with light and heavy SILAC amino acids respectively. Of the 428 proteins that were unambiguously identified, only 4 of these differed significantly between mutp53-expressing and p53 null cells (Fig. 3a; Supplementary Data 1). Podocalyxin (PODXL), a sialomucin associated with cancer aggressiveness[18], was significantly suppressed in mutp53^{R273H}-exosomes, and the ability of both the 175 and 273 H mutants of p53 to suppress exosomal PODXL was confirmed by western blotting (Fig. 3b). Moreover, sucrose density gradients indicated that PODXL precisely co-migrated with CD63 at a density of 1.1–1.15 g/mL indicating that PODXL is integrally associated with exosomes, and exosomal-associated PODXL is suppressed by mutp53 (Fig. 3c). RNAseq indicated that PODXL is the second-most significantly downregulated gene in mutp53-expressing H1299 cells - and qPCR and western blotting confirmed that PODXL mRNA and protein levels were suppressed by mutp53^{175H} or mutp53^{R273H} in H1299 cells (Fig. 3d; Supplementary Figure 5a; Supplementary Data 2). By contrast, induction of wild-type p53 did not affect PODXL levels (Supplementary Figure 5b). We and others have previously shown that mutant p53s exert pro-invasive gain-of-function by associating with and inhibiting p63[5,6]. We, therefore, knocked-down p63 and found that this suppressed PODXL level in H1299 cells to a similar extent as mutp53s (Supplementary Figure 5c). This indicates that PODXL expression is under the control of p63 and mutp53 likely suppresses PODXL levels by interfering with p63 function.

To investigate whether suppression of exosomal PODXL levels underpins the transfer of mutant p53's gain-of-function phenotype, we increased PODXL levels in p53^{R273H}-exosomes by expressing PODXL-GFP in H1299-p53^{R273H} cells (Supplementary Figure 5d). This did not influence the quantity or size distribution of mutp53^{R273H}-exosomes (Supplementary Figure 5e). However, expression of PODXL-GFP in donor cells significantly reduced the ability of mutp53^{R273H}-exosomes to drive receptor (α5β1 and cMET) recycling (Fig. 3e) and cell migration (Fig. 3f). In many reports, it is the presence (not the absence) of PODXL and other sialomucins has been linked to cancer progression[18]. Therefore, we were interested in determining the consequences of further reducing PODXL levels in mutp53-expressing cells. Exosomes from mutp53-expressing PODXL knockdown donor cells (Supplementary Figure 4a) had reduced ability to drive receptor recycling and cell migration in p53 null cells (Fig. 3e, f). By contrast, knockdown of α3β1 integrin

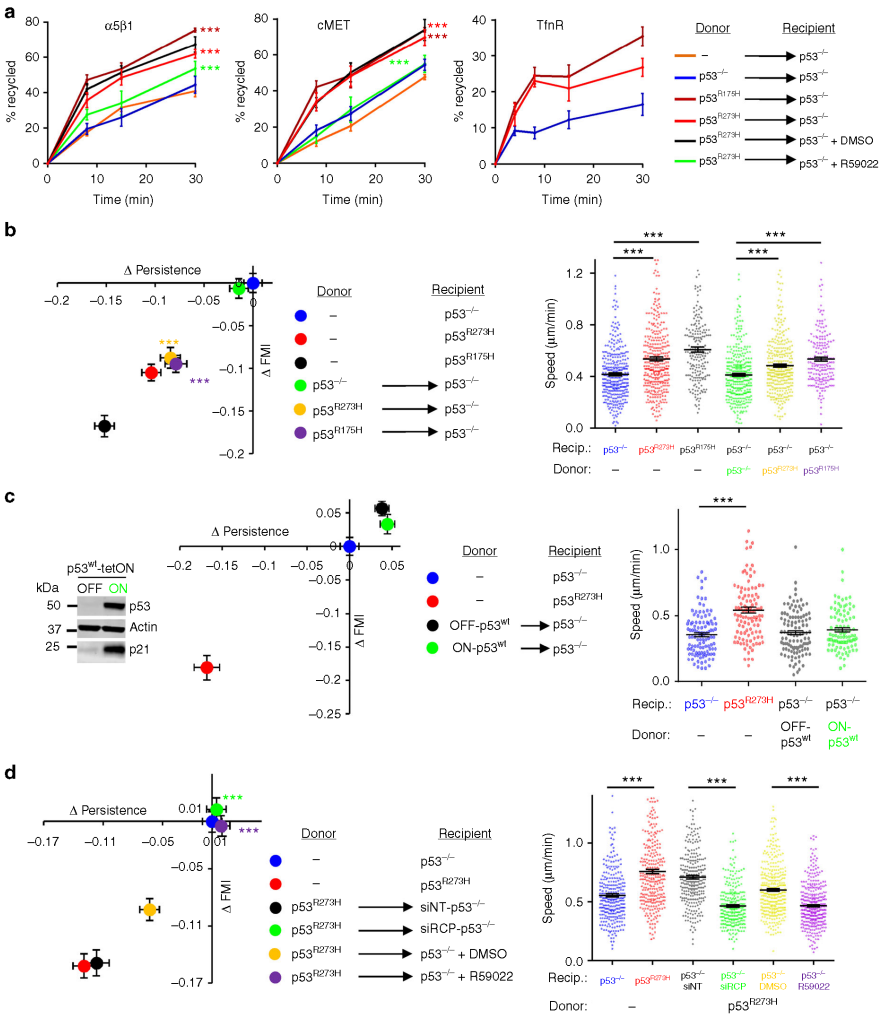

Fig. 2 Exosomes from mutant p53-expressing cells influence DGKα-dependent integrin trafficking and cell migration in p53 null cells. **a** H1299-p53$^{-/-}$ 'recipient' cells were pre-treated for 72 h with exosomes collected from H1299-p53$^{-/-}$, H1299-p53^{R273H} or H1299-p53^{R175H} 'donor' cells, or were left untreated. Recipient cells were then trypsinised and re-plated. Seventy-two hours following re-plating, recycling of integrin α5β1, cMET and TfnR was determined. Recipient cells were treated with R59022 (10 μM) or DMSO control as indicated. Values are mean ± SEM, $n = 6$; ***red versus blue, and ***green versus black are $p < 0.001$ ANOVA. **b** H1299-p53$^{-/-}$, H1299-p53^{R273H} or H1299-p53^{R175H} 'recipient' cells were pre-treated with exosomes collected from H1299-p53$^{-/-}$, H1299-p53^{R273H} or H1299-p53^{R175H} 'donor' cells, or were left untreated as indicated. Cells were then re-plated and the speed, ΔPersistence and ΔFMI of migration into scratch-wounds determined as for Supplementary Figure 1a–d. Values are mean ± SEM; $n > 195$ cells from three individual experiments; *** in the right panel, and ***yellow versus green and ***purple versus green in the left panel are $p < 0.001$, Mann–Whitney. **c** H1299-p53tetON cells were incubated in the presence or absence of doxycyclin and induction of wild-type p53 was confirmed by western blotting. Exosomes from these cells were incubated with H1299-p53$^{-/-}$ cells, the cells re-plated and the speed, ΔPersistence and ΔFMI of migration into scratch-wounds determined as for **b**. Values are mean ± SEM; $n > 110$ cells; *** are $p < 0.001$, Mann-Whitney. **d** H1299-p53$^{-/-}$ recipient cells were pre-treated with exosomes derived from H1299-p53^{R273H} donor cells. Recipient cells were then transfected with siRNAs targeting RCP (siRCP) or a non-targeting control (siNT), and the characteristics (ΔPersistence, ΔFMI and speed) of their migration into scratch-wounds was determined in the presence and absence of a DGK inhibitor (R59022; 10 μM) or DMSO control. Values are mean ± SEM; $n > 273$ cells; *** in right panel, and ***green versus black and ***purple versus yellow are $p < 0.001$, Mann-Whitney test

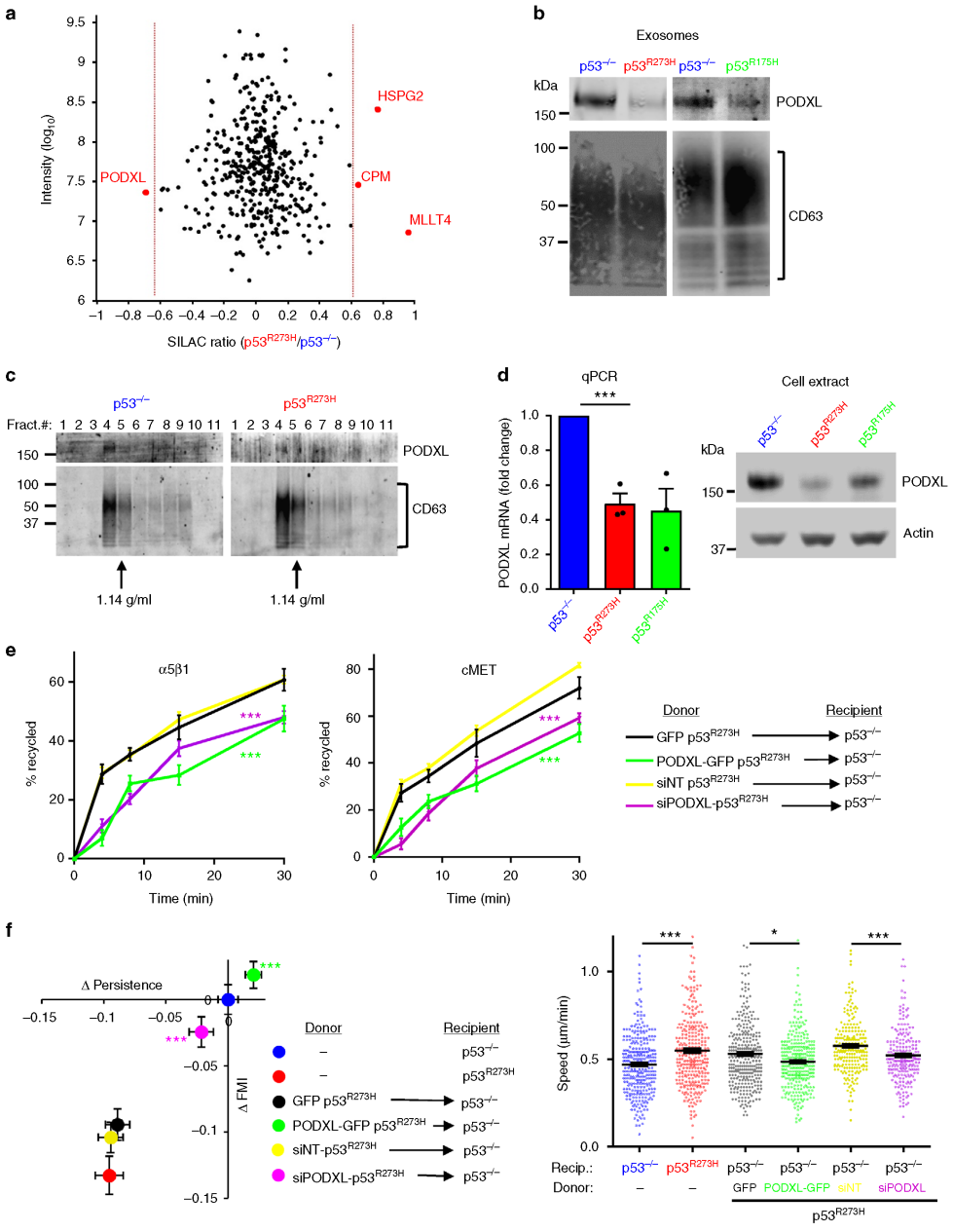
a
Intensity (log10)
SILAC ratio (p53R273H/p53−/−)
PODXL
HSPG2
CPM
MLLT4
b
Exosomes
p53−/− p53R273H p53−/− p53R175H
kDa
150
100
50
37
PODXL
CD63
c
p53−/−
p53R273H
Fract.#: 1 2 3 4 5 6 7 8 9 10 11
PODXL
CD63
1.14 g/ml
d
qPCR
PODXL mRNA (fold change)
Cell extract
Actin
e
α5β1
cMET
% recycled
Time (min)
Donor
Recipient
GFP p53R273H
PODXL-GFP p53R273H
siNT p53R273H
siPODXL-p53R273H
f
Δ Persistence
Δ FMI
Speed (μm/min)
Recip.:
Donor:
GFP
PODXL-GFP
siNT
siPODXL

Fig. 3 Mutant p53 controls exosomal podocalyxin levels to drive receptor trafficking and cell migration in p53 null cells. **a** H1299-p53$^{-/-}$ and H1299-p53^{R273H} cells were SILAC-labelled with heavy and light amino acids respectively. Conditioned media were collected from labelled cells, exosomes purified from these using differential centrifugation, and their proteome analysed by mass spectrometry. Scatter plot indicates the SILAC ratio H1299-p53^{R273H}/H1299-p53$^{-/-}$ (Log_2 scale) of each protein identified in the exosomal proteome. Proteins to the left and right of the red dotted lines are significantly down- and up-regulated respectively in exosomes from H1299-p53^{R273H} cells (Significance B statistic test, false discovery rate of 5%, Perseus software). These data are extracted from the table presented in Supplementary Data 1. **b** Exosomes from H1299-p53$^{-/-}$, H1299-p53^{R273H}, and H1299-p53^{R175H} cells were analysed by western blotting with an antibody recognising PODXL. CD63 was used as sample control. **c** Exosome pellets from H1299-p53$^{-/-}$ and H1299-p53^{R273H} cells were characterised using sucrose density gradient centrifugation followed by western blotting for PODXL and the exosome marker, CD63. **d** H1299-p53$^{-/-}$, H1299-p53^{R273H} and H1299-p53^{R175H} cells were lysed and assayed for the levels of mRNA encoding PODXL (left panel) using qPCR, and for PODXL protein using western blotting (right panel). Values in the left panel are mean ± SEM, $n = 3$; *** is $p < 0.001$ unpaired *t*-test. **e**, **f** Donor H1299-p53^{R273H} cells were transfected with GFP, or PODXL-GFP, siRNAs targeting PODXL (siPODXL) or non-targeting control (siNT). Exosomes collected from these cells were used to treat H1299-p53$^{-/-}$ recipient cells for 72 h before the cells were re-plated and recycling of α5β1 and cMET (**e**) and migratory characteristics of these cells into scratch-wounds (**f**) were determined as for Fig. 2a, b. Values are mean ± SEM. $N > 317$ cells; ***green versus black, and ***purple versus yellow are $p < 0.001$, Mann–Whitney test. In the right panel of **e**, *** is $p < 0.001$ and * is $p < 0.05$, Mann–Whitney

(ITGA3) (Supplementary Figure 4a)—the most abundant exosomal cargo—but whose levels do not differ between mutp53^{R273H} and p53$^{-/-}$-exosomes (Supplementary Data 1) did not oppose the ability of mutp53^{R273H}-exosomes to drive migration of recipient cells (Supplementary Figure 6a).

Taken together these data indicate that PODXL is required for exosomes to influence receptor trafficking, but that its levels must be within a certain range for this to occur. The role of mutant p53 is to drive transcriptional suppression of PODXL expression which reduces the exosomal content of this sialomucin to within this range, thus driving RCP-dependent receptor trafficking in recipient cells and allowing transfer of mutp53's gain-of-function to p53 null cells.

Rab35 associates with PODXL to influence its sorting to exosomes. PODXL binds to the Rab35 GTPase, and this association controls PODXL trafficking to the plasma membrane[19,20]. Rab35 and PODXL co-immunoprecipitated (Fig. 4a, e) to an extent that is commensurate with the expression levels of PODXL in p53$^{-/-}$ and mutp53-expressing cells respectively (Fig. 4a). Furthermore, knockdown of Rab35 (using SMARTPool siRNAs, an individual siRNA oligo or CRISPR gene editing) reduced PODXL at the cell surface (Fig. 4b; Supplementary Figure 6b, c). Interestingly, Rab35 knockdown led to accumulation of PODXL in CD63-positive late endosomes and, consistently, increased levels of PODXL in exosomes—while not affecting the number and size of exosomes released by H1299 cells (Fig. 4c, d). By contrast, knockdown of Rab27a and Rab27b did not influence the sorting of PODXL into exosomes (Fig. 4c). Mutation of residues in the juxtamembrane region of PODXL's cytoplasmic tail, that have previously been found to be important for Rab35–PODXL association (Val^{496} and Tyr^{500}), reduced their co-immunoprecipitation and led to increased trafficking of PODXL to CD63-positive late endosomes and exosomes (Fig. 4e–g). Consistently, the ability of H1299-p53^{R273H}-exosomes to influence recipient cell migration was completely opposed by Rab35 knockdown, whereas Rab27 knockdown (which does not influence sorting of PODXL to exosomes) was ineffective in this regard (Fig. 4h). Taken together, these data indicate that because Rab35 (but not Rab27) is required to transport PODXL to the plasma membrane, suppression of Rab35 diverts PODXL to late endosomes, thus increasing exosomal PODXL levels and disturbing exosome-mediated transfer of mutp53's migratory gain-of-function to recipient cells.

mutp53^{R273H}-exosomes promote integrin recycling in fibroblasts to influence ECM architecture. Treatment with mutp53^{R273H}-exosomes did not significantly increase the invasiveness of p53 null tumour cells in fibroblast-free Matrigel plugs (Supplementary Figure 7a). This raised the possibility that the fibroblasts in the organotypic plugs may contribute to transfer of mutp53's invasive gain-of-function. Indeed, pre-treatment with exosomes from mutant p53-expressing H1299 cells (either H1299-p53^{R273H} or H1288-p53^{R175H}) potently increased recycling (of α5β1 and TfnR) in TIFs, and this was opposed by inhibition of DGKα (Fig. 5a). Consistently, pre-treatment of TIFs with mutp53^{R273H} or mutp53^{R175H} exosomes increased their migration speed, decreased migratory persistence and FMI in scratch-wound assays (Fig. 5b), and increased random migration speed of subconfluent TIFs (Supplementary Figure 7b). Moreover, exosome-mediated transfer of these migratory characteristics to fibroblasts was opposed by CRISPR-mediated disruption of Rab35 or PODXL (Supplementary Figure 4b) or overexpression of PODXL-GFP in H1299-p53^{R273H} donor cells (Supplementary Figure 5d), indicating that control of PODXL levels in tumour cells is required for the transfer of mutant p53's migratory phenotype to fibroblasts (Fig. 5b).

To test whether altered DGKα-dependent integrin trafficking might influence ECM deposition, we allowed TIFs that had been pre-treated with mutp53^{R273H}-, mutp53^{R175H}- or p53$^{-/-}$-exosomes to deposit ECM for 8 days. Immunofluorescence indicated that ECM deposited by fibroblasts is normally organised into bundles of largely parallel filaments, and pre-incubation with p53$^{-/-}$-exosomes did not alter this (Fig. 5c). By contrast, pre-incubation with mutp53 (R273H or R175H) exosomes led to a more branched, orthogonal ECM network. To quantify this, we used grey level co-occurrence matrix (GLCM) analysis. This approach determines the probability (intensity correlation) that pixels at increasing distances (comparison distance) from a given point can be found to have similar intensities. Thus if an image consists mainly of long straight fibres it is possible to travel some distance in a straight line away from a given point without much alteration to intensity, and this will be reflected by long comparison distances for a given intensity correlation—i.e. a long mean decay distance. However, if an image is comprised mainly of short, orthogonally arrayed filaments then the correlation will fall more quickly as one travels away from a given point—yielding a shorter mean decay distance. The intensity correlation of ECM deposited by fibroblasts treated with mutp53^{R273H} or mutp53^{R175H}- exosomes decreased more quickly with distance than it did in ECM from untreated fibroblasts or those incubated with p53$^{-/-}$-exosomes (Fig. 5c). Furthermore, inhibition of DGKα (during the ECM deposition period) opposed deposition of orthogonal ECM with a short mean decay distance. Finally, second harmonic generation

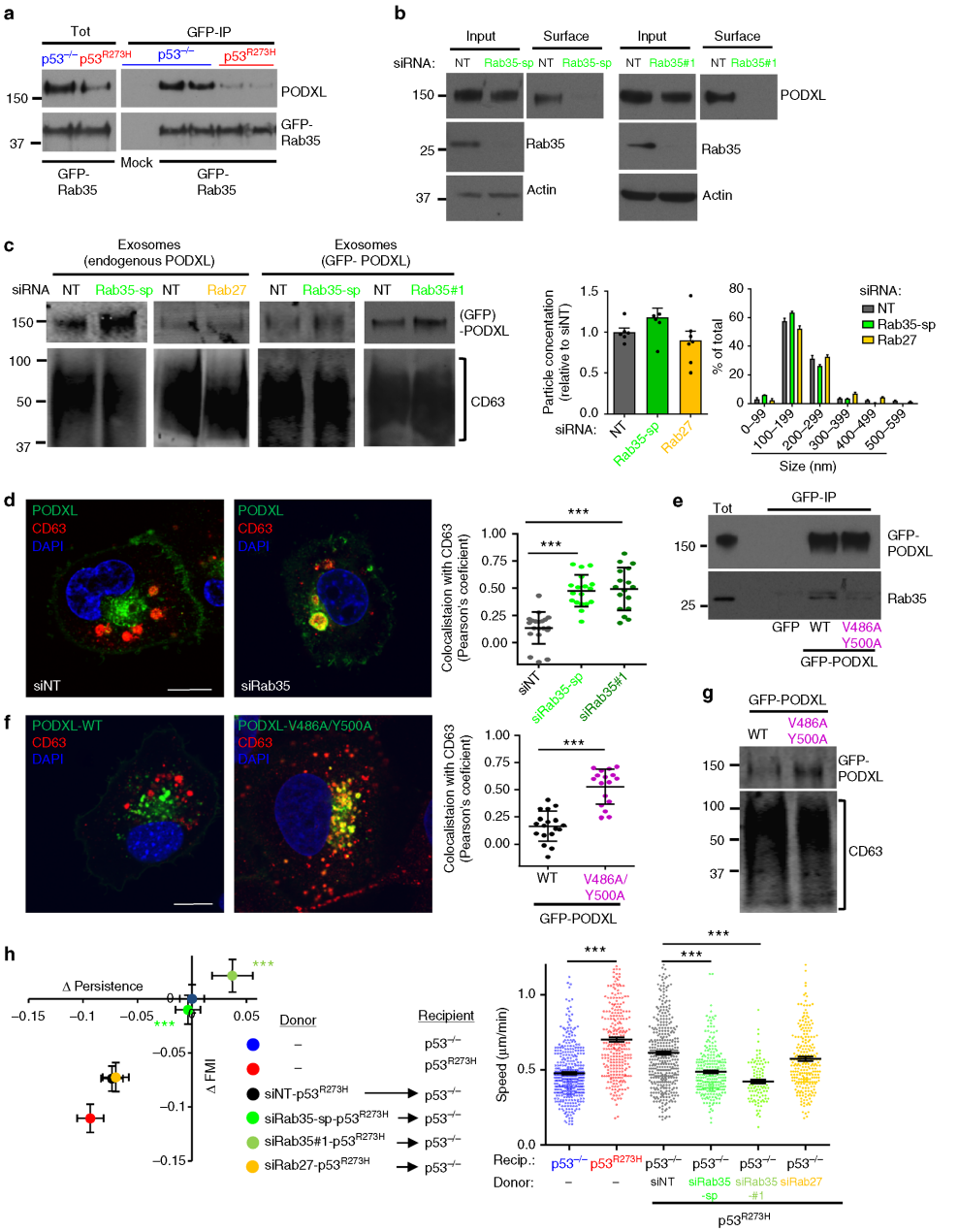
a
Tot
GFP-IP
p53−/− p53R273H
p53−/−
p53R273H
150
37
PODXL
GFP-Rab35
Mock
GFP-Rab35
GFP-Rab35
b
Input
Surface
Input
Surface
siRNA: NT Rab35-sp NT Rab35-sp NT Rab35#1 NT Rab35#1
150
25
37
PODXL
Rab35
Actin
Rab35
Actin
c
Exosomes (endogenous PODXL)
Exosomes (GFP- PODXL)
siRNA NT Rab35-sp NT Rab27 NT Rab35-sp NT Rab35#1
150
100
50
37
(GFP) -PODXL
CD63
Particle concentation (relative to siNT)
siRNA: NT Rab35-sp Rab27
% of total
siRNA: NT Rab35-sp Rab27
0-99
100-199
200-299
300-399
400-499
500-599
Size (nm)
d
PODXL
CD63
DAPI
siNT
siRab35
Colocalistaion with CD63 (Pearson's coeficient)
siNT
siRab35-sp
siRab35#1
e
Tot
GFP-IP
150
25
GFP-PODXL
Rab35
GFP WT V486A Y500A
GFP-PODXL
f
PODXL-WT
PODXL-V486A/Y500A
CD63
DAPI
Colocalistaion with CD63 (Pearson's coeficient)
WT
V486A/ Y500A
GFP-PODXL
g
GFP-PODXL
WT V486A Y500A
150
100
50
37
GFP-PODXL
CD63
h
Δ Persistence
Δ FMI
Donor
Recipient
siNT-p53R273H
siRab35-sp-p53R273H
siRab35#1-p53R273H
siRab27-p53R273H
p53−/−
p53R273H
Speed (μm/min)
Recip.: p53−/− p53R273H p53−/− p53−/− p53−/− p53−/−
Donor: – – siNT siRab35 -sp siRab35 -#1 siRab27
p53R273H

Fig. 4 Rab35 interacts with PODXL to influence its sorting to exosomes. **a** H1299 ($p53^{-/-}$ or $p53^{R273H}$) cells were transfected with GFP-Rab35 or mock transfected. GFP-tagged proteins were immunoprecipitated using an antibody recognising GFP conjugated to magnetic beads. Rab35 and PODXL were detected in the lysates (Tot) and immunoprecipitates (GFP-IP) using western blotting. **b** H1299-$p53^{R273H}$ cells were transfected with siRNAs targeting Rab35 (SMARTPool (Rab35-sp) or an individual siRNA (Rab35#1)) or a non-targeting control (NT). Cell surface proteins were labelled with NHS-Biotin at 4 °C and precipitated using streptavidin beads. Labelled (surface) and total (input) PODXL were then visualised by western blotting with actin as sample control. **c** H1299-$p53^{R273H}$ cells were transfected with siRNAs targeting Rab35 (Rab35-sp or Rab35#1), Rab27a/Rab27b (Rab27) or a non-targeting control (NT) ± GFP-PODXL. Exosomes were purified by differential centrifugation. Western blotting was used to determine exosomal levels of PODXL and GFP-PODXL with CD63 as sample control. Nanoparticle tracking was used to characterise exosomes (right panels), values are mean ± SEM, $n = 6$ movies from two individual experiments. **d** H1299-$p53^{R273H}$ cells were transfected with siRab35-sp, siRab35#1, or siNT. Cells were fixed and PODXL (green) and CD63 (red) were visualised by immunofluorescence. Bar, 15 µm. ImageJ was used to quantify co-localised pixels as determined by the Costes method. Values are mean ± SEM. $n > 16$ cells. *** is $p < 0.001$, Mann–Whitney. **e** H1299-$p53^{R273H}$ cells were transfected with GFP, GFP-PODXL or GFP-$PODXL^{V486A/Y500A}$. GFP-tagged proteins were immunoprecipitated and Rab35 and GFP-PODXL were detected in the immunoprecipitates as for **a**. **f** H1299-$p53^{R273H}$ cells were transfected with GFP-PODXL or GFP-$PODXL^{V486A/Y500A}$. Cells were fixed and PODXL (green) and CD63 (red) were visualised by immunofluorescence. Bar, 15 µm. Colocalisation was determined as for **d**. Values are mean ± SEM. $n > 16$ cells. *** is $p < 0.001$, unpaired *t*-test. **g** H1299-$p53^{R273H}$ cells were transfected with GFP-PODXL or GFP-$PODXL^{V486A/Y500A}$. Exosomes were collected by differential centrifugation. Western blotting was used to determine exosomal levels of GFP-PODXL with CD63 as a sample control. **h** H1299-$p53^{R273H}$ cells were transfected with siRab27, siRab35-sp, siRab35#1 or siNT. Exosomes collected from these cells were used to treat H1299-$p53^{-/-}$ cells and the characteristics of their migration into scratch-wounds was determined. Values are mean ± SEM; $n > 262$ cells; for siRab35#1 $n = 100$ cells; ***$p < 0.001$, Mann–Whitney

microscopy (SHG) in combination with GLCM analysis indicated that pre-incubation of fibroblasts with mutp53^{R273H}-exosomes prior to seeding them into collagen plugs significantly reduced the mean decay distance of fibrillar collagen within these plugs (Fig. 6b, d). Taken together, these data indicate that mutant p53-expressing tumour cells influences organisation of the ECM in 3D microenvironments by releasing exosomes which alter integrin trafficking in fibroblasts.

mutp53-exosomes encourage fibroblasts to generate a pro-invasive microenvironment. Exosome-driven alterations to the organisation of the ECM might be expected to influence its mechanical properties to affect tumour cell invasiveness. AFM analysis indicated that the ECM deposited by mutp53-treated TIFs had similar stiffness to that from untreated fibroblasts and, despite observations that pre-treatment with $p53^{-/-}$ exosomes encouraged the deposition of a slightly stiffer ECM (increased Young's modulus), this was not consistent with altered stiffness being associated with the altered properties of mutp53-fostered ECM (Fig. 5d). We, therefore, continued to use AFM to determine the adhesive properties of the ECM. We attached a silica bead to the tip of the AFM cantilever, allowed this to interact with the ECM for a defined time, and then measured the energy required to remove the bead. The energy required to remove a silica bead from the ECM deposited by untreated TIFs was unchanged by pre-treatment of TIFs with $p53^{-/-}$exosomes (Fig. 5d). However, pre-treatment of TIFs with mutp53-exosomes led to a three- to four-fold reduction in energy necessary to remove a bead from the ECM deposited by these fibroblasts (Fig. 5d). Because of this altered stickiness, we assessed the adhesions formed when cancer cells interacted with these matrices. Quantitative analysis of paxillin distribution indicated that MDA-MB-231 cancer cells assembled significantly fewer and smaller 3D cell:matrix contacts when they were plated into ECM deposited by fibroblasts pre-treated with mutp53-exosomes (Fig. 5e), indicating that cell:ECM contacts structures were less well-established in this less adhesive microenvironment. Therefore, we measured the speed at which tumour cells migrated through de-cellularised ECM deposited by exosome-treated fibroblasts. MDA-MB-231 breast cancer cells migrated significantly more quickly through ECM from fibroblasts that had previously been treated with mutp53^{R273H}-exosomes than they did through ECM from untreated fibroblasts or those treated with $p53^{-/-}$-exosomes (Fig. 6a). Furthermore, the ability of exosome-treated fibroblasts to assemble ECM which supported enhanced tumour cell migration was completely opposed by inhibition of DGKα (during the ECM deposition period). Finally, we incubated TIFs with exosomes and allowed them to pre-condition collagen plugs which were subsequently overlaid with H1299 tumour cells. This indicated that H1299 cells, irrespective of their p53 status, invaded efficiently into collagen plugs that had been conditioned by mutp53^{R273H}-exosome-treated TIFs (Fig. 6e). By contrast, pre-treatment of TIFs with $p53^{-/-}$-exosomes did not confer increased invadability to organotypic collagen plugs (Fig. 6e) despite increasing the overall levels of fibrillar collagen (Fig. 6c). Taken together, these data indicate that exosomes from mutant p53-expressing tumour cells influence the way that fibroblasts deposit and remodel the ECM so as to generate a micro-environment highly supportive of tumour cell migration and invasion.

Mutp53-expressing tumours influence ECM architecture in the lungs via PODXL and Rab35-dependent mechanisms. Exosomes released by a mutp53-expressing tumour in one organ might engender alteration to ECM organisation in other tissues. To test this, we subcutaneously implanted H1299-$p53^{-/-}$ cells or H1299s expressing mutp53^{273H} or mutp53^{175H} into nude mice. When the tumours had grown to 0.8 cm in diameter, we used SHG microscopy in combination with GLCM analysis to analyse ECM organisation in the lung parenchyma. It is important to note that we were unable to detect any H1299 cells in the lung, indicating that any alterations to the lung ECM were owing to factors (such as exosomes) released by the tumour cells and not migration of tumour cells to the lung. The total quantity of fibrillar collagen in the lung did not differ between non-tumour-bearing mice or those implanted with p53 null or mutp53-expressing tumours. However, the fibrillar collagen in the lung parenchyma of mutp53 tumour-bearing mice appeared to be more punctate and less well-organised into long fibres, and the mean decay distance of collagen filaments (as determined using GLCM) was significantly reduced by comparison with those animals with p53 null tumours or non-tumour-bearing animals (Fig. 7a). Importantly, deletion of either PODXL or Rab35 using CRISPR (Supplementary Figure 4b) opposed the ability of H1299-$p53^{273H}$ cells to alter lung ECM organisation in nude mice (Fig. 7a).

We used the KPC and $KP^{fl}C$ autochthonous models of pancreatic ductal adenocarcinoma (PDAC). In these, primary

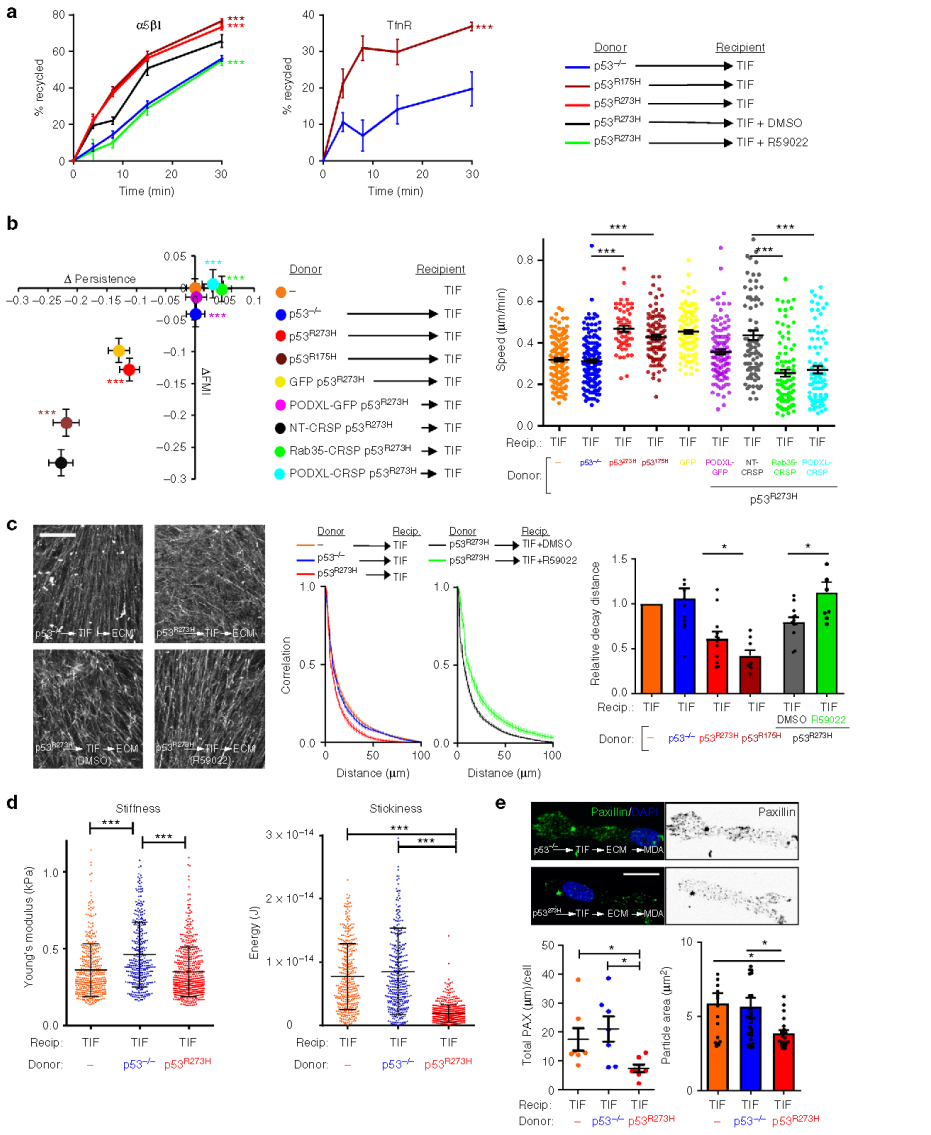

tumour initiation and growth is driven by expression of constitutively-active KRas (LSL-KRas^{G12D}) in combination with either deletion of an allele of p53 (p53$^{fl/+}$ generating the KP^{fl}C mouse) or expression of mutant p53s (either LSL-mutp53^{172H} or LSL-mutp53^{270H} generating the KP^{172}C and KP^{270}C mice respectively) under control of the pancreatic-specific Cre recombinase, Pdx-Cre. For comparison, we used KC mice which express LSL-KRas^{12G} under control of Pdx-Cre, but the resulting tumours do not readily progress past the pre-malignant PanIN (pancreatic intraepithelial neoplasm) stage. Importantly for this study, PDAC driven by LSL-KRas and LSL-mutp53^{172H} or LSL-mutp53^{270H} metastasise to the liver and lung. On the other hand, PDAC driven by KRas in combination with p53 loss (p53$^{fl/+}$) appear with similar penetrance, but do not metastasise[4]. We used SHG followed by GLCM analysis to assess the ECM of the lung parenchyma and perivascular regions at an age (10–12 weeks) in

Fig. 5 mutp53 exosomes promote integrin recycling in fibroblasts to influence ECM architecture. **a**, **b** mutp53-expressing R175H or R273H H1299 cells, or cells generated by CRISPR from the latter (PODXL-CRSP; Rab35-CRSP), were transfected with GFP or PODXL-GFP or were left untransfected. Exosomes collected from H1299-p53$^{-/-}$ and the transfected and untransfected mutant p53-expressing H1299 cells were used to treat TIFs and receptor recycling (**a**) and migratory characteristics of these (**b**) were determined as for Fig. 2a, b. In **a** R59022 (10 μM) or DMSO was added to TIFs as indicated. Mean ± SEM, $n = 6$. In **a** ***red versus blue, and ***green versus black are $p < 0.001$, ANOVA. In **b**, $n = >52$; ***red versus blue,***purple versus yellow, ***green versus black, ***light blue versus black are $p < 0.001$, Mann–Whitney. In the right panel of **b**, *** is $p < 0.001$, Mann–Whitney. **c** TIFs were incubated with exosomes from H1299 (p53$^{-/-}$, p53^{R273H}, p53^{R175H}) cells or left untreated and allowed to deposit ECM in the presence and absence of R59022 (10 μM) or DMSO. ECM was then de-cellularised, stained with antibodies recognising fibronectin and image stacks were collected using confocal microscopy. Extended focus projections of these stacks are displayed in the left panel of **c**, bar, 50 μm. The organisation of the ECM fibres in these was determined using GLCM. The decay curves and the weighted means of the decay distances derived from these are presented in the centre and right panels of **c** respectively. Weighted mean ± SEM, $n = 8$, * is $p < 0.05$, Mann–Whitney. **d** TIFs were treated with exosomes from H1299 (p53$^{-/-}$ or p53^{R273H}) cells or were left untreated and allowed to deposit ECM. De-cellularised ECM was analysed using AFM. The left and right panels indicate ECM stiffness and stickiness respectively. Mean ± SEM, $n > 6$ ECM preparations from two individual experiments *** is $p < 0.001$, Mann–Whitney. **e** MDA-MB-231 cells were seeded onto de-cellularised ECM deposited by exosome-treated TIFs as indicated. Cells were fixed and cell:ECM adhesions visualised by immunofluorescence. Top panel shows representative images (bar, 20 μm). Total area of paxillin per cell and average area of paxillin-positive particles are plotted in the bottom left ($n > 6$) and right panels ($n > 16$). Mean ± SEM, * is $p < 0.05$, Mann–Whitney

which primary tumour growth was underway, but metastases were not detectable in the liver or lung. Any animals with premature lung metastases visible by examination of paraffin-embedded, H&E-stained sections were excluded from the analysis —but these were rare. SHG indicated that collagen filaments in the perivascular regions and lung parenchyma of mutp53-driven KP^{172}C and KP^{270}C animals were shorter and less well-organised, and the mean decay distance (as assessed by GLCM analysis) of these fibres was reduced by comparison with that of KC (Fig. 7b, c) or normal animals. By contrast, for KP^{fl}C animals, in which tumours are driven by p53 loss, organisation of lung ECM was indistinguishable from KC animals (Fig. 7b, c). Taken together, these data indicate that hallmark alterations to ECM organisation, which we have established to be driven by the influence of mutp53^{R273H}- or mutp53^{175H}-exosomes on integrin trafficking in fibroblasts, may also be detected in the lungs of animals bearing autochthonous PDAC expressing the equivalent p53 mutations, but not in the lungs of animals with PDAC with p53 loss.

Exosomes from mutp53-expressing tumour cells derived from patients with squamous-type PDAC lead to ECM modification. We determined whether the mutp53 status of cells from human PDAC dictates the capacity of exosomes from these cells to influence ECM deposition. Human PDAC may be categorised into four main subtypes, and these are termed, progenitor, immunogenic, ADEX and squamous[21]. KPC tumours closely recapitulate the characteristics of the squamous subtype of PDAC, so we focussed on the three patient-derived cell lines (PDCLs) from this category. Of these, two (SQ2 and SQ3) expressed mutations that led to ablation of p53 protein expression and were considered, therefore, to be p53 null, while another (SQ1) expressed a mutant of p53 (M237I) with gain-of-function properties (Fig. 8a; Supplementary Figure 7c)[22]. We isolated exosomes from conditioned medium from these PDCLs and incubated them with fibroblasts. We assessed the migration of these exosome-exposed fibroblasts and found that only SQ1 (which expressed a mutant p53 protein) was able to increase migration speed and depress migratory persistence and FMI, as we had previously found for H1299 cells expressing mutant p53s (Fig. 8b). Furthermore, ECM deposited by fibroblasts pre-treated with exosomes from the SQ1 PDCL had reduced mean decay distance (Fig. 8c) and supported increased migration of cancer cells (Fig. 8d). Importantly, we found that knockdown of mutant p53 in SQ1 cells, while not significantly affecting the exosome quantity or size (Fig. 8a), led to increased PODXL levels (Fig. 8a) and opposed the ability of exosomes released from these cells to support altered fibroblast migration (Fig. 8b) and ECM deposition (Fig. 8c, d).

Discussion

We have recently reported that conditional deletion of RCP in pancreatic lineages (using Pdx-Cre) opposes metastasis in autochthonous models of mutant p53-expressing PDAC[23]. This is not owing to RCP's ability to control the recycling of α5β1 integrin, but via trafficking of the ephrin receptor, EphA2. However, this does not mean that RCP-mediated integrin trafficking has no role in PDAC metastasis. The progression of tumours from indolent to invasive and onwards to metastasis depends not only on the intrinsic invasiveness and dissemination of cancer cells, but on their ability to influence other cells to generate invasive microenvironments and to prime metastatic niches. Here we show that RCP-regulated α5β1 integrin trafficking is involved in the contribution made by fibroblasts to invasion and metastasis by controlling the way that the ECM is deposited by these cells. Furthermore, we show that mutant p53s expressed by tumour cells activates RCP-dependent integrin trafficking in fibroblasts via an exosome-mediated mechanism.

There are numerous reports that microRNAs and other non-coding RNAs are found within exosomes, and that these can drive processes such as tumour-associated inflammation and metastasis by influencing mRNA processing and translation in target cells[24]. Exosomes from mutant p53-expressing tumours may mediate transfer of a microRNA to influence the polarisation of macrophages to generate an immunosuppressive tumour microenvironment[25]. However, we have conducted extensive quantitative proteomic and RNAseq analyses and cannot demonstrate any alteration to the transcriptome or proteome of target cells following treatment with mutp53-exosomes. This indicates that the influence of exosomes on integrin trafficking does not involve detectable alterations to transcription or translation in target cells and is, therefore, more likely to be mediated by a more direct effect on the endosomal trafficking machinery of target cells. The exosome cargo that is most significantly altered by mutant p53 expression is the sialomucin, PODXL—and this is owing to mutp53's ability to influence PODXL levels in the exosome-producing cells. Alteration of cellular PODXL does not influence the quantity or the size of exosomes released by tumour cells, nor are exosomes with different PODXL content assimilated at different rates by target cells, so it is interesting to speculate how exosomal PODXL levels might influence receptor recycling

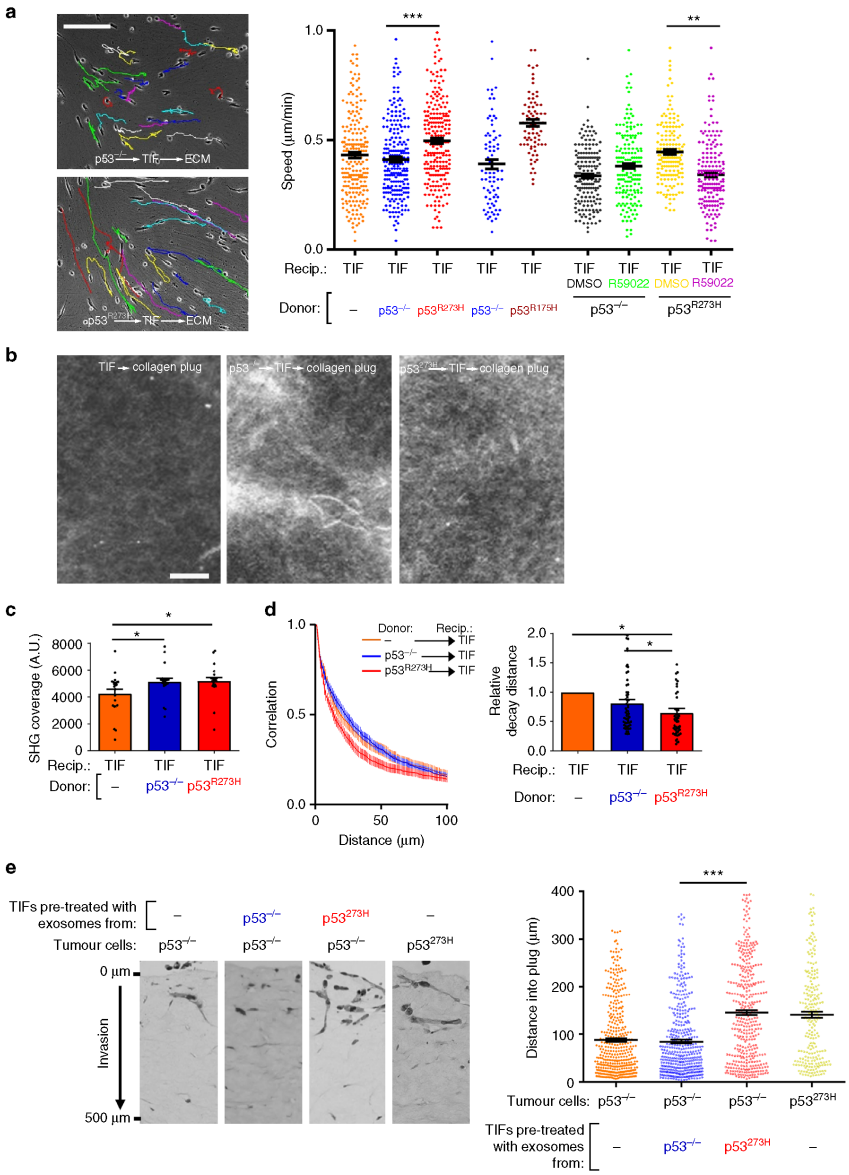

in target cells. PODXL is a glycocalyx component which, by virtue of negative charge imparted by sialylated N- and O- linked oligosaccharide residues, controls the separation of apposed lipid bilayers to promote the opening of lumens during morphogenesis, and to dictate the spacing of kidney podocytes. By respectively controlling PODXL expression and intracellular sorting, mutant p53 and Rab35 collude to tune levels of exosomal PODXL into a range which is just right for influencing receptor recycling. Any manipulation which places PODXL above or below this range (siRNA of PODXL, overexpression of PODXL, siRNA of Rab35) renders exosomes to be ineffective in driving receptor recycling. Given that sialomucins would be expected to contribute

Fig. 6 mutp53-exosomes encourage fibroblasts to generate a pro-invasive microenvironment. **a** TIFs were pre-treated with exosomes from H1299-p53$^{-/-}$, H1299-p53^{R273H} or H1299-p53^{R175H} cells and allowed to generate ECM in the presence and absence of R59022 as for Fig. 5c. ECM was then de-cellularised and MDA-MB-231 breast cancer cells plated onto these. The migration of MDA-MB-231 cells through the de-cellularised ECMs was recorded over a 16 h period using time-lapse video microscopy and cell tracking software. Representative tracks are indicated by the coloured lines in the left panels. Bar, 100 μm. The migration speed of the MDA-MB-231 cells was calculated and is presented in the right graph. Values are mean ± SEM, $n > 79$ cells; $^{**}p < 0.01$, $^{***}p < 0.001$, Mann–Whitney. **b**–**d** TIFs were incubated with exosomes from H1299-p53$^{-/-}$ (p53$^{-/-}$) or H1299-p53^{R273H} (p53^{R273}) cells for 72 h. Exosome pre-treated TIFs were trypsinised, mixed with acid-extracted collagen and the resulting organotypic plugs allowed to polymerise and contract for 3 days prior to collection of image stacks using second harmonic generation (SHG) microscopy. Representative optical slices from these are displayed in **b**. Bar, 4 μm. The coverage of the SHG signal (**c**) and organisation of the fibrillar collagen (**d**) was determined using GLCM as for Fig. 5c. The decay curves from these are presented in the left panels of **d** and the weighted means of the decay distances derived from these curves are displayed in the graph on the right. Values in **c** are mean ± SEM, $n = 22$ fields of view across three separate experiments. Values in **d** are weighted mean ± SEM, $n = 46$ fields of view across three separate experiments; * is $p < 0.05$, Mann–Whitney. **e** Collagen plugs were conditioned for 48 h with untreated TIFs or with TIFs that had been pre-treated for 72 h with exosomes from H1299-p53$^{-/-}$ or H1299-p53^{R273H} cells. Conditioned plugs were overlaid with H1299-p53$^{-/-}$ (p53$^{-/-}$) or H1299-p53^{R273H} (p53^{R273H}) cells and these were allowed to invade for 10 days. Plugs were then fixed and tumour cells visualised using H&E. The distance between each tumour cell and the top of the plug was determined using ImageJ. Bars are mean ± SEM, $n > 233$ cells; *** $p < 0.001$ Mann–Whitney test

to the surface charge of exosomes, our data suggest that exosomes within a defined charge range can influence integrin trafficking by acting within the endosomal system, and it will be interesting to determine how other factors which would be expected to influence exosome charge (such as post-translational modification of sialomucins) contribute to the ability of exosomes to interfere with endosomal processes.

CAF activation is associated with increased secretion of fibronectin. More recently, this process has been shown to be promoted by exosomes. Exosomes from PDAC cell lines can bind to liver macrophages to promote release of TGFβ leading to fibroblast activation and fibronectin deposition to prime pre-metastatic niche formation in the liver[16]. However, the alterations in collagen organisation that we find to be driven by mutp53-exosomes are not associated with events that accompany fibroblast activation, such as increased α-smooth muscle actin expression and fibronectin deposition. Rather mutp53-exosomes upregulate RCP-dependent integrin recycling without altering the profile of gene expression in target cells. Integrin endocytosis and recycling can influence ECM deposition and, as fibroblast migration is influenced by mutp53-exosomes, this is also likely to affect the ECM organisation. Long-term time-lapse experiments indicate that fibroblasts in a confluent monolayer normally migrate within a restricted area and this movement is directionally constrained. By contrast, mutp53-exosome-treated fibroblasts undergo much longer range and directionally adventitious movements, and this behaviour may be what leads to the more branched and disorganised ECM that they deposit. Mutant p53-expressing tumours can influence collagen organisation in the tumour stroma and this is associated with ECM cross-linking and assembly of parallel arrays of collagen fibres[26]. Indeed, SHG/GLCM analysis indicates that the mean decay distance of collagen filaments in the stroma of mutant p53-expressing (KPC) PDAC is significantly increased by comparison with the stromal regions of KfC tumours (Figure S7d). Thus, our findings clearly indicate that ECM alterations evoked at some distance from the primary tumour by mutp53 exosomes are distinct from those observed in the primary tumour. The orthogonal/tangled ECM that is deposited by lung fibroblasts under the influence of mutp53-exosomes may contribute to metastatic niche priming in more than one way—for instance by increasing the ability of circulating tumour cells to extravasate and colonise the lungs and/or by influencing the dormancy of micrometastatic colonies, and further work will determine how this occurs. Recently, it has been found that a p53-driven transcriptional programme supports many of the features of tumour-associated fibroblast behaviour, including ECM deposition which fosters cancer cell migration and invasion[27]. It will be interesting to determine whether regulation of fibroblast p53 function is associated with exosome-mediated transfer of mutp53-like phenotypes and the activation of fibroblast integrin trafficking, cell migration and ECM remodelling.

It is now clear that primary tumours release factors that influence the physiology of other organs to render them more receptive to metastatic seeding. A number of mechanisms have been shown to contribute to this, including mobilisation of immune cells, release of ECM-modifying enzymes (such as lysyl oxidase) and production of exosomes[14,15,28]. Although ECM modification is key to metastatic niche priming, the cellular mechanism through which tumour-derived exosomes lead to altered ECM deposition are not yet clear. Our findings describe a pathway in which a mutated tumour suppressor operates via a well-characterised gain-of-function mechanism to alter the ECM microenvironment to promote tumour cell invasive behaviour. Indeed, mutp53 and Rab35 collaborate to control the PODXL content of exosomes released by tumours cells, and these exosomes promote RCP/DGKα-dependent trafficking of α5β1 integrin in fibroblasts to influence the organisation and adhesive properties of the ECM that they deposit. Although further work will be necessary to determine how this more orthogonal and less adhesive ECM influences cell migration and invasion, this type of ECM organisation, which may be clearly detected in the lungs of mutant p53 tumour-bearing animals, is more conducive to the metastatic seeding of tumour cells. Thus, we have identified a new mechanism that may drive the morbidity of mutp53-expressing tumours and highlight an intercellular communication pathway consisting of a number of measurable well-characterised components (including Rab35, PODXL, RCP, DGKα, collagen organisation) which are amenable to pharmacological intervention and may constitute viable biomarkers to indicate the presence of metastatic tumours.

Methods

Cells, qPCR primers and antibodies. H1299 (p53 / and p53$^{R273H/R175H}$) (from ATCC) TIFs (in house, Beatson Institute) and MCF7 (ATCC) cells were cultured in Dulbecco's modified Eagle medium (DMEM, Life Technologies) supplemented with 10% fetal bovine serum (FBS) (Gibco), 1 mM L-glutamine, 100 μg/mL streptomycin and 100 U/mL penicillin. For all experiments involving exosomes, exosome-depleted serum was used throughout. PDCLs were generated as previously described[1–4] and cultured in M199/F12 HAM medium (1:1) (Life Technologies) supplemented with 7.5% filtered FBS (Hyclone, Thermo Scientific), 15 mM HEPES (Life Technologies), 2 mM L-glutamine (Life Technologies), 20 ng/mL EGF (Life Technologies), 40 ng/mL hydrocortisone (Sigma), 5 ng/mL apo-Transferrin (Sigma), 0.2 IU/mL Insulin ActRApid (Life Technologies), 0.06% glucose (Sigma), 0.5 pg/mL Tri-iodotyronine (Sigma), 1 × MEM vitamins (Life Technologies) and 2 μg/mL *O*-phosphoryl ethanolamine (Sigma). All cell lines were

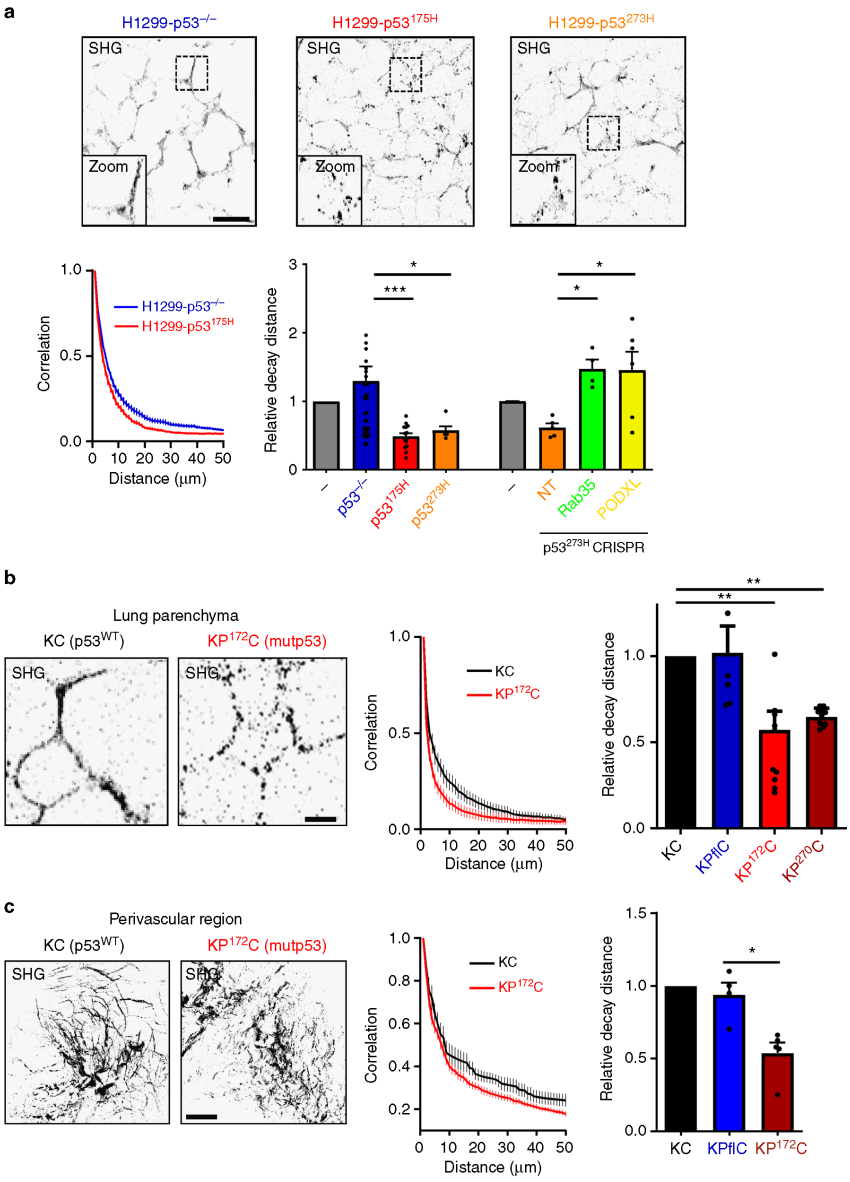

routinely tested for mycoplasma contamination. H1299 cells were transfected using the AMAXA system–Solution V with the X-001 electroporation protocol. PDCLs were transfected using Lipofectamine RNAiMAX (Thermo Scientific) according to the manufacturer's instructions. To suppress p53 the siRNA forward oligo was GACUCCAGUGGUAAUCUACUU, and for p63 it was UGA ACA GCA UGA ACA AGC U (TT). siRNAs for RCP, DGKα, PODXL, Rab35, Rab27a, Rab27b and ITGA3 were ON-TARGET siRNAs from Dharmacon. An individual siRNA was also used to target Rab35 and the sequence of this was GAUGAUGUGUGCCGAAUAU. Antibodies used were: CD63 (Pelicluster M1544, dilution for WB—1:1000; IF -1:200), p53 (in house, DO-1, 1:10000), Rab35 (Cell Signalling 9690S, 1:1000), RCP (in-house raised against RCP$^{379–649}$, 1:1000), PODXL (Abcam 150358, 1:1000), p63 (Abcam ab53039, 1:1000), α5 and α3 integrin (BD Pharmingen), cMET (R&D systems), GFP (Abcam ab6556, 1:1000), Actin (Sigma A2066, 1:3000), TSG101 (GeneTex GTX70255, 1:1000), HSPA8 (Cell signalling 8444S, 1:1000), Integrin β1 (BD Pharmingen 610467, 1:2000), CD9 (Abcam ab92726, 1:10000), DGKa (Protein tech 11547-1AP, 1:500), Rab27 (Abcam

Fig. 7 Mutant p53-expressing PDAC influences ECM architecture in the lungs. **a** H1299-p53$^{-/-}$, H1299-p53^{R273H} or H1299-p53^{R175H} cells, or H1299-p53^{R273H}cells in which Rab35 or Podocalyxin had been disrupted by CRISPR were injected subcutaneously into CD1 Nude mice. Mice were monitored for tumour growth and culled when tumours reached 0.8 cm diameter. Mice were sacrificed by IP injection of pentobarbital, and lungs were inflated with 2% low melting point agarose which was then allowed to solidify. Agarose-filled lungs were sliced using a vibratome, and parenchymal regions were imaged by SHG microscopy. Representative SHG pictures of lungs from CD1 nude mice transplanted with the respective cell line are displayed (top panels). Bar, 100 μm. Organisation of the fibrillar collagen was determined using GLCM as for Fig. 5c. The decay curves from these are presented in the bottom left panel of **a** and the weighted means of the decay distances derived from decay curves are displayed in the graph on the right. Values are weighted mean ± SEM; $n > 4$ animals per condition (except for H1299-p53^{R175H}, where $n = 3$); * is $p < 0.05$, *** is $p < 0.001$, Mann–Whitney. **b**, **c** KP^{172}C (Pdx1-Cre:KrasG12D/+:p53R172H/+) or KP^{270}C (Pdx1-Cre:KrasG12D/+:p53R270H/+), KP^{fl}C (Pdx1-Cre:KrasG12D/+:p53fl/+) or KC (Pdx1-Cre:KrasG12D/+) mice were sacrificed by IP injection of pentobarbital, and the parenchymal (**b**) and perivascular regions (**c**) of the lungs were and analysed by SHG microscopy as for **a**. Representative SHG pictures of lungs are displayed (left panel). Bar in **b**, 25 μm; bar in **c** 100 μm. Fibrillar collagen organisation was determined using GLCM. The decay curves from these are presented in the centre panels of **b**, **c**. Weighted means of the decay distances derived from decay curves are displayed in **b**, **c**, right panels). Values are weighted mean ± SEM. In **b**, $n > 7$ lung fields from three animals per condition (except for KC, where there were 6 animals); * is $p < 0.05$, Mann–Whitney. In **c**, $n = 3$ for KC, $n = 4$ for KP^{fl}C and $n = 5$ animals for KPC. * is $p < 0.05$, Mann–Whitney

ab55667, 1:1000), p21 (Cell signalling 2947, 1:1000), Fibronectin (BD Pharmingen 610078, 1:100), Paxillin (BD Pharmingen 610052, 1:100), Integrin α3 (Millipore AB1920, 1:1000). Uncropped blots corresponding to the main figures are presented in (Supplementary Figure 8). qPCR primers for PODXL and GAPDH were from QIAGEN.

For the CRISPR/Cas9 knockout of Rab35 and PODXL we used the lentiCRISPR vector (Addgene plasmid #52961) established by Zhang lab[29]. The guide RNAs sequences we used were GTAGCGAACGTGTCCGGCGT, which was generated by Wang et al.[30] as control, Rab35 guide TTGTCAACGTCAAGCGGTGG and PODXL guide GTGAGGTTCAGGACGAGCTG. The lentiviral constructs were cloned and transduced into H1299 cells as described in ref. [31].

Exosome purification and characterisation. Conditioned medium was collected and centrifuged to remove live cells (300*g*), dead cells (2000*g*) and finally to remove cell debris and larger lipid membrane fragments (10,000*g*). Exosomes were then pelleted using a 100,000*g* centrifugation in a SW32 rotor. The pellet was washed in PBS before a final pelleting centrifugation at 100,000 *g*, after which exosomes were resuspended in a small volume of PBS. For sucrose density gradient centrifugation, exosome pellets were mixed with 1 mL of a 2.5 M solution of sucrose at the bottom of a 12 mL centrifugation tube. Exosomes were overlaid with 11 layers of sucrose deceasing in concentration (from 2 to 0.4 M sucrose using 20 nm HEPES as the diluent). The gradient was centrifuged at 200,000 *g* overnight using an SW40 rotor. Exosomes were collected from each gradient fraction by a final centrifugation in PBS at 100,000 *g*.

Nanoparticle tracking analysis was carried out using the NanoSight LM10 instrument according to the manufacturer's instructions. Exosomes resuspended in 200 μL of filtered PBS were diluted 1:30 in filtered PBS before being introduced into the instrument for measurement.

When incubating recipient cells (H1299, A2780, or TIFs) with exosomes we routinely included these in the medium at a concentration of approx. 1×10^9 particles/mL.

Electron microscopy. Exosomes were fixed in 2% paraformaldehyde (Thermo Scientific Pierce) and subsequently adsorbed onto Formvar carbon coated EM grids overnight at 4 °C. Grids were washed with PBS and treated with 1% glutaraldehyde (Sigma) solution for 5 min. This was followed by eight washes with distilled water. Exosomes were visualised by negative staining, grids were incubated with uranyl oxalate (Polysciences) for 5 min and subsequently methyl cellulose-UA (Sigma) for 10 min at 4 °C. Air dried grids were imaged on a transmission electron microscope FEI Tecnai T20 running at 200 kV using Olympus Soft Imaging System software.

For immunogold staining, adsorbed exosomes were subject to four blocking washes with PBS containing 50 mM glycine after initial adsorption onto grids. A second blocking step was then carried out using PBS containing 5% BSA (Sigma) for 10 min. Exosomes were then exposed to CD63 primary antibody (Pelicluster, 1:200) or mouse IgG1 isotype control antibody (Pierce, 1:200) diluted in PBS containing 1% BSA for 30 min. Grids were washed in PBS containing 0.1% BSA six times for 5 min each. Grids were then incubated with anti-mouse 10 nm protein A-gold conjugate secondary antibodies (Cell Microscopy Centre) for 30 min before eight PBS washes. From this point onward the fixation and negative staining protocol was performed as described above. Images were analysed using ImageJ to determine the exosome size.

SILAC proteomics. H1299-p53$^{-/-}$ cells were cultured in heavy SILAC (lysine8, arginine10—Cambridge Isotope Labs) and H1299-p53^{R273H} in light SILAC medium. Conditioned media from these labelled cells were mixed and exosomes isolated by differential centrifugation. The exosome pellet was resuspended in 6 M urea for mass spectrometry analysis. Exosome proteins were reduced (10 mM dithiothreitol), alkylated (55 mM iodoacetamide) and digested (Lys C and trypsin). Peptides were cleaned using stage tips and re-dissolved in 5% acetonitrile/0.25% formic acid. Protein samples were then applied directly to an Orbitrap Elite (LC-MS). Data were searched and quantified using Swissprot (Human) database and MaxQuant software.

Receptor trafficking and cell migration. Recipient cells were cultured in the presence of purified exosomes for 72 h. Following this, cells were trypsinised and washed to remove exosomes, re-plated and grown for 48 h to achieve a confluence of 80–90% prior to conducting receptor recycling assays[32]. H1299-p53$^{-/-}$ cells were incubated in serum-free DMEM, transferred to ice, washed twice in cold PBS and surface-labelled at 4 C with 0.2 mg/mL NHS-SS-biotin (Pierce) in PBS for 30 min. Cells were transferred to serum-free DMEM for 30 min at 37 °C to allow internalisation of tracer. Cells were returned to ice, washed twice with ice-cold PBS and biotin was removed from proteins remaining at the cell surface by reduction with MesNa. The internalised fraction was then chased from the cells by returning them to 37 °C in serum-free DMEM. At the indicated times, cells were returned to ice and biotin removed from recycled proteins by a second reduction with MesNa. The DGK inhibitor (R59022) or DMSO control were added as the receptor internalised, and were maintained during the subsequent recycling period. Biotinylated α5β1, cMET and TfnR were then determined by capture-ELISA using Maxisorp (Nunc) plates coated with antibodies recognising human α5 integrin (BD Pharmingen 555651; 5 μg/mL), cMET (R&D systems AF276; 5 μg/mL)) or TfnR (BD Pharmingen 555534; 5 μg/mL)).

For scratch-wound assays, exosome-treated cells were trypsinised and re-plated for 24 h prior to scratch-wounding and analysis of cell migration.

De-cellularised ECM and organotypic approaches. Telomerase-immortalised human dermal fibroblasts (TIFs) were cultured in the presence of purified exosomes for 72 h. To produce de-cellularised ECM, gelatin-coated tissue culture-ware was cross-linked with glutaraldehyde, quenched and equilibrated in DMEM containing 10% FBS. Exosome-treated TIFs were trypsinised and re-plated at near confluence ($\sim 2 \times 10^4$ cells/cm^2) and grown for 8 days in DMEM containing 10% FBS and 50 μg/mL ascorbic acid. Matrices were denuded of living cells by incubation with PBS containing 20 mM NH_4OH and 0.5% Triton X-100, and DNA residue was removed by incubation with DNaseI[33]. For pre-conditioning of organotypic plugs of rat tail collagen, exosome-treated TIFs were seeded in plugs of rat tail collagen 1 which were allowed to contract in full DMEM (DMEM supplemented with 10% FBS) for 14 days. 4×10^4 H1299 cells were then plated on top of these plugs and cultured for 2 days. Plugs were then transferred to a metal grid and cultured with full DMEM for 1 week followed by fixation in 4% paraformaldehyde before paraffin embedding. Four micrometer sections were then cut and stained using hematoxylin and eosin[17].

Atomic force microscopy. The mechanical properties of the cell-derived ECM were carried out with an Atomic Force Microscope Nanowizard II (JPK Instruments) mounted on an inverted optical microscope (Zeiss Observe) with a cell heater attachment. Force indentation measurements were carried out using an AFM probe (Nanoworld, Arrow TL with a nominal spring constant of 0.03 N/m) attached with a 4.8 μm silica microsphere (Bang Labs) as described previously[34]. Thermal calibrations were performed to determine the spring constant of each cantilever before use. Force spectroscopy measurements were performed on 50 randomised locations on each sample by applying a 3 nN force indentation. The Hertzian spherical model was applied to the approach force–distance curves to deduce the elastic modulus of the ECM using an in-house algorithm written in R. The adhesive properties of the ECM were estimated through analysing the energy required to remove the probe from the matrix, which is the total areas of adhesion peaks in the retraction force–distance curves (JPK data analysis software).

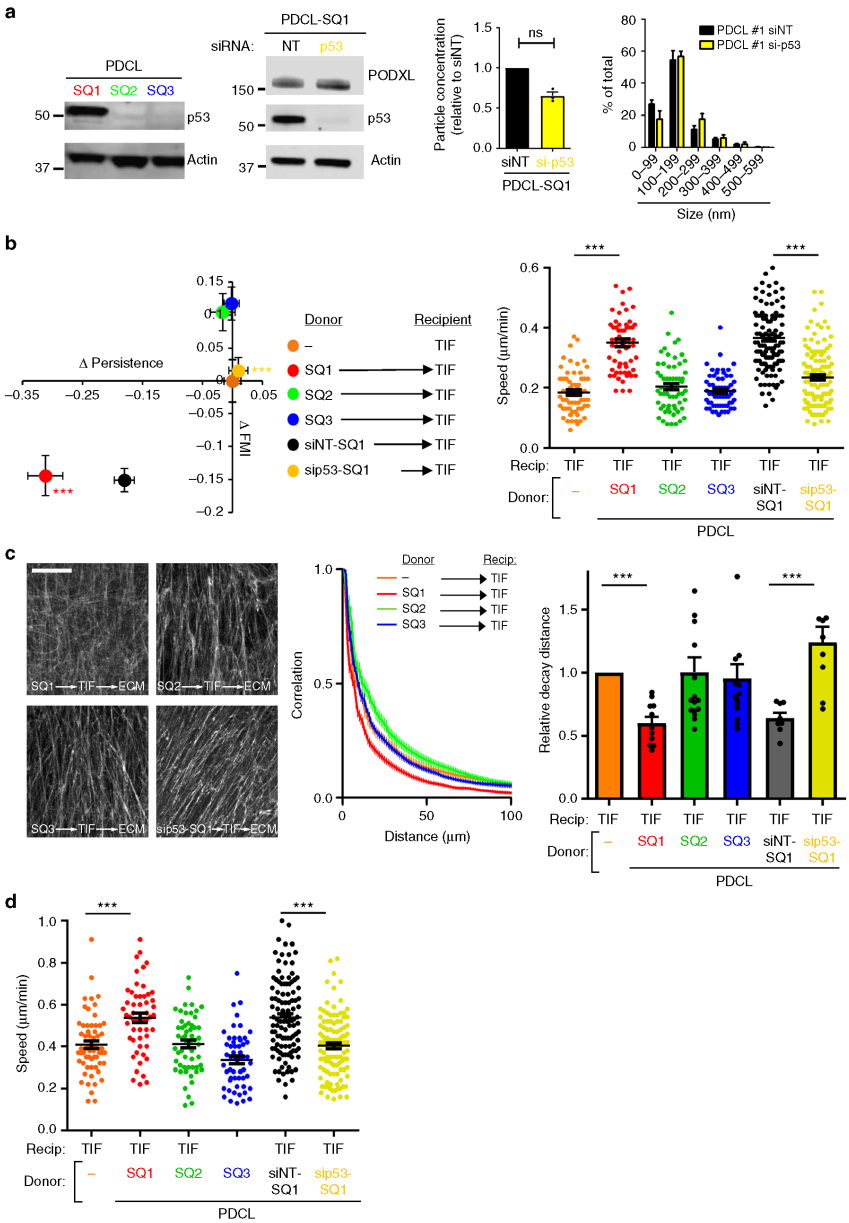

GLCM analysis of ECM organisation. Using image sets generated by second harmonic and immunofluorescence imaging, the structure and organisation of the ECM was analysed by applying grey level co-occurrence matrix (GLCM) analysis, a second-order statistical method. Briefly, the intensity of each pixel containing collagen signal is compared to the neighbouring pixels (up to 100 away, corresponding to 100 μm) and a 2D histogram of intensity occurrences compiled, from which statistical parameters of the intensity distribution are calculated such as correlation, homogeneity, contrast and entropy. This has the advantage of removing bias introduced by varying total amounts of signal, changes in the image acquisition and/or signal strength as compared to direct measurements from the raw image data. A bi-exponential model is applied to the correlation decay data and the fit parameters used to calculate a weighted

Fig. 8 Exosomes released by mutp53-expressing PDCL influence ECM architecture. **a** Levels of p53 in lysates from PDCLs expressing mutp53 – SQ1 – or null for p53 (SQ2 and SQ3) were assessed by western blotting (left panel). SQ1 cells were transfected with siRNAs targeting p53 (si-p53), or a non-targeting control (siNT) and levels of Podocalyxin and p53 in cell lysates were assessed by western blotting, with actin as a sample control (centre panel). Exosomes were collected from transfected cells and purified by differential centrifugation. Nanoparticle tracking was used to determine exosome number and size (right panels). Values are mean ± SEM. $n = 3$. **b** TIFs were left untreated or incubated with exosomes collected from SQ1, SQ2, or SQ3 cells, or from SQ1 cells transfected with si-p53, or siNT. Recipient TIFs were re-plated for a further 48 h and migratory characteristics of these cells into scratch-wounds were determined as for Fig. 2a, b. Values are mean ± SEM. $n > 60$ cells and *** is $p < 0.001$, Mann–Whitney. **c** TIFs were left untreated or incubated with exosomes for 72 h as described above (**b**). TIFs were then trypsinised, re-plated, and cultured for 8 days to allow deposition and remodelling of ECM. ECM was then de-cellularised, stained with antibodies recognising fibronectin and image stacks were collected using confocal microscopy. Extended focus projections of these stacks are displayed in the left panel of **c**, Bar, 50 µm. The organisation of the ECM fibres in these were determined using GLCM as for Fig. 5c. Decay curves from this are presented in the centre panels of **c** and the weighted means of the decay distances are displayed in the graph on the right. Values are weighted mean ± SEM, $n > 8$, *** is $p < 0.001$, Mann–Whitney. **d** De-cellularised ECMs were prepared as described above (**c**) and MDA-MB-231 breast cancer cells were plated onto these. The migration of MDA-MB-231 cells through the de-cellularised ECMs was recorded over a 16 h period using time-lapse video microscopy and cell tracking software. The migration speed of the MDA-MB-231 cells was calculated. Values are mean ± SEM, $n > 53$ cells; ***$p < 0.001$, Mann–Whitney

mean decay distance for use as a parameterisation metric between sample conditions.

Experimental animals. $KP^{172}C$ (Pdx1-Cre, $Kras^{G12D/+}$, $p53^{R172H/+}$), $KP^{270}C$ (Pdx1-Cre, $Kras^{G12D/+}$, $p53^{R270H/+}$), $KP^{fl}C$ (Pdx1-Cre, $Kras^{G12D/+}$, $p53^{fl/+}$) and KC (Pdx1-Cre, $Kras^{G12D/+}$) mice (mixed FVB/Bl6 strain) are as previously described[3]. Mice were monitored daily and kept in conventional animal facilities. All animal experiments were performed under UK Home Office licence and approved by the University of Glasgow Animal Welfare and Ethical Review Board. Tumourigenesis was assessed by gross pathology and confirmed by histology. For xenograft experiments, 1×10^6 H1299 cells were subcutaneously injected into 8-week-female CD1 nude mice. Subcutaneous tumour growth was measured by callipers three times a week until they reached a size endpoint of 8 mm. Mice were sacrificed by intraperitoneal injection of pentobarbital and lungs were inflated with 2% low melting point agarose. Briefly, a small incision was performed in the trachea and liquid agarose was injected with a blunted syringe needle. Mice were then left on ice for 10 min to allow agarose to solidify in lungs. Lungs were dissected and sliced using a vibratome (Campden Instruments 5100mz). Then, either fresh slices of lung were imaged using a Trimscope multiphoton microscope (Lavision) to visualise fibrillar collagen in the parenchyma by SHG, or to visualise fibrillar collagen in the perivascular/peribronchial area by SHG, the lung was fixed with 4% formaldehyde in PBS, sliced as before, mounted in Mowiol with 2.5% DABCO and imaged using an LSM 880 NLO multiphoton microscope (Zeiss).

Data availability

The data supporting the findings of this study are available within the article and its supplementary information files and from the corresponding author upon request. For the proteomics data, the raw MS files and search/identification files obtained with MaxQuant have been deposited to the ProteomeXchange Consortium via the PRIDE partner repository with the dataset identifier PXD011241.

Received: 27 June 2017 Accepted: 17 October 2018
Published online: 29 November 2018

References

1. Oren, M. & Rotter, V. Mutant p53 gain-of-function in cancer. *Cold Spring Harb. Perspect. Biol.* **2**, a001107 (2010).
2. Olive, K. P. et al. Mutant p53 gain of function in two mouse models of Li-Fraumeni syndrome. *Cell* **119**, 847–860 (2004).
3. Hingorani, S. R. et al. Trp53R172H and KrasG12D cooperate to promote chromosomal instability and widely metastatic pancreatic ductal adenocarcinoma in mice. *Cancer Cell* **7**, 469–483 (2005).
4. Morton, J. P. et al. Mutant p53 drives metastasis and overcomes growth arrest/senescence in pancreatic cancer. *Proc. Natl Acad. Sci. USA* **107**, 246–251 (2010).
5. Adorno, M. et al. A mutant-p53/Smad complex opposes p63 to empower TGFbeta-induced metastasis. *Cell* **137**, 87–98 (2009).
6. Muller, P. A. et al. Mutant p53 drives invasion by promoting integrin recycling. *Cell* **139**, 1327–1341 (2009).
7. Caswell, P. T. et al. Rab-coupling protein coordinates recycling of alpha5beta1 integrin and EGFR1 to promote cell migration in 3D microenvironments. *J. Cell Biol.* **183**, 143–155 (2008).
8. Rainero, E. et al. Diacylglycerol kinase alpha controls RCP-dependent integrin trafficking to promote invasive migration. *J. Cell Biol.* **196**, 277–295 (2012).
9. Levental, K. R. et al. Matrix crosslinking forces tumor progression by enhancing integrin signaling. *Cell* **139**, 891–906 (2009).
10. Tape, C. J. et al. Oncogenic KRAS regulates tumor cell signaling via stromal reciprocation. *Cell* **165**, 910–920 (2016).
11. Jones, M.C. et al. VEGFR1 (Flt1) regulates Rab4 recycling to control fibronectin polymerization and endothelial vessel branching. *Traffic* **10**, 754–766 (2009).
12. Shi, F. & Sottile, J. Caveolin-1-dependent beta1 integrin endocytosis is a critical regulator of fibronectin turnover. *J. Cell Sci.* **121**, 2360–2371 (2008).
13. Baker, A. M., Bird, D., Lang, G., Cox, T. R. & Erler, J. T. Lysyl oxidase enzymatic function increases stiffness to drive colorectal cancer progression through FAK. *Oncogene* **32**, 1863–1868 (2013).
14. Cox, T. R. et al. The hypoxic cancer secretome induces pre-metastatic bone lesions through lysyl oxidase. *Nature* **522**, 106–110 (2015).
15. Peinado, H. et al. Melanoma exosomes educate bone marrow progenitor cells toward a pro-metastatic phenotype through MET. *Nat. Med.* **18**, 883–891 (2012).
16. Costa-Silva, B. et al. Pancreatic cancer exosomes initiate pre-metastatic niche formation in the liver. *Nat. Cell Biol.* **17**, 816–826 (2015).
17. Timpson, P. et al. Organotypic collagen I assay: a malleable platform to assess cell behaviour in a 3-dimensional context. *J. Vis. Exp.* **56**, e3089 (2011).
18. Wang, J. et al. Prognostic role of podocalyxin-like protein expression in various cancers: a systematic review and meta-analysis. *Oncotarget* **8**, 52457–52464 (2016).
19. Klinkert, K., Rocancourt, M., Houdusse, A. & Echard, A. Rab35 GTPase couples cell division with initiation of epithelial apico-basal polarity and lumen opening. *Nat. Commun.* **7**, 11166 (2016).
20. Mrozowska, P. S. & Fukuda, M. Regulation of podocalyxin trafficking by Rab small GTPases in 2D and 3D epithelial cell cultures. *J. Cell Biol.* **213**, 355–369 (2016).
21. Bailey, P. et al. Genomic analyses identify molecular subtypes of pancreatic cancer. *Nature* **531**, 47–52 (2016).
22. Kang, H. J., Chun, S. M., Kim, K. R., Sohn, I. & Sung, C. O. Clinical relevance of gain-of-function mutations of p53 in high-grade serous ovarian carcinoma. *PLoS ONE* **8**, e72609 (2013).
23. Gundry, C. et al. Phosphorylation of Rab-coupling protein by LMTK3 controls Rab14-dependent EphA2 trafficking to promote cell:cell repulsion. *Nat. Commun.* **8**, 14646 (2017).
24. Melo, S. A. et al. Cancer exosomes perform cell-independent microRNA biogenesis and promote tumorigenesis. *Cancer Cell* **26**, 707–721 (2014).
25. Cooks, T. et al. Mutant p53 cancers reprogram macrophages to tumor supporting macrophages via exosomal miR-1246. *Nat. Commun.* **9**, 771 (2018).
26. Miller, B. W. et al. Targeting the LOX/hypoxia axis reverses many of the features that make pancreatic cancer deadly: inhibition of LOX abrogates metastasis and enhances drug efficacy. *EMBO Mol. Med.* **7**, 1063–1076 (2015).
27. Arandkar, S. et al. Altered p53 functionality in cancer-associated fibroblasts contributes to their cancer-supporting features. *Proc. Natl Acad. Sci. USA* **115**, 6410–6415 (2018).
28. Coffelt, S. B. et al. IL-17-producing gammadelta T cells and neutrophils conspire to promote breast cancer metastasis. *Nature* **522**, 345–348 (2015).
29. Shalem, O. et al. Genome-scale CRISPR-Cas9 knockout screening in human cells. *Science* **343**, 84–87 (2014).

30. Wang, T., Wei, J. J., Sabatini, D. M. & Lander, E. S. Genetic screens in human cells using the CRISPR-Cas9 system. *Science* **343**, 80–84 (2014).
31. O'Prey, J. et al. Application of CRISPR/Cas9 to autophagy research. *Methods Enzymol.* **588**, 79–108 (2017).
32. Roberts, M., Barry, S., Woods, A., van der Sluijs, P. & Norman, J. PDGF-regulated rab4-dependent recycling of alphavbeta3 integrin from early endosomes is necessary for cell adhesion and spreading. *Curr. Biol.* **11**, 1392–1402 (2001).
33. Bass, M. D. et al. Syndecan-4-dependent Rac1 regulation determines directional migration in response to the extracellular matrix. *J. Cell Biol.* **177**, 527–538 (2007).
34. McPhee, G., Dalby, M. J., Riehle, M. & Yin, H. Can common adhesion molecules and microtopography affect cellular elasticity? A combined atomic force microscopy and optical study. *Med Biol. Eng. Comput.* **48**, 1043–1053 (2010).

Acknowledgements

This work was funded by Cancer Research UK and Breast Cancer Now. We acknowledge the Cancer Research UK Glasgow Centre (C596/A18076) and the BSU facilities at the Cancer Research UK Beatson Institute (C596/A17196).

Author contributions

D.N., N.H., L.M., G.C., A. M.F., D.R., L.C., J. K., M.C., E.M.G., J.S., E.D., L.M.C., F.K., D.S., S.M., J.M., and J.N. performed the experiments and analysed experimental data. A. E., K.V., I.M., K.B., P.B., H.Y., L.M.C., J.M., S.Z., and J.N. supervised the experimental work and/or assisted with the planning of experiments. K.K. and A.E. provided reagents. D.N. and J.N. prepared the figures and wrote the manuscript.

Additional information

Supplementary Information accompanies this paper at https://doi.org/10.1038/s41467-018-07339-y.

Competing interests: The authors declare no competing interests.

Reprints and permission information is available online at http://npg.nature.com/reprintsandpermissions/

Publisher's note: Springer Nature remains neutral with regard to jurisdictional claims in published maps and institutional affiliations.

Appendix III – Novo et al., 2018

Novo, D., Heath, N., Mitchell, L., Caligiuri, G., MacFarlane, A., Reijmer, D., Charlton, L., Knight, J., Calka, M., McGhee, E., Dornier, E., Sumpton, D., Mason, S., Echard, A., Klinkert, K., Secklehner, J., Kruiswijk, F., Vousden, K., Macpherson, I.R., Blyth, K., Bailey, P., Yin, H., Carlin, L.M., Morton, J., Zanivan, S., Norman, J.C., 2018. Mutant p53s generate pro-invasive niches by influencing exosome podocalyxin levels. Nature Communications. 9.

References

Admyre, C., Grunewald, J., Thyberg, J., Gripenbäck, S., Tornling, G., Eklund, A., Scheynius, A., Gabrielsson, S., 2003. Exosomes with major histocompatibility complex class II and co-stimulatory molecules are present in human BAL fluid. Eur. Respir. J. 22, 578–583.

Adorno, M., Cordenonsi, M., Montagner, M., Dupont, S., Wong, C., Hann, B., Solari, A., Bobisse, S., Rondina, M.B., Guzzardo, V., Parenti, A.R., Rosato, A., Bicciato, S., Balmain, A., Piccolo, S., 2009. A Mutant-p53/Smad Complex Opposes p63 to Empower TGFβ-Induced Metastasis. Cell 137, 87–98.

Ahn, S.-G., 2003. Redox regulation of mammalian heat shock factor 1 is essential for Hsp gene activation and protection from stress. Genes & Development 17, 516–528.

Akthar, S., Patel, D.F., Beale, R.C., Peiró, T., Xu, X., Gaggar, A., Jackson, P.L., Blalock, J.E., Lloyd, C.M., Snelgrove, R.J., 2015. Matrikines are key regulators in modulating the amplitude of lung inflammation in acute pulmonary infection. Nature Communications 6.

Albrengues, J., Bourget, I., Pons, C., Butet, V., Hofman, P., Tartare-Deckert, S., Feral, C.C., Meneguzzi, G., Gaggioli, C., 2014. LIF Mediates Proinvasive Activation of Stromal Fibroblasts in Cancer. Cell Reports 7, 1664–1678.

Albrengues, J., Shields, M.A., Ng, D., Park, C.G., Ambrico, A., Poindexter, M.E., Upadhyay, P., Uyeminami, D.L., Pommier, A., Küttner, V., Bružas, E., Maiorino, L., Bautista, C., Carmona, E.M., Gimotty, P.A., Fearon, D.T., Chang, K., Lyons, S.K., Pinkerton, K.E., Trotman, L.C., Goldberg, M.S., Yeh, J.T.-H., Egeblad, M., 2018. Neutrophil extracellular traps produced during inflammation awaken dormant cancer cells in mice. Science 361, eaao4227.

Al-Nedawi, K., Meehan, B., Kerbel, R.S., Allison, A.C., Rak, J., 2009. Endothelial expression of autocrine VEGF upon the uptake of tumor-derived microvesicles containing oncogenic EGFR. Proceedings of the National Academy of Sciences 106, 3794–3799.

Al-Nedawi, K., Meehan, B., Micallef, J., Lhotak, V., May, L., Guha, A., Rak, J., 2008. Intercellular transfer of the oncogenic receptor EGFRvIII by microvesicles derived from tumour cells. Nat Cell Biol 10, 619–624.

Anderberg, C., Li, H., Fredriksson, L., Andrae, J., Betsholtz, C., Li, X., Eriksson, U., Pietras, K., 2009. Paracrine Signaling by Platelet-Derived Growth Factor-CC Promotes Tumor Growth by Recruitment of Cancer-Associated Fibroblasts. Cancer Res 69, 369–378.

Antonyak, M.A., Wilson, K.F., Cerione, R.A., 2012. R(h)oads to microvesicles. Small GTPases 3, 219–224.

Arjonen, A., Kaukonen, R., Mattila, E., Rouhi, P., Högnäs, G., Sihto, H., Miller, B.W., Morton, J.P., Bucher, E., Taimen, P., Virtakoivu, R., Cao, Y., Sansom, O.J., Joensuu, H., Ivaska, J., 2014. Mutant p53–associated myosin-X upregulation promotes breast cancer invasion and metastasis. J. Clin. Invest. 124, 1069–1082.

Augsten, M., 2014. Cancer-Associated Fibroblasts as Another Polarized Cell Type of the Tumor Microenvironment. Front. Oncol. 4.

Baglio, S.R., Lagerweij, T., Pérez-Lanzón, M., Ho, X.D., Léveillé, N., Melo, S.A., Cleton-Jansen, A.-M., Jordanova, E.S., Roncuzzi, L., Greco, M., Eijndhoven, M.A.J. van, Grisendi, G., Dominici, M., Bonafede, R., Lougheed, S.M., Gruijl, T.D. de, Zini, N., Cervo, S., Steffan, A., Canzonieri, V., Martson, A., Maasalu, K., Köks, S., Wurdinger, T., Baldini, N., Pegtel, D.M., 2017. Blocking Tumor-Educated MSC Paracrine Activity Halts Osteosarcoma Progression. Clin Cancer Res 23, 3721–3733.

Baietti, M.F., Zhang, Z., Mortier, E., Melchior, A., Degeest, G., Geeraerts, A., Ivarsson, Y., Depoortere, F., Coomans, C., Vermeiren, E., Zimmermann, P., David, G., 2012.

Syndecan–syntenin–ALIX regulates the biogenesis of exosomes. Nat Cell Biol 14, 677–685.

Bailey, P., Australian Pancreatic Cancer Genome Initiative, Chang, D.K., Nones, K., Johns, A.L., Patch, A.-M., Gingras, M.-C., Miller, D.K., Christ, A.N., Bruxner, T.J.C., Quinn, M.C., Nourse, C., Murtaugh, L.C., Harliwong, I., Idrisoglu, S., Manning, S., Nourbakhsh, E., Wani, S., Fink, L., Holmes, O., Chin, V., Anderson, M.J., Kazakoff, S., Leonard, C., Newell, F., Waddell, Nick, Wood, S., Xu, Q., Wilson, P.J., Cloonan, N., Kassahn, K.S., Taylor, D., Quek, K., Robertson, A., Pantano, L., Mincarelli, L., Sanchez, L.N., Evers, L., Wu, J., Pinese, M., Cowley, M.J., Jones, M.D., Colvin, E.K., Nagrial, A.M., Humphrey, E.S., Chantrill, L.A., Mawson, A., Humphris, J., Chou, A., Pajic, M., Scarlett, C.J., Pinho, A.V., Giry-Laterriere, M., Rooman, I., Samra, J.S., Kench, J.G., Lovell, J.A., Merrett, N.D., Toon, C.W., Epari, K., Nguyen, N.Q., Barbour, A., Zeps, N., Moran-Jones, K., Jamieson, N.B., Graham, J.S., Duthie, F., Oien, K., Hair, J., Grützmann, R., Maitra, A., Iacobuzio-Donahue, C.A., Wolfgang, C.L., Morgan, R.A., Lawlor, R.T., Corbo, V., Bassi, C., Rusev, B., Capelli, P., Salvia, R., Tortora, G., Mukhopadhyay, D., Petersen, G.M., Munzy, D.M., Fisher, W.E., Karim, S.A., Eshleman, J.R., Hruban, R.H., Pilarsky, C., Morton, J.P., Sansom, O.J., Scarpa, A., Musgrove, E.A., Bailey, U.-M.H., Hofmann, O., Sutherland, R.L., Wheeler, D.A., Gill, A.J., Gibbs, R.A., Pearson, J.V., Waddell, Nicola, Biankin, A.V., Grimmond, S.M., 2016. Genomic analyses identify molecular subtypes of pancreatic cancer. Nature 531, 47–52.

Baker, S.J., Preisinger, A.C., Jessup, J.M., Paraskeva, C., Markowitz, S., Willson, J.K.V., Hamilton, S., Vogelstein, B., 1990. p53 Gene Mutations Occur in Combination with 17p Allelic Deletions as Late Events in Colorectal Tumorigenesis 7.

Barbazán, J., Matic Vignjevic, D., 2019. Cancer associated fibroblasts: is the force the path to the dark side? Current Opinion in Cell Biology 56, 71–79.

Bargonetti, J., Friedman, P.N., Kern, S.E., Prives, C., 1991. Wild-Type but Not Mutant ~53 lmmunopurified Proteins Bind to Sequences Adjacent to the SV40 Origin of Replication 9.

Bargonetti, J., Manfredi, J.J., Chen, X., Marshak, D.R., Prives, C., 1993. A proteolytic fragment from the central region of p53 has marked sequence-specific DNA-binding activity when generated from wild-type but not from oncogenic mutant p53 protein. Genes Dev. 7, 2565–2574.

Baroni, S., Romero-Cordoba, S., Plantamura, I., Dugo, M., D'Ippolito, E., Cataldo, A., Cosentino, G., Angeloni, V., Rossini, A., Daidone, M.G., Iorio, M.V., 2016. Exosome-mediated delivery of miR-9 induces cancer-associated fibroblast-like properties in human breast fibroblasts. Cell Death Dis 7, e2312–e2312.

Barres, C., Blanc, L., Bette-Bobillo, P., Andre, S., Mamoun, R., Gabius, H.-J., Vidal, M., 2010. Galectin-5 is bound onto the surface of rat reticulocyte exosomes and modulates vesicle uptake by macrophages. Blood 115, 696–705.

Bensaad, K., Tsuruta, A., Selak, M.A., Vidal, M.N.C., Nakano, K., Bartrons, R., Gottlieb, E., Vousden, K.H., 2006. TIGAR, a p53-Inducible Regulator of Glycolysis and Apoptosis. Cell 126, 107–120.

Bianco, F., Perrotta, C., Novellino, L., Francolini, M., Riganti, L., Menna, E., Saglietti, L., Schuchman, E.H., Furlan, R., Clementi, E., Matteoli, M., Verderio, C., 2009. Acid sphingomyelinase activity triggers microparticle release from glial cells. EMBO J 28, 1043–1054.

Binnewies, M., Roberts, E.W., Kersten, K., Chan, V., Fearon, D.F., Merad, M., Coussens, L.M., Gabrilovich, D.I., Ostrand-Rosenberg, S., Hedrick, C.C., Vonderheide, R.H., Pittet, M.J., Jain, R.K., Zou, W., Howcroft, T.K., Woodhouse, E.C., Weinberg, R.A., Krummel, M.F., 2018. Understanding the tumor immune microenvironment (TIME) for effective therapy. Nat Med 24, 541–550.

Boman, K., Andersson, G., Wennersten, C., Nodin, B., Ahlgren, G., Jirström, K., 2017. Podocalyxin-like and RNA-binding motif protein 3 are prognostic biomarkers in urothelial bladder cancer: a validatory study. Biomark Res 5, 10.

Boman, K., Larsson, A.H., Segersten, U., Kuteeva, E., Johannesson, H., Nodin, B., Eberhard, J., Uhlén, M., Malmström, P.-U., Jirström, K., 2013. Membranous expression of podocalyxin-like protein is an independent factor of poor prognosis in urothelial bladder cancer. Br J Cancer 108, 2321–2328.

Bourhis, J.-M., Mariano, N., Zhao, Y., Harlos, K., Exposito, J.-Y., Jones, E.Y., Moali, C., Aghajari, N., Hulmes, D.J.S., 2012. Structural basis of fibrillar collagen trimerization and related genetic disorders. Nat Struct Mol Biol 19, 1031–1036.

Brodsky, B., Persikov, A.V., 2005. Molecular Structure of the Collagen Triple Helix. In: Advances in Protein Chemistry. Elsevier, pp. 301–339.

Bu, L., Baba, H., Yoshida, N., Miyake, K., Yasuda, T., Uchihara, T., Tan, P., Ishimoto, T., 2019. Biological heterogeneity and versatility of cancer-associated fibroblasts in the tumor microenvironment. Oncogene 38, 4887–4901.

Buschow, S.I., Nolte-'t Hoen, E.N.M., van Niel, G., Pols, M.S., ten Broeke, T., Lauwen, M., Ossendorp, F., Melief, C.J.M., Raposo, G., Wubbolts, R., Wauben, M.H.M., Stoorvogel, W., 2009. MHC II in dendritic cells is targeted to lysosomes or T cell-induced exosomes via distinct multivesicular body pathways. Traffic 10, 1528–1542.

Calvo, F., Ege, N., Grande-Garcia, A., Hooper, S., Jenkins, R.P., Chaudhry, S.I., Harrington, K., Williamson, P., Moeendarbary, E., Charras, G., Sahai, E., 2013. Mechanotransduction and YAP-dependent matrix remodelling is required for the generation and maintenance of cancer-associated fibroblasts. Nat Cell Biol 15, 637–646.

Caswell, P.T., Chan, M., Lindsay, A.J., McCaffrey, M.W., Boettiger, D., Norman, J.C., 2008. Rab-coupling protein coordinates recycling of α5β1 integrin and EGFR1 to promote cell migration in 3D microenvironments. J Cell Biol 183, 143–155.

Chanda, D., Otoupalova, E., Hough, K.P., Locy, M.L., Bernard, K., Deshane, J.S., Sanderson, R.D., Mobley, J.A., Thannickal, V.J., 2019. Fibronectin on the Surface of Extracellular Vesicles Mediates Fibroblast Invasion. Am J Respir Cell Mol Biol 60, 279–288.

Chapman, A., Fernandez del Ama, L., Ferguson, J., Kamarashev, J., Wellbrock, C., Hurlstone, A., 2014. Heterogeneous Tumor Subpopulations Cooperate to Drive Invasion. Cell Reports 8, 688–695.

Chen, G., Huang, A.C., Zhang, W., Zhang, G., Wu, M., Xu, W., Yu, Z., Yang, J., Wang, B., Sun, H., Xia, H., Man, Q., Zhong, W., Antelo, L.F., Wu, B., Xiong, X., Liu, X., Guan, L., Li, T., Liu, S., Yang, R., Lu, Youtao, Dong, L., McGettigan, S., Somasundaram, R., Radhakrishnan, R., Mills, G., Lu, Yiling, Kim, J., Chen, Y.H., Dong, H., Zhao, Y., Karakousis, G.C., Mitchell, T.C., Schuchter, L.M., Herlyn, M., Wherry, E.J., Xu, X., Guo, W., 2018. Exosomal PD-L1 contributes to immunosuppression and is associated with anti-PD-1 response. Nature 560, 382–386.

Chen, J., 2016. The Cell-Cycle Arrest and Apoptotic Functions of p53 in Tumor Initiation and Progression. Cold Spring Harb Perspect Med 6.

Cho, H., Kim, J.-H., Jun, C.-D., Jung, D.-W., Williams, D.R., 2019. CAF-Derived IL6 and GM-CSF Cooperate to Induce M2-like TAMs–Response. Clin Cancer Res 25, 894–895.

Clark, A.G., Vignjevic, D.M., 2015. Modes of cancer cell invasion and the role of the microenvironment. Current Opinion in Cell Biology 36, 13–22.

Clark, K., 2005. A specific 5 1-integrin conformation promotes directional integrin translocation and fibronectin matrix formation. Journal of Cell Science 118, 291–300.

Clore, G.M., Ernst, J., Clubb, R., Omichinski, J.G., Kennedy, W.M.P., Sakaguchi, K., Appella, E., Gronenborn, A.M., 1995. Refined solution structure of the oligomerization domain of the tumour suppressor p53. Nat Struct Mol Biol 2, 321–333.

Coffill, C.R., Muller, P.A.J., Oh, H.K., Neo, S.P., Hogue, K.A., Cheok, C.F., Vousden, K.H., Lane, D.P., Blackstock, W.P., Gunaratne, J., 2012. Mutant p53 interactome identifies nardilysin as a p53R273H-specific binding partner that promotes invasion. EMBO Rep 13, 638–644.

Collisson, E.A., Bailey, P., Chang, D.K., Biankin, A.V., 2019. Molecular subtypes of pancreatic cancer. Nat Rev Gastroenterol Hepatol 16, 207–220.

Colombo, M., Moita, C., van Niel, G., Kowal, J., Vigneron, J., Benaroch, P., Manel, N., Moita, L.F., Théry, C., Raposo, G., 2013. Analysis of ESCRT functions in exosome biogenesis, composition and secretion highlights the heterogeneity of extracellular vesicles. J Cell Sci 126, 5553–5565.

Como, C.J.D., Prives, C., 1998. Human tumor-derived p53 proteins exhibit binding site selectivity and temperature sensitivity for transactivation in a yeast-based assay. Oncogene 16, 2527–2539.

Conklin, M.W., Eickhoff, J.C., Riching, K.M., Pehlke, C.A., Eliceiri, K.W., Provenzano, P.P., Friedl, A., Keely, P.J., 2011. Aligned Collagen Is a Prognostic Signature for Survival in Human Breast Carcinoma. The American Journal of Pathology 178, 1221–1232.

Cooks, T., Pateras, I.S., Jenkins, L.M., Patel, K.M., Robles, A.I., Morris, J., Forshew, T., Appella, E., Gorgoulis, V.G., Harris, C.C., 2018. Mutant p53 cancers reprogram macrophages to tumor supporting macrophages via exosomal miR-1246. Nat Commun 9, 771.

Costa-Silva, B., Aiello, N.M., Ocean, A.J., Singh, S., Zhang, H., Thakur, B.K., Becker, A., Hoshino, A., Mark, M.T., Molina, H., Xiang, J., Zhang, T., Theilen, T.-M., García-Santos, G., Williams, C., Ararso, Y., Huang, Y., Rodrigues, G., Shen, T.-L., Labori, K.J., Lothe, I.M.B., Kure, E.H., Hernandez, J., Doussot, A., Ebbesen, S.H., Grandgenett, P.M., Hollingsworth, M.A., Jain, M., Mallya, K., Batra, S.K., Jarnagin, W.R., Schwartz, R.E., Matei, I., Peinado, H., Stanger, B.Z., Bromberg, J., Lyden, D., 2015. Pancreatic cancer exosomes initiate pre-metastatic niche formation in the liver. Nat Cell Biol 17, 816–826.

Crighton, D., Wilkinson, S., O'Prey, J., Syed, N., Smith, P., Harrison, P.R., Gasco, M., Garrone, O., Crook, T., Ryan, K.M., 2006. DRAM, a p53-induced modulator of autophagy, is critical for apoptosis. Cell 126, 121–134.

Dang, C.V., 2012. Links between metabolism and cancer. Genes & Development 26, 877–890.

De Boeck, A., Hendrix, A., Maynard, D., Van Bockstal, M., Daniëls, A., Pauwels, P., Gespach, C., Bracke, M., De Wever, O., 2013. Differential secretome analysis of cancer-associated fibroblasts and bone marrow-derived precursors to identify microenvironmental regulators of colon cancer progression. Proteomics 13, 379–388.

Di Agostino, S., Sorrentino, G., Ingallina, E., Valenti, F., Ferraiuolo, M., Bicciato, S., Piazza, S., Strano, S., Del Sal, G., Blandino, G., 2016. YAP enhances the pro-proliferative transcriptional activity of mutant p53 proteins. EMBO Rep 17, 188–201.

Di Agostino, S., Strano, S., Emiliozzi, V., Zerbini, V., Mottolese, M., Sacchi, A., Blandino, G., Piaggio, G., 2006. Gain of function of mutant p53: The mutant p53/NF-Y protein complex reveals an aberrant transcriptional mechanism of cell cycle regulation. Cancer Cell 10, 191–202.

Di Micco, R., Fumagalli, M., Cicalese, A., Piccinin, S., Gasparini, P., Luise, C., Schurra, C., Garre', M., Nuciforo, P.G., Bensimon, A., Maestro, R., Pelicci, P.G., d'Adda di

Fagagna, F., 2006. Oncogene-induced senescence is a DNA damage response triggered by DNA hyper-replication. Nature 444, 638–642.

Di Modica, M., Regondi, V., Sandri, M., Iorio, M.V., Zanetti, A., Tagliabue, E., Casalini, P., Triulzi, T., 2017. Breast cancer-secreted miR-939 downregulates VE-cadherin and destroys the barrier function of endothelial monolayers. Cancer Letters 384, 94–100.

Dias, M.V.S., Teixeira, B.L., Rodrigues, B.R., Sinigaglia-Coimbra, R., Porto-Carreiro, I., Roffé, M., Hajj, G.N.M., Martins, V.R., 2016. PRNP/prion protein regulates the secretion of exosomes modulating CAV1/caveolin-1-suppressed autophagy. Autophagy 12, 2113–2128.

Ding, X., Ji, J., Jiang, J., Cai, Q., Wang, C., Shi, M., Yu, Y., Zhu, Z., Zhang, J., 2018. HGF-mediated crosstalk between cancer-associated fibroblasts and MET-unamplified gastric cancer cells activates coordinated tumorigenesis and metastasis. Cell Death Dis 9, 867.

Doyonnas, R., Kershaw, D.B., Duhme, C., Merkens, H., Chelliah, S., Graf, T., McNagny, K.M., 2001. Anuria, Omphalocele, and Perinatal Lethality in Mice Lacking the Cd34-Related Protein Podocalyxin. J Exp Med 194, 13–28.

el-Deiry, W.S., Kern, S.E., Pietenpol, J.A., Kinzler, K.W., Vogelstein, B., 1992. Definition of a consensus binding site for p53. Nat. Genet. 1, 45–49.

Erler, J.T., Bennewith, K.L., Cox, T.R., Lang, G., Bird, D., Koong, A., Le, Q.-T., Giaccia, A.J., 2009. Hypoxia-Induced Lysyl Oxidase Is a Critical Mediator of Bone Marrow Cell Recruitment to Form the Premetastatic Niche. Cancer Cell 15, 35–44.

Escola, J.-M., Kleijmeer, M.J., Stoorvogel, W., Griffith, J.M., Yoshie, O., Geuze, H.J., 1998. Selective Enrichment of Tetraspan Proteins on the Internal Vesicles of Multivesicular Endosomes and on Exosomes Secreted by Human B-lymphocytes. J. Biol. Chem. 273, 20121–20127.

Fader, C.M., Sánchez, D.G., Mestre, M.B., Colombo, M.I., 2009. TI-VAMP/VAMP7 and VAMP3/cellubrevin: two v-SNARE proteins involved in specific steps of the autophagy/multivesicular body pathways. Biochimica et Biophysica Acta (BBA) - Molecular Cell Research 1793, 1901–1916.

Fernández, D., Larrucea, S., Nowakowski, A., Pericacho, M., Parrilla, R., Ayuso, M.S., 2011. Release of podocalyxin into the extracellular space. Biochimica et Biophysica Acta (BBA) - Molecular Cell Research 1813, 1504–1510.

Freed-Pastor, W.A., Mizuno, H., Zhao, X., Langerød, A., Moon, S.-H., Rodriguez-Barrueco, R., Barsotti, A., Chicas, A., Li, W., Polotskaia, A., Bissell, M.J., Osborne, T.F., Tian, B., Lowe, S.W., Silva, J.M., Børresen-Dale, A.-L., Levine, A.J., Bargonetti, J., Prives, C., 2012. Mutant p53 Disrupts Mammary Tissue Architecture via the Mevalonate Pathway. Cell 148, 244–258.

Freed-Pastor, W.A., Prives, C., 2012. Mutant p53: one name, many proteins. Genes & Development 26, 1268–1286.

Frum, R.A., Love, I.M., Damle, P.K., Mukhopadhyay, N.D., Palit Deb, S., Deb, S., Grossman, S.R., 2016. Constitutive Activation of DNA Damage Checkpoint Signaling Contributes to Mutant p53 Accumulation via Modulation of p53 Ubiquitination. Molecular Cancer Research 14, 423–436.

Garcia, N.A., González-King, H., Grueso, E., Sánchez, R., Martinez-Romero, A., Jávega, B., O'Connor, J.E., Simons, P.J., Handberg, A., Sepúlveda, P., 2019. Circulating exosomes deliver free fatty acids from the bloodstream to cardiac cells: Possible role of CD36. PLoS One 14.

Girardini, J.E., Napoli, M., Piazza, S., Rustighi, A., Marotta, C., Radaelli, E., Capaci, V., Jordan, L., Quinlan, P., Thompson, A., Mano, M., Rosato, A., Crook, T., Scanziani, E., Means, A.R., Lozano, G., Schneider, C., Del Sal, G., 2011. A Pin1/Mutant p53 Axis Promotes Aggressiveness in Breast Cancer. Cancer Cell 20, 79–91.

Glentis, A., Oertle, P., Mariani, P., Chikina, A., El Marjou, F., Attieh, Y., Zaccarini, F., Lae, M., Loew, D., Dingli, F., Sirven, P., Schoumacher, M., Gurchenkov, B.G., Plodinec, M., Vignjevic, D.M., 2017. Cancer-associated fibroblasts induce metalloprotease-independent cancer cell invasion of the basement membrane. Nat Commun 8, 924.

Göhler, T., Jäger, S., Warnecke, G., Yasuda, H., Kim, E., Deppert, W., 2005. Mutant p53 proteins bind DNA in a DNA structure-selective mode. Nucleic Acids Res. 33, 1087–1100.

Grant, T.J., Hua, K., Singh, A., 2016. Molecular Pathogenesis of Pancreatic Cancer. In: Progress in Molecular Biology and Translational Science. Elsevier, pp. 241–275.

Grenard, P., Bresson-Hadni, S., El Alaoui, S., Chevallier, M., Vuitton, D.A., Ricard-Blum, S., 2001. Transglutaminase-mediated cross-linking is involved in the stabilization of extracellular matrix in human liver fibrosis. Journal of Hepatology 35, 367–375.

Guerra, F., Bucci, C., 2016. Multiple Roles of the Small GTPase Rab7. Cells 5, 34.

Guix, F.X., Sannerud, R., Berditchevski, F., Arranz, A.M., Horré, K., Snellinx, A., Thathiah, A., Saido, T., Saito, T., Rajesh, S., Overduin, M., Kumar-Singh, S., Radaelli, E., Corthout, N., Colombelli, J., Tosi, S., Munck, S., Salas, I.H., Annaert, W., De Strooper, B., 2017. Tetraspanin 6: a pivotal protein of the multiple vesicular body determining exosome release and lysosomal degradation of amyloid precursor protein fragments. Mol Neurodegeneration 12, 25.

Gupta, S., Rawat, S., Arora, V., Kottarath, S.K., Dinda, A.K., Vaishnav, P.K., Nayak, B., Mohanty, S., 2018. An improvised one-step sucrose cushion ultracentrifugation method for exosome isolation from culture supernatants of mesenchymal stem cells. Stem Cell Res Ther 9, 180.

Gusachenko, O.N., Zenkova, M.A., Vlassov, V.V., 2013. Nucleic acids in exosomes: Disease markers and intercellular communication molecules. Biochemistry Moscow 78, 1–7.

Hanahan, D., Weinberg, R.A., 2000. The Hallmarks of Cancer. Cell 100, 57–70.

Handorf, A.M., Zhou, Y., Halanski, M.A., Li, W.-J., 2015. Tissue Stiffness Dictates Development, Homeostasis, and Disease Progression. Organogenesis 11, 1–15.

Hashimoto, S., Furukawa, S., Hashimoto, A., Tsutaho, A., Fukao, A., Sakamura, Y., Parajuli, G., Onodera, Y., Otsuka, Y., Handa, H., Oikawa, T., Hata, S., Nishikawa, Y., Mizukami, Y., Kodama, Y., Murakami, M., Fujiwara, T., Hirano, S., Sabe, H., 2019. ARF6 and AMAP1 are major targets of *KRAS* and *TP53* mutations to promote invasion, PD-L1 dynamics, and immune evasion of pancreatic cancer. Proc Natl Acad Sci USA 201901765.

Herchenhan, A., Uhlenbrock, F., Eliasson, P., Weis, M., Eyre, D., Kadler, K.E., Magnusson, S.P., Kjaer, M., 2015. Lysyl Oxidase Activity Is Required for Ordered Collagen Fibrillogenesis by Tendon Cells. J. Biol. Chem. 290, 16440–16450.

Heusermann, W., Hean, J., Trojer, D., Steib, E., von Bueren, S., Graff-Meyer, A., Genoud, C., Martin, K., Pizzato, N., Voshol, J., Morrissey, D.V., Andaloussi, S.E.L., Wood, M.J., Meisner-Kober, N.C., 2016. Exosomes surf on filopodia to enter cells at endocytic hot spots, traffic within endosomes, and are targeted to the ER. J Cell Biol 213, 173–184.

Hillen, F., Griffioen, A.W., 2007. Tumour vascularization: sprouting angiogenesis and beyond. Cancer Metastasis Rev 26, 489–502.

Hingorani, S.R., Wang, L., Multani, A.S., Combs, C., Deramaudt, T.B., Hruban, R.H., Rustgi, A.K., Chang, S., Tuveson, D.A., 2005. Trp53R172H and KrasG12D cooperate to promote chromosomal instability and widely metastatic pancreatic ductal adenocarcinoma in mice. Cancer Cell 7, 469–483.

Hogan, M.C., Johnson, K.L., Zenka, R.M., Cristine Charlesworth, M., Madden, B.J., Mahoney, D.W., Oberg, A.L., Huang, B.Q., Leontovich, A.A., Nesbitt, L.L., Bakeberg, J.L., McCormick, D.J., Robert Bergen, H., Ward, C.J., 2014.

Subfractionation, characterization, and in-depth proteomic analysis of glomerular membrane vesicles in human urine. Kidney International 85, 1225–1237.

Holmes, D.F., Gilpin, C.J., Baldock, C., Ziese, U., Koster, A.J., Kadler, K.E., 2001. Corneal collagen fibril structure in three dimensions: Structural insights into fibril assembly, mechanical properties, and tissue organization. Proceedings of the National Academy of Sciences 98, 7307–7312.

Hoshino, A., Costa-Silva, B., Shen, T.-L., Rodrigues, G., Hashimoto, A., Tesic Mark, M., Molina, H., Kohsaka, S., Di Giannatale, A., Ceder, S., Singh, S., Williams, C., Soplop, N., Uryu, K., Pharmer, L., King, T., Bojmar, L., Davies, A.E., Ararso, Y., Zhang, T., Zhang, H., Hernandez, J., Weiss, J.M., Dumont-Cole, V.D., Kramer, K., Wexler, L.H., Narendran, A., Schwartz, G.K., Healey, J.H., Sandstrom, P., Jørgen Labori, K., Kure, E.H., Grandgenett, P.M., Hollingsworth, M.A., de Sousa, M., Kaur, S., Jain, M., Mallya, K., Batra, S.K., Jarnagin, W.R., Brady, M.S., Fodstad, O., Muller, V., Pantel, K., Minn, A.J., Bissell, M.J., Garcia, B.A., Kang, Y., Rajasekhar, V.K., Ghajar, C.M., Matei, I., Peinado, H., Bromberg, J., Lyden, D., 2015. Tumour exosome integrins determine organotropic metastasis. Nature 527, 329–335.

Hsu, C., Morohashi, Y., Yoshimura, S., Manrique-Hoyos, N., Jung, S., Lauterbach, M.A., Bakhti, M., Grønborg, M., Möbius, W., Rhee, J., Barr, F.A., Simons, M., 2010. Regulation of exosome secretion by Rab35 and its GTPase-activating proteins TBC1D10A–C. J Cell Biol 189, 223–232.

Hyenne, V., Apaydin, A., Rodriguez, D., Spiegelhalter, C., Hoff-Yoessle, S., Diem, M., Tak, S., Lefebvre, O., Schwab, Y., Goetz, J.G., Labouesse, M., 2015. RAL-1 controls multivesicular body biogenesis and exosome secretion. J Cell Biol 211, 27–37.

Ikenouchi, J., Hirata, M., Yonemura, S., Umeda, M., 2013. Sphingomyelin clustering is essential for the formation of microvilli. Journal of Cell Science 126, 3585–3592.

Inda, M. -d.-M., Bonavia, R., Mukasa, A., Narita, Y., Sah, D.W.Y., Vandenberg, S., Brennan, C., Johns, T.G., Bachoo, R., Hadwiger, P., Tan, P., DePinho, R.A., Cavenee, W., Furnari, F., 2010. Tumor heterogeneity is an active process maintained by a mutant EGFR-induced cytokine circuit in glioblastoma. Genes & Development 24, 1731–1745.

Ingallina, E., Sorrentino, G., Bertolio, R., Lisek, K., Zannini, A., Azzolin, L., Severino, L.U., Scaini, D., Mano, M., Mantovani, F., Rosato, A., Bicciato, S., Piccolo, S., Del Sal, G., 2018. Mechanical cues control mutant p53 stability through a mevalonate–RhoA axis. Nat Cell Biol 20, 28–35.

Jacquemet, G., Green, D.M., Bridgewater, R.E., von Kriegsheim, A., Humphries, M.J., Norman, J.C., Caswell, P.T., 2013. RCP-driven α5β1 recycling suppresses Rac and promotes RhoA activity via the RacGAP1–IQGAP1 complex. J Cell Biol 202, 917–935.

Jansen, K.A., Atherton, P., Ballestrem, C., 2017. Mechanotransduction at the cell-matrix interface. Seminars in Cell & Developmental Biology 71, 75–83.

Jimenez, G.S., Nister, M., Stommel, J.M., Beeche, M., Barcarse, E.A., Zhang, X.Q., O'Gorman, S., Wahl, G.M., 2000. A transactivation-deficient mouse model provides insights into Trp53 regulation and function. Nat. Genet. 26, 37–43.

Jones, M.C., Caswell, P.T., Moran-Jones, K., Roberts, M., Barry, S.T., Gampel, A., Mellor, H., Norman, J.C., 2009. VEGFR1 (Flt1) Regulates Rab4 Recycling to Control Fibronectin Polymerization and Endothelial Vessel Branching. Traffic 10, 754–766.

Jordan, J.J., Menendez, D., Inga, A., Nourredine, M., Bell, D., Resnick, M.A., 2008. Noncanonical DNA Motifs as Transactivation Targets by Wild Type and Mutant p53. PLoS Genet 4, e1000104.

Kalluri, R., 2016. The biology and function of fibroblasts in cancer. Nat Rev Cancer 16, 582–598.

Kang, H.J., Chun, S.-M., Kim, K.-R., Sohn, I., Sung, C.O., 2013. Clinical Relevance of Gain-Of-Function Mutations of p53 in High-Grade Serous Ovarian Carcinoma. PLoS ONE 8, e72609.

Kaplan, R.N., Riba, R.D., Zacharoulis, S., Bramley, A.H., Vincent, L., Costa, C., MacDonald, D.D., Jin, D.K., Shido, K., Kerns, S.A., Zhu, Z., Hicklin, D., Wu, Y., Port, J.L., Altorki, N., Port, E.R., Ruggero, D., Shmelkov, S.V., Jensen, K.K., Rafii, S., Lyden, D., 2005. VEGFR1-positive haematopoietic bone marrow progenitors initiate the pre-metastatic niche. Nature 438, 820–827.

Kaprio, T., Hagström, J., Fermér, C., Mustonen, H., Böckelman, C., Nilsson, O., Haglund, C., 2014. A comparative study of two PODXL antibodies in 840 colorectal cancer patients. BMC Cancer 14, 494.

Kastan, M.B., Onyekwere, O., Sidransky, D., Vogelstein, B., Craig, R.W., 1991. Participation of p53 Protein in the Cellular Response to DNA Damage 9.

Kastenhuber, E.R., Lowe, S.W., 2017. Putting p53 in Context. Cell 170, 1062–1078.

Kato, S., Han, S.-Y., Liu, W., Otsuka, K., Shibata, H., Kanamaru, R., Ishioka, C., 2003. Understanding the function–structure and function–mutation relationships of p53 tumor suppressor protein by high-resolution missense mutation analysis. PNAS 100, 8424–8429.

KellokumpuS, S., Sormunengn, R., Heikkinennll, J., n.d. Lysyl Hydroxylase, a Collagen Processing Enzyme, Exemplifies a Novel Class of Luminallyloriented Peripheral Membrane Proteins in the Endoplasmic Reticulum 6.

Kern, S.E., Kinzler, K.W., Bruskin, A., Jarosz, D., Friedman, P., Prives, C., Vogelstein, B., 1991. Identification of p53 as a Sequence-Specific DNA-Binding Protein. Science, New Series 252, 1708–1711.

Klibi, J., Niki, T., Riedel, A., Pioche-Durieu, C., Souquere, S., Rubinstein, E., Le Moulec, S., Guigay, J., Hirashima, M., Guemira, F., Adhikary, D., Mautner, J., Busson, P., 2009. Blood diffusion and Th1-suppressive effects of galectin-9-containing exosomes released by Epstein-Barr virus-infected nasopharyngeal carcinoma cells. Blood 113, 1957–1966.

Klinkert, K., Rocancourt, M., Houdusse, A., Echard, A., 2016. Rab35 GTPase couples cell division with initiation of epithelial apico-basal polarity and lumen opening. Nature Communications 7.

Kloecker, G.H., Rabinowits, G., Gercel-Taylor, C., Day, J.M., Taylor, D.D., 2008. Exosomal microRNA: A Diagnostic Marker for Lung Cancer. Clinical Lung Cancer 9, 295.

Klotzsch, E., Smith, M.L., Kubow, K.E., Muntwyler, S., Little, W.C., Beyeler, F., Gourdon, D., Nelson, B.J., Vogel, V., 2009. Fibronectin forms the most extensible biological fibers displaying switchable force-exposed cryptic binding sites. Proceedings of the National Academy of Sciences 106, 18267–18272.

Koga, T., Hashimoto, S., Sugio, K., Yoshino, I., Nakagawa, K., Yonemitsu, Y., Sugimachi, K., Sueishi, K., 2001. Heterogeneous distribution of P53 immunoreactivity in human lung adenocarcinoma correlates with MDM2 protein expression, rather than with P53 gene mutation. International Journal of Cancer 95, 232–239.

Koles, K., Budnik, V., 2012. Exosomes go with the Wnt. Cellular Logistics 2, 169–173.

Koles, K., Nunnari, J., Korkut, C., Barria, R., Brewer, C., Li, Y., Leszyk, J., Zhang, B., Budnik, V., 2012. Mechanism of Evenness Interrupted (Evi)-Exosome Release at Synaptic Boutons. J. Biol. Chem. 287, 16820–16834.

Kwon, S.-H., Liu, K.D., Mostov, K.E., 2014. Intercellular Transfer of GPRC5B via Exosomes Drives HGF-Mediated Outward Growth. Current Biology 24, 199–204.

Labernadie, A., Kato, T., Brugués, A., Serra-Picamal, X., Derzsi, S., Arwert, E., Weston, A., González-Tarragó, V., Elosegui-Artola, A., Albertazzi, L., Alcaraz, J., Roca-Cusachs, P., Sahai, E., Trepat, X., 2017. A mechanically active heterotypic E-cadherin/N-cadherin adhesion enables fibroblasts to drive cancer cell invasion. Nat Cell Biol 19, 224–237.

Lancaster, G.I., Febbraio, M.A., 2005. Exosome-dependent Trafficking of HSP70: A NOVEL SECRETORY PATHWAY FOR CELLULAR STRESS PROTEINS. J. Biol. Chem. 280, 23349–23355.

Lang, G.A., Iwakuma, T., Suh, Y.-A., Liu, G., Rao, V.A., Parant, J.M., Valentin-Vega, Y.A., Terzian, T., Caldwell, L.C., Strong, L.C., El-Naggar, A.K., Lozano, G., 2004. Gain of Function of a p53 Hot Spot Mutation in a Mouse Model of Li-Fraumeni Syndrome. Cell 119, 861–872.

Lauwers, E., Wang, Y.-C., Gallardo, R., Van der Kant, R., Michiels, E., Swerts, J., Baatsen, P., Zaiter, S.S., McAlpine, S.R., Gounko, N.V., Rousseau, F., Schymkowitz, J., Verstreken, P., 2018. Hsp90 Mediates Membrane Deformation and Exosome Release. Molecular Cell 71, 689-702.e9.

Leach, J., Morton, J.P., Sansom, O.J., 2019. Neutrophils: Homing in on the myeloid mechanisms of metastasis. Molecular Immunology 110, 69–76.

LeBleu, V.S., Kalluri, R., 2018. A peek into cancer-associated fibroblasts: origins, functions and translational impact. Dis. Model. Mech. 11, dmm029447.

Lespagnol, A., Duflaut, D., Beekman, C., Blanc, L., Fiucci, G., Marine, J.-C., Vidal, M., Amson, R., Telerman, A., 2008. Exosome secretion, including the DNA damage-induced p53-dependent secretory pathway, is severely compromised in TSAP6/Steap3-null mice. Cell Death Differ 15, 1723–1733.

Levental, K.R., Yu, H., Kass, L., Lakins, J.N., Egeblad, M., Erler, J.T., Fong, S.F.T., Csiszar, K., Giaccia, A., Weninger, W., Yamauchi, M., Gasser, D.L., Weaver, V.M., 2009. Matrix Crosslinking Forces Tumor Progression by Enhancing Integrin Signaling. Cell 139, 891–906.

Levine, A.J., Oren, M., 2009. The first 30 years of p53: growing ever more complex. Nat Rev Cancer 9, 749–758.

Li, B., Antonyak, M.A., Zhang, J., Cerione, R.A., 2012. RhoA triggers a specific signaling pathway that generates transforming microvesicles in cancer cells. Oncogene 31, 4740–4749.

Li, D., Yallowitz, A., Ozog, L., Marchenko, N., 2014. A gain-of-function mutant p53–HSF1 feed forward circuit governs adaptation of cancer cells to proteotoxic stress. Cell Death Dis 5, e1194–e1194.

Li, I., Nabet, B.Y., 2019. Exosomes in the tumor microenvironment as mediators of cancer therapy resistance. Mol Cancer 18, 32.

Lin, D.-C., Hao, J.-J., Nagata, Y., Xu, L., Shang, L., Meng, X., Sato, Y., Okuno, Y., Varela, A.M., Ding, L.-W., Garg, M., Liu, L.-Z., Yang, H., Yin, D., Shi, Z.-Z., Jiang, Y.-Y., Gu, W.-Y., Gong, T., Zhang, Y., Xu, X., Kalid, O., Shacham, S., Ogawa, S., Wang, M.-R., Koeffler, H.P., 2014. Genomic and molecular characterization of esophageal squamous cell carcinoma. Nat Genet 46, 467–473.

Liu, K., Ling, S., Lin, W.-C., 2011. TopBP1 Mediates Mutant p53 Gain of Function through NF-Y and p63/p73. Molecular and Cellular Biology 31, 4464–4481.

Liu, Y., Gu, Y., Han, Y., Zhang, Q., Jiang, Z., Zhang, X., Huang, B., Xu, X., Zheng, J., Cao, X., 2016. Tumor Exosomal RNAs Promote Lung Pre-metastatic Niche Formation by Activating Alveolar Epithelial TLR3 to Recruit Neutrophils. Cancer Cell 30, 243–256.

Mackay, H.L., Moore, D., Hall, C., Birkbak, N.J., Jamal-Hanjani, M., Karim, S.A., Phatak, V.M., Piñon, L., Morton, J.P., Swanton, C., Le Quesne, J., Muller, P.A.J., 2018. Genomic instability in mutant p53 cancer cells upon entotic engulfment. Nature Communications 9.

Malkin, D., Li, F.P., Strong, L.C., Fraumeni, J.F., Nelson, C.E., Kim, D.H., Kassel, J., Gryka, M.A., Bischoff, F.Z., Tainsky, M.A., Et, A., 1990. Germ line p53 mutations in a familial syndrome of breast cancer, sarcomas, and other neoplasms. Science 250, 1233–1238.

Mantovani, F., Collavin, L., Del Sal, G., 2019. Mutant p53 as a guardian of the cancer cell. Cell Death Differ 26, 199–212.

Margolis, L., Sadovsky, Y., 2019. The biology of extracellular vesicles: The known unknowns. PLoS Biol 17, e3000363.

Mathieu, M., Martin-Jaular, L., Lavieu, G., Théry, C., 2019. Specificities of secretion and uptake of exosomes and other extracellular vesicles for cell-to-cell communication. Nat Cell Biol 21, 9–17.

Matsumoto, A., Takahashi, Y., Nishikawa, M., Sano, K., Morishita, M., Charoenviriyakul, C., Saji, H., Takakura, Y., 2017. Accelerated growth of B16BL6 tumor in mice through efficient uptake of their own exosomes by B16BL6 cells. Cancer Sci. 108, 1803–1810.

Mayle, K.M., Le, A.M., Kamei, D.T., 2012. The intracellular trafficking pathway of transferrin. Biochimica et Biophysica Acta (BBA) - General Subjects 1820, 264–281.

Messenger, S.W., Woo, S.S., Sun, Z., Martin, T.F.J., 2018. A Ca2+-stimulated exosome release pathway in cancer cells is regulated by Munc13-4. J Cell Biol 217, 2877–2890.

Midgley, A.C., Rogers, M., Hallett, M.B., Clayton, A., Bowen, T., Phillips, A.O., Steadman, R., 2013. Transforming Growth Factor-β1 (TGF-β1)-stimulated Fibroblast to Myofibroblast Differentiation Is Mediated by Hyaluronan (HA)-facilitated Epidermal Growth Factor Receptor (EGFR) and CD44 Co-localization in Lipid Rafts. J. Biol. Chem. 288, 14824–14838.

Midgley, C.A., Lane, D.P., 1997. p53 protein stability in tumour cells is not determined by mutation but is dependent on Mdm2 binding. Oncogene 15, 1179–1189.

Miller, B.W., Morton, J.P., Pinese, M., Saturno, G., Jamieson, N.B., McGhee, E., Timpson, P., Leach, J., McGarry, L., Shanks, E., Bailey, P., Chang, D., Oien, K., Karim, S., Au, A., Steele, C., Carter, C.R., McKay, C., Anderson, K., Evans, T.R.J., Marais, R., Springer, C., Biankin, A., Erler, J.T., Sansom, O.J., 2015. Targeting the LOX / HYPOXIA axis reverses many of the features that make pancreatic cancer deadly: inhibition of LOX abrogates metastasis and enhances drug efficacy. EMBO Mol Med 7, 1063–1076.

Minciacchi, V.R., Freeman, M.R., Di Vizio, D., 2015. Extracellular Vesicles in Cancer: Exosomes, Microvesicles and the Emerging Role of Large Oncosomes. Seminars in Cell & Developmental Biology 40, 41–51.

Mohanaiah, P., Sathyanarayana, P., GuruKumar, L., 2013. Image Texture Feature Extraction Using GLCM Approach 3, 5.

Morelli, A.E., 2004. Endocytosis, intracellular sorting, and processing of exosomes by dendritic cells. Blood 104, 3257–3266.

Morton, J.P., Timpson, P., Karim, S.A., Ridgway, R.A., Athineos, D., Doyle, B., Jamieson, N.B., Oien, K.A., Lowy, A.M., Brunton, V.G., Frame, M.C., Evans, T.R.J., Sansom, O.J., 2010. Mutant p53 drives metastasis and overcomes growth arrest/senescence in pancreatic cancer. Proceedings of the National Academy of Sciences 107, 246–251.

Mouw, J.K., Ou, G., Weaver, V.M., 2014. Extracellular matrix assembly: a multiscale deconstruction. Nat Rev Mol Cell Biol 15, 771–785.

Mrozowska, P.S., Fukuda, M., 2016. Regulation of podocalyxin trafficking by Rab small GTPases in 2D and 3D epithelial cell cultures. J Cell Biol 213, 355–369.

Muller, P.A.J., Caswell, P.T., Doyle, B., Iwanicki, M.P., Tan, E.H., Karim, S., Lukashchuk, N., Gillespie, D.A., Ludwig, R.L., Gosselin, P., Cromer, A., Brugge, J.S., Sansom, O.J., Norman, J.C., Vousden, K.H., 2009. Mutant p53 Drives Invasion by Promoting Integrin Recycling. Cell 139, 1327–1341.

Muller, P.A.J., Trinidad, A.G., Caswell, P.T., Norman, J.C., Vousden, K.H., 2014. Mutant p53 Regulates Dicer through p63-dependent and -independent Mechanisms to Promote an Invasive Phenotype. J. Biol. Chem. 289, 122–132.

Muller, P.A.J., Trinidad, A.G., Timpson, P., Morton, J.P., Zanivan, S., van den Berghe, P.V.E., Nixon, C., Karim, S.A., Caswell, P.T., Noll, J.E., Coffill, C.R., Lane, D.P., Sansom, O.J., Neilsen, P.M., Norman, J.C., Vousden, K.H., 2013. Mutant p53 enhances MET trafficking and signalling to drive cell scattering and invasion. Oncogene 32, 1252–1265.

Munir, R., Lisec, J., Swinnen, J.V., Zaidi, N., 2019. Lipid metabolism in cancer cells under metabolic stress. Br J Cancer 120, 1090–1098.

Muralidharan-Chari, V., Clancy, J., Plou, C., Romao, M., Chavrier, P., Raposo, G., D'Souza-Schorey, C., 2009. ARF6-regulated shedding of tumor cell-derived plasma membrane microvesicles. Curr. Biol. 19, 1875–1885.

Nabhan, J.F., Hu, R., Oh, R.S., Cohen, S.N., Lu, Q., 2012. Formation and release of arrestin domain-containing protein 1-mediated microvesicles (ARMMs) at plasma membrane by recruitment of TSG101 protein. Proceedings of the National Academy of Sciences 109, 4146–4151.

Nazarenko, I., Rana, S., Baumann, A., McAlear, J., Hellwig, A., Trendelenburg, M., Lochnit, G., Preissner, K.T., Zoller, M., 2010. Cell Surface Tetraspanin Tspan8 Contributes to Molecular Pathways of Exosome-Induced Endothelial Cell Activation. Cancer Research 70, 1668–1678.

Neri, S., Miyashita, T., Hashimoto, H., Suda, Y., Ishibashi, M., Kii, H., Watanabe, H., Kuwata, T., Tsuboi, M., Goto, K., Menju, T., Sonobe, M., Date, H., Ochiai, A., Ishii, G., 2017. Fibroblast-led cancer cell invasion is activated by epithelial–mesenchymal transition through platelet-derived growth factor BB secretion of lung adenocarcinoma. Cancer Letters 395, 20–30.

Neuzillet, C., Tijeras-Raballand, A., Ragulan, C., Cros, J., Patil, Y., Martinet, M., Erkan, M., Kleeff, J., Wilson, J., Apte, M., Tosolini, M., Wilson, A.S., Delvecchio, F.R., Bousquet, C., Paradis, V., Hammel, P., Sadanandam, A., Kocher, H.M., 2019. Inter- and intra-tumoural heterogeneity in cancer-associated fibroblasts of human pancreatic ductal adenocarcinoma. J. Pathol. 248, 51–65.

O'Brien, K., Rani, S., Corcoran, C., Wallace, R., Hughes, L., Friel, A.M., McDonnell, S., Crown, J., Radomski, M.W., O'Driscoll, L., 2013. Exosomes from triple-negative breast cancer cells can transfer phenotypic traits representing their cells of origin to secondary cells. European Journal of Cancer 49, 1845–1859.

Olive, K.P., Tuveson, D.A., Ruhe, Z.C., Yin, B., Willis, N.A., Bronson, R.T., Crowley, D., Jacks, T., 2004. Mutant p53 Gain of Function in Two Mouse Models of Li-Fraumeni Syndrome. Cell 119, 847–860.

Olivier, M., Hollstein, M., Hainaut, P., 2010. TP53 Mutations in Human Cancers: Origins, Consequences, and Clinical Use. Cold Spring Harbor Perspectives in Biology 2, a001008–a001008.

O'Reilly, P.J., Ding, Q., Akthar, S., Cai, G., Genschmer, K.R., Patel, D.F., Jackson, P.L., Viera, L., Roda, M., Locy, M.L., Bernstein, E.A., Lloyd, C.M., Bernstein, K.E., Snelgrove, R.J., Blalock, J.E., 2017. Angiotensin-converting enzyme defines matrikine-regulated inflammation and fibrosis. JCI Insight 2, e91923.

Orgel, J.P.R.O., Irving, T.C., Miller, A., Wess, T.J., 2006. Microfibrillar structure of type I collagen in situ. Proceedings of the National Academy of Sciences 103, 9001–9005.

Oria, R., Wiegand, T., Escribano, J., Elosegui-Artola, A., Uriarte, J.J., Moreno-Pulido, C., Platzman, I., Delcanale, P., Albertazzi, L., Navajas, D., Trepat, X., García-Aznar, J.M., Cavalcanti-Adam, E.A., Roca-Cusachs, P., 2017. Force loading explains spatial sensing of ligands by cells. Nature 552, 219–224.

Ostrowski, M., Carmo, N.B., Krumeich, S., Fanget, I., Raposo, G., Savina, A., Moita, C.F., Schauer, K., Hume, A.N., Freitas, R.P., Goud, B., Benaroch, P., Hacohen, N., Fukuda, M., Desnos, C., Seabra, M.C., Darchen, F., Amigorena, S., Moita, L.F., Thery, C., 2010. Rab27a and Rab27b control different steps of the exosome secretion pathway. Nat Cell Biol 12, 19–30.

Özdemir, B.C., Pentcheva-Hoang, T., Carstens, J.L., Zheng, X., Wu, C.-C., Simpson, T.R., Laklai, H., Sugimoto, H., Kahlert, C., Novitskiy, S.V., De Jesus-Acosta, A., Sharma, P., Heidari, P., Mahmood, U., Chin, L., Moses, H.L., Weaver, V.M., Maitra, A., Allison, J.P., LeBleu, V.S., Kalluri, R., 2014. Depletion of Carcinoma-Associated Fibroblasts and Fibrosis Induces Immunosuppression and Accelerates Pancreas Cancer with Reduced Survival. Cancer Cell 25, 719–734.

Park, J., Wysocki, R.W., Amoozgar, Z., Maiorino, L., Fein, M.R., Jorns, J., Schott, A.F., Kinugasa-Katayama, Y., Lee, Y., Won, N.H., Nakasone, E.S., Hearn, S.A., Kuttner, V., Qiu, J., Almeida, A.S., Perurena, N., Kessenbrock, K., Goldberg, M.S., Egeblad, M., 2016. Cancer cells induce metastasis-supporting neutrophil extracellular DNA traps. Science Translational Medicine 8, 361ra138-361ra138.

Paul, N.R., Allen, J.L., Chapman, A., Morlan-Mairal, M., Zindy, E., Jacquemet, G., Fernandez del Ama, L., Ferizovic, N., Green, D.M., Howe, J.D., Ehler, E., Hurlstone, A., Caswell, P.T., 2015. α5β1 integrin recycling promotes Arp2/3-independent cancer cell invasion via the formin FHOD3. J Cell Biol 210, 1013–1031.

Pearce, O.M.T., Delaine-Smith, R.M., Maniati, E., Nichols, S., Wang, J., Böhm, S., Rajeeve, V., Ullah, D., Chakravarty, P., Jones, R.R., Montfort, A., Dowe, T., Gribben, J., Jones, J.L., Kocher, H.M., Serody, J.S., Vincent, B.G., Connelly, J., Brenton, J.D., Chelala, C., Cutillas, P.R., Lockley, M., Bessant, C., Knight, M.M., Balkwill, F.R., 2018. Deconstruction of a Metastatic Tumor Microenvironment Reveals a Common Matrix Response in Human Cancers. Cancer Discov 8, 304–319.

Peinado, H., Alečković, M., Lavotshkin, S., Matei, I., Costa-Silva, B., Moreno-Bueno, G., Hergueta-Redondo, M., Williams, C., García-Santos, G., Ghajar, C.M., Nitadori-Hoshino, A., Hoffman, C., Badal, K., Garcia, B.A., Callahan, M.K., Yuan, J., Martins, V.R., Skog, J., Kaplan, R.N., Brady, M.S., Wolchok, J.D., Chapman, P.B., Kang, Y., Bromberg, J., Lyden, D., 2012. Melanoma exosomes educate bone marrow progenitor cells toward a pro-metastatic phenotype through MET. Nat Med 18, 883–891.

Peinado, H., Zhang, H., Matei, I.R., Costa-Silva, B., Hoshino, A., Rodrigues, G., Psaila, B., Kaplan, R.N., Bromberg, J.F., Kang, Y., Bissell, M.J., Cox, T.R., Giaccia, A.J., Erler, J.T., Hiratsuka, S., Ghajar, C.M., Lyden, D., 2017. Pre-metastatic niches: organ-specific homes for metastases. Nat Rev Cancer 17, 302–317.

Peng, Y., Chen, L., Li, C., Lu, W., Chen, J., 2001. Inhibition of MDM2 by hsp90 Contributes to Mutant p53 Stabilization. J. Biol. Chem. 276, 40583–40590.

Petitjean, A, Achatz, M.I.W., Borresen-Dale, A.L., Hainaut, P., Olivier, M., 2007. TP53 mutations in human cancers: functional selection and impact on cancer prognosis and outcomes. Oncogene 26, 2157–2165.

Petitjean, Audrey, Mathe, E., Kato, S., Ishioka, C., Tavtigian, S.V., Hainaut, P., Olivier, M., 2007. Impact of mutant p53 functional properties on *TP53* mutation patterns and tumor phenotype: lessons from recent developments in the IARC TP53 database. Hum. Mutat. 28, 622–629.

Plebanek, M.P., Angeloni, N.L., Vinokour, E., Li, J., Henkin, A., Martinez-Marin, D., Filleur, S., Bhowmick, R., Henkin, J., Miller, S.D., Ifergan, I., Lee, Y., Osman, I., Thaxton, C.S., Volpert, O.V., 2017. Pre-metastatic cancer exosomes induce immune surveillance by patrolling monocytes at the metastatic niche. Nat Commun 8, 1319.

Poggi, A., Musso, A., Dapino, I., Zocchi, M.R., 2014. Mechanisms of tumor escape from immune system: Role of mesenchymal stromal cells. Immunology Letters 159, 55–72.

Pollet, H., Conrard, L., Cloos, A.-S., Tyteca, D., 2018. Plasma Membrane Lipid Domains as Platforms for Vesicle Biogenesis and Shedding? Biomolecules 8, 94.

Polotskaia, A., Xiao, G., Reynoso, K., Martin, C., Qiu, W.-G., Hendrickson, R.C., Bargonetti, J., 2015. Proteome-wide analysis of mutant p53 targets in breast cancer

identifies new levels of gain-of-function that influence PARP, PCNA, and MCM4. Proc Natl Acad Sci USA 112, E1220–E1229.

Principe, D.R., DeCant, B., Mascarinas, E., Wayne, E.A., Diaz, A.M., Akagi, N., Hwang, R., Pasche, B., Dawson, D.W., Fang, D., Bentrem, D.J., Munshi, H.G., Jung, B., Grippo, P.J., 2016. TGF Signaling in the Pancreatic Tumor Microenvironment Promotes Fibrosis and Immune Evasion to Facilitate Tumorigenesis. Cancer Research 76, 2525–2539.

Proux-Gillardeaux, V., Raposo, G., Irinopoulou, T., Galli, T., 2007. Expression of the Longin domain of TI-VAMP impairs lysosomal secretion and epithelial cell migration. Biology of the Cell 99, 261–271.

Purushothaman, A., Bandari, S.K., Liu, J., Mobley, J.A., Brown, E.E., Sanderson, R.D., 2016. Fibronectin on the Surface of Myeloma Cell-derived Exosomes Mediates Exosome-Cell Interactions. J. Biol. Chem. 291, 1652–1663.

Qian, B.-Z., Li, J., Zhang, H., Kitamura, T., Zhang, J., Campion, L.R., Kaiser, E.A., Snyder, L.A., Pollard, J.W., 2011. CCL2 recruits inflammatory monocytes to facilitate breast-tumour metastasis. Nature 475, 222–225.

Rahman, M.A., Barger, J.F., Lovat, F., Gao, M., Otterson, G.A., Nana-Sinkam, P., 2016. Lung cancer exosomes as drivers of epithelial mesenchymal transition. Oncotarget 7.

Rainero, E., Caswell, P.T., Muller, P.A.J., Grindlay, J., McCaffrey, M.W., Zhang, Q., Wakelam, M.J.O., Vousden, K.H., Graziani, A., Norman, J.C., 2012. Diacylglycerol kinase α controls RCP-dependent integrin trafficking to promote invasive migration. J Cell Biol 196, 277–295.

Rajagopal, C., Harikumar, K.B., 2018. The Origin and Functions of Exosomes in Cancer. Front. Oncol. 8, 66.

Rajkumar, V.S., Shiwen, X., Bostrom, M., Leoni, P., Muddle, J., Ivarsson, M., Gerdin, B., Denton, C.P., Bou-Gharios, G., Black, C.M., Abraham, D.J., 2006. Platelet-Derived Growth Factor-β Receptor Activation Is Essential for Fibroblast and Pericyte Recruitment during Cutaneous Wound Healing. The American Journal of Pathology 169, 2254–2265.

Rath, N., Morton, J.P., Julian, L., Helbig, L., Kadir, S., McGhee, E.J., Anderson, K.I., Kalna, G., Mullin, M., Pinho, A.V., Rooman, I., Samuel, M.S., Olson, M.F., 2017. ROCK signaling promotes collagen remodeling to facilitate invasive pancreatic ductal adenocarcinoma tumor cell growth. EMBO Mol Med. 9, 198–218.

Resnick, M.A., Inga, A., 2003. Functional mutants of the sequence-specific transcription factor p53 and implications for master genes of diversity. PNAS 100, 9934–9939.

Ringuette Goulet, C., Bernard, G., Tremblay, S., Chabaud, S., Bolduc, S., Pouliot, F., 2018. Exosomes Induce Fibroblast Differentiation into Cancer-Associated Fibroblasts through TGFβ Signaling. Mol Cancer Res 16, 1196–1204.

Rippin, T.M., Bykov, V.J.N., Freund, S.M.V., Selivanova, G., Wiman, K.G., Fersht, A.R., 2002. Characterization of the p53-rescue drug CP-31398 in vitro and in living cells. Oncogene 21, 2119–2129.

Roca-Cusachs, P., Gauthier, N.C., del Rio, A., Sheetz, M.P., 2009. Clustering of 5 1 integrins determines adhesion strength whereas v 3 and talin enable mechanotransduction. Proceedings of the National Academy of Sciences 106, 16245–16250.

Rodrigues, N.R., Rowan, A., Smith, M.E., Kerr, I.B., Bodmer, W.F., Gannon, J.V., Lane, D.P., 1990. p53 mutations in colorectal cancer. Proceedings of the National Academy of Sciences 87, 7555–7559.

Rønnov-Jessen, L., Petersen, O.W., Koteliansky, V.E., Bissell, M.J., 1995. The origin of the myofibroblasts in breast cancer. Recapitulation of tumor environment in culture unravels diversity and implicates converted fibroblasts and recruited smooth muscle cells. J. Clin. Invest. 95, 859–873.

Royo, F., Cossío, U., Ruiz de Angulo, A., Llop, J., Falcon-Perez, J.M., 2019. Modification of the glycosylation of extracellular vesicles alters their biodistribution in mice. Nanoscale 11, 1531–1537.

Sablina, A.A., Budanov, A.V., Ilyinskaya, G.V., Agapova, L.S., Kravchenko, J.E., Chumakov, P.M., 2005. The antioxidant function of the p53 tumor suppressor. Nat Med 11, 1306–1313.

Sanz-Moreno, V., Gaggioli, C., Yeo, M., Albrengues, J., Wallberg, F., Viros, A., Hooper, S., Mitter, R., Féral, C.C., Cook, M., Larkin, J., Marais, R., Meneguzzi, G., Sahai, E., Marshall, C.J., 2011. ROCK and JAK1 Signaling Cooperate to Control Actomyosin Contractility in Tumor Cells and Stroma. Cancer Cell 20, 229–245.

Saukkonen, K., Hagström, J., Mustonen, H., Juuti, A., Nordling, S., Fermér, C., Nilsson, O., Seppänen, H., Haglund, C., 2015. Podocalyxin Is a Marker of Poor Prognosis in Pancreatic Ductal Adenocarcinoma. PLoS ONE 10, e0129012.

Scaffidi, A.K., Mutsaers, S.E., Moodley, Y.P., McAnulty, R.J., Laurent, G.J., Thompson, P.J., Knight, D.A., 2002. Oncostatin M stimulates proliferation, induces collagen production and inhibits apoptosis of human lung fibroblasts. British Journal of Pharmacology 136, 793–801.

Schegg, B., Hulsmeier, A.J., Rutschmann, C., Maag, C., Hennet, T., 2009. Core Glycosylation of Collagen Is Initiated by Two (1-O)Galactosyltransferases. Molecular and Cellular Biology 29, 943–952.

Schlienger, S., Campbell, S., Claing, A., 2014. ARF1 regulates the Rho/MLC pathway to control EGF-dependent breast cancer cell invasion. Mol. Biol. Cell 25, 17–29.

Schofield, H.K., Zeller, J., Espinoza, C., Halbrook, C.J., Vecchio, A. del, Magnuson, B., Fabo, T., Daylan, A.E.C., Kovalenko, I., Lee, H.-J., Yan, W., Feng, Y., Karim, S.A., Kremer, D.M., Kumar-Sinha, C., Lyssiotis, C.A., Ljungman, M., Morton, J.P., Galbán, S., Fearon, E.R., Magliano, M.P. di, 2018. Mutant p53R270H drives altered metabolism and increased invasion in pancreatic ductal adenocarcinoma [WWW Document]. URL https://insight.jci.org/articles/view/97422/pdf (accessed 7.20.19).

Schwarzbauer, J.E., DeSimone, D.W., 2011. Fibronectins, Their Fibrillogenesis, and In Vivo Functions. Cold Spring Harb Perspect Biol 3, a005041.

Shalem, O., Sanjana, N.E., Hartenian, E., Shi, X., Scott, D.A., Mikkelsen, T.S., Heckl, D., Ebert, B.L., Root, D.E., Doench, J.G., Zhang, F., 2014. Genome-Scale CRISPR-Cas9 Knockout Screening in Human Cells. Science 343, 84–87.

Sharma, R., Huang, X., Brekken, R.A., Schroit, A.J., 2017. Detection of phosphatidylserine-positive exosomes for the diagnosis of early-stage malignancies. Br J Cancer 117, 545–552.

Shi, F., Sottile, J., 2008. Caveolin-1-dependent β1 integrin endocytosis is a critical regulator of fibronectin turnover. J Cell Sci 121, 2360–2371.

Skog, J., Würdinger, T., van Rijn, S., Meijer, D.H., Gainche, L., Curry, W.T., Carter, B.S., Krichevsky, A.M., Breakefield, X.O., 2008. Glioblastoma microvesicles transport RNA and proteins that promote tumour growth and provide diagnostic biomarkers. Nat Cell Biol 10, 1470–1476.

Skotland, T., Sandvig, K., Llorente, A., 2017. Lipids in exosomes: Current knowledge and the way forward. Progress in Lipid Research 66, 30–41.

Snyder, K.A., Hughes, M.R., Hedberg, B., Brandon, J., Hernaez, D.C., Bergqvist, P., Cruz, F., Po, K., Graves, M.L., Turvey, M.E., Nielsen, J.S., Wilkins, J.A., McColl, S.R., Babcook, J.S., Roskelley, C.D., McNagny, K.M., 2015. Podocalyxin enhances breast tumor growth and metastasis and is a target for monoclonal antibody therapy. Breast Cancer Res 17, 46.

Soldevilla, B., Rodríguez, M., San Millán, C., García, V., Fernández-Periañez, R., Gil-Calderón, B., Martín, P., García-Grande, A., Silva, J., Bonilla, F., Domínguez, G., 2014. Tumor-derived exosomes are enriched in ΔNp73, which promotes oncogenic

potential in acceptor cells and correlates with patient survival. Human Molecular Genetics 23, 467–478.

Song, H., Hollstein, M., Xu, Y., 2007. p53 gain-of-function cancer mutants induce genetic instability by inactivating ATM. Nat Cell Biol 9, 573–580.

Sorrentino, G., Ruggeri, N., Specchia, V., Cordenonsi, M., Mano, M., Dupont, S., Manfrin, A., Ingallina, E., Sommaggio, R., Piazza, S., Rosato, A., Piccolo, S., Del Sal, G., 2014. Metabolic control of YAP and TAZ by the mevalonate pathway. Nat Cell Biol 16, 357–366.

Sottile, J., Chandler, J., 2005. Fibronectin Matrix Turnover Occurs through a Caveolin-1–dependent Process. Mol Biol Cell 16, 757–768.

Sottile, J., Hocking, D.C., 2002. Fibronectin Polymerization Regulates the Composition and Stability of Extracellular Matrix Fibrils and Cell-Matrix Adhesions. Mol Biol Cell 13, 3546–3559.

Stambolsky, P., Tabach, Y., Fontemaggi, G., Weisz, L., Maor-Aloni, R., Sigfried, Z., Shiff, I., Kogan, I., Shay, M., Kalo, E., Blandino, G., Simon, I., Oren, M., Rotter, V., 2010. Modulation of the Vitamin D3 Response by Cancer-Associated Mutant p53. Cancer Cell 17, 273–285.

Stanhope-Baker, P., Kessler, P.M., Li, W., Agarwal, M.L., Williams, B.R.G., 2004. The Wilms Tumor Suppressor-1 Target Gene Podocalyxin Is Transcriptionally Repressed by p53. J. Biol. Chem. 279, 33575–33585.

Strano, S., Fontemaggi, G., Costanzo, A., Rizzo, M.G., Monti, O., Baccarini, A., Del Sal, G., Levrero, M., Sacchi, A., Oren, M., Blandino, G., 2002. Physical Interaction with Human Tumor-derived p53 Mutants Inhibits p63 Activities. J. Biol. Chem. 277, 18817–18826.

Su, X., Chakravarti, D., Cho, M.S., Liu, L., Gi, Y.J., Lin, Y.-L., Leung, M.L., El-Naggar, A., Creighton, C.J., Suraokar, M.B., Wistuba, I., Flores, E.R., 2010. TAp63 suppresses metastasis through coordinate regulation of Dicer and miRNAs. Nature 467, 986–990.

Sullivan, K.D., Galbraith, M.D., Andrysik, Z., Espinosa, J.M., 2018. Mechanisms of transcriptional regulation by p53. Cell Death Differ. 25, 133–143.

Sun, B., Zhou, Y., Fang, Y., Li, Z., Gu, X., Xiang, J., 2019. Colorectal cancer exosomes induce lymphatic network remodeling in lymph nodes. Int. J. Cancer 145, 1648–1659.

Tang, D., Gao, J., Wang, S., Ye, N., Chong, Y., Huang, Y., Wang, J., Li, B., Yin, W., Wang, D., 2016. Cancer-associated fibroblasts promote angiogenesis in gastric cancer through galectin-1 expression. Tumor Biol. 37, 1889–1899.

Tang, Y.-T., Huang, Y.-Y., Li, J.-H., Qin, S.-H., Xu, Y., An, T.-X., Liu, C.-C., Wang, Q., Zheng, L., 2018. Alterations in exosomal miRNA profile upon epithelial-mesenchymal transition in human lung cancer cell lines. BMC Genomics 19, 802.

Teichgräber, V., Monasterio, C., Chaitanya, K., Boger, R., Gordon, K., Dieterle, T., Jäger, D., Bauer, S., 2015. Specific inhibition of fibroblast activation protein (FAP)-alpha prevents tumor progression in vitro. Adv Med Sci 60, 264–272.

Terakawa, T., Kenzaki, H., Takada, S., 2012. p53 Searches on DNA by Rotation-Uncoupled Sliding at C-Terminal Tails and Restricted Hopping of Core Domains. J. Am. Chem. Soc. 134, 14555–14562.

Terzian, T., Suh, Y.-A., Iwakuma, T., Post, S.M., Neumann, M., Lang, G.A., Pelt, C.S.V., Lozano, G., 2008. The inherent instability of mutant p53 is alleviated by Mdm2 or p16INK4a loss. Genes Dev. 22, 1337–1344.

Testa, J.S., Apcher, G.S., Comber, J.D., Eisenlohr, L.C., 2010. Exosome-Driven Antigen Transfer for MHC Class II Presentation Facilitated by the Receptor Binding Activity of Influenza Hemagglutinin. The Journal of Immunology 185, 6608–6616.

Tian, T., Zhu, Y.-L., Zhou, Y.-Y., Liang, G.-F., Wang, Y.-Y., Hu, F.-H., Xiao, Z.-D., 2014. Exosome Uptake through Clathrin-mediated Endocytosis and Macropinocytosis and Mediating miR-21 Delivery. J. Biol. Chem. 289, 22258–22267.

Timpson, P., Mcghee, E.J., Erami, Z., Nobis, M., Quinn, J.A., Edward, M., Anderson, K.I., 2011a. Organotypic Collagen I Assay: A Malleable Platform to Assess Cell Behaviour in a 3-Dimensional Context. J Vis Exp.

Timpson, P., McGhee, E.J., Morton, J.P., Kriegsheim, A. von, Schwarz, J.P., Karim, S.A., Doyle, B., Quinn, J.A., Carragher, N.O., Edward, M., Olson, M.F., Frame, M.C., Brunton, V.G., Sansom, O.J., Anderson, K.I., 2011b. Spatial Regulation of RhoA Activity during Pancreatic Cancer Cell Invasion Driven by Mutant p53. Cancer Res 71, 747–757.

Tocci, P., Cianfrocca, R., Di Castro, V., Rosanò, L., Sacconi, A., Donzelli, S., Bonfiglio, S., Bucci, G., Vizza, E., Ferrandina, G., Scambia, G., Tonon, G., Blandino, G., Bagnato, A., 2019. β-arrestin1/YAP/mutant p53 complexes orchestrate the endothelin A receptor signaling in high-grade serous ovarian cancer. Nat Commun 10, 3196.

Toledo, F., Lee, C.J., Krummel, K.A., Rodewald, L.-W., Liu, C.-W., Wahl, G.M., 2007. Mouse Mutants Reveal that Putative Protein Interaction Sites in the p53 Proline-Rich Domain Are Dispensable for Tumor Suppression. Molecular and Cellular Biology 27, 1425–1432.

Tommelein, J., Verset, L., Boterberg, T., Demetter, P., Bracke, M., De Wever, O., 2015. Cancer-Associated Fibroblasts Connect Metastasis-Promoting Communication in Colorectal Cancer. Front. Oncol. 5.

Trajkovic, K., Hsu, C., Chiantia, S., Rajendran, L., Wenzel, D., Wieland, F., Schwille, P., Brügger, B., Simons, M., 2008. Ceramide Triggers Budding of Exosome Vesicles into Multivesicular Endosomes. Science 319, 1244–1247.

Treps, L., Perret, R., Edmond, S., Ricard, D., Gavard, J., 2017. Glioblastoma stem-like cells secrete the pro-angiogenic VEGF-A factor in extracellular vesicles. Journal of Extracellular Vesicles 6, 1359479.

Vader, P., Breakefield, X.O., Wood, M.J.A., 2014. Extracellular vesicles: emerging targets for cancer therapy. Trends in Molecular Medicine 20, 385–393.

Valenti, F., Fausti, F., Biagioni, F., Shay, T., Fontemaggi, G., Domany, E., Yaffe, M.B., Strano, S., Blandino, G., Di Agostino, S., 2011. Mutant p53 oncogenic functions are sustained by Plk2 kinase through an autoregulatory feedback loop. Cell Cycle 10, 4330–4340.

van Niel, G., D'Angelo, G., Raposo, G., 2018. Shedding light on the cell biology of extracellular vesicles. Nat Rev Mol Cell Biol 19, 213–228.

Varadaraj, A., Jenkins, L.M., Singh, P., Chanda, A., Snider, J., Lee, N.Y., Amsalem-Zafran, A.R., Ehrlich, M., Henis, Y.I., Mythreye, K., 2017. TGF-β triggers rapid fibrillogenesis via a novel TβRII-dependent fibronectin-trafficking mechanism. MBoC 28, 1195–1207.

Vennin, C., Australian Pancreatic Genome Initiative (APGI), Mélénec, P., Rouet, R., Nobis, M., Cazet, A.S., Murphy, K.J., Herrmann, D., Reed, D.A., Lucas, M.C., Warren, S.C., Elgundi, Z., Pinese, M., Kalna, G., Roden, D., Samuel, M., Zaratzian, A., Grey, S.T., Da Silva, A., Leung, W., Mathivanan, S., Wang, Y., Braithwaite, A.W., Christ, D., Benda, A., Parkin, A., Phillips, P.A., Whitelock, J.M., Gill, A.J., Sansom, O.J., Croucher, D.R., Parker, B.L., Pajic, M., Morton, J.P., Cox, T.R., Timpson, P., 2019. CAF hierarchy driven by pancreatic cancer cell p53-status creates a pro-metastatic and chemoresistant environment via perlecan. Nat Commun 10, 3637.

Villarroya-Beltri, C., Baixauli, F., Mittelbrunn, M., Fernández-Delgado, I., Torralba, D., Moreno-Gonzalo, O., Baldanta, S., Enrich, C., Guerra, S., Sánchez-Madrid, F., 2016. ISGylation controls exosome secretion by promoting lysosomal degradation of MVB proteins. Nat Commun 7, 13588.

Vinay, D.S., Ryan, E.P., Pawelec, G., Talib, W.H., Stagg, J., Elkord, E., Lichtor, T., Decker, W.K., Whelan, R.L., Kumara, H.M.C.S., Signori, E., Honoki, K., Georgakilas, A.G., Amin, A., Helferich, W.G., Boosani, C.S., Guha, G., Ciriolo, M.R., Chen, S., Mohammed, S.I., Azmi, A.S., Keith, W.N., Bilsland, A., Bhakta, D., Halicka, D., Fujii, H., Aquilano, K., Ashraf, S.S., Nowsheen, S., Yang, X., Choi, B.K., Kwon, B.S., 2015. Immune evasion in cancer: Mechanistic basis and therapeutic strategies. Seminars in Cancer Biology 35, S185–S198.

Vogiatzi, F., Brandt, D.T., Schneikert, J., Fuchs, J., Grikscheit, K., Wanzel, M., Pavlakis, E., Charles, J.P., Timofeev, O., Nist, A., Mernberger, M., Kantelhardt, E.J., Siebolts, U., Bartel, F., Jacob, R., Rath, A., Moll, R., Grosse, R., Stiewe, T., 2016. Mutant p53 promotes tumor progression and metastasis by the endoplasmic reticulum UDPase ENTPD5. Proc Natl Acad Sci USA 113, E8433–E8442.

Walerych, D., Lisek, K., Sommaggio, R., Piazza, S., Ciani, Y., Dalla, E., Rajkowska, K., Gaweda-Walerych, K., Ingallina, E., Tonelli, C., Morelli, M.J., Amato, A., Eterno, V., Zambelli, A., Rosato, A., Amati, B., Wiśniewski, J.R., Del Sal, G., 2016. Proteasome machinery is instrumental in a common gain-of-function program of the p53 missense mutants in cancer. Nat Cell Biol 18, 897–909.

Walker, K.K., Levine, A.J., 1996. Identification of a novel p53 functional domain that is necessary for efficient growth suppression. Proceedings of the National Academy of Sciences 93, 15335–15340.

Wang, J., Zhao, Y., Qi, R., Zhu, X., Huang, C., Cheng, S., Wang, S., Qi, X., 2017. Prognostic role of podocalyxin-like protein expression in various cancers: A systematic review and meta-analysis. Oncotarget 8.

Webber, J.P., Spary, L.K., Sanders, A.J., Chowdhury, R., Jiang, W.G., Steadman, R., Wymant, J., Jones, A.T., Kynaston, H., Mason, M.D., Tabi, Z., Clayton, A., 2015. Differentiation of tumour-promoting stromal myofibroblasts by cancer exosomes. Oncogene 34, 290–302.

Wei, Y., Wang, D., Jin, F., Bian, Z., Li, L., Liang, H., Li, M., Shi, L., Pan, C., Zhu, D., Chen, X., Hu, G., Liu, Y., Zhang, C.-Y., Zen, K., 2017. Pyruvate kinase type M2 promotes tumour cell exosome release via phosphorylating synaptosome-associated protein 23. Nat Commun 8, 14041.

Weissmueller, S., Manchado, E., Saborowski, M., Morris, J.P., Wagenblast, E., Davis, C.A., Moon, S.-H., Pfister, N.T., Tschaharganeh, D.F., Kitzing, T., Aust, D., Markert, E.K., Wu, J., Grimmond, S.M., Pilarsky, C., Prives, C., Biankin, A.V., Lowe, S.W., 2014. Mutant p53 drives pancreatic cancer metastasis through cell-autonomous PDGF receptor β signaling. Cell 157, 382–394.

White, D.P., Caswell, P.T., Norman, J.C., 2007. αvβ3 and α5β1 integrin recycling pathways dictate downstream Rho kinase signaling to regulate persistent cell migration. J Cell Biol 177, 515–525.

Willis, A., Jung, E.J., Wakefield, T., Chen, X., 2004. Mutant p53 exerts a dominant negative effect by preventing wild-type p53 from binding to the promoter of its target genes. Oncogene 23, 2330–2338.

Wilson, G.M., Fielding, A.B., Simon, G.C., Yu, X., Andrews, P.D., Hames, R.S., Frey, A.M., Peden, A.A., Gould, G.W., Prekeris, R., 2005. The FIP3-Rab11 Protein Complex Regulates Recycling Endosome Targeting to the Cleavage Furrow during Late Cytokinesis□D □V. Molecular Biology of the Cell 16, 12.

Wolf, D., Harris, N., Rotter, V., 1984. Reconstitution of p53 expression in a nonproducer Ab-MuLV-transformed cell line by transfection of a functional p53 gene. Cell 38, 119–126.

Wolfers, J., Lozier, A., Raposo, G., Regnault, A., Théry, C., Masurier, C., Flament, C., Pouzieux, S., Faure, F., Tursz, T., Angevin, E., Amigorena, S., Zitvogel, L., 2001. Tumor-derived exosomes are a source of shared tumor rejection antigens for CTL cross-priming. Nat Med 7, 297–303.

Wollert, T., Hurley, J.H., 2010. Molecular mechanism of multivesicular body biogenesis by ESCRT complexes. Nature 464, 864–869.

Wortzel, I., Dror, S., Kenific, C.M., Lyden, D., 2019. Exosome-Mediated Metastasis: Communication from a Distance. Developmental Cell 49, 347–360.

Xu, J., Reumers, J., Couceiro, J.R., De Smet, F., Gallardo, R., Rudyak, S., Cornelis, A., Rozenski, J., Zwolinska, A., Marine, J.-C., Lambrechts, D., Suh, Y.-A., Rousseau, F., Schymkowitz, J., 2011. Gain of function of mutant p53 by coaggregation with multiple tumor suppressors. Nat Chem Biol 7, 285–295.

Yan, H.H., Jiang, J., Pang, Y., Achyut, B.R., Lizardo, M., Liang, X., Hunter, K., Khanna, C., Hollander, C., Yang, L., 2015. CCL9 Induced by TGF Signaling in Myeloid Cells Enhances Tumor Cell Survival in the Premetastatic Organ. Cancer Research 75, 5283–5298.

Yáñez-Mó, M., Siljander, P.R.-M., Andreu, Z., Bedina Zavec, A., Borràs, F.E., Buzas, E.I., Buzas, K., Casal, E., Cappello, F., Carvalho, J., Colás, E., Cordeiro-da Silva, A., Fais, S., Falcon-Perez, J.M., Ghobrial, I.M., Giebel, B., Gimona, M., Graner, M., Gursel, I., Gursel, M., Heegaard, N.H.H., Hendrix, A., Kierulf, P., Kokubun, K., Kosanovic, M., Kralj-Iglic, V., Krämer-Albers, E.-M., Laitinen, S., Lässer, C., Lener, T., Ligeti, E., Linē, A., Lipps, G., Llorente, A., Lötvall, J., Manček-Keber, M., Marcilla, A., Mittelbrunn, M., Nazarenko, I., Nolte-'t Hoen, E.N.M., Nyman, T.A., O'Driscoll, L., Olivan, M., Oliveira, C., Pállinger, É., del Portillo, H.A., Reventós, J., Rigau, M., Rohde, E., Sammar, M., Sánchez-Madrid, F., Santarém, N., Schallmoser, K., Stampe Ostenfeld, M., Stoorvogel, W., Stukelj, R., Van der Grein, S.G., Helena Vasconcelos, M., Wauben, M.H.M., De Wever, O., 2015. Biological properties of extracellular vesicles and their physiological functions. Journal of Extracellular Vesicles 4, 27066.

Yang, C., Guo, W. -b., Zhang, W. -s., Bian, J., Yang, J. -k., Zhou, Q. -z., Chen, M. -k., Peng, W., Qi, T., Wang, C. -y., Liu, C. -d., 2017. Comprehensive proteomics analysis of exosomes derived from human seminal plasma. Andrology 5, 1007–1015.

Yeh, Y.-C., Ling, J.-Y., Chen, W.-C., Lin, H.-H., Tang, M.-J., 2017. Mechanotransduction of matrix stiffness in regulation of focal adhesion size and number: reciprocal regulation of caveolin-1 and β1 integrin. Sci Rep 7, 15008.

Yu, X., Harris, S.L., Levine, A.J., 2006. The Regulation of Exosome Secretion: a Novel Function of the p53 Protein. Cancer Res 66, 4795–4801.

Yu, X., Prekeris, R., Gould, G.W., 2007. Role of endosomal Rab GTPases in cytokinesis. European Journal of Cell Biology 86, 25–35.

Zhang, C., Liu, J., Liang, Y., Wu, R., Zhao, Y., Hong, X., Lin, M., Yu, H., Liu, L., Levine, A.J., Hu, W., Feng, Z., 2013. Tumour-associated mutant p53 drives the Warburg effect. Nat Commun 4, 2935.

Zhang, G., Ezura, Y., Chervoneva, I., Robinson, P.S., Beason, D.P., Carine, E.T., Soslowsky, L.J., Iozzo, R.V., Birk, D.E., 2006. Decorin regulates assembly of collagen fibrils and acquisition of biomechanical properties during tendon development. J. Cell. Biochem. 98, 1436–1449.

Zhang, H., Deng, T., Liu, R., Bai, M., Zhou, L., Wang, Xia, Li, S., Wang, Xinyi, Yang, H., Li, J., Ning, T., Huang, D., Li, H., Zhang, L., Ying, G., Ba, Y., 2017. Exosome-delivered EGFR regulates liver microenvironment to promote gastric cancer liver metastasis. Nat Commun 8, 15016.

Zhang, H., Freitas, D., Kim, H.S., Fabijanic, K., Li, Z., Chen, H., Mark, M.T., Molina, H., Martin, A.B., Bojmar, L., Fang, J., Rampersaud, S., Hoshino, A., Matei, I., Kenific, C.M., Nakajima, M., Mutvei, A.P., Sansone, P., Buehring, W., Wang, H., Jimenez, J.P., Cohen-Gould, L., Paknejad, N., Brendel, M., Manova-Todorova, K., Magalhães, A., Ferreira, J.A., Osório, H., Silva, A.M., Massey, A., Cubillos-Ruiz, J.R., Galletti, G., Giannakakou, P., Cuervo, A.M., Blenis, J., Schwartz, R., Brady, M.S., Peinado, H., Bromberg, J., Matsui, H., Reis, C.A., Lyden, D., 2018.

Identification of distinct nanoparticles and subsets of extracellular vesicles by asymmetric flow field-flow fractionation. Nat Cell Biol 20, 332–343.

Zhang, M., Tsimelzon, A., Chang, C.-H., Fan, C., Wolff, A., Perou, C.M., Hilsenbeck, S.G., Rosen, J.M., 2015. Intratumoral heterogeneity in a p53 null mouse model of human breast cancer. Cancer Discov 5, 520–533.

Zhong, Y., Macgregor-Das, A., Saunders, T., Whittle, M.C., Makohon-Moore, A., Kohutek, Z.A., Poling, J., Herbst, B.T., Javier, B.M., Cope, L., Leach, S.D., Hingorani, S.R., Iacobuzio-Donahue, C.A., 2017. Mutant p53 Together with TGFβ Signaling Influence Organ-Specific Hematogenous Colonization Patterns of Pancreatic Cancer. Clin Cancer Res 23, 1607–1620.

Zhou, G., Wang, J., Zhao, M., Xie, T.-X., Tanaka, N., Sano, D., Patel, A.A., Ward, A.M., Sandulache, V.C., Jasser, S.A., Skinner, H.D., Fitzgerald, A.L., Osman, A.A., Wei, Y., Xia, X., Songyang, Z., Mills, G.B., Hung, M.-C., Caulin, C., Liang, J., Myers, J.N., 2014. Gain-of-Function Mutant p53 Promotes Cell Growth and Cancer Cell Metabolism via Inhibition of AMPK Activation. Molecular Cell 54, 960–974.

Zimmerman, B., Kelly, B., McMillan, B.J., Seegar, T.C.M., Dror, R.O., Kruse, A.C., Blacklow, S.C., 2016. Crystal Structure of a Full-Length Human Tetraspanin Reveals a Cholesterol-Binding Pocket. Cell 167, 1041-1051.e11.

Zomer, A., Maynard, C., Verweij, F.J., Kamermans, A., Schäfer, R., Beerling, E., Schiffelers, R.M., de Wit, E., Berenguer, J., Ellenbroek, S.I.J., Wurdinger, T., Pegtel, D.M., van Rheenen, J., 2015. In Vivo Imaging Reveals Extracellular Vesicle-Mediated Phenocopying of Metastatic Behavior. Cell 161, 1046–1057.